マス・フォア・インダストリ研究 No.18

New technologies for non-destructive and non-invasive inspections and their applications

Organizer:

Takashi Takiguchi

Institute of Mathematics for Industry
Kyushu University

About the Mathematics for Industry Research

The Mathematics for Industry Research was founded on the occasion of the certification of the Institute of Mathematics for Industry (IMI), established in April 2011, as a MEXT Joint Usage/Research Center – the Joint Research Center for Advanced and Fundamental Mathematics for Industry – by the Ministry of Education, Culture, Sports, Science and Technology (MEXT) in April 2013. This series publishes mainly proceedings of workshops and conferences on Mathematics for Industry (MfI). Each volume includes surveys and reviews of MfI from new viewpoints as well as up-to-date research studies to support the development of MfI.

October 2018
Osamu Saeki
Director
Institute of Mathematics for Industry

New technologies for non-destructive and non-invasive inspections and their applications

Organizer: Takashi Takiguchi

Preface

These are the proceedings of the workshop "New technologies for non-destructive and non-invasive inspections and their applications", held at IMI, Kyushu University, from October twenty eighth to October thirty first, 2019. In this workshop, the following researches were reported and lively discussions were had on them.

- Dr. Kenji Hashizume : Development and operation of the non-destructive inspection methods for infrastructures

- Prof. Cheng Hua : Mathematical modeling and analysis of Rayleigh wave

- Takashi Takiguchi : An overview of ultrasonic imaging and its development

- Prof. Daisuke Kawagoe : Regularity of solutions to the stationary transport equation and its application to the optical tomography

- Prof. Makoto Maruya : 3D reconstruction of the asteroid Ryugu as an inverse problem

- Prof. Kazumi Tanuma : Perturbations of Rayleigh waves in anisotropic elasticity and Bleustein-Gulyaev waves in piezoelectricity

On the first day of the workshop, Doctor Kenji Hashizume introduced the inspection deveices for the infrasturcures developed by West Nippon Expressway Engineering Shikoku Company Limited, as well as their applications to non-destructive inspections and to prediction of the potholes on the road. It is surprising that his talk necessarily contains new technology developed by West Nippon Expressway Engineering Shikoku Company Limited every year. Now our research team is studying how to apply the device *J-SYSTEM* developed by West Nippon Expressway Engineering Shikoku Company Limited for a non-destructive ispection of stone statues in China. It is a serious problem in China that old stone statues collapse naturally and there are a number of such statues.

In the morning on the second day, Professor Cheng Hua gave a presentation on the Rayleigh waves in the viscoelastic media. It was one of the main topics in this workshop to study how to establish a non-destructive inspection technique for the concrete cover in RC (reinforced concrete) structures by application of the Rayleigh waves. In his talk, Prof. Hua studied the uniqueness problem of the Rayleigh waves in the viscoelastic media. It must be solved bofore the application to non-destructive inspections are discussed and it could be a basic theory for applications of the Rayleigh waves.

In the afternoon, the organizer overviewed the development of ulrtasonic imaging technique (USI). For the time being, the USI has been being developed by applying the idea by G. N. Hounsfield for the first practicalization of the X-ray computerized tomography. The organizer reviewed such development and posed some open problems for further development of USI.

In the morning on October 30th, Professor Daisuke Kawagoe presented his research on the regularity of solution of the transport equation and its application to optical tomography. In this talk, he theoretically succeeded in taking out the Radon transform of the absorption coefficients of infra-red ray in the human tissue by observation of the infra-red laser transportation, which is a very nice and interesting result. From the viewpoint of practical application, a very important problem is left open; how to practicalize his idea. It was one of the main topic in this workshop to study new non-destructive inspection (NDI) or non-invasive inspection (NII) techniques without X-ray nor magnetic resonance. Being excellent techniques for non-destructive or non-invasive inspections, X-ray tomography and MRI have shortcomings such as the expensive cost in both the devices themselves and their protection facilities, harmful side effects of the X-rays and strong magnetic fields to human bodies and to the environment and so on. Therefore, it is required to develop new, cheaply running, safe and reliable NII and NDI techniques. The talks by Prof. Kawagoe and the origanizer are very closely related to this topic.

In the afternoon, Professor Makoto Maruya introduced his research on remote sensing. He belongs to Hayabusa 2 project. He introduced the idea applied for the reconstruction of the 3D image of the asteroid Ryugu. On this problem, many improvements were proposed by the audience and we decided to begin the research to improve this 3D reconstruction. He also introduced an algorithm for GNNS. We created several problems to improve the algorithm for GNNS, which are being studied.

On the final day, Professor Kazumi Tanuma presented his research in the Rayleigh waves in anisotropic elasticitic media and in Bleustein-Gulyaev waves in piezoelectric media. In his research, Prof. Tanuma treated the Rayleigh waves in in anisotropic elasticitic media as the Rayleigh waves in isotropic elasticitic media and their small perturbations. The same idea was applied for the study of the Bleustein-Gulyaev waves in piezoelectric media. His idea can be of help in the study to apply Rayleigh wave in a non-destructive inspection technique for the concrete cover in RC structures, since concrete is an anistropic viscoelastic medium.

In this workshop, we have created new research tasks to be solved by industry-academia and interdisciplinary collaboration, which are being studied now. We wish that we would have more opportunities to hold such workshops to study these important problems. We also hope that such collaboration be much more popular.

At the end of Preface, I would express my gratefulness to Ms. Chiemi Furutani and Ms. Mika Tomonaga, the secretaries of this workshop, for their kind help.

January 31, 2020

Takashi Takiguchi

Table of Contents

New technologies for non-destructive and non-invasive inspections and their applications

October 28-31, 2019

IMI, Ito Campus, Kyushu University
Room M W1-C-512, West Zone 1,
744 Motooka, Nishi-ku Fukuoka 819-0395, Japan

October 28, Monday
13:50   Opening

(Chair: D. Kawagoe)
14:00-15:30 Kenji Hashizume
             (West Nippon Expressway Shikoku Engineering Company Limited, Japan)
             Development and operation of the non-destructive inspection methods
             for infrastructures

15:30-16:30 Discussion

October 29, Tuesday
(Chair: K. Tanuma)
11:00-12:30 Cheng Hua (Fudan University, China)
             Mathematical modeling and analysis of Rayleigh wave

12:30-14:00 Discussion over lunch

14:00-15:30 Takashi Takiguchi (National Defense Academy of Japan, Japan)
             An overview of ultrasonic imaging and its develpment

15:30-16:30 Discussion

October 30, Wednesday
(Chair: T. Takiguchi)
11:00-12:30 Daisuke Kawagoe (Kyoto University, Japan)
             Regularity of solutions to the stationary transport equation
             and its application to the optical tomography

12:30-14:00 Discussion over lunch

14:00-15:30 Makoto Maruya
             (National Institute of Advanced Industrial Science and Technology/
              Geo Insight LLC, Japan)
             3D reconstruction of the asteroid Ryugu as an inverse problem

15:30-16:30 Discussion

October 31, Thursday

(Chair: C. Hua)

11:00-12:30   Kazumi Tanuma (Gunma University, Japan)
        Perturbations of Rayleigh waves in anisotropic elasticity
        and Bleustein-Gulyaev waves in piezoelectricity

12:30-14:00   Discussion over lunch

14:00   Closing

Organizer:
Takashi Takiguchi (National Defense Academy of Japan)

Supported by:
IMI, Kyushu University

Development and operation of the non-destructive inspection methods for infrastructures

Kenji Hashizume

West Nippon Expressway Engineering Shikoku Company Limited

3-1-1 Hanazono-cho, Takamatsu-shi, Kagawa 760-0072, Japan

Email: kenji.hashizume@w-e-shikoku.co.jp

In this talk, we introduce the latest trend about our inspection devices and the techniques, which are introduced into the inspection of expressway. We suggest the development of the devices, which enable objective evaluation and record for inspection of bridge, tunnel and pavement. We also introduce how we manage roads by the devices we have developed.

Key Words: inspection, non-destructive, infrared, light cutting method

1. Introduction

  In order to secure the social durability of infrastructure, the following matters are indispensable. (1) To maintain and manage the organized infrastructure efficiently and effectively. (2) To prevent the outbreak of risk events of damage due to aging of infrastructure. Therefore, it is important to inspect and repair the infrastructure efficiently and effectively.

Accordingly the efficient and effective inspection and repairing would be very important. For the given purpose, the efficient and effective inspections and maintenance practice shall be necessary. The inspection method using the non-destructive inspection devices for the bridges, tunnels, and pavements inspections with objective evaluations and keeping their records is now proposed. In this talk, we suggest the development of the devices, which enable objective evaluation and record for inspection of bridge, tunnel and pavement. We also introduce how we manage roads by the devices we have developed.

2. New devices for inspection
2.1 Bridge Inspections

We now explain the "J-System" (Figure-1) for the inspection method using the infrared cameras. The reinforced concrete fulfill its role with the joint functioning of rebar and concrete for the concrete structure. When the rebar gathers rust in the concrete, cracks appear on the concrete surface along the rebar, the surface concrete spalls, and so its durability is to be reduced. We have been inspecting the cracks triggered by the concrete delaminations along the rebar through the hammering. The infrared cameras inspection is the new one detecting the damaged areas such as concrete delaminations and cracks through photographing the concrete surface by using infrared cameras from remote palaces, and keeping the records of the concrete surface conditions using digital cameras. The inspections of bridges surface by infrared cameras are done by the passive method, and the followings are the important elements;

figure -1   J-system

i. **Cameras Quality (Is the cameras suitable for the inspection environment?)**

Inspections are done basically during night, so it is important to extend the surveillance hours of the day and increase the annual surveillance days by using the camera with a short- wave type which has no the environmental reflections during night and with a enforcing-cooling-system type with a small thermal resolution.
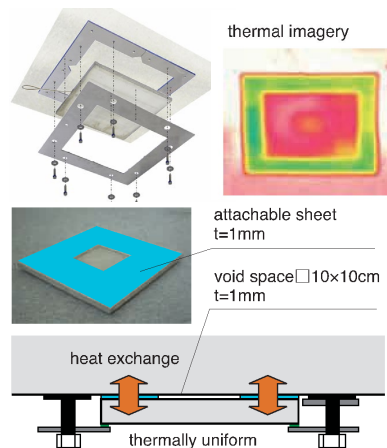
figure -2   J-system EM(S)

ii. **Judgment on time zone of the day when inspections can be done (Do we inspect at a suitable time ?)**

We implement the night- time inspection basically, because there are various bridge types and bridge members which are not suitable to inspect during daytime. The time zone of the day when inspection is possible is based on data

of the EMS (Environment Measuring System)(Figure-2) mounted on the inspection bridges.

iii. Simple and Objective Evaluation Method (Is it possible and easy to evaluate objectively?)

There could be, for individuals, differences among the inspection judgments because it is sometime impossible to judge the damage evaluation such as delamination and spalling for the bridge members and damaged parts only by looking at the infrared images. It is also impossible to judge the crack's depth along the rebar. However, the red, yellow, and blue cracks' judgment- images at the 1, 2, 3 cm depth from the surface are shown at the camera monitor (Figure -3).
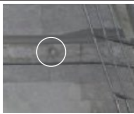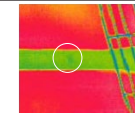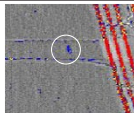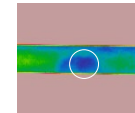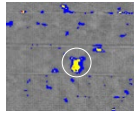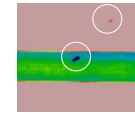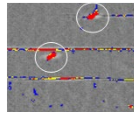
Damage grade	Visible image	Infrared image	3 level indication
Observation Abnormal sound			
Caution Possibility of falling down near future			
Warning Require emergency measure			

figure -3   J-System Monitor Image

2.2 Tunnel and Pavement Inspection
2.2.1 Tunnel and Pavement Inspection

We now explain the "L & L System" (Figure-4) inspection method which uses the Line Censor Camera and Laser Marker. Line Censor cameras mount the visual image censors, and can photograph seamless and continuous imageries. They can also be applied for the tunnel and pavement inspections.Light Cutting method is photographing the laser marker images from a upper and oblique position by using the laser which is irradiated vertically down on measuring surfaces and obtain the object shape. This method is used for road surface profile measuring.

figure -4   L&L   System

i. Tunnel Inspection

It is possible to obtain the fine and colorful continuous images (Figure-5) of tunnel lining by using Line Censor cameras mounted on the inspection cars with high speed (less than 100km/h). The cracks of tunnel lining can be detected up to 0.2mm, and water leakage and lime isolation can be also found. The damage spreading drawings and their diagonal charts can easily be produced based on the captive pictures, and so we inspect only the areas where further close
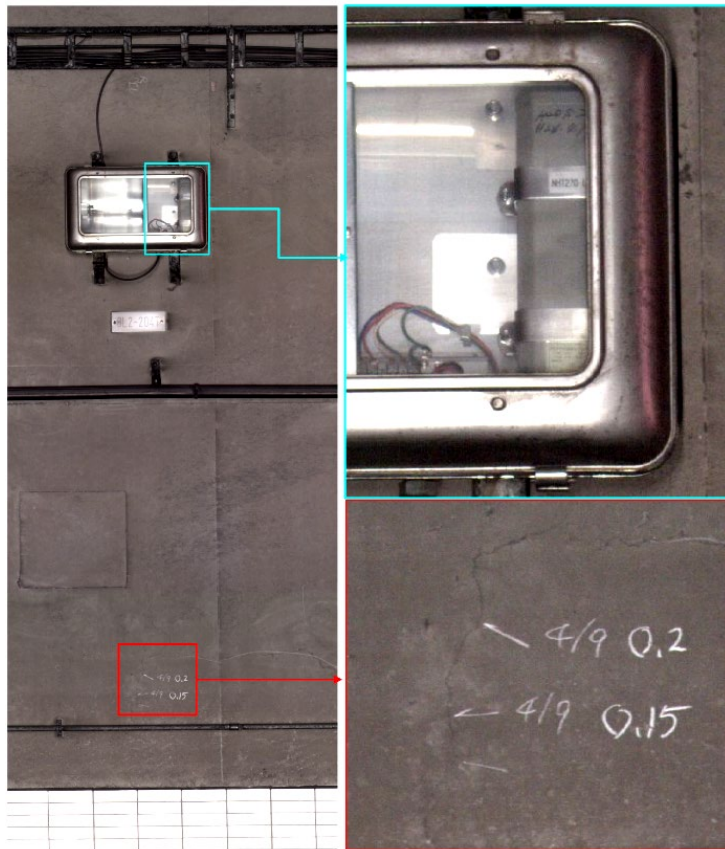
figure -5   Visual image with cracks and the accessories

and detail investigations are necessary. And we can clearly watch the conditions of rusted accessories in tunnels, and so it is now possible to apply them for the accessories inspections.

ii. Pavement Inspection

We can inspect the pavement conditions such as cracks and potholes, and conditions of bridge expansion joints by using Line Censer cameras mounted on the vehicle with high speed (less than 100km/h). At the same time, we can also measure rutting, bumps, and upheaval through using laser cameras, and measure road surface profile such as height, and also evaluate the evenness, bump and IRI values.

We can also display the grade evaluation for the cracks, rutting, bumps,

evenness, and IRI values obtained by the road surface measurements, and we can also easily sort and extract some of the data with abnormal ranges which show more than a certain threshold (Figure-6). Thus, the repairing and renewal plans of road pavement and the bumps will be made easier.

Visual image（pavement）

Processed surface height image(red:rutting10mm or deeper)

Transversal cross section (Left red line)   Cracks can be detected as a difference of height.

IRI DATA
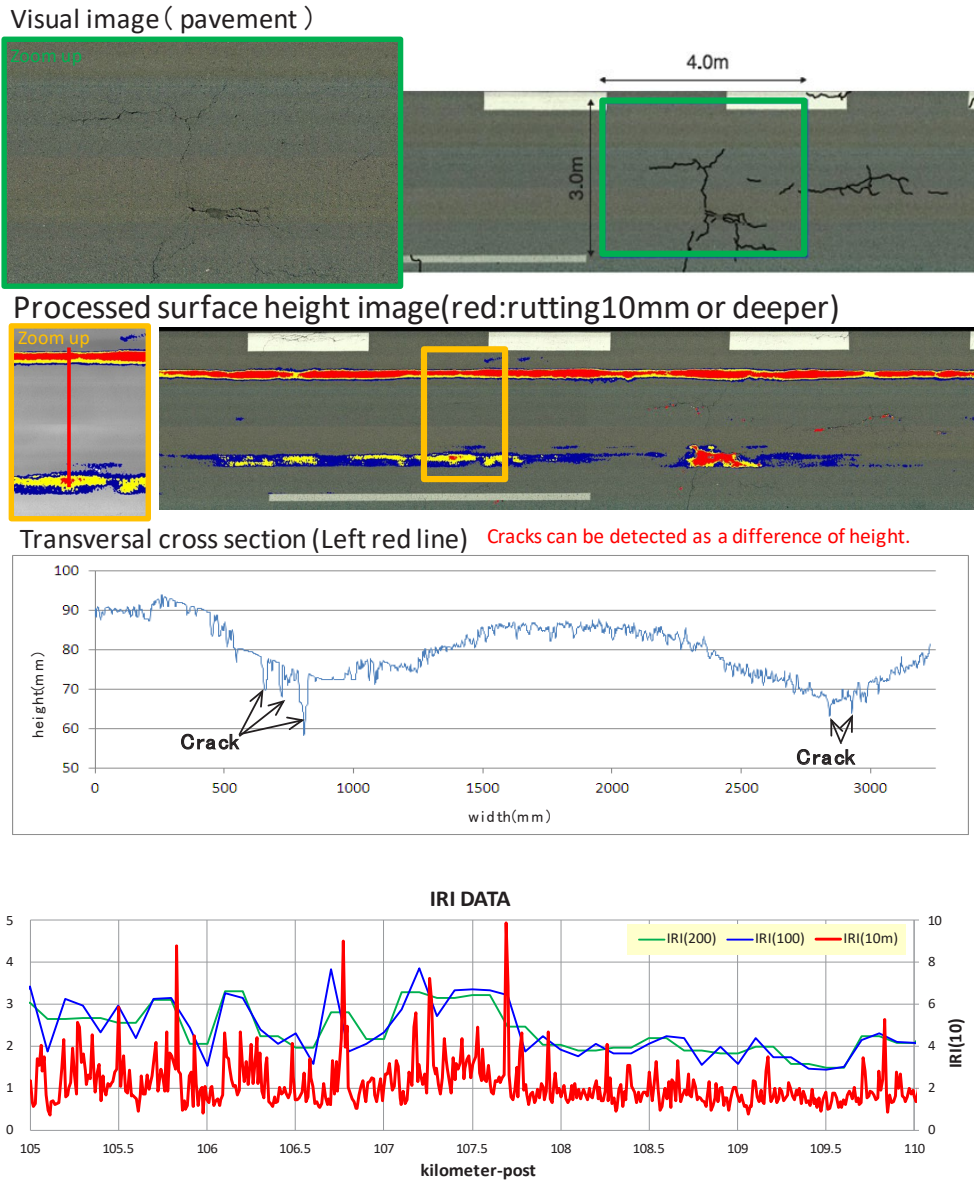
figure -6   Pavement evaluation

We have analyzed the periodically measured data using the high-accuracy pavement-condition measuring vehicle in expressways of Shikoku, to fully understand the progress of porous asphalt pavement damages. As a result, it is found that when the local subsidence phenomena occur, they would develop from cracks to potholes in a short time. It is very difficult to find these damages earlier even through the conventional evaluation indexes (cracks, rutting, flatness) or survey frequency. This study is to propose the new evaluation factors to the porous asphalt pavement based on the analysis of the high-accuracy surface profile.

First, an evaluation by the local subsidence amount is proposed (Figure-7). This method is an evaluation method for extracting local collapse points indicating a prediction of the occurrence of potholes that cannot be grasped by conventional evaluation methods and survey frequency. In this method, the data presented in a chronological order and measured periodically were used. The evaluation index based on the amount of local subsidence can be calculated with the conventional measurement data obtained by investigating the road properties, making it possible to grasp the generation risk of the current potholes. In addition, the prediction results based on the damage growth curve model can be utilized as a mid-to-long-term repair planning document.

Depth of local
subsidence amount

dashed line：the representative road surface shape
　the representative rut depth which is the central value of the maximum rut depth in a vicinity of 10m.
solid line：the road surface shape of target point
　the rut depth of the objective point
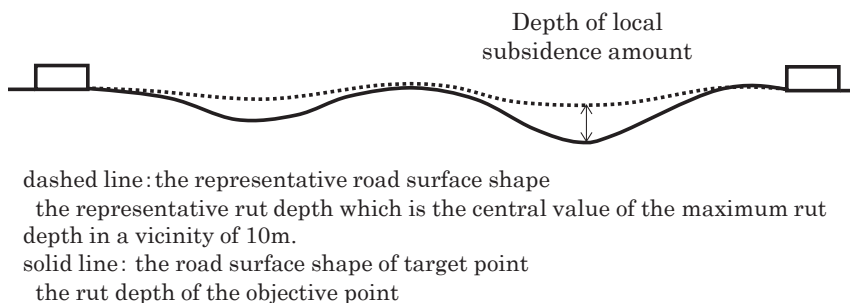
figure -7　　Local subsidence amount

Second, the cracking of porous asphalt proceeds with aggregate scattering; however, by using this vehicle, a surface texture depth (mean profile depth: MPD) evaluation can be applied to the full lane width (Figure-8). The MPD is a quantitative evaluation method used for evaluating the progress of aggregate scattering and cracking peculiar to porous asphalt. Acquiring highly accurate shape data of the road surface makes it possible to quantitatively evaluate the MPD of the full lane width in a planar way.

This study will be the basic documents for the repair planning which will prolong the porous asphalt pavement life, and contribute to reducing the pothole occurrence risks by proposing the quantifying evaluation flow based on the analysis results.
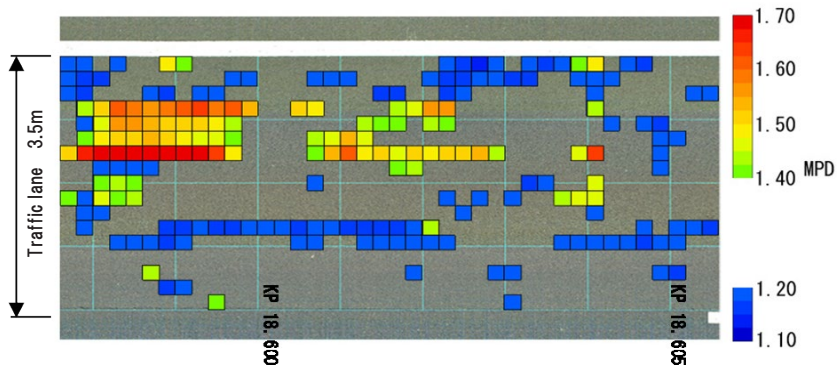
Warm color ⇒ Large MPD
Large quantity of aggregate scattering is observed.
Cool color ⇒ Small MPD
A place which will likely be clogged.

figure -8　Mean profile depth

3. Topic technology

3.1 Tunnel Inspection new system "Smart-Eagle type-T"

We are considering a method to evaluate the risk of crashing of tunnel concrete (Figure-9). In this technique, we measure the unevenness of the surface with shape measurement precisely and judge the danger from its shape. In the future, I would like to propose unique evaluation methods based on visible and shape data.

figure -9   Smart Eagle type-T

3.2 Pavement Inspection new system "Smart-Eagle type-P"

Currently, a technology that can easily grasp each index of the road surface properties required for pavement management attracts attention (Figure-10). This technology reduces the investigation cost which was the problem of the conventional road surface property investigation, and shortens the analysis time. This system has the following features

laser × 1
3D-camera × 1

gyro × 1
Light cutting unit × 1
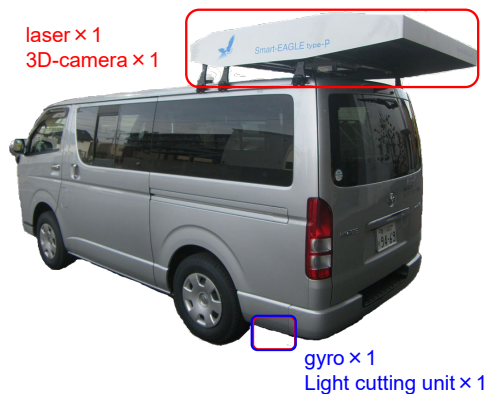
figure -10   Smart Eagle type-P

- ➢ Automatic analysis
- ➢ Proposing a new evaluation indicator to extract damage
   (Local subsidence amount & MPD by vehicle)

By measuring with high frequency, it is possible to grasp the current situation quickly. Also, by analyzing accumulated data, it can contribute to formulation of inspection and repair plan according to the actual situation (Figure-11).
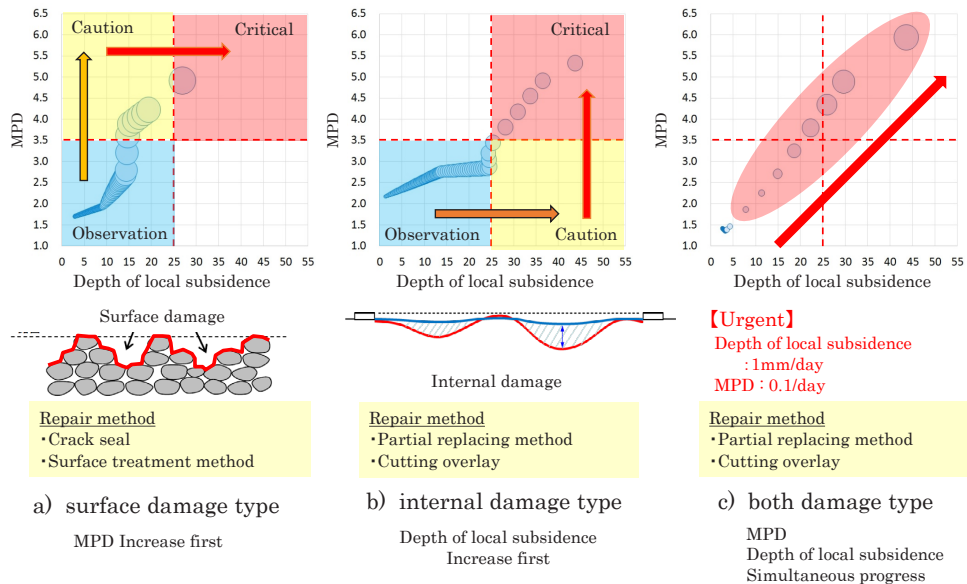
figure -11   Damage formed by a simple road survey property

4. Conclusion

The bridges, tunnels, and pavement inspections by cameras can be used for the assistances for the on-site inspections or their alternatives, and we can maintain the objective evaluations and predict the future damages through their annual transitions. Also the repairing plan can be made easily and efficiently.
The proposed inspection method using the cameras makes it possible to use, select and combine those inspection tools economically and effectively in accordance with budges and utilizations patterns of each organization based on their different road structure maintenance and repairing standards.

This work is partially based on the discussions at 2019 IMI Joint Use Research Program Workshop (II) "New technologies for non-destructive and non-invasive inspections and their applications"

Reference

1) A study for detection accuracy improvement in the infrared thermography method,J.JCI,vol.34,No.1,1696-1701,2012
2) Predictive probability of the concrete delamination and damage by an infrared thermography method, ,J.JCI,vol.35,No.1,1813-1818,2013
3) One approach of the forecasting method for the pot-hole occurred by the deterioration of deeper than binder course on porous asphalt pavement,J.JSCE,Ser.E1,vol.70,No.3,I_17-I_24,2014
4) Study on damage form analysis and road surface management using simple road surface survey technology ,J.JSCE 2019 Annual Meeting ,5-446,sep.2019

Development and operation of the non-destructive inspection methods for infrastructures

NEXCO
エンジニアリング四国

West Nippon Expressway Shikoku Company Limited.

West's Japan highway business area Map

Map showing NEXCO-West's business area

Korea Osaka Japan Tokyo Nagoya

Tottori Obama Matsue Kyoto Yokaichi Koka-tsuchiyama Kobe Nara Osaka

CHUGOKU Okayama KANSAI Wakayama

Hiroshima Takamatsu

Yamaguchi Tokushima

Kitakyushu Matsuyama

My company business area

SHIKOKU Kochi

Fukuoka

Saga

KYUSHU

Kumamoto

Nagasaki

West's Highways in Operation 3,427km

OKINAWA Miyazaki

Kagoshima

Naha

Business data

Expressways business

Expressways in operation 3,427km
Daily traffic volume .... 2.82 million/day (fiscal 2013 results)
Operating revenue .... JPY 605.3 billion (fiscal 2013 results)
Expressways under construction .... 141 km
Expressways under construction .... 187 km
(Section developed by the central government)

Development business

Service areas (SA) .... 98 locations
Parking areas (PA) .... 200 locations
Sales .... JPY 151 billion (fiscal 2013 results)

<Legend> Expressways
— Expressways in operation
— Expressways under construction
— Expressways under construction (Section developed by the central government)
— Other expressways

http://global.w-nexco.co.jp/

1

The NEXCO-West Group Policy

100% Safety and Reliability

2

Operation and Maintenance Management

Inspection Planning

Scheduling for inspection activities using stored inspection data

Conducting designs and repair works

Inspection

Conducting inspections

Design and Repair

Decision Making Meeting

Deciding the necessity of repair works with updated bridge inventory

Planning for Design and Repair

Scheduling for designs and repair works
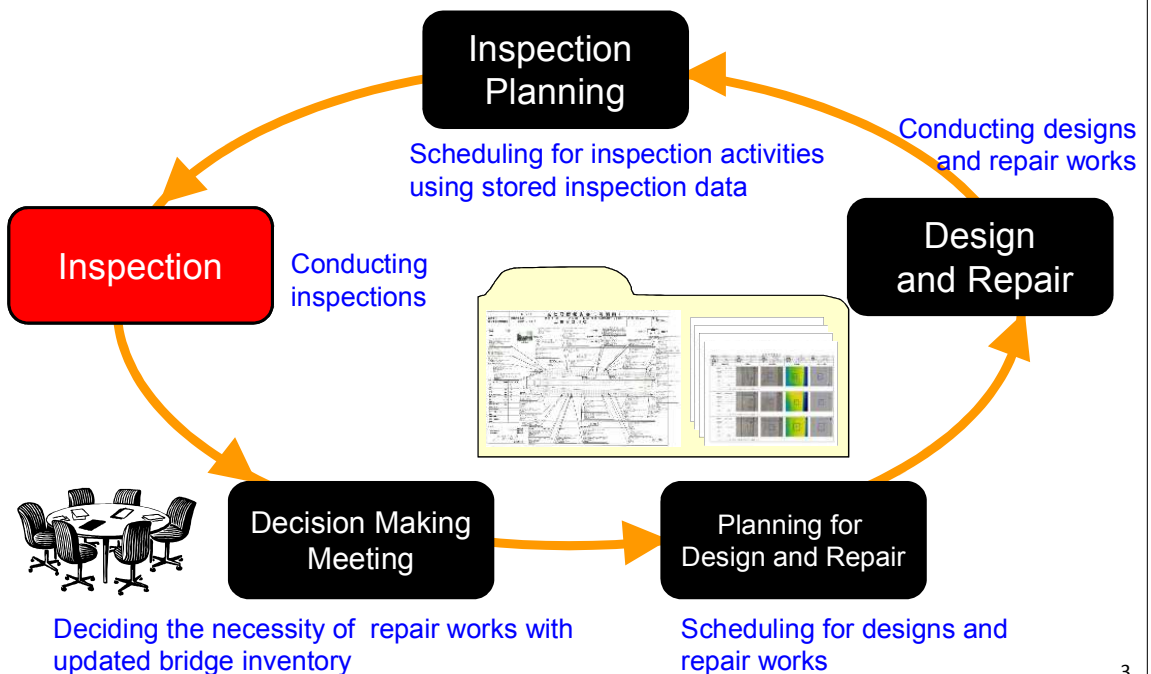
3

Inspection Types

| Type	Procedure	Frequency
Daily Inspection	Visible unusual conditions and deformations of structures are daily inspected behind the wheels.	Once every two days to Once every four days (Dependent on traffic volume)
Routine Inspection	The safety of the structure is regularly confirmed by distant visual inspection, cross visual inspection and hammering test.	More than once a year
Detailed Inspection	The safety of the structure is understood by cross visual inspection and hammering test more in detail.	Once every five years

4

Budgeting for O&M Activities(West's Japan highway)

Operation and Maintenance Costs : 15.6 bn. US$

（planned, in2013 fiscal year ）

Repair Costs
327mn. US$

Maintenance Costs
830mn. US$

Toll Collection Costs
399mn. US$
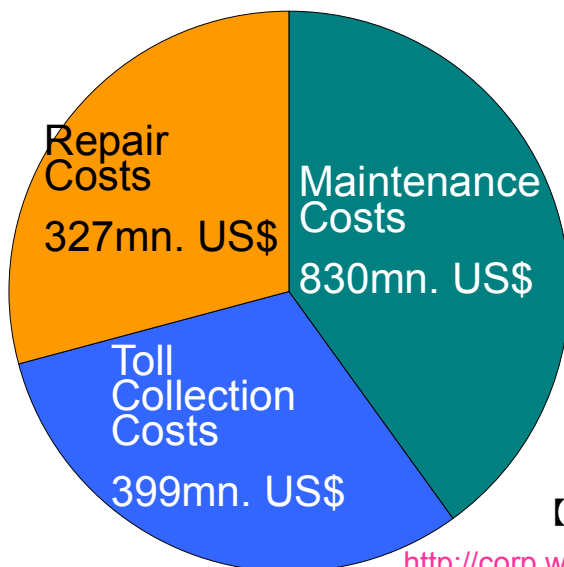
Inspection Costs
84mn. US$

【Note】Exchange Rate 1 USD=115 JPY

http://corp.w-nexco.co.jp/corporate/disclosure/h25/

5

Inspection of Japan highway

Bridges

Tunnels

Pavement

6

Proposal of new technology

Bridges

J-System

Tunnels

Pavement

L&L System

Analyzer with Laser & Line sensor

7

Proposal of our technology

J-System

> We developed this technology to gain effective inspection in order to comply Road Management rule
> After analyzing accumulated data we propose an Evaluation Indicator that related in order to understand deterior mechanism of Architectural structure and to do a preventive action

【Our approachment】
Not just hand over a complete system, but we submit a proposal by finding out the needs from user and design the machine based on measurement accuracy as needed and customize soft ware that easy to use

Eagle

8

Contents

Ⅰ. Approach and issues for
    preventing concrete accident flaking

  Ⅰ-1. Bridge
      （ reinforced concrete structure）

  Ⅰ-2. Tunnel
      （unreinforced concrete structure）

Ⅱ. Approach and issues for
        identity of pavement damages

9

Bridge Inspection

J -SYSTEM

A new concrete inspection and assessment method with safer manipulating, higher performance, and lower cost based on infrared thermography technology.

J-SYSTEM

- EM(S) Test-Piece
- J Monitor
- J Software
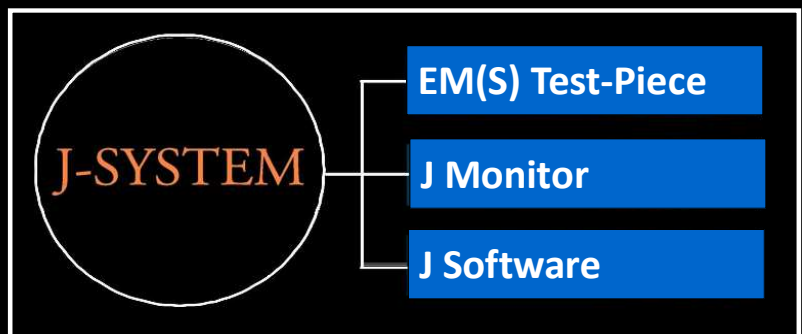
Sounding inspection for prevention measure against flaking

Present method needs a lot of costs and time

12

Infrared inspection situation

Visible image camera

Monitor

Infrared camera

Battery

conventional sounding test (requires lane closure)

J-SYSTEM (does not require lane closure)

13

Basic Theory of Infrared Thermography

Inspection must be done when the temperature difference between air and concrete is large enough.

Air temp.

Temp. difference

Flawed area temp.
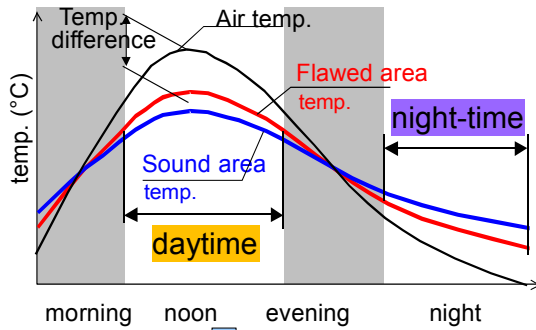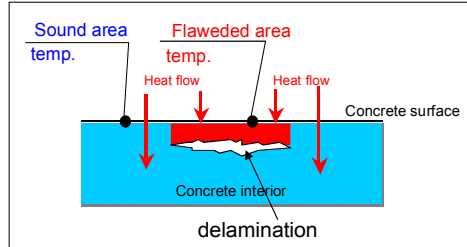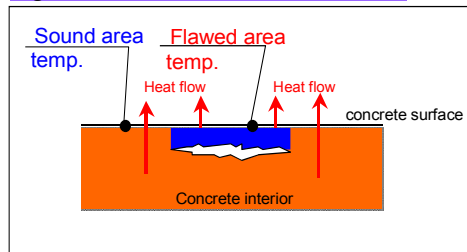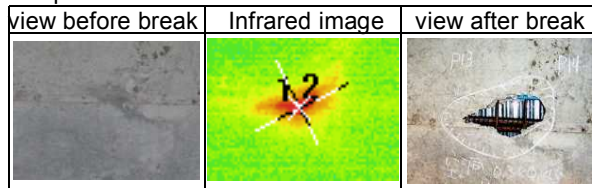
Sound area temp.

temp. (°C)

daytime

night-time

morning　noon　evening　night

Temp. differences creates thermal anomalies

view before break	Infrared image	view after break

daytime : sound <flawed < air

Sound area temp.　Flaweded area temp.

Heat flow　Heat flow

Concrete surface

Concrete interior

delamination

night-time : sound > flawed >air

Sound area temp.　Flawed area temp.

Heat flow　Heat flow

concrete surface

Concrete interior

14

Relationship between Inspection time, and bridge type or part

Direction of heat flow and temperature in damage part

Section	Surface to be inspected	Direct effect	Indirect effect
All bridges	Surface to be inspected / Damaged part / Pavement	Sunlight / Temperature rises due to effect of sunlight	Temperature decreases due effect of sunlight / Sunlight
Metal bridge	Damaged part / Pavement / Surface to be inspected	Surface to be inspected is not directly exposed to sunlight	Sunlight / Temperature decreases due to effect of sunlight
Box beam bridge	Pavement / Damaged part / Surface to be inspected / Surface to be inspected	Surface to be inspected is not directly exposed to sunlight	Sunlight / Temperature decreases due to effect of sunlight / Temperature rises due to effect of sunlight

Inspection time should be selected by bridge type or part

15

Inspection time period of each bridge type

Seto Inland Sea climate during summer/autumn
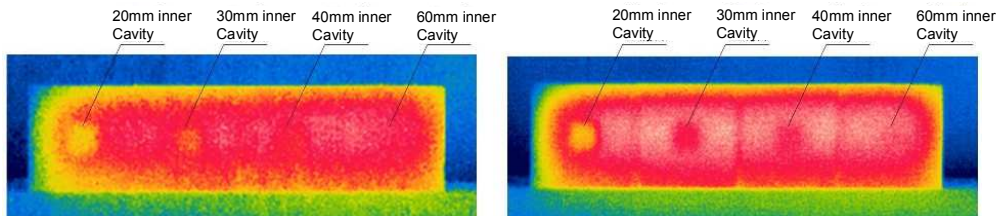
Inspection time period

Bridge type	Section	Time											
		6	8	10	12	14	16	18	20	22	24	2	4
All bridges	Wall balustrade		▬▬▬▬▬▬				▬▬▬▬▬▬▬▬▬▬▬▬▬▬						
RC bridge	Overhang								▬▬▬▬▬▬▬▬▬▬				
	Floor slab			▬▬▬▬▬▬					▬▬▬▬▬▬▬▬				
Me bridge	Overhang	▬							▬▬▬▬▬▬▬▬▬▬▬▬				
	Floor slab	▬							▬▬▬▬▬▬▬▬▬▬▬▬				
Box beam bridge	Overhang	▬							▬▬▬▬▬▬▬▬▬▬▬▬				
	Floor slab								▬▬▬▬▬▬▬▬▬▬▬▬▬				
PC bridge	Overhang	▬							▬▬▬▬▬▬▬▬▬▬▬▬				
	Girder				▬▬▬▬▬▬				▬▬▬▬▬▬▬▬				
	Floor slab	▬							▬▬▬▬▬▬▬▬▬▬▬▬				

Almost all bridge types and bridge sections can be investigated during night time.
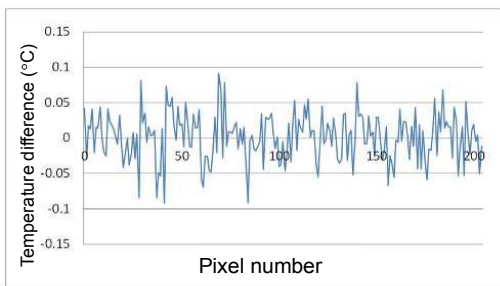
16

Images of damage from different minimum detected temperatures

Thermal images of different minimum detected temperatures (NETD)
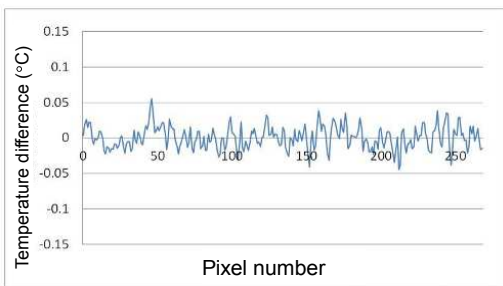(Daily range = 10°C: photographed at 0 a.m.)

20mm inner Cavity　30mm inner Cavity　40mm inner Cavity　60mm inner Cavity

20mm inner Cavity　30mm inner Cavity　40mm inner Cavity　60mm inner Cavity

a) Thermal image photographed by Camera A

b) Thermal image photographed by Camera B

Standard deviation = 0.034 °C

Standard deviation = 0.016 °C
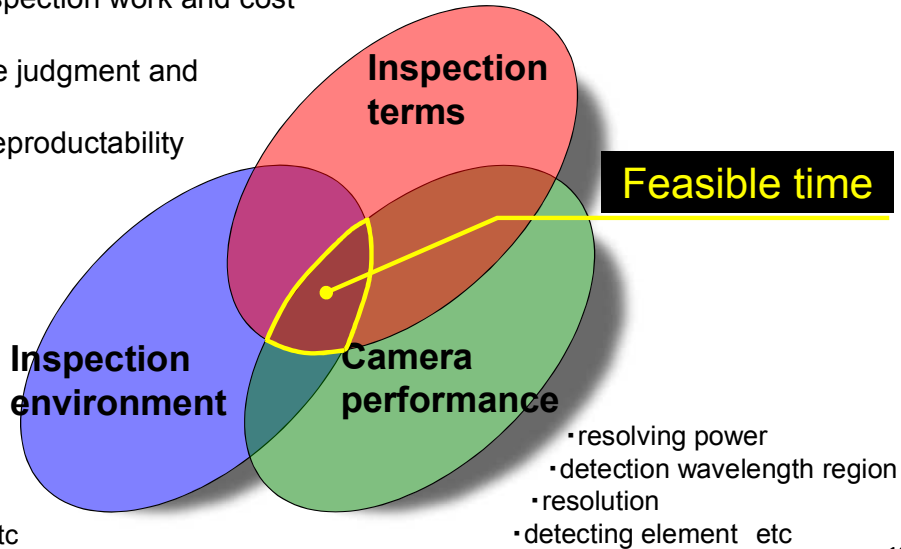
a) Temperature variation of Camera A

b) Temperature variation of Camera B

17

−19−

Issues for accurate infrared inspection

・clarification of inspection depth
・quality guarantee and prevention of missing damage
・high efficient inspection work and cost performance
・efficient damage judgment and objectivity
・recording and reproductability

・kind of bridge, part
・detection depth
・photographing distance etc

Inspection terms

Feasible time

Inspection environment

Camera performance

・daily range
・solar radiation
・wind and rain etc

・resolving power
・detection wavelength region
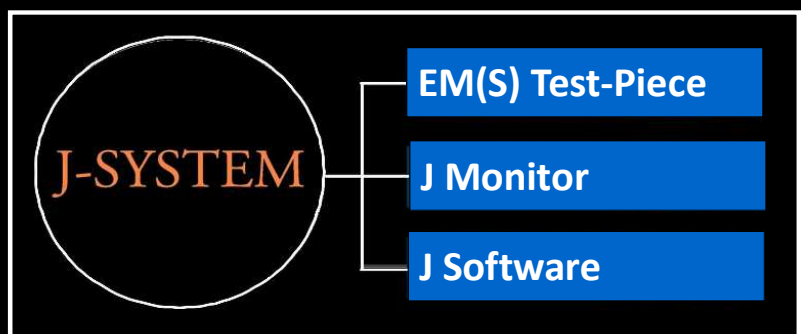・resolution
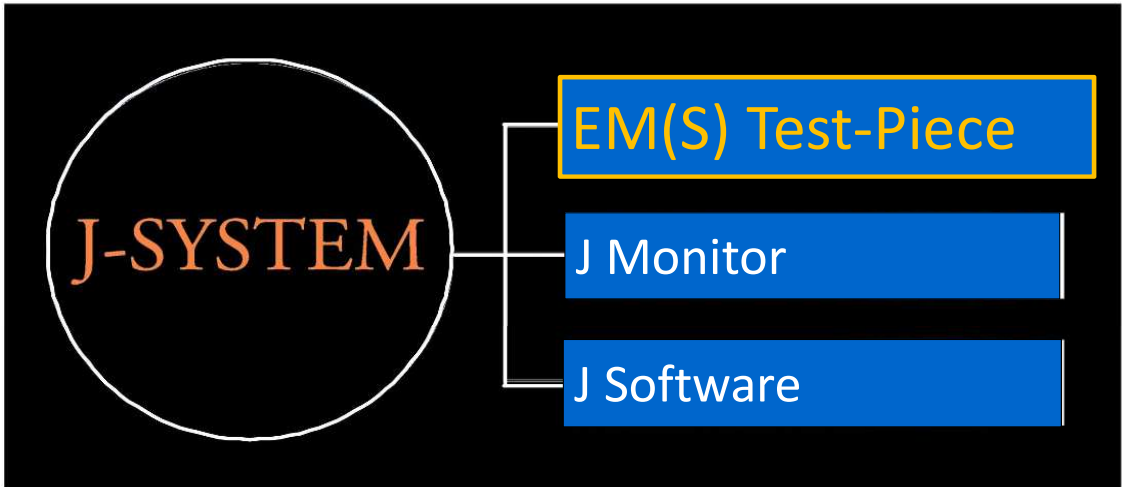・detecting element etc

18

J -SYSTEM

A new concrete inspection and assessment method with safer manipulating, higher performance, and lower cost based on infrared thermography technology.
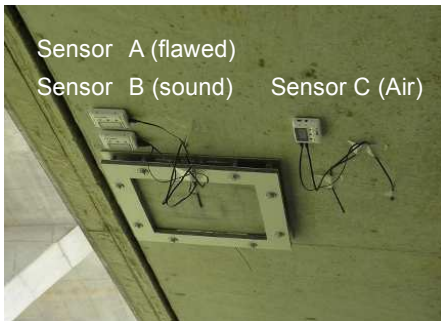
J-SYSTEM

- **EM(S) Test-Piece**
- **J Monitor**
- **J Software**

EM(S): On-the-spot Test Piece
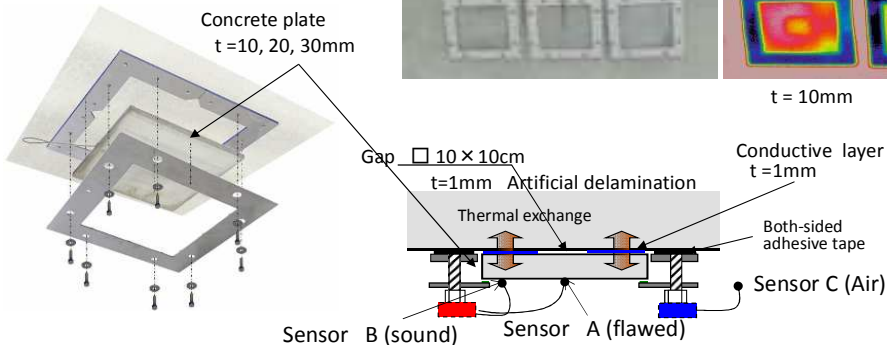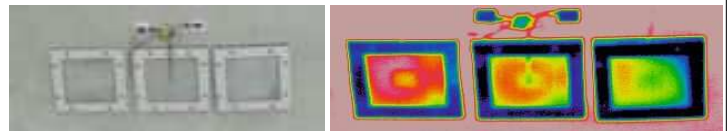

EM(S) Test-Piece

J Monitor

J Software

To ensure thermal condition of real structure for infrared testing before and during infrared inspection

20

EM(S) : On-the-spot Test-Piece

Sensor A (flawed)

Sensor B (sound)　Sensor C (Air)

To obtain real temperature data under actual conditions element by element

Gulf side

Ocean side

Concrete plate
t =10, 20, 30mm

t = 10mm　　20mm　　30mm

Gap　□ 10 × 10cm
t=1mm　Artificial delamination

Conductive layer
t =1mm

Thermal exchange

Both-sided
adhesive tape

Sensor C (Air)

Sensor B (sound)　Sensor A (flawed)
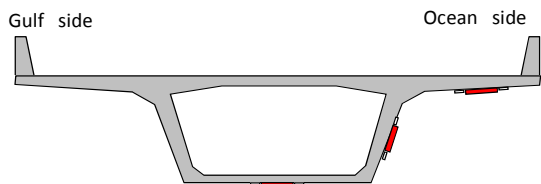
21

Do we inspect at a suitable time ?
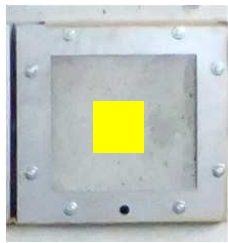
EM（S）

Checking central Void
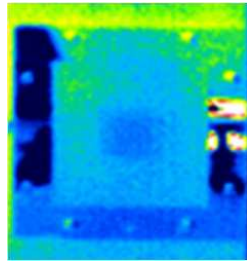
IR Image
Central cavity is observed.
→ OK

IR Image
Cavity is not observed.
→ NG

The thermal environment should be precisely obtained by an EM(S) device before any investigation

22

J Monitor：A Display for IR images in Real Time

J-SYSTEM

EM(S) Equipment

J Monitor

J Software
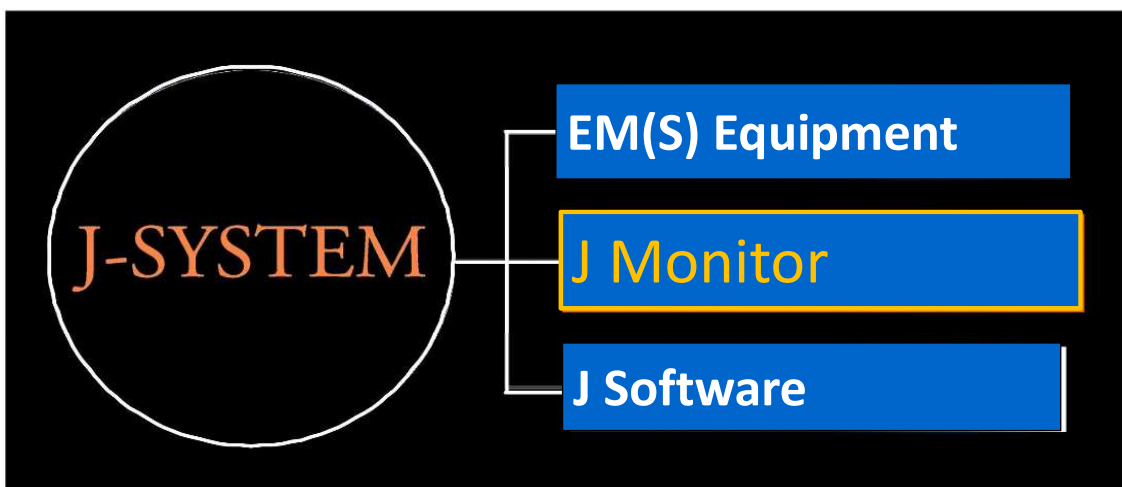
23

J Monitor, inspection situation

24

J Monitor

J **Monitor**

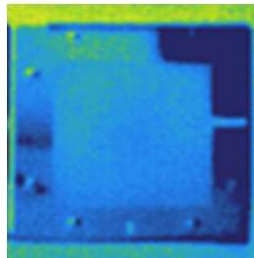IR Raw Image | IR Prosess Image
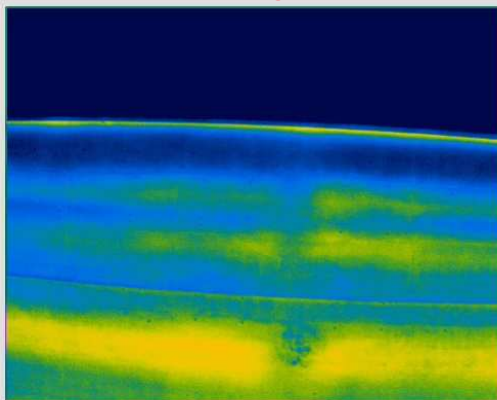
25

J Software: Infrared Image Processing Software

J-SYSTEM
- EM(S) Equipment
- J Monitor
- J Software
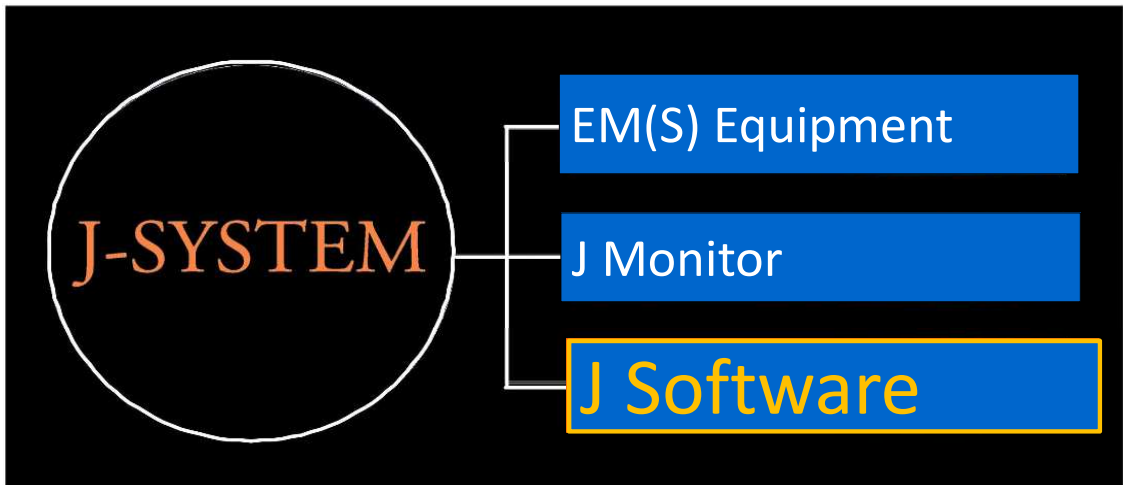
26

Image Emphasizing Thermal Anomalies

sunlight

delamination

thermal anomaly = 0.1℃

The thermal gradient of a structure is filtered to emphasize thermal anomalies.

Thermo-image

Filtered image

Rating image

foreign body

plastic (5cm)

hard to spot

easy to spot

temp.

around 5℃

thermal anomaly = 0.1℃

Thermal gradient of structure

27

−24−
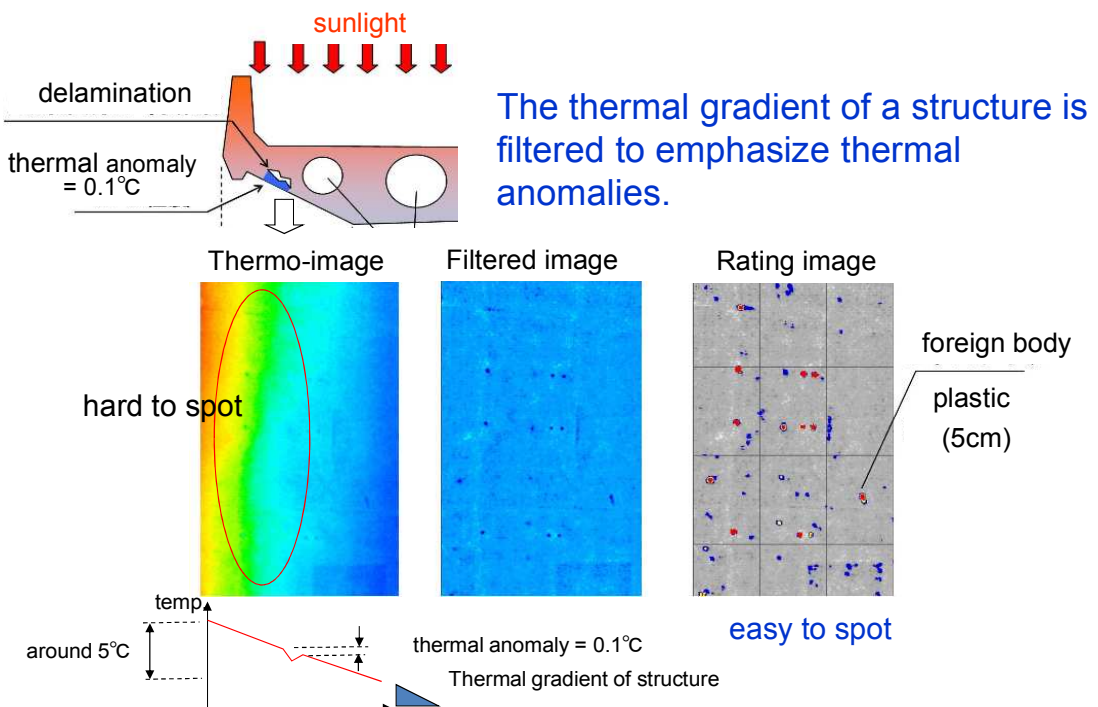
J Software: Damage Ratings

Temperature distribution is interpreted into damage ratings by using a comprehensive database of temperature patterns.

Visible image：EM(S) test-piece

1cm   2cm   3cm

IR raw image
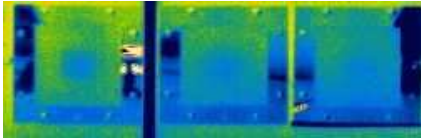
IR Process image
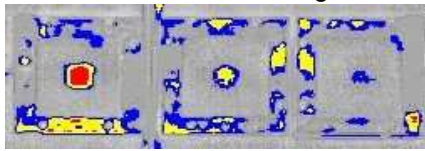
Damage level		
Damage pattern		indication
crack reinforcement Depth ≧ 4cm Concrete surface		Observation （Insignificant）
crack reinforcement Depth ≧ 2cm Concrete surface		Caution
reinforcement Reaching surface crack Concrete surface		Critical Emergency measures required

28

Comparison Between New and Conventional

29

Is it possible and easy to evaluate objectively?

observation (blue)
caution (yellow)
critical (red)
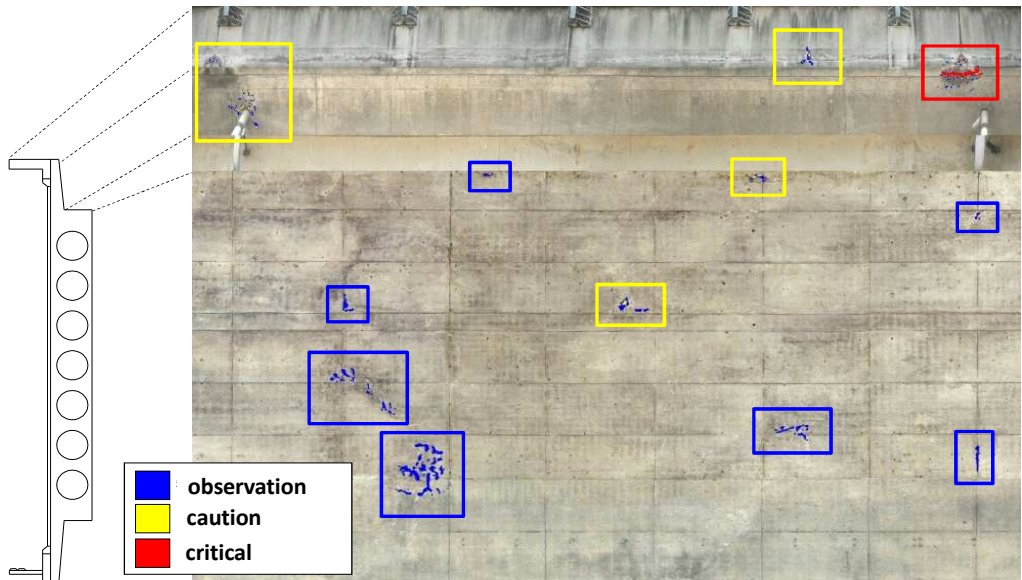
Your resources can be focused on the areas that need the most work.

30

Overpass slab without crushing inspection robot （RABIT™）development

- This robot is included of Impact Echo, Electrical resistivityh, Ultrasonic surface wave, GPR, High-definition imaging, GPS
- At first, it is decided to use it to 24 bridges in states at Northeast are in USA. In the next 5 years targeted to use it at 1,000 bridges
- Company to manufacture and sales RABIT™ was established.
- Currently, in addition 5 units are in production.

31

Proposal for RABIT™（December 2013 ）
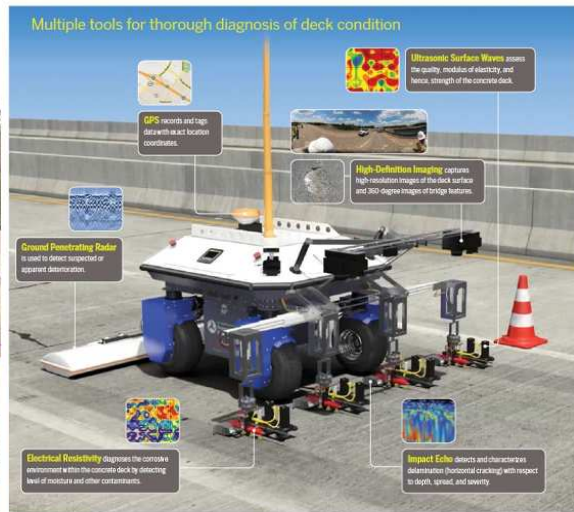
Overpass slab without crushing inspection robot was developed by Federal Highway Administration (FHWA) and Rutgers University

32

Accuracy verification by RUTGERS University

Verification at Test Room

Bridge model at Rutgers University
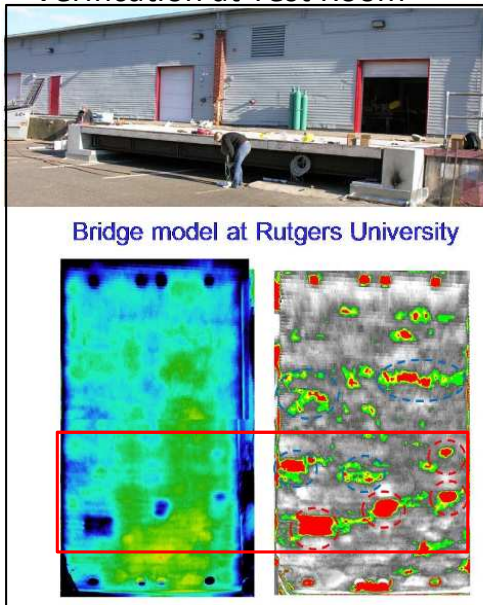
Verification at actual bridge

Tunnel (South-West)
IR raw image

Bridge in Bloomsbury, NJ

Processed image at delaminated area

Conducted on 04/17/2014, 8 -11 pm
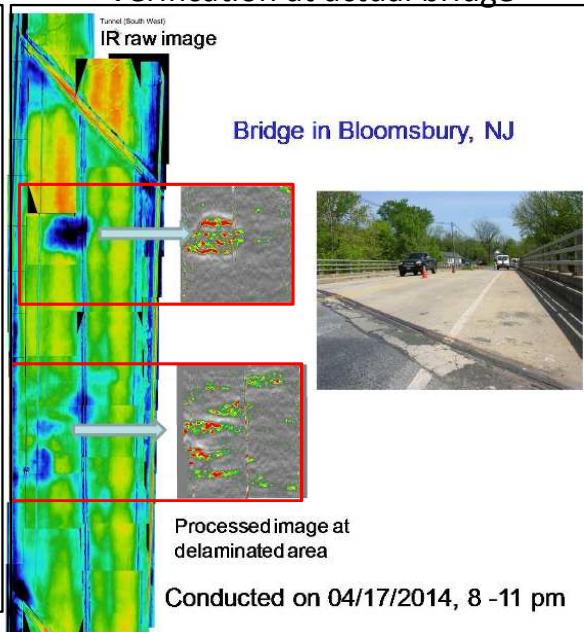
33

J-System Features

Proper investigable time can be assessed.

Damage depth can be obtained in real time

Absolute quality assurance
& Oversight prevention

"J-System" supports investigations conducted by customers

34

Current of Issues (improvement)①

【Improvement】
Further accuracy improvement of identified and analyzed damage by J-System

【Current issues】
Clearing noise (filtering) on the image after analysis by J-System

35

Features analyzed image by results of hammering sound

removal or flaking	Cavity	Slag	Foreign substances	Normal
Surrounding form is complexity, Red is out of center.	Surrounding form is smooth, Red is in the center.	Form is long thin, surrounding form is complexity.	Form is square, Red occupancy is high.	Yellow occupancy is high, Red's barycenter is in the midst.

36

Extraction of feature amount on analyzed image

Thermal image

Analyzed image

Area of Red (scale -up）

R:幅

R:高さ

重心位置（x,y）　　　　周囲長

矩形高さ

面積

矩形幅

Concept figure of analyzed image

×　面積　　　×　周囲長

Feature amount
Area（s）＝Σ ×
Boundary length（L）＝Σ ×
Complexity（c)=L/S
Degree of circularity（c_L）＝4πS／L^2

37

Increasing prediction accuracy （reclassification)

Thermal pictures detection

- Spalling   13%
- Delamination 18%
- Efflorescence   6%
- Sound   58%
- Other materials 4%

- Repair marks 8%
- Free lime 17%
- Color unevenness 33%
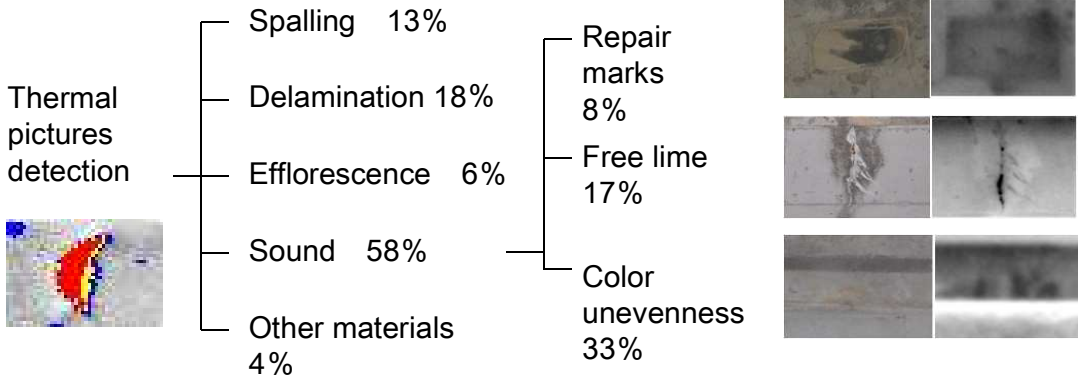
60% of sound parts

Redistribution of sound parts = repair marks, free lime, and color unevenness

Examining algorism of classifying 7 categories

Utilizing thermal pictures textures

38

Situations of thermal pictures textures

Thermal recording of foreign substances

Surface adhesion

Efflorescence
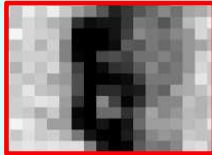
Free Lime
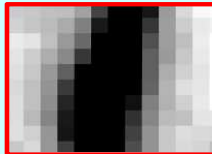
Lacing

Repair Marks

Foreign substance lacing

Measuring thermal movement through detection

Sound （color unevenness）

Spalling Area

Delamination Area
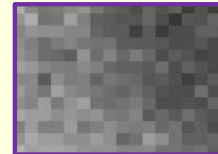
With contrast （even ）

Local contrast

With contrast （uneven ）

39

Texture Analysis by Gray-Level Co-occurrence Matrix

Texture Analysis by GLCM
（GLCM：Gray-Level Co-occurrence Matrix）

Method of inspecting colorful density location
of remote two-pixel pair at certain area

Computing GLCM

Computing 14 different
character values

Effective character value for
evaluating damage level

40

Texture Analysis by GLCM

G L C M
(Probability Matrix)

Probability P. δ (i, j) where a
relative pixel's density is j at a
distance δ= (r ,θ) from a
subject pixel density i

Movement σ

Distance
r

Relative pixel
(density, j)

θ

Subject pixel
(density i)

1	2	0	3
1	2	2	3
2	0	3	2
1	3	0	2

$$P_{\delta} = \begin{array}{c} \\ 0 \\ 1 \\ 2 \\ i\downarrow \quad 3 \end{array} \begin{array}{cccc} 0 & 1 & 2 & 3 \\ \left[\begin{array}{cccc} 0 & 0 & 1 & 2 \\ 0 & 0 & 2 & 1 \\ 2 & 0 & 1 & 1 \\ 1 & 0 & 1 & 0 \end{array}\right] \end{array} \rightarrow j$$

$(r, \theta) = (1, 0°)$
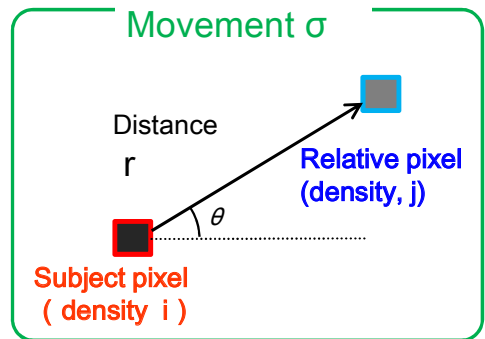
Enlarged thermal picture

Converting the probability of movement
appearance frequency

41

Character value arising from GLCM①

- Multiple Comparison Result

Sum of square (y-axis: 0–80)
ノロ / 異物混入 ※ / 健全 ※ / 剥離 / 浮き / 補修跡 / 遊離石灰

Sum Average (y-axis: 0–40)
ノロ / 異物混入 / 健全 / 剥離 ※ / 浮き / 補修跡 / 遊離石灰

Sum Variance (y-axis: 0–300)
ノロ / 異物混入 ※ / 健全 ※ / 剥離 / 浮き / 補修跡 / 遊離石灰

Contrast (y-axis: 0–100)
ノロ / 異物混入 / 健全 ※ / 剥離 / 浮き ※ / 補修跡 / 遊離石灰

※：Under5%
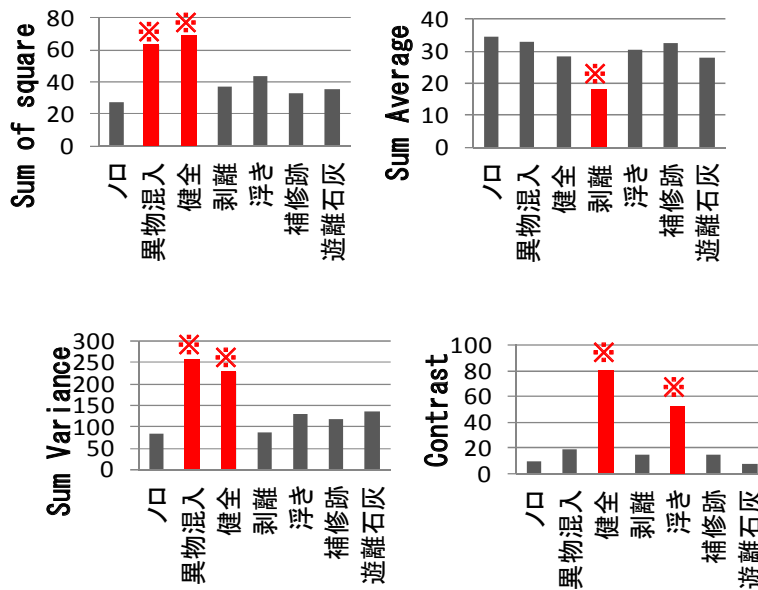
42

Character value arising from GLCM②

	Character value	Significance probability
1	Angular Second Moment	0.405
2	Contrast	0.000 ※※
3	Correlation	0.108
4	Sum of Square:variance	0.000 ※※
5	Inverse Difference Moment	0.109
6	Sum Average	0.000 ※※
7	Sum Variance	0.000 ※※
8	Sum Entropy	0.140
9	Entropy	0.374
10	Difference Variance	0.160
11	Difference Entropy	0.135
12	Information Measure of Correlation1	0.045 ※
13	Information Measure of Correlation2	0.871
14	Maximal Correlation Coefficient	0.621

43

Further improvement

【Form for wanting to be removed by filtering】
Remove "flicker", still exiting through restriction of inspection term
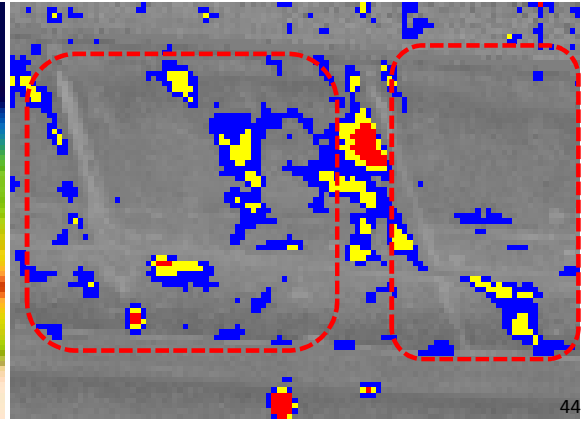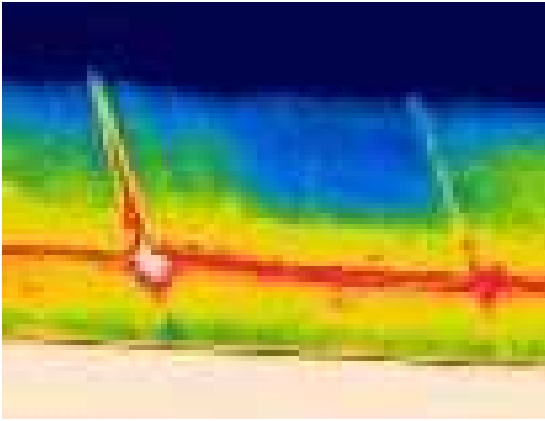
44

Tunnel Inspection

45

Background

Conventional visible inspection adds damage conditions of tunnel linings concrete , such as flaking concrete to be caused critical accident, adopted camera technical and developed vehicle to inspect higher accurate

46

Flow chart for tunnel inspection

Ⅰ. The captured image of the tunnel

Ⅱ. Creating an image of the tunnel

Ⅲ. Analyzing

Ⅳ. Inspection

47

Investigation of cracking and other damages

➢ The width, length, and number of cracks, efflorescence, and water leakage can be investigated with high precision.
➢ Color images allow the inspection of corrosion and damage to the accessories attached to the tunnel lining.
➢ High-precision photography/analysis enables a comparison between the previous investigation and the current damage progress.

48

Visual image（ tunnel ）
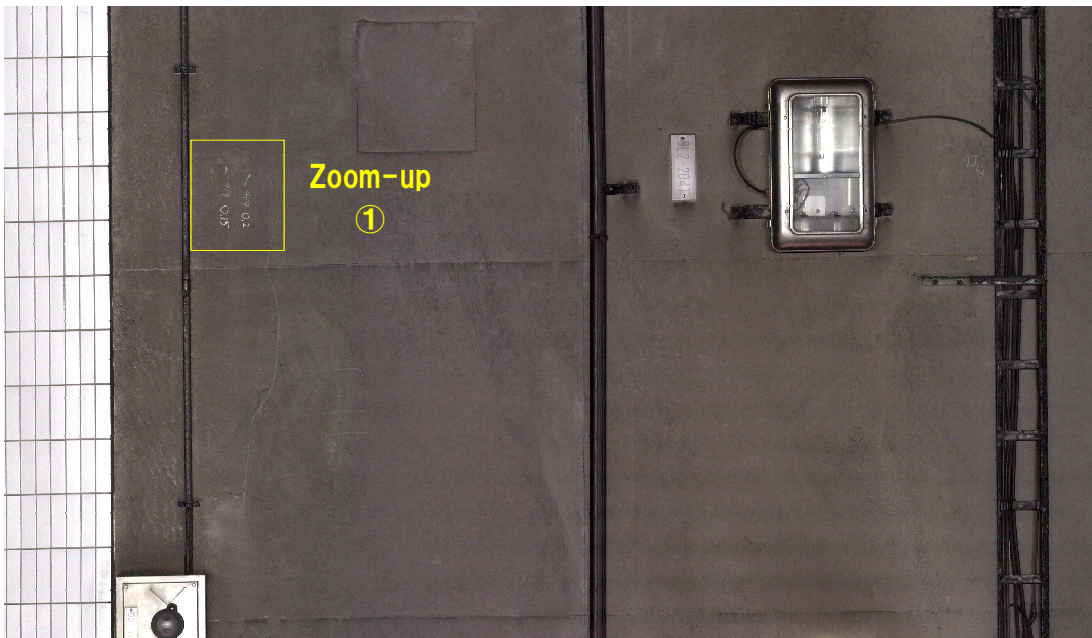
Zoom-up
①

49

Zoom-up visual image（Cracks ）
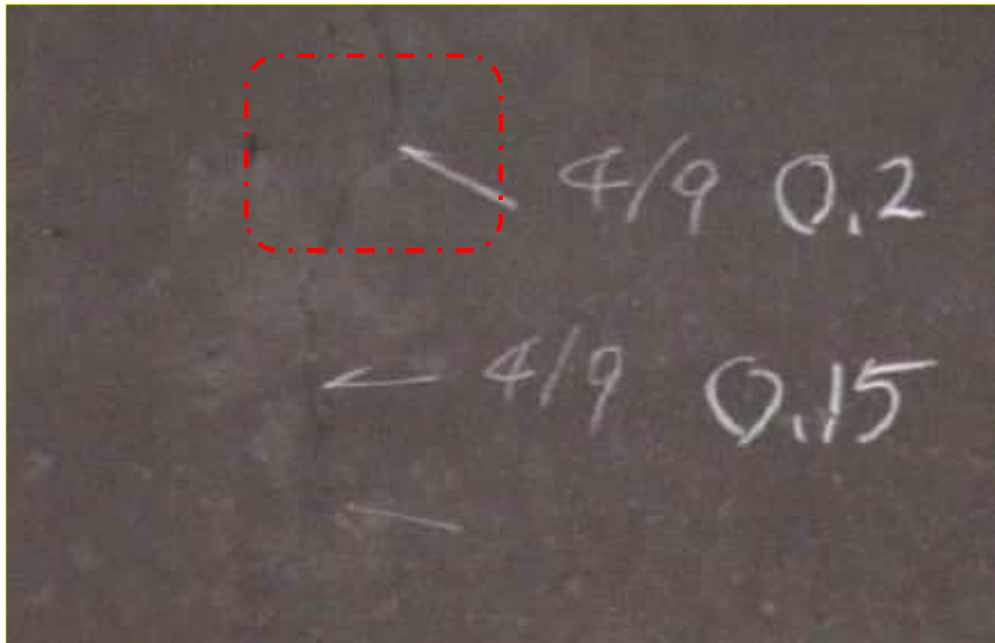
50

Further improvement

Tunnel lining concrete which is plain concrete causes concrete flaking accidents.
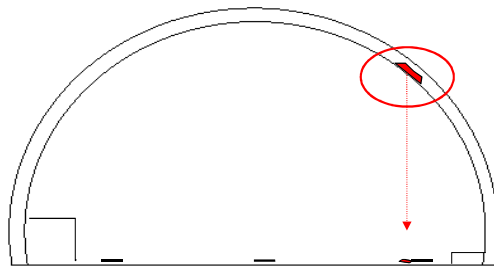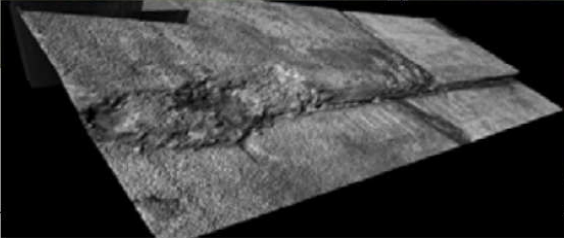
Surface status（visual image)
　　　　　　& surface profiling (height data）
⇒Need method for predicting flaking
　（Theory from deterioration to flaking）

51

Approach for identifying hazardous areas

Infrared can not be used（TN）→ We need a new approach！

Current problems	New technique
No judgeing by the front of image whether the crack may be falling or not	Detecting flaking point by obtaining height data of tunnel lining surface.

52

Smart EAGLE type-T(Tunnel) Completion

vehicle speed of 65km/h （H29）

Now, Trying at 80 to 100 km / h

53

Measuring unit

B）Surface profiling unit   A）Visual image unit
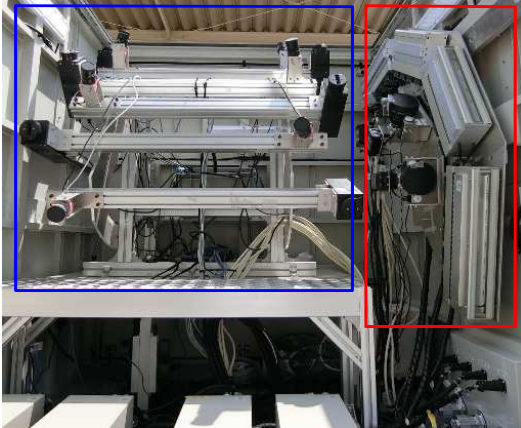
PC & Monitor

A）Visible image

Cracking evaluation

B）Surface profiling

（height data）

**Extract dangerous spots
from concrete surface
profiling**

スリットレーザーを
トンネル軸に直行して
ＴＮ覆工面に照射

進行方向
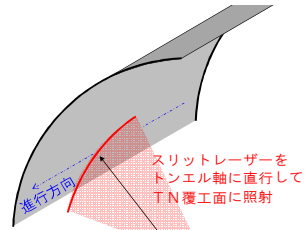
エリアカメラで斜めから
レーザーを撮影して
覆工面の形状を計測

54

Measurement of tunnel conditions by height data

Damage of inside
tunnel for verification
(photo-shooting by
digital camera)

Visual Image   Height Image

55
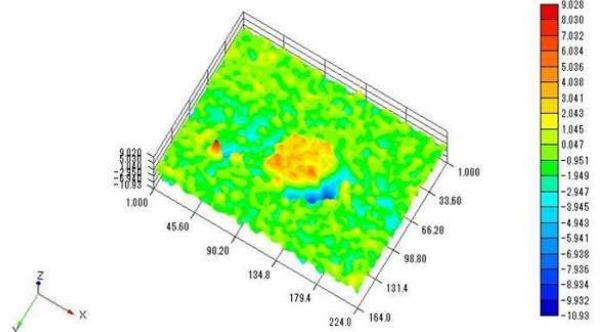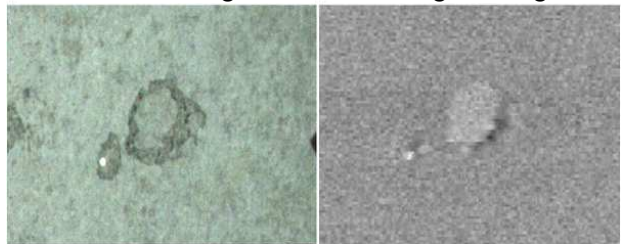
Overview of proposed measuring technology ②

① Visual image

0.5mm   1.0mm   1.7mm   2.3mm   5.6mm

Simulation step thickness

② Height image

Simulation step thickness

0.5mm   1.0mm   1.7mm   2.3mm   5.6mm

③ Process image

Simulation step thickness

0.5mm   1.0mm   1.7mm   2.3mm   5.6mm
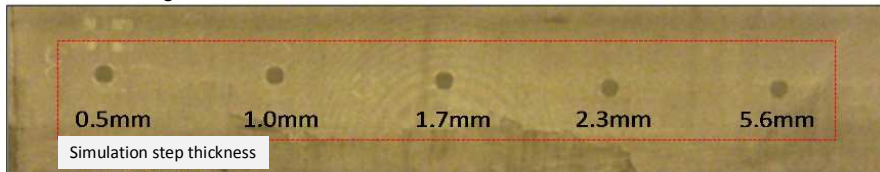
Simulate gap

□100×100mm

Thickness 0.5～5.6㎜

凡 例

-0.3
-1.1
-2.0
-2.8
-3.6
-4.5
-5.3
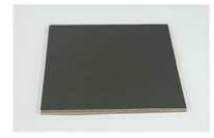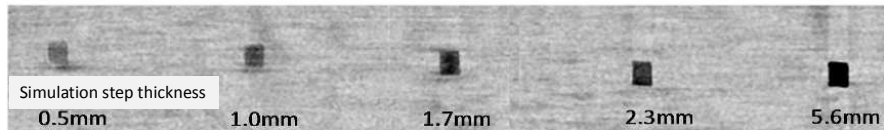
Black
=Large gap
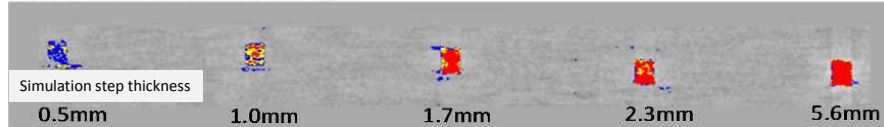
observation

caution

critical

56

Height measurement result of actual tunnel

【Visual image】　　　　　　【Height image】
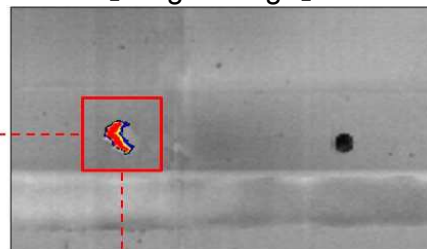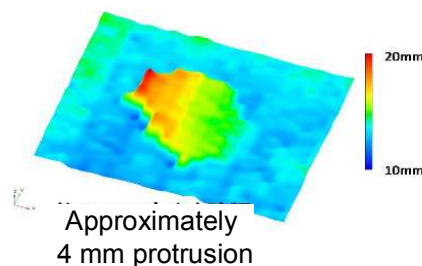
【3D image】　　　　　【Zoom-up photo of changes after inspection 】

Approximately
4 mm protrusion

20mm

10mm

Remove repair
section of filled
trace （50mm
× 50mm）

57

Extraction of damaged points
（Calculation of shape feature amount ）

・"Shape feature amount" is calculated for each area of red, yellow, and blue which is determined by setting a threshold value as emphasis index

■Processed image

Colored part: convex part

Feature amount extraction in white frame

W

H
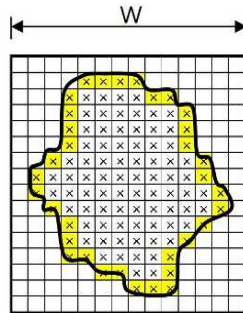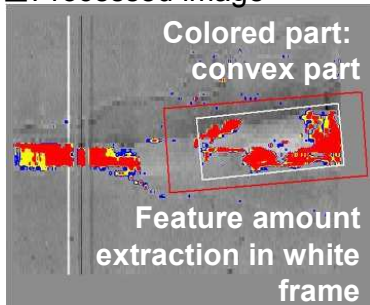
① Boundary length(L)
② Area(S)
③ Occupancy (O)
④ Complexity (C)
⑤ Degree of Circularity (CC)

(S) = number of "X"
(O) = S/(H*W)
(C) = L/S
(CC) = $4\pi S/L^2$

☐ Boundary length(L)

【Threshold setting image】

Surface shape

2.2mm or more

1.8 mm or more and less than 2.2 mm

1.4 mm or more and less than 1.8 mm
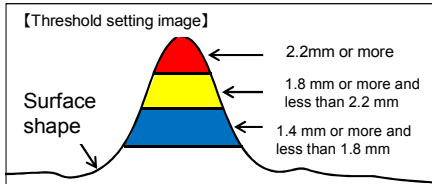
※shape feature amount
⇒Numerical representation of items ①〜⑤ of unique shape change areas

58

Extraction of damaged points
（ Prediction method of damage type ）

Feature amount to use for variables of formula	Construction of prediction model	Answer to the formula （ Result of hammering ）

【 Independent variable 】

◎ Feature amount
・Length
・Area
・Occupancy
・Complexity
・Circularity

◎ Feature amount by texture analysis （14types）

・Dispersion
・Total
・Distributed total
・Contrast
  ・
  ・

【 Multivariate analysis 】

↓Various models

◎Neural network
・Logistic regression analysis
・Discrimination analysis
・Decision tree analysis
      ：

Analysis is performed with multiple multivariate analysis models and select model with high correlation.

Adopt analysis result by neural network

【 Dependent variable 】

Result of hammering N=149

Damage Float
         Separation
         Sheet peeling
         Rock pocket

Sound protrusion
         Sound
         Step
         Repair mark
         Free lime
         Contamination

59

（Prediction method of damage type）

Analysis result

Area of hammering：5,900㎡

149points where unique shapes were detected

			Analysis (estimation) result										
			Damage				Inspection	Sound					total
			Float	Separation	Sheet peeling	Rock pocket	Protrusion	Sound	Step	Repair mark	Free lime	Contamination	
tapping result	Damage	Float	36	1			1						38
		Separation		4									4
		Sheet peeling			8								8
		Rock pocket				1							1
	Sound	Protrusion					30						30
		Sound	1				2	41			1		45
		Step							17				17
		Repair mark								1			1
		Free lime									3		3
		Contamination										2	2
	total		37	5	8	1	33	41	17	1	4	2	149

Damage points :51

Screening points: 84

Oversight is 0（ 84 points of hammering inspection)

60

Prospect of tunnel inspection

Height measurement is effective as screening technology of hammering !

1）Current tunnel lining image shooting ⇒
    tunnel lining shooting ＋ Height measurement

2）Detailed inspection ・all hammering ⇒
    Hammering at only the screening points

⇒It is also possible to increase the frequency of detailed inspection with only hammering at screening points.

61

Pavement Inspection

Inspection Methods

Daily Inspection (Behind the wheel)

Detailed Inspection   pavement investigation

《Our product》

Control Item

■ Maintenance Target Values of Pavement

Rutting (mm)	Difference in Level（mm）		Coefficient of Sliding Friction （μV）	Flatness IRI（mm/m）	Cracking Ratio （%）
	Bridge Mounting	Crossing Structure Mounting			
25	20	30	0.25	3.5	20

■ Cracks Evaluation（Conceptual Diagram）

《Legend》 ——— : Cracks ⌐ ¬ :Crack Measurement

One Lane

Evaluation Unit：100m
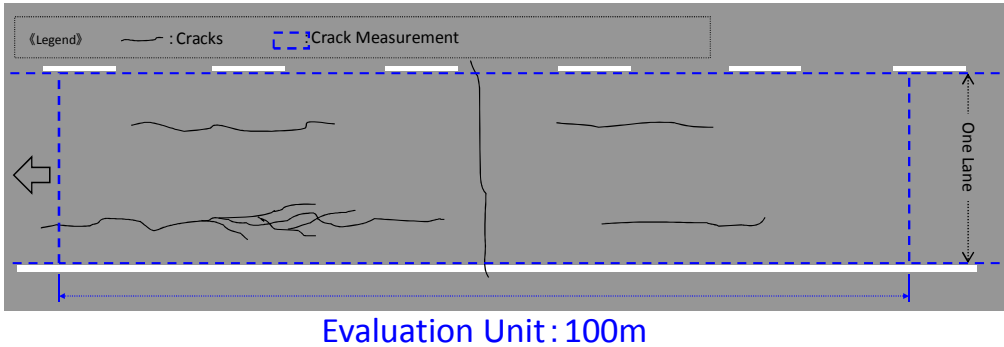
64

Data Acquisition by Periodic Inspection

Road Surface Measurement（3 Elements）

Company-owned vehicle

Cracks　　　**Ruts**　　　**Flatness**

65

L&L System

Visual image

Camera

Direction of movement

Line Sensor

Illumination area
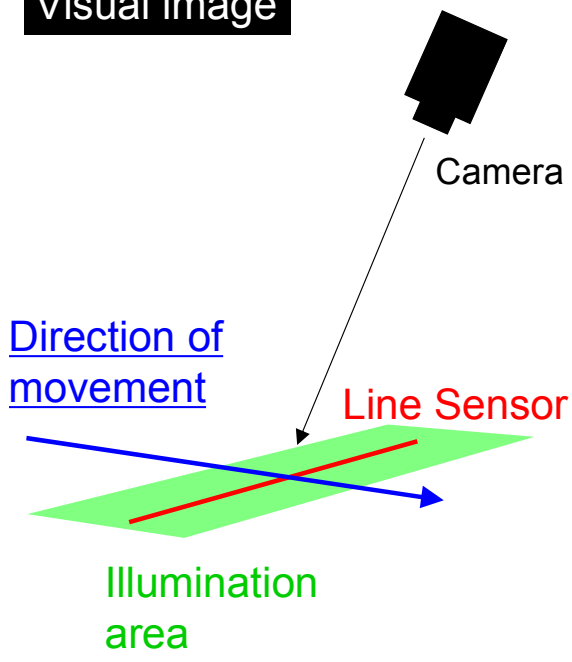
Height image | Width profile

Camera

Slit Laser

photographed with an area camera by a slant

The slit laser is situated in directions **perpendicular.**

66
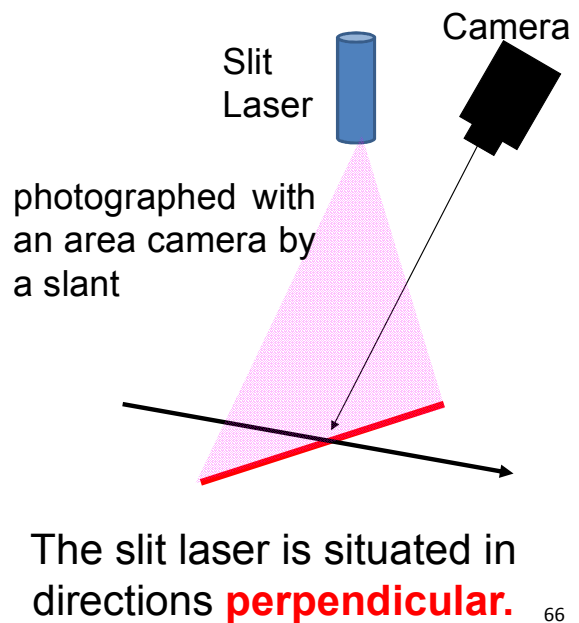
Certified in the performance confirmation test in FY2018

■Examination date
May 22, 23, 24, 2018

■Testing place
The testing track of the National Institute for Land and Infrastructure Management, and others

■Performance confirmation result (**Pass**)
"Performance Confirmation Certificate No.3027"

Test items	Assessment scope	Time	Result
Accuracy of distance measurement	The vehicle obtains accuracy within +/− 5% accuracy for of the value measured by an optical measuring device.	Night	Pass
Accuracy of cracking measurement	The vehicle obtains accuracy capable of identifying cracking with width of 1mm or greater.	Night	Pass
Accuracy of rutting measurement	The vehicle obtains accuracy within +/− 3 mm of the rut depth measured by a cross-section profile meter.	Night	Pass
Accuracy of flatness measurement	The vehicle obtains accuracy within +/− 30% of the standard deviation value measured by a longitudinal profile meter.	Night	Pass

67

Movie

68

Visual image（ pavement ）

Accuracy at a speed of 100km/h
～Detecting cracks～
Shooting width=4.5m(Color image)
Resolution 0.8mm x 0.8mm/pixel

69

Calculation of cracking ratio

Aerial view taken by the Line Scanning Camera

Semi-automatic identification of cracking damage   develop
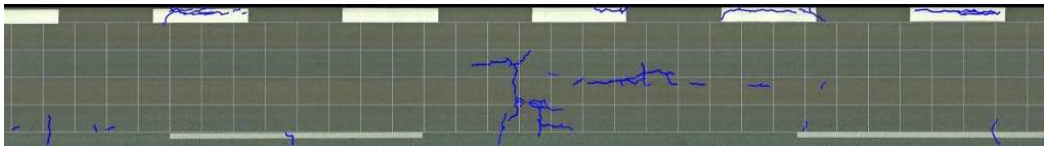
Fully-automatic line/surface Analysis (Accuracy rate is 99%)

70

Height image

Surface height image

3.0m

4.0m
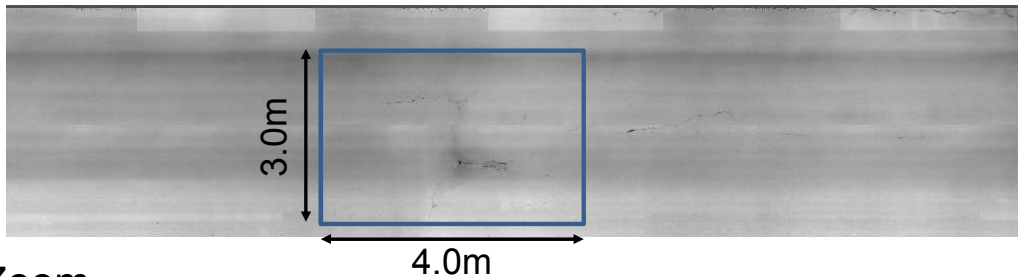
Zoom
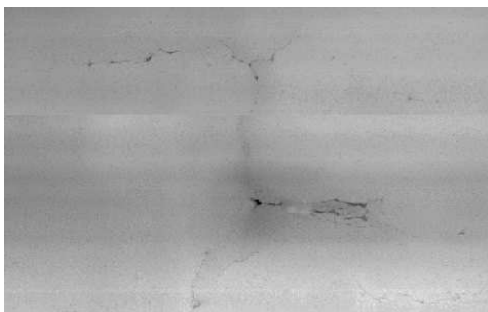
Accuracy at a speed of 100km/h
～Rutting Measurement～
Shooting width=4.4m
Dimension of rutting:1mm or less
Resolution 1.27mm(Transversal)
           2.70mm (Longitudinal)
           0.50mm (Depth)

71

Ruts

Height image (Black part is low.)

Cracking
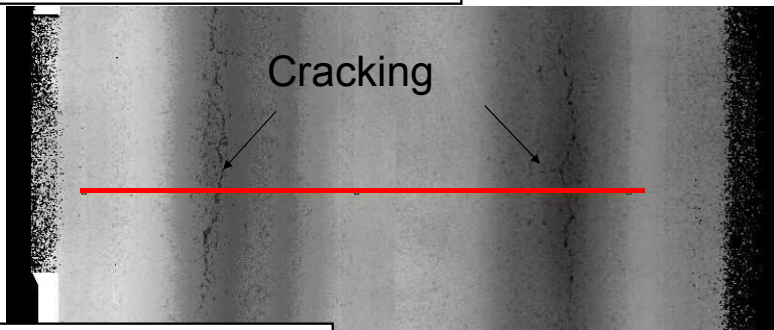
Ruts on the red line above

Cracking

Cracking

72
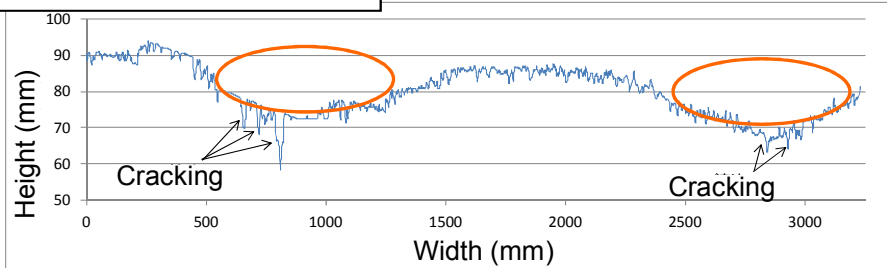
Flatness (Longitudinal profiling)

High-resolution allows us to accurately profile the longitudinal shape of a <u>microscopic</u> bump.

1st measurement
2nd measurement
3rd measurement
Level measurement

Bump

Bump

Gap5mm

Gap12mm

Scale 10mm

Driving direction

Simulated
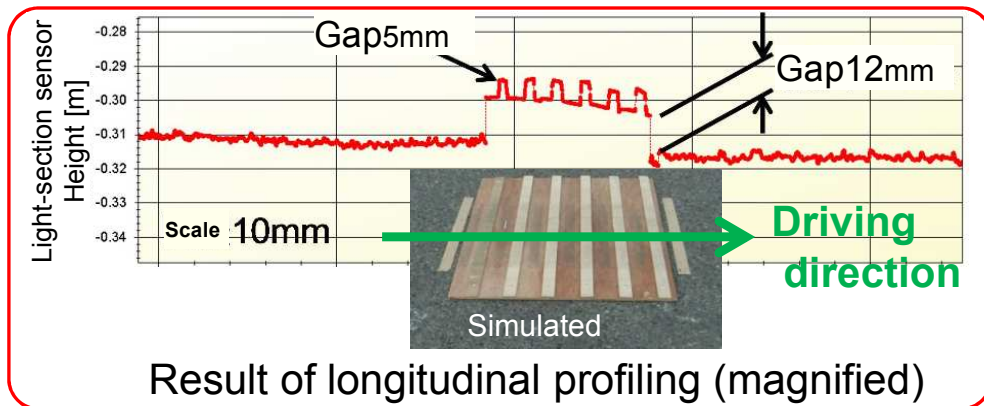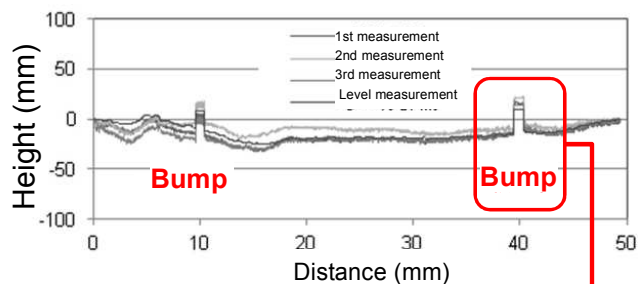
Result of longitudinal profiling (magnified)

73

Analyzing highly accurate longitudinal profile

74

Analyzing highly accurate longitudinal profile

Visual image

Surface height image

Manhole Cover profile area
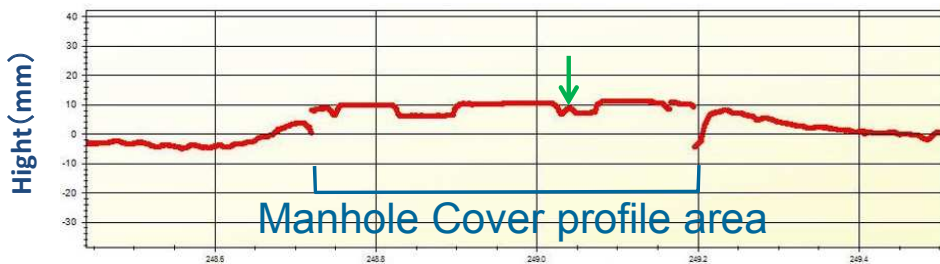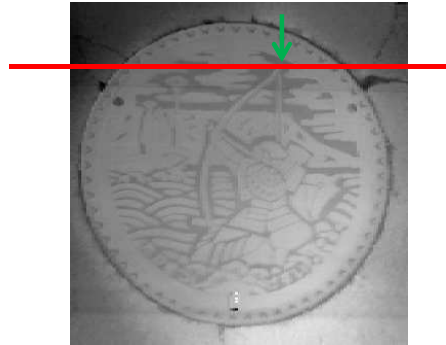
75

Analyzing highly accurate longitudinal profile

Future: IRI can be measured thanks to no speed dependanc
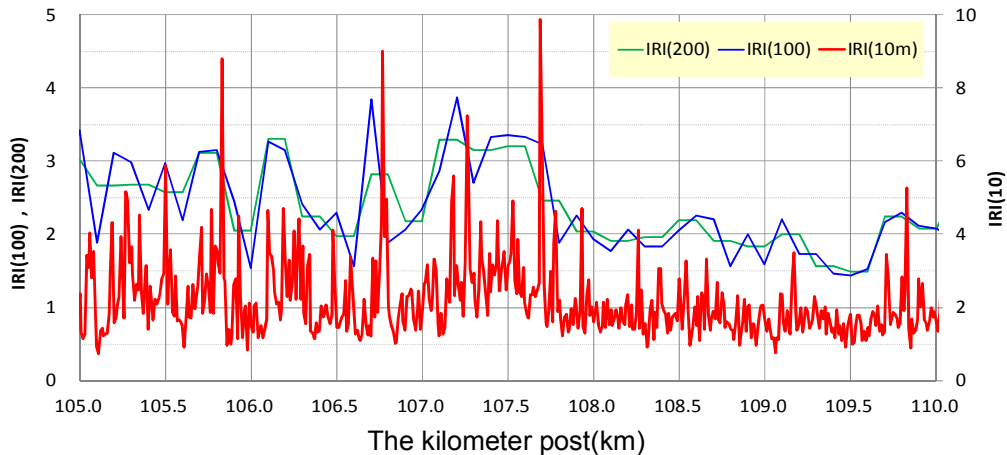
Developmental event of pothole on Porous asphalt pavement

Done to review the objective of preventive maintenance
➢Proposal new evaluation indicator to apply for Porous asphalt pavement
➢Proposal method of predicting of occurrence of pot hole

Data from periodic measurement

Visual image

| Oct. 2013 | Nov. 2013 | Dec. 2013 | Jan. 2014 |

Data from periodic measurement

Height image
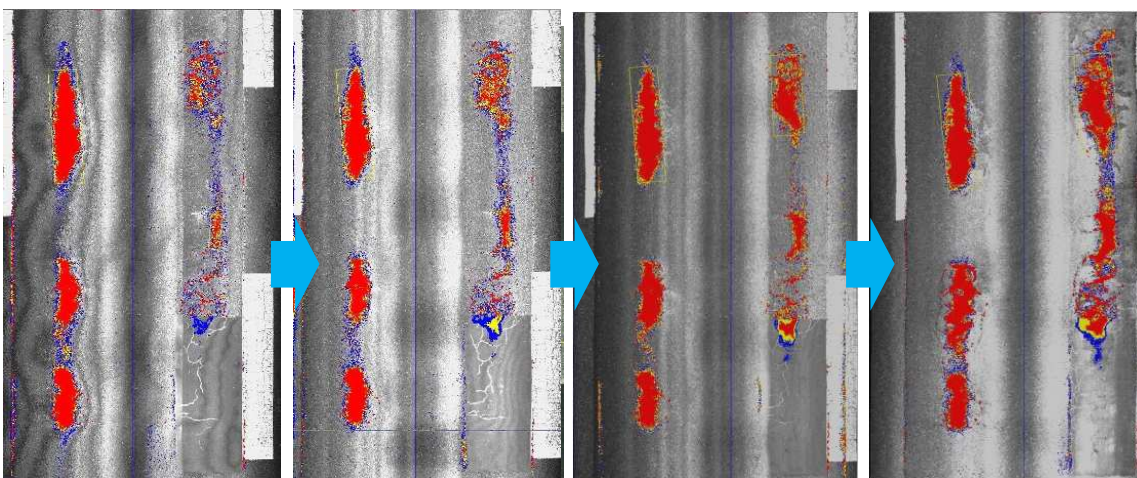
| Oct. 2013 | Nov. 2013 | Dec. 2013 | Jan. 2014 |

Proposal of a new evaluation indicator

(1) Area where the overall depth of the rut is high

Red: Shape of the rut at the objective point
Blue: Representative shape of the rut

Lane marking **Depth of local subsidence** Lane marking

The depth of the rut is high, but that of local subsidence is low.
⇒ Low risk of pothole occurrence

(2) Area where the overall depth of the rut is low

Depth of local subsidence

The depth of the rut is low, but that of local subsidence is high.
⇒ Potential risk of pothole occurrence ⇒ Dangerous
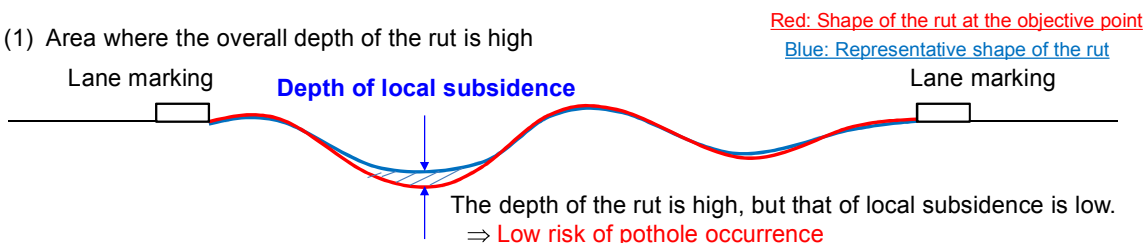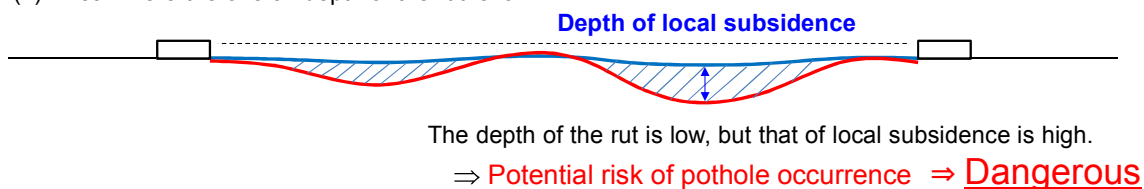
Proposal method [Evaluation based on the depth of local subsidence]

The relative depth of local subsidence is calculated as the depth of local subsidence by calculating the difference between the rut depth of the objective point and the representative rut depth which is the central value of the maximum rut depth in a vicinity of 10m.

80

Proposal of a new evaluation method (Aggregate scattering) (1)

■Current issues

Due to the spread of Porous asphalt-related road surfaces, problems caused by aggregate scattering have increased.

(1) Less noise reduction functionality

(2) Less driving safety and comfort

⇒ A quantitative evaluation method has not been established.
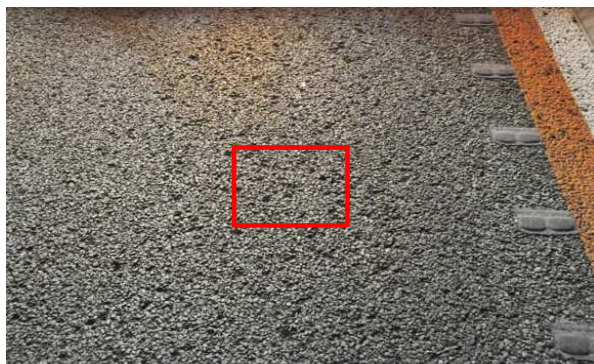
81

Proposal of a new evaluation method (Aggregate scattering) (2)
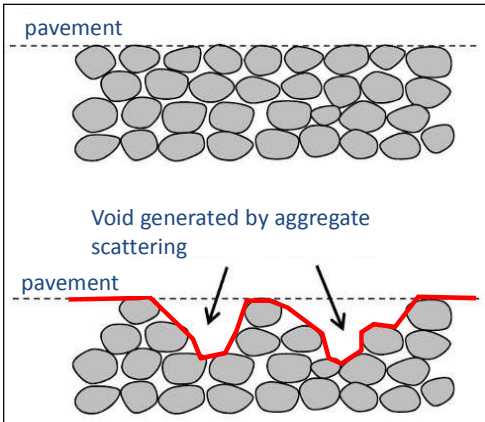
Image of aggregate scattering

3D shape measurement by Light-Section Method allows us to measure the form of a pavement with high precision.

We focus on the relationship between aggregate scattering and mean profile depth (MPD).

Dents

Dents

a) Visible image

b) Height image

Height (mm)

1.6

−13.3

82
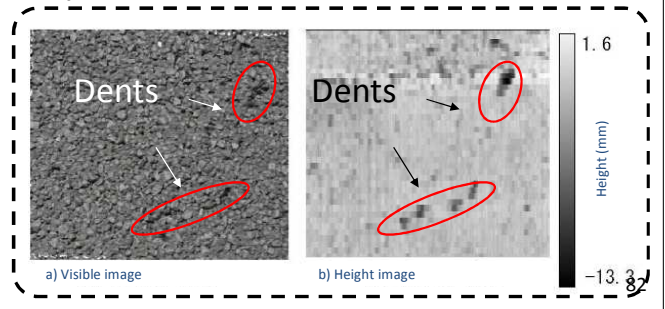
Superficial (MPD) quantitative evaluation of aggregate scattering
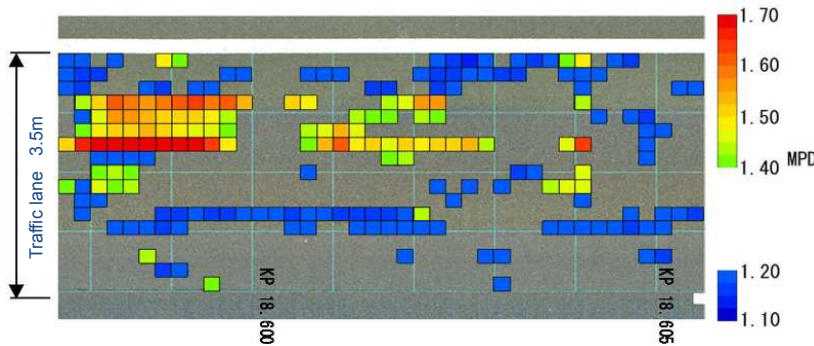
Traffic lane 3.5m

KP 18.600

KP 18.606

Warm color: Large MPD
⇒Large quantity of aggregate scattering is observed.

Cool color: Small MPD
⇒A place which will likely be clogged.
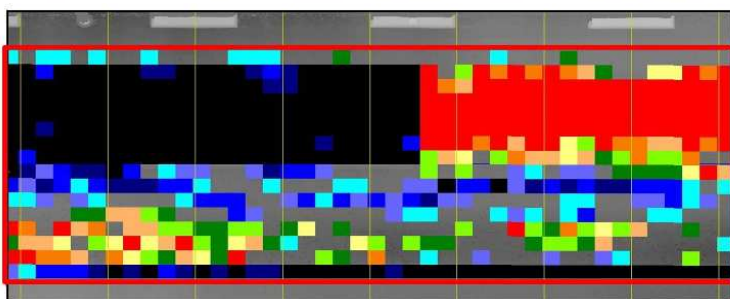
Large MPD

Small MPD

83

High risk event

Pot-hole
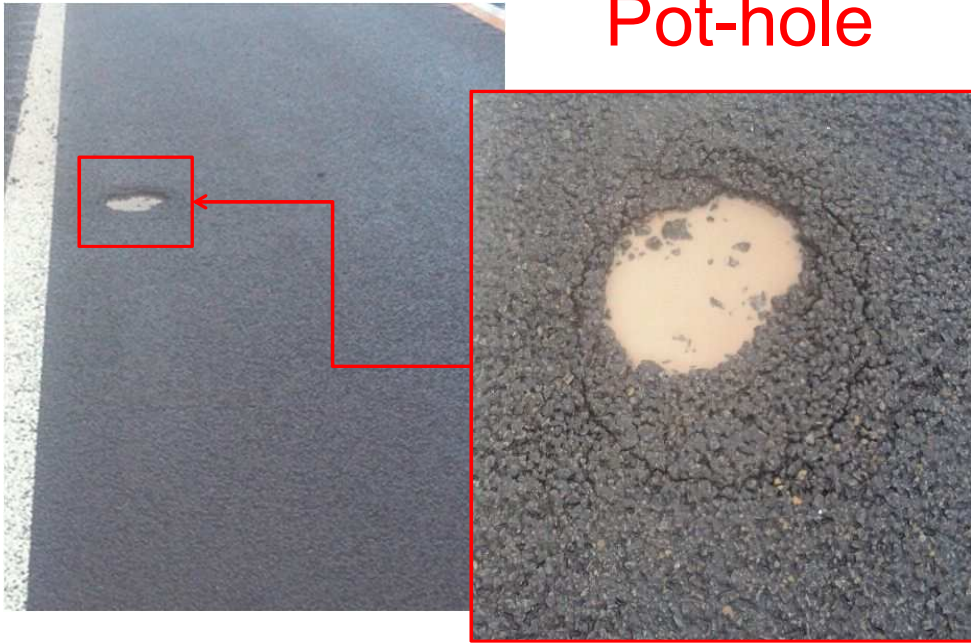
84

Pot hole repair method

Pothole

Repair work

Cold ashalt mixture

Compacting machine

85

Current status of road surface management

①Surface inspection

Inspection frequency
**Once every 3 years
(Shikoku-area)**

② Daily check（ On-board inspection ）

Inspection frequency
5days/2weeks
（According to traffic volume ）

【Current status】Discover pothole by daily inspection
→ Emergency treatment ⇒ **Post-maintenance**

86

Smart EAGLE type-P(Pavement) Completion

Crack, Rut, GPS

IRI
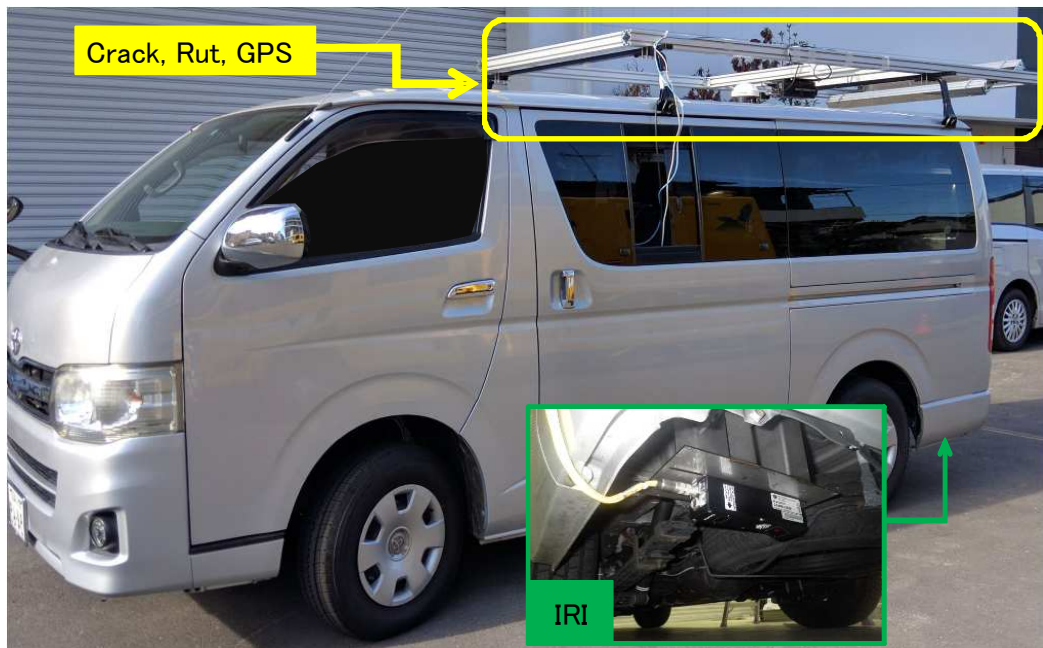
87

Proposal of Simple Road Survey Method by Smart Eagle

Characteristic

・Production cost is low

（Measuring equipment of road surface shape ×1set, IRI- equipment ×1set, GPS）

- Fully automated analysis by simplified method, so analyzing cost is low
- Grasp damaged points beforehand by increasing frequency

laser×1
3D-camera×1

Get velocity from vehicle speed pulse

GPS-unit×1

gyro×1, Light cutting unit×1

88
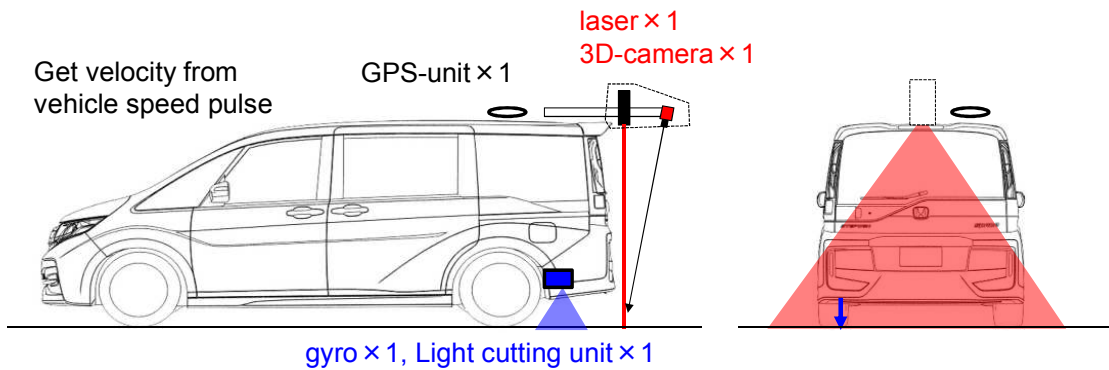
Proposal of Simple Road Inspection Method by Smart Eagle

Smart Eagle Evaluation index that automatic analysis possible

Evaluation index	Analysis value of this system
Crack ratio	Crack ratio by simplified method
Ruts amount	Test method manual・NEXCO-Test method compliance
IRI	Evaluation length can be set arbitrarily
Depth of local subsidence	Depth of local subsidence against the representative ruts
MPD	The Value calculated MPD from transverse shape data in a plane

Prediction of pothole occurrence
Evaluation index focused on this time
⇒ **Depth of local subsidence & MPD**

89

Proposal on operation method of road surface management by Smart Eagle ①

Vehicle equipped with Smart Eagle
（In the future to be installed in daily inspection vehicles）

Measurement data

Provide aging information
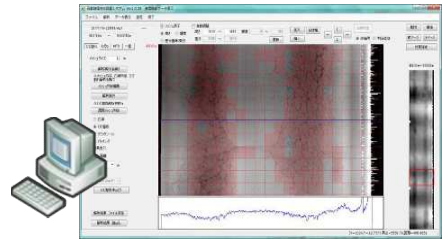
Automatic analysis

Cloud server

90
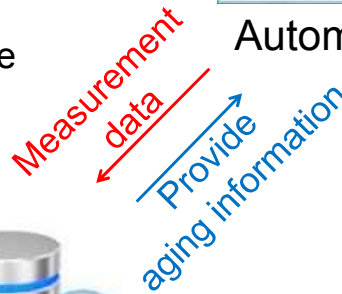
Damage form by simple road survey property technology

a) surface damage type
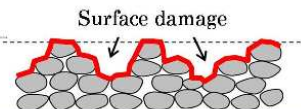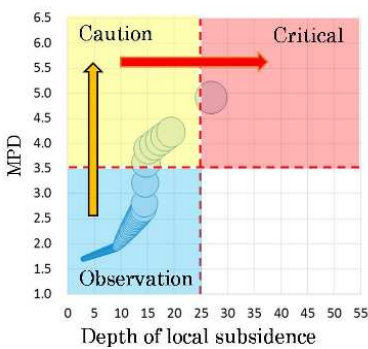
MPD Increase first
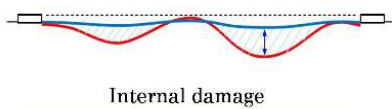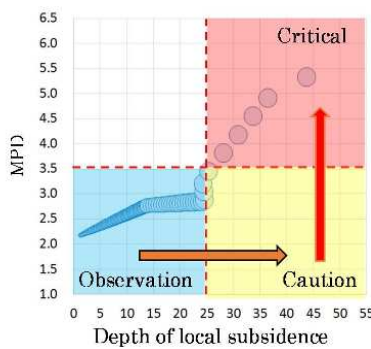
Repair method
・Crack seal
・Surface treatment method

b) internal damage type

Depth of local subsidence Increase first

Repair method
・Partial replacing method
・Cutting overlay

c) both damage type

MPD
Depth of local subsidence
Simultaneous progress

Repair method
・Partial replacing method
・Cutting overlay
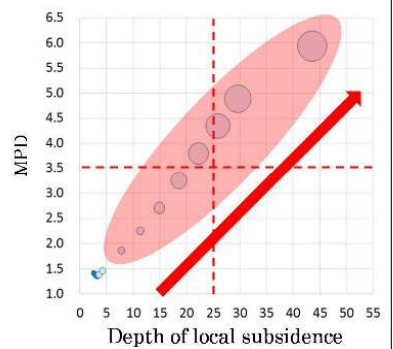
【Urgent】
Depth of local subsidence
: 1mm/day
MPD : 0.1/day

91

Proposal on operation method of road surface management by Smart Eagle ②

Periodic measurement（10 days pitch ）

Evaluation of increase
→ Display of caution points etc.

Prevent the pothole occurrence by risk management
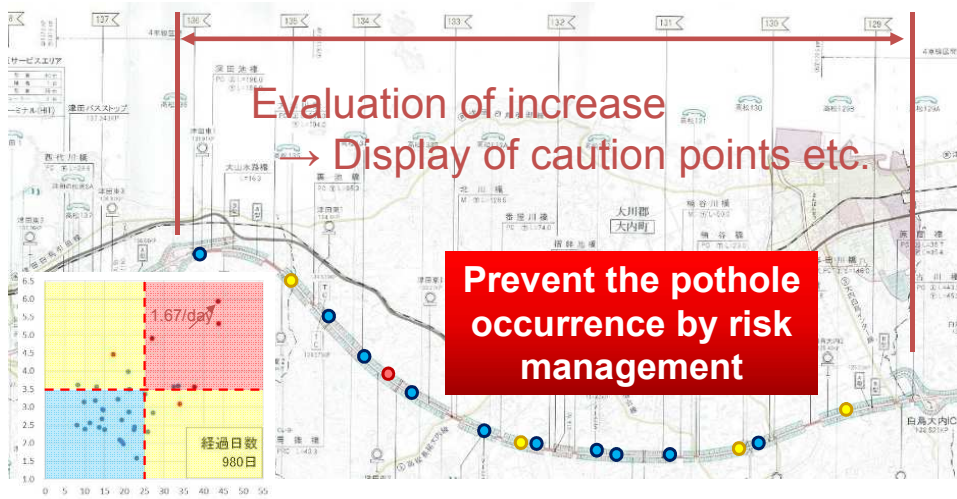
April 2019 trial introduction scheduled

92

Mathematical modelling and analysis of Rayleigh Wave

Cheng Hua

Department of Aeronautics and Astronautics, Fudan University, Shanghai, China

Abstract: Waves that propagate in elastic solid can be divided into two main categories: body waves and surface waves. Two and only two types of body waves in an unbounded solid, namely longitudinal wave (P-wave) and shear waves (SV-wave and SH-wave), can be propagated independently. Rayleigh wave is one kind of surface waves which propagates along the free boundary and decays exponentially away from the boundary. Rayleigh wave is essentially the formation of interference on the surface of the medium of P-wave and SV-wave. Therefore, it was firstly introduced as a solution of the free boundary problem for an elastic half space by Lord Rayleigh (1885) [1], who summed it up as the simultaneous solution of the equations of P-wave and SV-wave. Yet to this day, the method of the characteristic equation of surface wave velocity he deduced is still the important way to seek for Rayleigh wave [2].

It is important to realize that since a solution (Rayleigh wave) can be found using Elastic theory and Helmholtz decomposition, it can also be seen as the superposition of two separate components: one P-wave and the other SV-wave. So, we think it is necessary to review in detail the mechanical process and mathematical method of deducing Rayleigh wave so far. In this report another main attention is a new and simplified characteristic equation about Rayleigh wave, which is the result recently deduced with special aim at future purposes in viscoelastic media.

In this report an overview will also be given about propagation properties of Rayleigh wave, such as velocity of propagation, particle motion, wave attenuation factor. Velocity of propagation is one of the most important features of Rayleigh wave, in fact, the characteristic equation is exactly what it is about Rayleigh wave speed. Concerning the combined effect of material and geometrical attenuation as the wave spreads out from the source, the exponential decay of particle motion with depth is another important property that helps to build the mathematical model of Rayleigh wave.

Keywords: Rayleigh wave; Rayleigh's equation; Rayleigh wave speed; characteristic equation

Elastic Wave

Mechanical wave is a disturbance that propagates in a solid, liquid, or gaseous medium. Examples of mechanical waves include the elastic waves generated in the earth's crust during earthquakes and sound waves and ultrasonic waves in liquids and gases. When elastic waves propagate, the energy of elastic deformation is transferred in the absence of a flow of matter, which occurs only in special cases, such as during an acoustic wind. Every harmonic elastic wave is characterized by the amplitude and vibration frequency of the particles of the medium, a wavelength, phase and group velocities, and a law governing the distribution of displacements and stresses over the wave front. A special feature of elastic waves is that their phase and group velocities are independent of the wave amplitude and the wave geometry. An elastic wave may be a plane, spherical, or cylindrical wave.

An elastic wave is a deformation of elastic body that travels throughout the body in all directions. We can examine the deformation over a period of time by fixing our look on just one point in space. This is the case of Lagrangian description.

We will begin by a simple case, assuming that we have an isotropic medium, which is the elastic properties or wave velocity is not directionally dependent and that our medium is continuous. By examining a balance of forces across an elemental volume and relating the forces on the volume to an ideal elastic response of the volume using Hooke's Law we will derive one form of the elastic wave equation.

Let us begin by examining the balance of forces and mass (Newton's Second Law) for a very small elemental volume. The effect of traction forces and additional body forces ($\vec{f}$) is to generate an acceleration ($\ddot{\vec{u}}$) per unit volume of mass or density ρ:

$$\rho\, \ddot{u}_i = \sigma_{ij,j} + f_i \qquad\qquad (1)$$

where the double-dot above u, denotes the second partial derivative with respect to time ($\dfrac{\partial^2 u_i}{\partial t^2}$). The deformation in the body is achieved by displacing individual particles about their central resting point. Because we consider that the behavior is essentially elastic the particles will eventually come to rest at their original point of rest. Displacement for each point in space is described by a vector with a tail at that point.

$$\vec{u} = (u_1, u_2, u_3)$$

Each component of the displacement, u_i depends on the location within the body and at what stage of the wave propagation we are considering.

Density ρ is a scalar property that depends on what point in 3-D space we consider:

$$\rho = \rho(x, x_2, x_3) \text{ or, in other words}$$

$$\rho(x_1, x_2, x_3) = \rho(\vec{x})$$

Body forces all the forces external to the elastic medium except in the immediate vicinity of the elemental volume. For example, commonly the effect of gravity is discarded as is the effect of the seismic source if the case is relatively 'distant' from the cause, so that the homogeneous (partial differential) equation for motion states that the acceleration a particle of solid undergoes while under the influence of traction forces is proportional to the stress gradients across its surface, and that the acceleration is greater for smaller volume densities, i.e.:

$$\ddot{u}_i = \frac{\partial \sigma_{ij}}{\partial x_j} = \frac{\partial \sigma_{i1}}{\partial x_1} + \frac{\partial \sigma_{i2}}{\partial x_2} + \frac{\partial \sigma_{i3}}{\partial x_3} \quad \text{(for j=1,2,3)} \qquad (2)$$

Each basis vector component of the acceleration as for example $i = 1$ is expressed as

$$u_1 \hat{x}_1 = \left(\frac{\partial \sigma_{11}}{\partial x_1} + \frac{\partial \sigma_{12}}{\partial x_2} + \frac{\partial \sigma_{13}}{\partial x_3} \right) \hat{x}_1$$

Finally, in complete indicial notation: $\ddot{u}_i = \sigma_{ij,j}$

By using the relation between strain and displacement, the infinitesimal deformation at each point depends on the gradients in the displacement field:

$$\begin{aligned} e_{pq} &= \frac{1}{2}(u_{p,q} + u_{q,p}) \\ &= \frac{1}{2}(\frac{\partial u_p}{\partial x_q} + \frac{\partial u_q}{\partial x_p}) \end{aligned} \qquad (3)$$

Empirically, it has been shown that for small strains (10^{-5}), and over short periods of time, solids behave as ideal elastic solids. The most general form of Hooke's Law for an ideal elastic solid is:

$$\sigma_{ij} = c_{ijpq} e_{pq} \qquad (4)$$

where c_{ijpq} is a fourth-order tensor containing 3^4=81 elastic constants or matrix components that define the elastic properties of the material in the an anisotropic and inhomogeneous medium. Each component c_{ijpq} or elastic constant has dimensions of pressure. Each component c_{ijpq} is independent of the strain e_{ij} and for this reason is called a 'constant' although elastic constants vary throughout space as a function of position.

We can reduce the number of constants to two in various steps. Firstly we can reduce the number to 36 because it follows that since σ_{ij} and e_{ij} are symmetric:

$$c_{jipq} = c_{ijpq} \quad \text{and} \quad c_{ijqp} = c_{ijpq}.$$

Through thermodynamic considerations we can demonstrate that

$$c_{pqij} = c_{ijpq}$$

So that even in the case of anisotropy the number of constants can be reduced to 21. However, it is possible to often solve many geological problems by considering that rocks have isotropic elastic properties. The assumption of isotropy reduces the number of independent elastic constants to just two. In summary for an isotropic, continuous medium we can reduce the elastic constant tensor to the following:

$$c_{ijpq} = \lambda \delta_{ij} \delta_{pq} + \mu(\delta_{ip} \delta_{jq} + \delta_{iq} \delta_{jp}) \qquad (5)$$

where λ and μ are known as the Lamé elastic parameters or properties. Lamé parameters λ and μ can be expressed in terms of other familiar elastic parameters such as Young's modulus E and Poisson's ratio σ:

$$\lambda = \frac{E\sigma}{(1+\sigma)(1-2\sigma)} \; ; \mu = \frac{E}{2(1+\sigma)} \qquad (6)$$

Other elastic parameters can also be expressed in terms of λ and μ. For example, incompressibility K relates the change in pressure surrounding a body to the corresponding relative change in volume of the body:

$$K = -V\frac{\Delta P}{\Delta V} = \lambda + \frac{2}{3}\mu = \frac{E}{3(1-2\sigma)} \qquad (7)$$

Substitution of equation (5) into equation (4) shows that traction forces and strain are related for an isotropic medium in the following manner:

$$\sigma_{ij} = \left[\lambda\delta_{ij}\delta_{pq} + \mu\left(\delta_{ip}\delta_{jq} + \delta_{iq}\delta_{jp}\right)\right]e_{pq}$$

$$= \lambda\delta_{ij}\delta_{pq}e_{pq} + \mu\delta_{ip}\delta_{jq}e_{pq} + \mu\delta_{iq}\delta_{jp}e_{pq}$$

If we add over repeated sub-indices:

$$= \lambda\delta_{ij}\left(\delta_{11}e_{11} + \delta_{22}e_{22} + \delta_{33}e_{33}\right)$$
$$+ \mu\delta_{i(p=1,2,3)}\delta_{jq}\left(e_{1q} + e_{2q} + e_{3q}\right)$$
$$+ \mu\delta_{iq}\delta_{j(p=1,2,3)}\left(e_{1q} + e_{2q} + e_{3q}\right)$$

From the definition of a Kronecker delta, the only terms that will be non-zero and contribute to the stress tensor will be those which make the sub-indices equal. That is for the second term on the right of the equals sign, values exist if $p = i$ and $q = j$. Similarly, for the third term on the right of the equals sign values exist if $p = j$ and $q = i$. With this simplification we arrive at:

$$= \lambda\delta_{ij}e_{kk} + \mu\delta_{ii}\delta_{jj}e_{ij} + \mu\delta_{ii}\delta_{jj}e_{ji}$$

Because the deformation tensor is symmetric $e_{ij} = e_{ji}$ leading to the result that

$$\sigma_{ij} = \lambda\delta_{ij}e_{kk} + 2\mu e_{ij} \qquad (8a)$$

In experiments we observe displacement, ground velocity and acceleration so it makes sense to express the stresses in terms displacements,

$$\sigma_{ij} = \lambda\delta_{ij}\frac{\partial u_k}{\partial x_k} + \mu\left(\frac{\partial u_i}{\partial x_j} + \frac{\partial u_j}{\partial x_i}\right) \text{ or, in complete indicial notation:}$$

$$\sigma_{ij} = \lambda\delta_{ij}u_{k,k} + \mu(u_{i,j} + u_{j,i}) \qquad (8b)$$

since

$$e_{ij} = \frac{1}{2}\left(u_{i,j} + u_{j,i}\right) \text{ and } e_{kk} = e_{11} + e_{22} + e_{33} = u_{k,k} = \nabla\cdot\vec{u}$$

Note that $\nabla \cdot \vec{u} = \dfrac{\Delta V}{V}$, (where ΔV is the relative change in volume, for infinitesimal deformations)

We obtain the wave equation for displacements in a general isotropic medium by substituting (8b) into the equation of motion

$$\rho \ddot{\vec{u}}_i = \sigma_{ij,j} + f_i \ (1)$$

$$= \left[\lambda \delta_{ij} u_{k,k} + \mu(u_{i,j} + u_{j,i}) \right]_{,j} + f_i$$

$$= (\lambda \delta_{ij} u_{k,k})_{,j} + \mu_{,j}(u_{i,j} + u_{j,i}) + \mu(u_{i,jj} + u_{j,ij}) + f_i,$$

$$= \lambda_{,i} \delta_{ij} u_{k,k} + \lambda \delta_{ij} u_{k,k} + (\mu(u_{i,j} + u_{j,i}))_{,j} + \mu(u_{i,jj} + u_{j,ij}) + f_i$$

After expansion using the product rule. Let us take each of the terms on the right hand side separately to demonstrate the application of indicial notation. For each term i only the case where j=i can contribute in the Kronecker delta, so

$$\lambda_{,i} \delta_{ij} u_{k,k} = \lambda_{,i} \delta_{ii} u_{k,k}$$

$$= \lambda_{,i} u_{k,k}$$

$$\equiv \lambda_{,i} u_{j,j}$$

Because we can interchange the repeated k's by repeated j's because they both signify summation over the range of values for j; i.e., 1 through 3.

$$= \underline{(\lambda + \mu)u_{j,ij}} + \underline{\mu u_{i,jj}} + \underline{\lambda_{,i} u_{j,j}} + \underline{\mu_{,j}(u_{i,j} + u_{j,i})} + f_i \qquad (9)$$

$$ \quad I \qquad\qquad II \qquad III \qquad\quad IV$$

In order to show the steps in detail, let us examine each of the terms I through IV on the right hand side of equation (9).

Starting with I :

$$u_{k,ki} = \frac{\partial^2 u_1}{\partial x_1 \partial x_i} + \frac{\partial^2 u_2}{\partial x_2 \partial x_i} + \frac{\partial^2 u_3}{\partial x_3 \partial x_i}$$

$$= \frac{\partial}{\partial x_1}\left(\frac{\partial u_1}{\partial x_i}\right) + \frac{\partial}{\partial x_1}\left(\frac{\partial u_2}{\partial x_i}\right) + \frac{\partial}{\partial x_1}\left(\frac{\partial u_3}{\partial x_i}\right)$$

$$= u_{ki,k} \equiv u_{j,ij}$$

For II :

$$u_{i,jj} = \frac{\partial^2 u_i}{\partial x_1 \partial x_1} + \frac{\partial^2 u_i}{\partial x_2 \partial x_2} + \frac{\partial^2 u_i}{\partial x_3 \partial x_3}$$

$$= \nabla^2 (u_i)$$

After some algebra we show that an alternative expression can be obtained by adding (9) vectorially from $i = 1,2,3$ to arrive at:

$$\rho\ddot{\vec{u}} = (\lambda + \mu)\nabla(\nabla \bullet \vec{u}) + \mu\nabla^2\vec{u} + \nabla\lambda\nabla \bullet \vec{u} + \nabla\mu \times \nabla \times \vec{u} + 2(\nabla\mu \bullet \nabla)\vec{u} + \vec{f} \qquad (10)$$

Two fundamental body wave types: P wave and S wave

From the equation of motion (10) in vectorial form, we can demonstrate (by Poisson, Cauchy, and George G. Stokes), that in an infinite elastic, and isotropic, homogeneous medium two types of particle motion associated with traveling trains of deformation can be predicted. These are called body waves. In the faster type, called longitudinal, dilational, irrotational wave, or simply P wave, the particle motion is in the same direction as that of wave propagation; in the slower type, called transverse, shear, rotational wave, or simply S wave, it is perpendicular to the propagation direction. We next show the existence of the two types of elastic deformation waves which could propagate through isotropic elastic solids.

Since λ and μ are constant in a homogeneous medium, we have that $\nabla\lambda$ and $\nabla\mu$ both equal zero because there are no spatial changes in their values. This leaves:

$$\rho\frac{\partial^2\vec{u}}{\partial t^2} = (\lambda + \mu)\nabla(\nabla \bullet \vec{u}) + \mu\nabla^2\vec{u}$$

But we can use the identity:

$$\mu(\nabla \times \nabla \times \vec{u}) = \mu\nabla(\nabla \bullet \vec{u}) - (\nabla^2\vec{u})\mu \text{, (identity 1) so that}$$

$$\rho\frac{\partial^2\vec{u}}{\partial t^2} = (\lambda + 2\mu)\nabla(\nabla \bullet \vec{u}) - \mu(\nabla \times \nabla \times \vec{u}) \quad (11)$$

Now, if we take the divergence of (11) while keeping in mind that:

$$\nabla \bullet (\nabla \times "vector") \equiv 0 \text{ and that} \qquad \text{(identity 2)}$$

$$\nabla \times \nabla("scalar") \equiv 0 , \qquad \text{(identity 3)}$$

We can simplify the expression to because the second term on the right becomes zero because $\nabla \times \vec{u}$ is a vector quantity, and its rotational is zero (identity 2):

$$\nabla\left(\rho\frac{\partial^2\vec{u}}{\partial t^2}\right) = \nabla[(\lambda + 2\mu)\nabla(\nabla \bullet \vec{u})]$$

$$\rho\frac{\partial^2(\nabla \bullet \vec{u})}{\partial t^2} = \nabla^2(\nabla \bullet \vec{u})(\lambda + 2\mu)$$

We can change variable names by defining a new scalar field variable $\Theta = \nabla \bullet \vec{u}$ so that the immediately preceding expression looks like:

$$\rho\frac{\partial^2\Theta}{\partial t^2} = \nabla^2\Theta(\lambda + 2\mu)$$

$$\frac{\rho}{\lambda + 2\mu}\ddot{\Theta} = \nabla^2\Theta \text{ , where } \ddot{\Theta} = \frac{\partial^2\Theta}{\partial t^2}$$

In order to propagate this type of deformation through the medium the body must expand and contract (divergence is non-zero), in which the particles of the medium vibrate in the direction of wave propagation, can propagate also in liquids and gases, which are elastic with respect to volume but not with respect to shape. This is P wave that can be transmitted by both solid and liquid materials in the Earth's interior. With P wave, the particles of the medium vibrate in a manner similar to sound waves—the transmitting media is alternately compressed and expanded.

Now, if we take the rotational of the general equation of motion as expressed in equation (11) i.e.,

$$\nabla \times (\rho\ddot{\bar{u}}) = \nabla \times [(\lambda + 2\mu)\nabla(\nabla \bullet \bar{u}) - \mu(\nabla \times \nabla \times \bar{u})]$$

$$\rho\frac{\partial^2(\nabla \times \bar{u})}{\partial t^2} = (\lambda + 2\mu)\nabla \times \nabla(\nabla \bullet \bar{u}) - \mu\nabla \times \nabla \times (\nabla \times \bar{u})$$

Because $\nabla \bullet \bar{u}$ is a scalar field and the rotational of the gradient of this field is zero (identity 3). the first term on the right of the equation goes to zero:

$$\rho\frac{\partial^2(\nabla \times \bar{u})}{\partial t^2} = -\mu\nabla \times \nabla \times (\nabla \times \bar{u})$$

We can now change variable names by defining a new vector field variable $\bar{\Omega} = \nabla \times \bar{u}$ so that the immediately preceding expression looks like:

$$\rho\frac{\partial^2\Omega}{\partial t^2} = -\mu\nabla \times (\nabla \times \bar{\Omega})$$

$$= -\mu\{\nabla(\nabla \bullet [(\nabla \times \bar{\Omega})])\} + \nabla^2\bar{\Omega}$$

$$= -\frac{\mu}{\rho}\bar{\Omega}$$

because the first term goes to zero since the divergence of the rotational of $\bar{\Omega}$ is zero (identity 2), the above equation represents another type of body wave, the slower one, the S wave, travels only through solid material. With S waves, the particle motion is transverse to the direction of travel and involves a shearing of the transmitting rock.

References:

[1] Rayleigh, L. (1885) On Waves Propagated along the Plane Surface of an Elastic Solid. *Proceedings of the London Mathematical Society*, **17**, 4-11.

[2] Eric A. Ash, Edward G. Paige. (1985) Rayleigh-wave Theory and Application. *Proceedings of an International Symposium Organized by The Rank Prize Funds at The Royal Institution*, London, 15–17 July, 1985.

Mathematical modeling and analysis of Rayleigh Wave

Cheng HUA

Department of Aeronautics and Astronautics (Department of Mechanics)

Fudan University

2019 IMI 会議, 日本福岡

CONTENT

1 弾性波の説明とその分類
Description and classification of elastic waves

2 Rayleigh波の数学モデル
Mathematical modeling of Rayleigh waves

3 粘弾性Rayleigh波の特性方程式
Characteristic equation of viscoelastic Rayleigh waves

4 進行中の計算例
Calculation example in progress

5 总结、不足和展望
Summary, lack and outlook

02

PART ONE 1

Description and classification of elastic waves

弾性波の説明とその分類

03

---

1. 弾性波の説明とその分類

弾性論の基礎方程式（等方性線形弾性体）

運動方程式（応力のつり合い式）

Navier より

$$\rho \frac{\partial^2 u_i}{\partial t^2} = \sigma_{ji,j} + f_i \quad (\sigma_{ij} = \sigma_{ji})$$

構成方程式

Lame より
または
Hooke より

$$\sigma_{ij} = \lambda \varepsilon_{kk} \delta_{ij} + 2\mu \varepsilon_{ij}$$

$$\varepsilon_{ij} = \frac{1+\upsilon}{E} \sigma_{ij} - \frac{\upsilon}{E} \sigma_{kk} \delta_{ij}$$

ひずみと変位関係

Cauchy より

$$\varepsilon_{ij} = \frac{1}{2}(u_{i,j} + u_{j,i})$$

σ_{ij} : Stress tensor $\quad \varepsilon_{ij}$: Strain tensor $\quad u_i$: Displacement vector $\quad f_i$: Body force
ρ : Density $\quad (\lambda, \mu)$: Lame coefficients $\quad E$: Young modulus $\quad \upsilon$: Poisson's ratio

04

Lame-Navier方程式(変位を未知変数とする基礎方程式)

For isotropic linear elasticity, Motion Equation:

$$\rho \frac{\partial^2 u_i}{\partial t^2} = (\lambda + \mu) u_{j,ji} + \mu u_{i,jj} + f_i \qquad \text{テンソル記号}$$

$$\rho \frac{\partial^2 \vec{u}}{\partial t^2} = (\lambda + \mu)\nabla(\nabla \cdot \vec{u}) + \mu\Delta\vec{u} + \vec{f} \qquad \text{ベクトル記号}$$

$$\rho \frac{\partial^2 \vec{u}}{\partial t^2} = (\lambda + 2\mu)\nabla(\nabla \cdot \vec{u}) - \mu\nabla \times \nabla \times \vec{u} + \vec{f} \qquad \text{ベクトル記号（他の形式-1）}$$

$$\rho \frac{\partial^2 \vec{u}}{\partial t^2} = \lambda\nabla(\nabla \cdot \vec{u}) + \mu(\nabla(\nabla \cdot \vec{u}) + (\nabla \cdot \nabla)\vec{u}) + \vec{f} \qquad \text{ベクトル記号（他の形式-2）}$$

For anisotropic linear elasticity, Motion Equation:

$$\rho \frac{\partial^2 u_i}{\partial t^2} = C_{ijkl} u_{k,jl} + f_i \qquad \text{テンソル記号を使うと明確です}$$

05

動的問題の弾性解、弾性波の波動方程式(物体力が作用しない)

$$\rho \frac{\partial^2 \vec{u}}{\partial t^2} = (\lambda + 2\mu)\nabla(\nabla \cdot \vec{u}) - \mu\nabla \times \nabla \times \vec{u} \qquad \text{ベクトル記号（他の形式-1）}$$

ベクトル場に関するHelmholtzの定理によれば（ベクトル場の分解）

$$\vec{u} = \vec{u}_p + \vec{u}_s \qquad \text{ただし} \qquad \begin{aligned} \nabla \times \vec{u}_p &= 0 \\ \nabla \cdot \vec{u}_s &= 0 \end{aligned}$$

$$\begin{cases} \rho\dfrac{\partial^2 \vec{u}_p}{\partial t^2} = (\lambda + 2\mu)\Delta\vec{u}_p \\[2mm] \rho\dfrac{\partial^2 \vec{u}_s}{\partial t^2} = \mu\Delta\vec{u}_s \end{cases} \quad\Rightarrow\quad \begin{cases} \dfrac{\partial^2 \vec{u}_p}{\partial t^2} = v_p^2\Delta\vec{u}_p \quad v_p^2 = \dfrac{\lambda + 2\mu}{\rho} \quad \text{(P wave)} \\[3mm] \dfrac{\partial^2 \vec{u}_s}{\partial t^2} = v_s^2\Delta\vec{u}_s \quad v_s^2 = \dfrac{\mu}{\rho} \quad \text{(S wave)} \end{cases}$$

06

無限等方性線形弾性体において，P波とS波2種類しかない！

以下のように説明します。
弾性波が伝播する物質点の変位成分は：

$$\begin{cases} u = u(xl + ym + zn - ct) \\ v = v(xl + ym + zn - ct) \\ w = w(xl + ym + zn - ct) \end{cases}$$

$xl+ym+zn$ - ctに関する関数である。l, m, nは弾性波の法線方向、波の伝播方向と一致している。Cは波の速度。

また、

$$\nabla \cdot \vec{u} = \varepsilon_x + \varepsilon_y + \varepsilon_z = \frac{\partial u}{\partial x} + \frac{\partial v}{\partial y} + \frac{\partial w}{\partial z} = lu' + mv' + nw'$$

なお、上式の'は $xl+ym+zn$ - ct についての導関数を求めるという意味です。$Lame{-}Navier$方程式に代入すれば：

$$\begin{cases} (\lambda + \mu)(l^2 u'' + lmv'' + nlw'') = (\rho c^2 - \mu)u'' \\ (\lambda + \mu)(lmu'' + m^2 v'' + mnw'') = (\rho c^2 - \mu)v'' \\ (\lambda + \mu)(nlu'' + mnv'' + n^2 w'') = (\rho c^2 - \mu)w'' \end{cases}$$

$$\left(l^2 - \frac{\rho c^2 - \mu}{\lambda + \mu} \right)u'' + lmv'' + nlw'' = 0$$

$$lmu'' + \left(m^2 - \frac{\rho c^2 - \mu}{\lambda + \mu} \right)v'' + mnw'' = 0$$

$$nlu'' + mnv'' + \left(n^2 - \frac{\rho c^2 - \mu}{\lambda + \mu} \right)w'' = 0$$

弾性波の物質点の変位が存在するなら、上式の加速度は必ずゼロ解ではないから、

上式の係数行列式はゼロではない：

$$\begin{vmatrix} l^2 - \dfrac{\rho c^2 - \mu}{\lambda + \mu} & lm & nl \\[2mm] lm & m^2 - \dfrac{\rho c^2 - \mu}{\lambda + \mu} & mn \\[2mm] nl & mn & n^2 - \dfrac{\rho c^2 - \mu}{\lambda + \mu} \end{vmatrix} = 0$$

簡略化して次の式を得る：

$$\left(\mu - \rho c^2\right)^2 \left(\lambda + 2\mu - \rho c^2\right) = 0$$

$$c = \sqrt{\dfrac{\mu}{\rho}} = v_S, \quad c = \sqrt{\dfrac{\lambda + 2\mu}{\rho}} = v_P$$

これによって、無限等方性線形弾性体において，弾性波の波速が2つしかないので、P波とS波二種類だけの弾性波について説明できる。

09

Body Waves: P and S waves

P波 とS波の形

(a) Undisturbed material

Compression Expansion Compression Expansion Compression

Undisturbed material

(b) Primary wave　Direction of wave movement

|← Wavelength →|

(c) Secondary wave

Surface
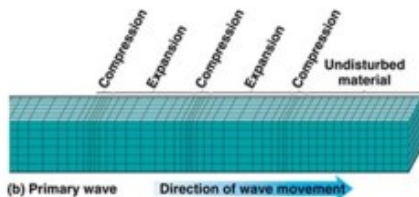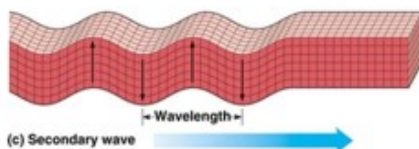
Focus
(d)

©2001 Brooks/Cole - Thomson Learning
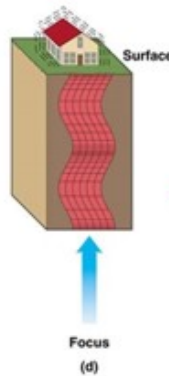
- Body waves
  - P or primary waves
    - fastest waves
    - travel through solids, liquids, or gases
    - compressional wave, material movement is in the same direction as wave movement
  - S or secondary waves
    - slower than P waves
    - travel through solids only
    - shear waves - move material perpendicular to wave movement

10

1. 弾性波の説明とその分類
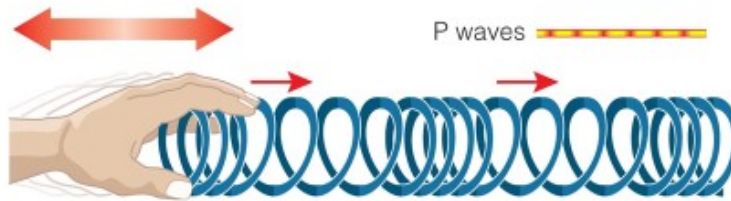
P waves

P waves result from compression and stretching in the direction of travel.

Body waves
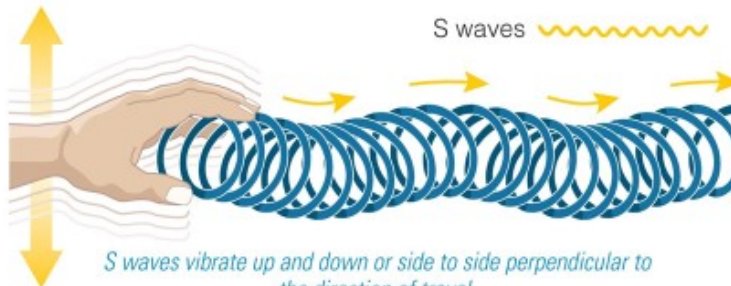
S waves

S waves vibrate up and down or side to side perpendicular to the direction of travel.

Copyright © 2008 Pearson Education, Inc., publishing as Pearson Addison-Wesley.

11

PART TWO 2

Mathematical modeling of Rayleigh waves

Rayleigh波の数学モデル

無限等方性線形弾性体ではなく、境界がある（例え半無限空間）

Rayleigh wave

12

Body waves (P-wave, S-wave) and surface wave

Longitudinal wave (P-wave)   **Shear wave (S-wave)**
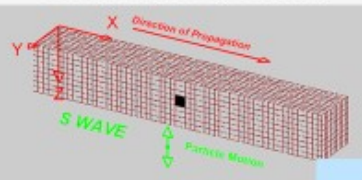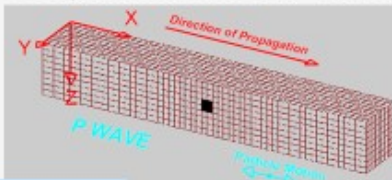
$$\Delta^2\varphi - \frac{1}{v_P^2}\frac{\partial^2\varphi}{\partial t^2} = 0$$

$$\vec{u} = grad\,\phi + rot\,\vec{\psi}$$

$$\Delta^2\vec{\psi} - \frac{1}{v_S^2}\frac{\partial^2\vec{\psi}}{\partial t^2} = 0$$

interference   **at a surface**

L. Rayleigh in 1885:

- ◆ Isotropic elastic media
- ◆ Along the surface of solids
- ◆ Quick attenuation with depth
- ◆ Particle in elliptical retrograde motion
- ◆ slower than body wave velocities, etc

Rayleigh Surface wave

13

---
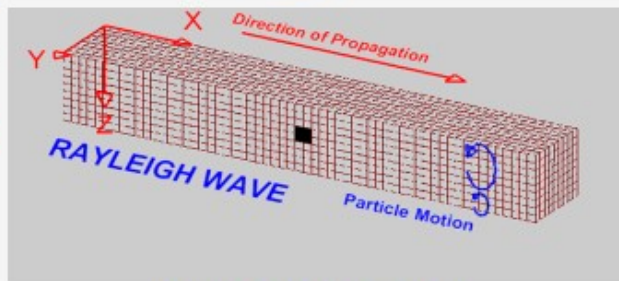
2. Rayleigh波の数学モデル

P波、S波、Rayleigh波の信号

14
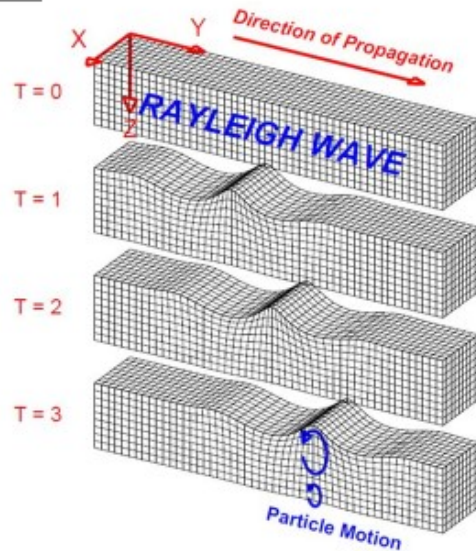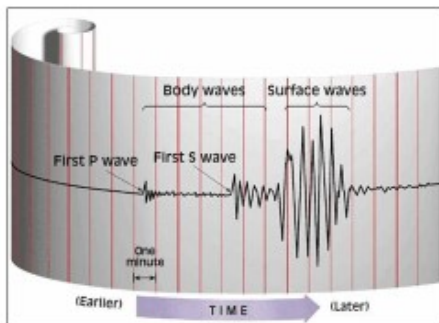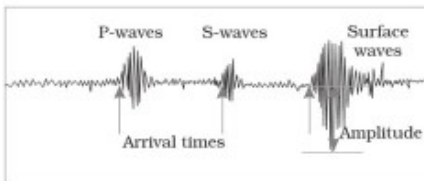
2. Rayleigh波の数学モデル

Here,

a, b : attenuation coefficient (positive real number)

A, B : For unknown coefficients

ψ_V: SV Component of S-Wave

φ : Functions of Solutions of P Wave

$$\begin{cases} \Delta^2\varphi - \dfrac{1}{v_P^2}\dfrac{\partial^2\varphi}{\partial t^2} = 0 & \text{(P wave)} \\[3mm] \Delta^2\bar{\psi} - \dfrac{1}{v_S^2}\dfrac{\partial^2\bar{\psi}}{\partial t^2} = 0 & \text{(S wave)} \end{cases}$$

Assume that the solution of the two equations

(considering the two components of the surface wave) is :

$$\begin{cases} \varphi = A\cdot e^{-aZ}\cdot e^{i(k_R x - \omega t)} \\[2mm] \psi_V = B\cdot e^{-bZ}\cdot e^{i(k_R x - \omega t)} \end{cases}$$

ω, v_R : **Circular frequency and velocity of Rayleigh Wave**

$k_R = \omega / v_R$: **Circular Wave Number of Rayleigh Wave**

15

In some detail

- Well-known equation for Rayleigh wave in elastic medium (Rayleigh 1885), its circular wavenumber k_R is obtained by

$$(2k_R^2 - k_S^2)^2 - 4k_R^2\sqrt{(k_R^2 - k_P^2)(k_R^2 - k_S^2)} = 0 \quad \textbf{characteristic equation}$$

  and it has been proved that there is only one solution, for example, in Poisson'solid (Lame elastic coefficients $\lambda = \mu$) ,the ratio of Rayleigh wave velocity to shear wave velocity is *0.919*.

  Here, k_R, k_P and k_S is wave numbers of Rayleigh, longitudinal and shear waves, respectively: $\quad k_R = \omega / v_R \qquad k_P = \omega / v_P \qquad k_S = \omega / v_S$

- **There is no accepted Rayleigh wave equation in viscoelastic media, and is a controversy about the uniqueness of solutions of viscoelastic Rayleigh waves.**

- **In this report**, the characteristic equation of viscoelastic Rayleigh wave is discussed by using **complex modulus** which is commonly used in dynamic analysis of viscoelastic materials.

16

簡単な回顧と整理 (Summary, Elastic→Viscoelastic)

Personage	Relevant Viewpoints of Rayleigh Waves in Viscoelastic Media
Rayleigh 1885[1]	Elastic Rayleigh wave equation, has been proved only one solution.
Scholte 1947[2] Bland 1960[3, p.75]	**The existence of Rayleigh waves in viscoelastic media is demonstrated mathematically, but it is speculated that there may be another type of Rayleigh waves.** The question of the existence and uniqueness of Rayleigh wave in viscoelastic media "It has not yet been shown that for any viscoelastic material there is one and only one such root".
Currie 1977[4]	There may be more than one Rayleigh wave.
Romeo 2001[5]	Using complex modulus to generalize elastic Rayleigh wave equation to viscoelastic medium, it is considered that there is only one Rayleigh wave.
Ivanov 2005[6]	The study of Rayleigh wave properties at fixed wavelength supports Romeo's view.
Chirita 2014[7]	Similarly, the Rayleigh wave equation is established by using complex modulus, which supports Currie's viewpoint.

[1] L. Rayleigh, OnWaves Propagated along the Plane Surface of an Elastic Solid, *Proceedings of the London Mathematical Society.* 1885, 17(1): 4-11.
[2] Scholte J G. On Rayleigh waves in visco-elastic media. *Physica*, 1947, 13: 245-250
[3] Bland, D. R. The Theory of Linear Viscoelasticity, Pergamon, Oxford, (1960)
[4] Currie P K, Hayes M A, O'Leary P M. Viscoelastic Rayleigh waves. *Quarterly of Applied Mathematics*, 1977, 35:35-53
[5] Romeo M. Rayleigh waves on a viscoelastic solid half-space. *Journal of the Acoustical Society of America*, 2001, 110: 59-67
[6] Ivanov T P, Savova R. Viscoelastic surface waves of an assigned wavelength. *European Journal of Mechanics - A/Solids*,2005, 24(2):305-310.
[7] Chirita S, Ciarletta M, Tibullo V. Rayleigh Surface Waves on a Kelvin-Voigt Viscoelastic Half-Space. *Journal of Elasticity*, 2014, 115(1):61-76.

17

---

03 PART THREE

Characteristic equation of viscoelastic Rayleigh waves

粘弾性Rayleigh波の特性方程式

両方

これは弾性Rayleigh波の特性方程式を求めていく過程と似ているところがあります。

wave source — Rayleigh wave propagation along a free surface
O — x
free surface
amplitude
z
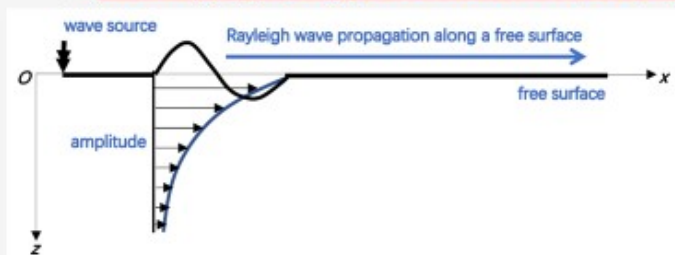
18

Viscoelastic wave equation

1D

$$\sigma_1 = E\varepsilon \qquad \sigma_2 = \eta\frac{d\varepsilon}{dt}$$

$\lambda, \mu \qquad \sigma \qquad \lambda', \mu'$

Kelvin model

◆ Dynamical equilibrium equation（*Newton's law*）

$$\rho\frac{\partial^2 u_i}{\partial t^2} = \sigma_{ij,j}$$

◆ Constitutive equation of linear isotropic viscoelastic medium

$$\sigma_{ij} = \lambda(t)\delta_{ij} * du_{k,k} + \mu(t) * \left[du_{i,j} + du_{j,i}\right]$$

2D/3D

λ, μ elastic Lame coefficients
λ', μ' viscoelastic Lame coefficients

Kelvin Viscoelastic Media, Motion Equation:

$$\rho\frac{\partial^2 u_i}{\partial t^2} = \left[(\lambda+\mu)+(\lambda'+\mu')\frac{\partial}{\partial t}\right]u_{j,ji} + \left(\mu+\mu'\frac{\partial}{\partial t}\right)u_{i,jj} \qquad (1)$$

Helmholtz Decomposition of Displacement Vector Field

$$u_i = \Phi_{,i} + e_{ijk}\Psi_{k,j}, \qquad \Psi_{k,k} = 0$$

Φ scalar potential (longitudinal wave)
Ψ_k vector potential (shear wave)

The longitudinal and shear wave equation based on potential function

$$\rho\frac{\partial^2\Phi}{\partial t^2} = (\lambda+2\mu)\Phi_{,jj} + (\lambda'+2\mu')\left(\frac{\partial\Phi}{\partial t}\right)_{,jj}$$

$$\rho\frac{\partial^2\Psi_k}{\partial t^2} = \mu\Psi_{k,jj} + \mu'\left(\frac{\partial\Psi_k}{\partial t}\right)_{,jj} \qquad (2)$$
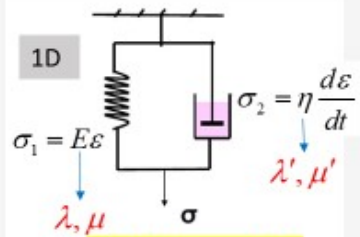
`19`

Characteristic equation in viscoelastic medium

Direction of propagation x

Half-space plane Oxz

Amplitude

z
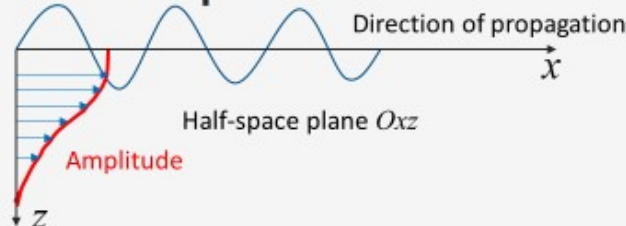
The wave equations of potential function in half-space plane can be expressed as follows :

$$\rho\frac{\partial^2\Phi}{\partial t^2} = (\lambda+2\mu)\left(\frac{\partial^2\Phi}{\partial x^2}+\frac{\partial^2\Phi}{\partial z^2}\right) + (\lambda'+2\mu')\frac{\partial}{\partial t}\left(\frac{\partial^2\Phi}{\partial x^2}+\frac{\partial^2\Phi}{\partial z^2}\right)$$

$$\rho\frac{\partial^2\Psi_k}{\partial t^2} = \mu\left(\frac{\partial^2\Psi_k}{\partial x^2}+\frac{\partial^2\Psi_k}{\partial z^2}\right) + \mu'\frac{\partial}{\partial t}\left(\frac{\partial^2\Psi_k}{\partial x^2}+\frac{\partial^2\Psi_k}{\partial z^2}\right) \qquad (3)$$

The simultaneous equation (3) means Rayleigh wave is formed by the interference superposition of longitudinal and shear waves. Suppose its solutions Φ and Ψ_y take the same form as follows： *A case similar to elasticity, but K, α, β*

α, β
Representing attenuation with depth

$$\Phi(x,z,t) = ae^{-\alpha z}\, e^{i(Kx-\omega t)}$$

$$\Psi_y(x,z,t) = be^{-\beta z}\, e^{i(Kx-\omega t)} \qquad (4)$$

The same K denotes the complex circular wave number.

a, b : unknown but non-zero real coefficients

K's imaginary part reflects the effect of viscosity. Both the real part and the imaginary part should be positive.

`20`

Characteristic equation in viscoelastic medium

In order to determine K, the stress boundary conditions at the free surface must be applied:

$$\sigma_{zx}|_{z=0} = 0$$
$$\sigma_{zz}|_{z=0} = 0$$

By using Kelvin viscoelastic constitutive equation (1), the stress σ_{zx}, σ_{zz} can be expressed as displacements u_x, u_z and then replaced by **Substitute** potential function (4):

Substitute

$$\Phi(x,z,t) = a e^{-\alpha z}\, e^{i(Kx-\omega t)}$$
$$\Psi_y(x,z,t) = b e^{-\beta z}\, e^{i(Kx-\omega t)}$$

non-zero real coefficients

$$\sigma_{zx} = M\left(\frac{\partial^2 \Psi_y}{\partial x^2} - \frac{\partial^2 \Psi_y}{\partial z^2} + 2\frac{\partial^2 \Phi}{\partial x \partial z}\right)$$

$$\sigma_{zz} = (\Lambda+2M)\frac{\partial^2 \Phi}{\partial z^2} + \Lambda\frac{\partial^2 \Phi}{\partial x^2} + 2M\frac{\partial^2 \Psi_y}{\partial x \partial z}$$

Here $\quad \Lambda = \lambda - i\omega\lambda'$
$\qquad M = \mu - i\omega\mu'$
That is the Lame coefficient in the form of complex numbers

$$2iMK\alpha \cdot a + M(K^2 + \beta^2)\cdot b = 0$$
$$\left[(\Lambda+2M)\alpha^2 - \Lambda K^2\right]\cdot a - 2iMK\beta \cdot b = 0$$

$$\begin{vmatrix} 2iMK\alpha & M(K^2+\beta^2) \\ (\Lambda+2M)\alpha^2 - \Lambda K^2 & -2iMK\beta \end{vmatrix} = 0$$

The above equations have non-zero solutions, and **the determinant** of their coefficients is required to be equal to zero.

$$\Lambda K^4 + [\Lambda\beta^2 - (\Lambda+2M)\alpha^2 + 4M\alpha\beta]K^2 - \alpha^2\beta^2(\Lambda+2M) = 0 \quad (5)$$

α, β to be handled

21

Characteristic equation in viscoelastic medium

In the above equation, α, β remain unknown. In order to find their value, substituting the potential function (4) into the wave equation (3), we can get

$$\alpha^2 = K^2 - K_P^2$$
$$\beta^2 = K^2 - K_S^2 \qquad (6)$$

here, $K_P^2 = \dfrac{\rho\omega^2}{\Lambda+2M}$, $K_S^2 = \dfrac{\rho\omega^2}{M}$ refer to the wavenumber of P-wave and S-wave in viscoelastic medium respectively, similar to Rayleigh wave number K, also in the plural form, therefore α, β are actually in the plural form.

By substituting (6) into (5), we can get

$$(2K^2 - K_S^2)^2 - 4K^2\sqrt{(K^2 - K_P^2)(K^2 - K_S^2)} = 0 \qquad (7)$$

The above equation is formally related to the Rayleigh's characteristic equation in the **elastic medium** below

$$(2k_R^2 - k_S^2)^2 - 4k_R^2\sqrt{(k_R^2 - k_P^2)(k_R^2 - k_S^2)} = 0 \quad \text{Rayleigh's characteristic equation}$$

the same form, but equation (7) is about complex numbers.

By equation (7), if material parameters $\lambda, \mu, \lambda', \mu'$ and circular frequency ω are given, we can obtain the corresponding Rayleigh wave number K.

22

Simplification of Characteristic Equation

$$16(K_S^2 - K_P^2)K^6 + (16K_P^2K_S^2 - 24K_S^4)K^4 + 8K_S^6K^2 - K_S^8 = 0 \quad (8)$$

let $R = \dfrac{K}{K_S}$ — **Ratio of Rayleigh Complex Wave Number to Shear wave one**

$$16\left(1 - \frac{K_P^2}{K_S^2}\right)R^6 + \left(16\frac{K_P^2}{K_S^2} - 24\right)R^4 + 8R^2 - 1 = 0$$

$$\frac{K_P^2}{K_S^2} = \frac{M}{\Lambda + 2M}$$

let $Z = \dfrac{\Lambda}{M}$ — **Ratio of Complex Modulus**

$$16(Z+1)R^6 - 8(3Z+4)R^4 + 8(Z+2)R^2 - (Z+2) = 0 \quad (9)$$

Only one coefficient Z in (4.2) !

for complex numbers $Z = p + qi$, here $p = \dfrac{\lambda\mu + (\omega\lambda')(\omega\mu')}{\mu^2 + (\omega\mu')^2}$, $q = \dfrac{\lambda(\omega\mu') - \mu(\omega\lambda')}{\mu^2 + (\omega\mu')^2}$

reflects ratios of the material parameters for elasticity and viscoelasticity.

For equation (9), for different p, q, **the corresponding R root can be obtained, from which the number of Rayleigh waves can be analyzed.**

since $p>0$, meanwhile q takes positive or negative values will correspond to conjugate roots, respectively. So take $q>0$ too. Considering the Possible Material Coefficient, Take separately $p \in [0.01, 100]$, $q \in [0.001, 10]$

23

The true one of viscoelastic Rayleigh waves

Because Rayleigh waves are formed by the interference of longitudinal and shear waves, therefore Rayleigh wave velocity should be less than shear wave velocity.

Since $v_R = \dfrac{\omega}{\mathrm{Re}(K)}$, $v_S = \dfrac{\omega}{\mathrm{Re}(K_S)}$, then

The true Rayleigh wave:

$$v_R < v_S \qquad \mathrm{Re}(K) > \mathrm{Re}(K_S)$$

from $K_S^2 = \dfrac{\rho\omega^2}{M}$, $M = \mu - i\omega\mu'$, K_S's argument $\theta_{K_S} \in \left[0, \dfrac{\pi}{4}\right)$, $\dfrac{\sqrt{2}}{2}|K_S| < \mathrm{Re}(K_S) \leq |K_S|$

$$\mathrm{Re}(K) = \omega/v_R \qquad \mathrm{Re}(K_P) = \omega/v_P \qquad \mathrm{Re}(K_S) = \omega/v_S$$

We can put forward a condition to determine which is the true one?

$\mathrm{Re}(K) > \mathrm{Re}(K_S)$

$v_R < v_S$

true

$\mathrm{Re}(K) < \mathrm{Re}(K_S)$

$v_R > v_S$

false

24

Numerical example in progress

PART FOUR

進行中の計算例

---

4. 進行中の計算例

数値モデル形状の概略図

Model of Rayleigh wave

$$\left(2k_\beta{}^2 - k_s{}^2\right)^2 - 4k_\beta{}^2\sqrt{\left(k_\beta{}^2 - k_p{}^2\right)\left(k_\beta{}^2 - k_s{}^2\right)} = 0$$
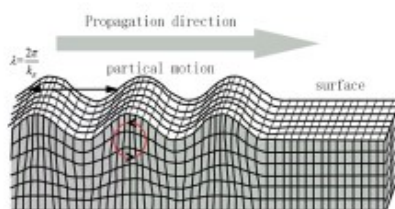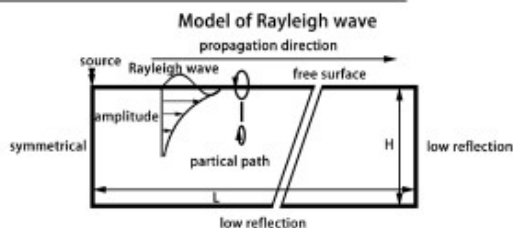
Characteristic equation for elastic medium

➤インターリーブメッシュ差分法と有限要素法の数値手法をそれぞれ適用して，直接反復アルゴリズムを用いて，二次元粘弾性波動方程式の数値解を実施する。

➤具体的なメッシュモデルについて計算例検証、比較分析を行う。

$$\rho\frac{\partial^2 u_i}{\partial t^2} = [\lambda(t) + \mu(t)] * \mathrm{d}u_{j,ji} + \mu(t) * \mathrm{d}u_{i,jj}$$
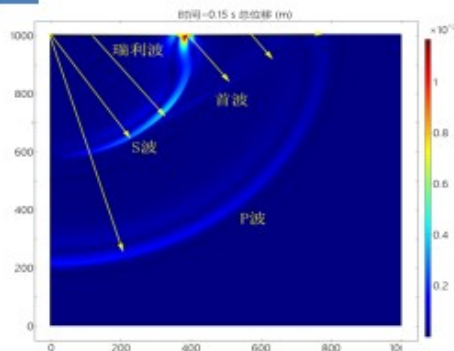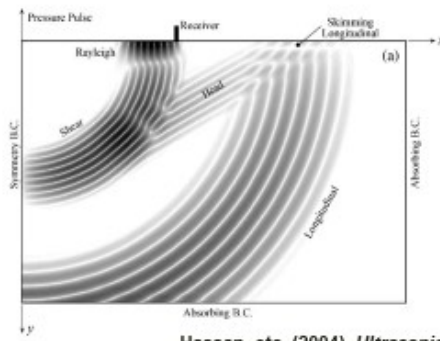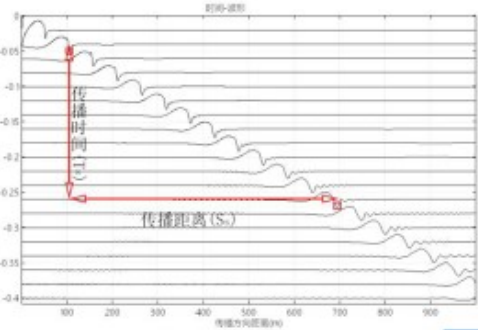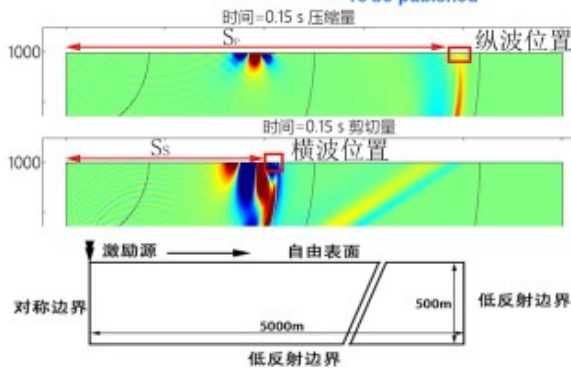
4. 進行中の計算例

具体的な計算例の差分計算、有限要素結果
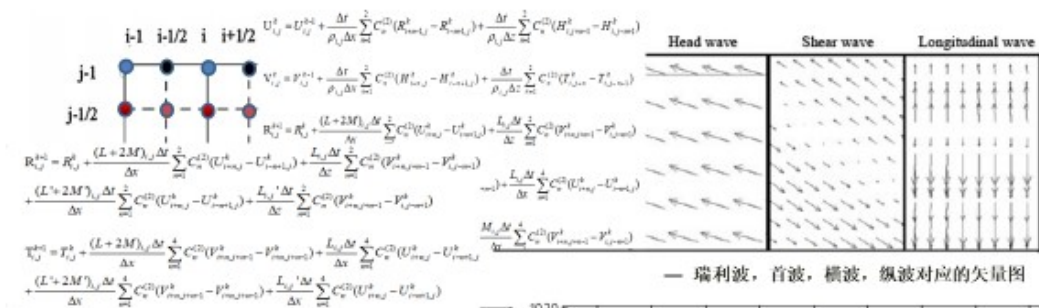
> 弾性と粘弾性計算結果の比較

瑞利波総位移(m)
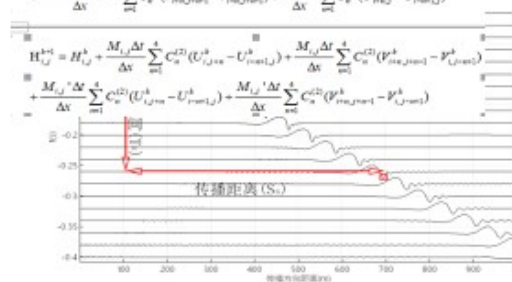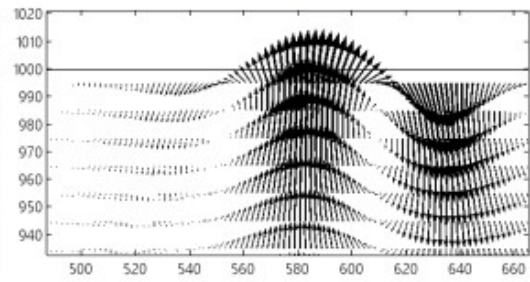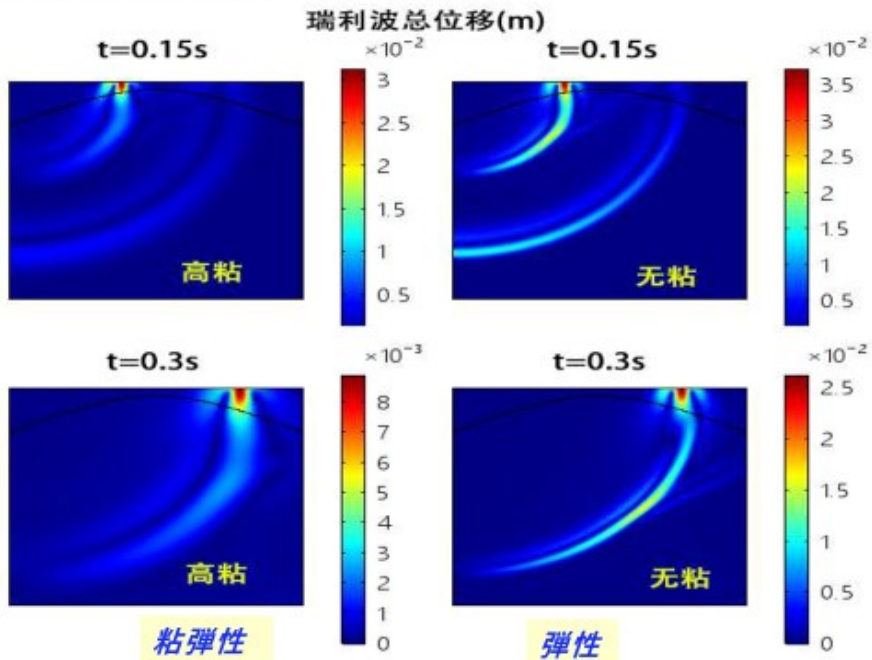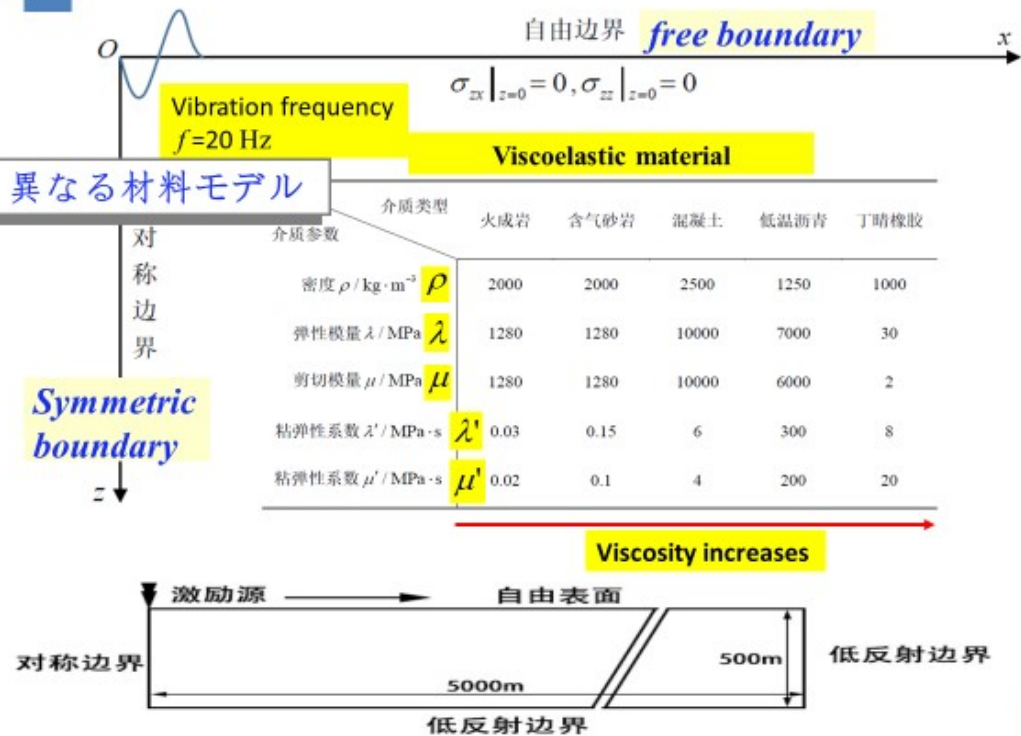
Analysis of numerical results

Solutions of Characteristic Equations in Different Media K

波数 介质	K_1 / m^{-1}	K_2 / m^{-1}	K_3 / m^{-1}	弹性解 k_R
火成岩	$0.1708 + 0.0002i$	$0.0884 + 0.0001i$	$0.0785 + 0.0001i$	0.1708
含气砂岩	$0.1708 + 0.0009i$	$0.0884 + 0.0006i$	$0.0785 + 0.0003i$	0.1708
混凝土	$0.0683 + 0.0018i$	$0.0353 + 0.0012i$	$0.0314 + 0.0006i$	0.0683
低温沥青	$0.0234 + 0.0185i$	$0.0121 + 0.0077i$	$0.0105 + 0.0102i$	0.0622
丁晴橡胶	$0.0625 + 0.0619i$	$0.0364 + 0.0359i$	$0.0257 + 0.0255i$	0.9581

Viscosity increases

Rayleigh wave velocity in different media calculated

介质 波速	火成岩	含气砂岩	混凝土	低温沥青	丁晴橡胶
v_p / m·s^{-1}	1386	1386	3469	10904	3453
v_s / m·s^{-1}	800.0	800.0	2002	5792	2233
v / m·s^{-1}	735.5	735.5	1840	5375	2011

from K_1, Rayleigh wave velocity v is about 0.9 times that of S-wave velocity v_S

Re(K_1) is almost the same as that of elastic medium when the viscosity is small.

31

Some simulation results

Displacements under 20 meters tend to 0

Deformation is large on the surface, gradually weakening along the depth direction, and it is difficult to see the deformation at about 20 meters depth.
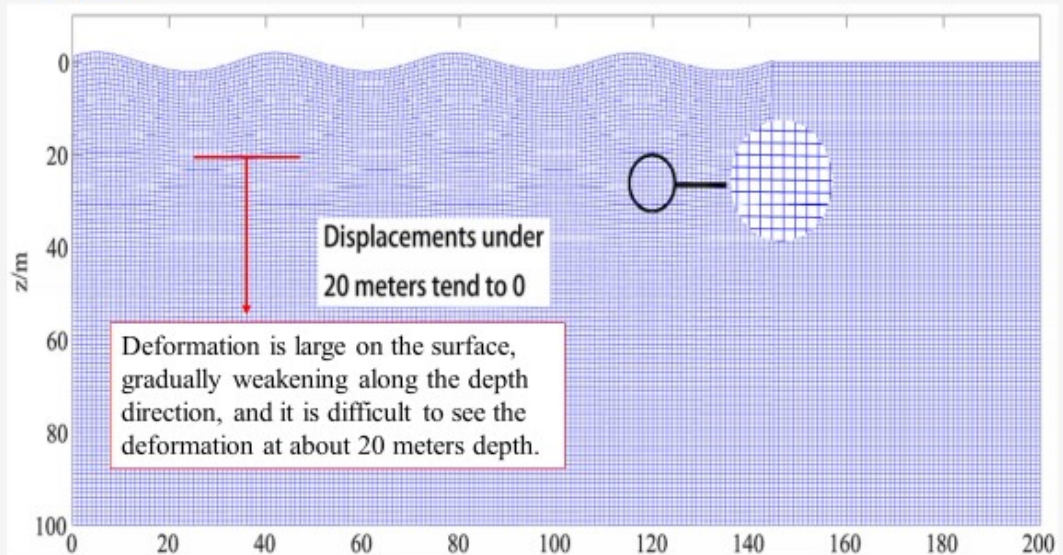
32

Some simulation results

Trajectory diagram of particle motion, Oblique ellipse

z/m

wavelength

attenuation

弹性时为正椭圆

x/m
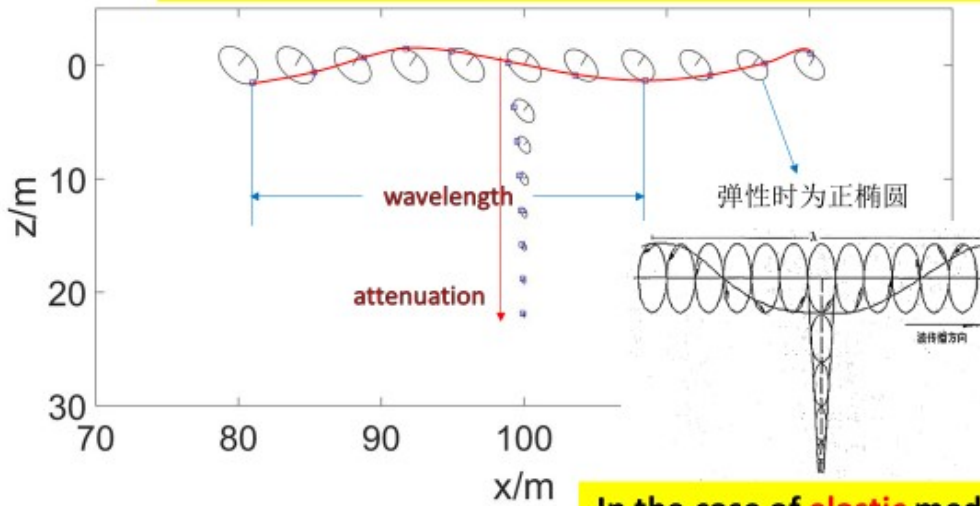
In the case of elastic medium normal ellipse

33

05 PART FIVE Summary, lack and outlook

まとめ、不足と展望

34

Summary

- The mathematical model and analysis method of Rayleigh wave are briefly introduced.

- A **simplified characteristic equation** of Rayleigh wave is derived in Kelvin viscoelastic half-space in terms of complex wavenumber.

$$16(K_S^2 - K_P^2)K^6 + (16K_P^2K_S^2 - 24K_S^4)K^4 + 8K_S^6K^2 - K_S^8 = 0$$

$$16(Z+1)R^6 - 8(3Z+4)R^4 + 8(Z+2)R^2 - (Z+2) = 0$$

- The **uniqueness** of the Rayleigh wave should be proved **under a natural condition** that the speed of Rayleigh wave is slower than P- and S-wave.

- **Examples** of several specific media are numerically calculated to verify some fundamental features.

35

Lack

- The assumption is **Kelvin viscoelastic** material, this study hasn't discussed viscoelastic media in general sense.

$$Z = p + qi \qquad p = \frac{\lambda\mu + (\omega\lambda')(\omega\mu')}{\mu^2 + (\omega\mu')^2}, q = \frac{\lambda(\omega\mu') - \mu(\omega\lambda')}{\mu^2 + (\omega\mu')^2}$$

$$p \in [0.01, 100], q \in [0.001, 10]$$

$$\sigma_1 = E\varepsilon \qquad \sigma_2 = \eta\frac{d\varepsilon}{dt}$$
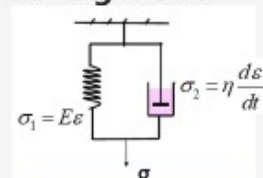
Kelvin model

- The **convenient way** to discuss the validity of characteristic roots is supposed **in the finite range** of real and imaginary parts of complex **Z**.

- The **uniqueness problem** is discussed but is not proved.

- **Characteristic equation** of Rayleigh surface wave is derived, but it is **not dynamic equation of** Rayleigh wave.

36
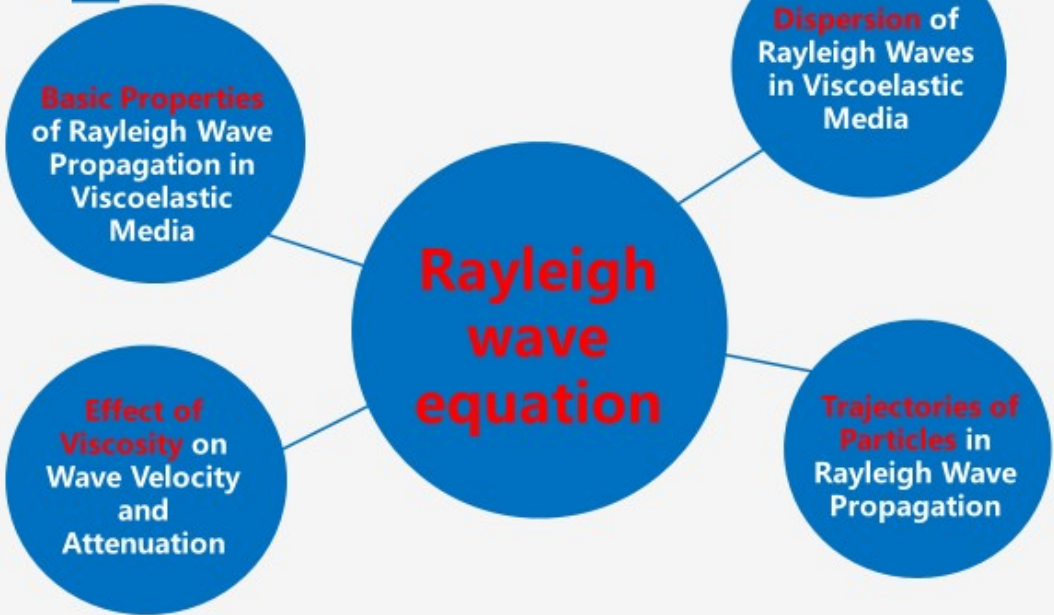
An overview of ultrasonic imaging and its development

Takashi TAKIGUCHI*

Abstract

In this paper, we give an overview of the development of the ultrasonic imaging. We introduce a mathematical model for the ultrasonic imaging developed by Mita-Takiguchi, whose numerical solutions are also discussed. In our numerical approach to the ultrasonic imaging, the idea by G. N. Hounsfield, who first developed a device for medical computerized tomography, for the practicalization of the computerized tomography, plays an important role.

Key words : ultrasound, non-destructive inspection, least square solution

AMS subject classifications : 44A12, 45Q05, 15A60

1   Introduction

In this paper, we review the development of the ultrasonic imaging (USI). The X-ray tomography (CT) and the magnetic resonance imaging (MRI) being excellent techniques for non-destructive or non-invasive inspections, they have shortcomings such as the expensive cost in both the devices themselves and their protection facilities, harmful side effects of the X-rays and the strong electromagnetic field to both human bodies and the environment and so on. Therefore, it is required to develop new, cheaply running, safe and reliable tomographic techniques without X-ray nor magnetic resonance, especially in medical imaging and in the non-destructive inspections. There are new tomographic techniques under development such as optical tomography ([3]), photo-acoustic tomography ([8]), ultrasonic imaging ([1, 10]) and so on, among which we take the ultrasonic imaging as the main topic in this paper. We refer the readers to [14] for a review of new tomographic techniques without X-ray nor magnetic resonance.

It may be very hard for USI to be as accurate as CT and MRI, since CT and MRI are very sharp and accurate. We, however, believe that USI would be a cheaply running and safe alternative to CT or MRI, because we can reconstruct sharper and more accurate images by USI with the numerical approach established in [14, 15] than the optical tomography and the photo-acoustic tomography, which is why we focus on USI.

We develop our theory in the following way. In this section, as the introduction of this article, we introduce the motivation of this paper. In the next section, we review the

---
*Department of Mathematics, National Defense Academy of Japan, 1-10-20, Hashirimizu, Yokosuka, Kanagawa, 239-8686, JAPAN   tel: +81-46-841-3810 (ext. 3249)   fax: +81-46-844-5902 (shared)   email: takashi@nda.ac.jp

mathematical problem for the practicalization of USI posed by Mita-Takiguchi [10]. In the third section, we shall review the idea by G. N. Hounsfield to practicalize CT, which serves as the key idea for our numerical solution to USI developed in the fourth section. In Section 4, we shall introduce an numerical approach to the mathematical problem of USI posed in the second section. We also make a comparison between USI and CT from the viewpoint of accuracy and discuss why the development of USI is important. In the final section, we summarize the conclusion of this review and mention open problems for USI to be practicalized in various field; medical imaging, non-destructive inspection for concrete structures and so on.

2 Mathematical model for ultrasonic imaging

In this section, we review the mathematical model for USI. There existing a number of non-destructive inspection methods. Confer [5, 13] for non-destructive inspections of concrete structures applying ultrasonic waves. Almost all of known techniques applying ultrasound utilize the "echo technique". It is very helpful to apply echo techniques when we can access the concrete structure from only its one side. Applying this technique, however, we obtain only rough sketches of the inclusion or the cavity which lies very close to the side we can access, which is far from concretely interior-describing non-destructive inspection we are trying to establish. We can find very few paper like [9] where the study is given in a similar method to ours. Even in the paper [9], its main result is to detect the combination defect in the masonry, which is very rough and strongly depends on a priori information of the structure, which is also far from the non-destructive inspection technique the we are trying to develop. Mita and the author [10], verified the propagation of the ultrasonic primary waves by experiments, which reads as;

Property 2.1. *The ultrasonic primary wave takes the route in the object where the travel time would be the shortest.*

We call this route *the fastest route*. In view of Property 2.1, Mita and the author posed a mathematical problem for USI with the observation data of only the first arriving ultrasonic waves, which reads as follows.

Problem 2.1 (Problem to develop USI (cf. [10]))**.** *Let $\Omega \subset \mathbb{R}^3$ be a domain and $f(x)$ be the propagation velocity the ultrasound at the point $x \in \Omega$. For $\alpha, \beta \in \partial\Omega$, we denote by $\gamma_{\alpha,\beta}$ a route from α to β contained in Ω. In this case, reconstruct $f(x)$ $(x \in \Omega)$ out of the data*

$$\min_{\gamma_{\alpha,\beta}} \int_{\gamma_{\alpha,\beta}} 1/f(x)d\gamma, \tag{1}$$

for $\forall \alpha, \beta \in \partial\Omega$.

Remark 2.1 (Remarks on Problem 2.1)**.**

- In general, solutions to Problem 2.1 are not unique. It is impossible to reconstruct the information of some points x's where $C(x)$'s are very small. For example, we cannot reconstruct the ultrasonic velocity of the styrofoam if it is included near the center of the test piece of concrete since no ultrasound wave would go through it.

However, it does not matter very much. Since, for some problems, we only focus on the part where the density (accordingly, the ultrasonic velocity) is relatively large for other problems, it is very important to determine the part where the density is so small that the ultrasound would not go through it, where the exact velocity does not matter. Remark that, in practice, it being very important to determine the exact place where the density is relatively small, for example, to determine the place where the steel is corroded or concrete would not pour in well in the RC structures, it is not so important to determine the exact density (ultrasonic velocity) of the place where the density is relatively small.

- We also note that it is possible to determine the exact place where the ultrasonic velocity is so small that no ultrasound would go through it, by USI, without knowing the ultrasonic velocity at such points.

- It is an interesting problem to determine the optimal subset reconstructible by USI.

In the same paper [10], they also verified that there is no decay in the velocity of the ultrasonic waves with respect to the length in concrete structures, if the length less than 1200mm, by which, together with Property 2.1, they gave how to non-destructively inspect cover concrete in reinforced concrete (RC) structures. Let us shortly review it.

For simplicity, let us assume a simple structure where only one rebar is imbedded as designed in Figure 1, which is a section of the three dimensional structure. We assume that the rebar is imbedded as designed where the rebar is parallel to surfaces of the test piece. We established the basic theory for our non-destructive inspection technique for concrete cover. By modification, our method can be applied for real RC structures.
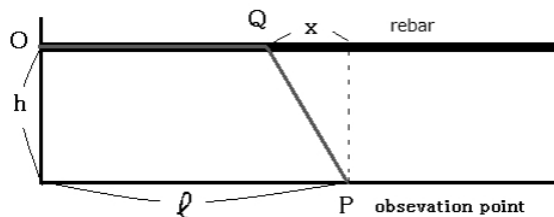
Figure 1: Propagation of an ultrasonic wave

Concrete structure being inhomogeneous, we homogenize the ultrasonic velocity in the concrete by application of the idea of the least square solution (cf. [10]), by which we denote the velocity in the steel by V and that in the concrete by v. In general, it is known that $4000m/s < v < 5200m/s$ and $5500m/s < V < 6500m/s$. Therefore we can assume that $v < V$.

We first determine the ultrasonic velocity in the steel V. By homogenization of the ultrasonic velocity in the concrete, the first-arriving ultrasound projected from the point $O(0, h)$ propagates along the spline $\overline{OQ} \cup \overline{QP}$ and is received at the point $P(l, 0)$, whose travel time we denote by t_0. If we project the ultrasonic wave from the point O and receive it at the point $P_i(l+l_i, 0)$ with travel time t_i, then we obtain approximate ultrasonic

velocity in the steel by $l_i/(t_i - t_0)$. Take observation points $P_1, \cdots, P_n$ as many as possible and take the least square solution

$$V = \frac{l_1(t_1 - t_0) + \cdots + l_n(t_n - t_0)}{(t_1 - t_0)^2 + \cdots + (t_n - t_0)^2} \tag{2}$$

to the system of linear equation which trivially has no solution

$$V(t_1 - t_0) = l_1, \cdots, V(t_n - t_0) = l_n. \tag{3}$$

We also comment that the least square solution V is the minimizer of the function

$$(V(t_1 - t_0) - l_1)^2 + \cdots + (V(t_n - t_0) - l_n)^2, \tag{4}$$

which was introduced in [10], it may be better if we give the minimizer of

$$l_1^k(V(t_1 - t_0) - l_1)^2 + \cdots + l^k(V(t_n - t_0) - l_n)^2, \tag{5}$$

for k=1 or 2, as a weighted least square solution, which shall be discussed in our forthcoming paper. Whichever minimizer is applied, our non-destructive inspection for cover concrete works well.

We then give an average ultrasonic velocity $\bar{v}$ as in [10]. For given V and v, x and the length L of the segment QP in Figure 1 are calculated as

$$x = \frac{vh}{\sqrt{V^2 - v^2}}, \quad x = \frac{Vh}{\sqrt{V^2 - v^2}}. \tag{6}$$

We let $v_0 = 3500 m/s$ then the ultrasonic wave projected from the point $O_i(0, h_i)$, $\bar{h}_i < h$ linearly propagates in the concrete to the observation point $R_j(r_j, 0)$, $r_j < \frac{vh}{\sqrt{V^2 - v_0^2}}$. Take as many pairs of source and observation points $\{O_i, R_j\}$ which gives the length L_{ij} of the segment where the ultrasonic wave propagates, and the travel time t_{ij}. Therefore we obtain the first step value v_1 of the homogenized acoustic velocity in the concrete by

$$v_1 = \frac{\sum t_{ij} L_{ij}}{\sum t_{ij}^2}. \tag{7}$$

Replacing v_0 by v_1 and repeating the same procedure, we obtain the the second step values $v_2 = \bar{v}$, which we determine as the homogenized acoustic velocity in the concrete. If necessary, we make the sequence $\{v_k\}$ until it approximately converges. In giving average ultrasonic velocity $\bar{v}$, we can give a modification of applying the idea of a weighted least square solution, which also shall be discussed in our another paper.

By the knowledge of the ultrasonic velocities, V in the steel and $\bar{v}$ in the concrete, and the route where the ultrasound propagates, we can propose a non-destructive inspection technique for concrete cover.

In Figure 1, when we observe the travel time the primary ultrasonic wave between the points O and P, the calculated travel time is

$$\frac{l - \frac{\bar{v}h}{\sqrt{V^2 - \bar{v}^2}}}{V} + \frac{Vh}{\bar{v}\sqrt{V^2 - \bar{v}^2}} \tag{8}$$

and the one in the segment QP is

$$\tilde{t} = \frac{Vh}{\bar{v}\sqrt{V^2 - \bar{v}^2}}. \tag{9}$$

If the velocity $\tilde{v}$ in the segment QP is much smaller than the homogenized velocity $\bar{v}$, for example, $\bar{v} - \tilde{v} > 200m/s$, then one or more of the following could happen.

- There is a cavity in the segment QP.

- There is a water route around the rebar.

- Some part of the rebar may get corroded.

In any case, we have to shave the concrete cover and have to repair the defect. Shaved concrete cover can be easily re-fixed by filling the cavity by shaving with better concrete. Therefore, what is important is to establish how to find where to shave in a non-destructive way, an answer of which is given as the above way.

3   G. N. Hounsfield's idea

In this section, we review the idea by G. N. Hounsfield for the practicalization of CT, which plays an important role in our main theory in the next section.

Consider a section of the human body by a plane, where we define the coordinate in order that this plane is given by $\{(x, y, z) \in \mathbb{R}^3|\ z = 0\}$. Let $f(x, y) = f(x, y, 0)$ be the density of the human body in the plane $\{(x, y, z) \in \mathbb{R}^3 \mid z = 0\}$. The mathematical problem of CT is introduced as follows.

Problem 3.1. *Reconstruct the function $f(x, y)$ defined on $\mathbb{R}^2$ by its line integrals $\int_l f(x, y)dl$ along all lines l's in $\mathbb{R}^2$.*

For the properties of the X-rays, introduction of the mathematical model for CT and the introduction of Problem 3.1, we refer the readers to [6, 11] for example. In general, for a function $f(x)$ defined on $\mathbb{R}^n$ and $d < n$, its d-dimensional Radon transform $R_d f(\xi)$ is defined as its integration on a d-dimensional plane ξ. For $d = n - 1$, we omit to write the term $n - 1$ and denote Rf, which is called the Radon transform of f. Problem 3.1 is a problem of the Radon transform on $\mathbb{R}^2$. For the general theory of the Radon transform, cf. [4, 6, 7]. As a reference of the Radon transform in connection with CT, we recommend [11]. In 1917, J. Radon [12] (cf. also the appendix in [4]) gave inversion formulas for the Radon transform for $n = 2, 3$. Radon's reconstruction formula being not stable under errors, some regularization and discretization treatment was necessary for the practicalization of CT. Therefore, there arose the following problem.

Problem 3.2. *Assume that for two functions $f_1(x, y), f_2(x, y)$ defined on $\mathbb{R}^2$ and for any line $l \subset \mathbb{R}^2$, their Radon transforms are close, that is,*

$$Rf_1(l) \approx Rf_2(l) \quad \text{for } \forall l \subset \mathbb{R}^2. \tag{10}$$

In this case, is it true that

$$f_1(x, y) \approx f_2(x, y) \quad \text{for } \forall(x, y) \in \mathbb{R}^2? \tag{11}$$

This problem was solved, about a decade after the practicalization of CT, by giving suitable filters applicable to the Radon's inversion formula to cut-off the unstable or the high frequency factors. This method is called "the filtered back projection method", which gives a better reconstruction image than Hounsfield's method.

Hounsfield, independently of the above discussion, considered the problem of practical CT formulated as follows.

Problem 3.3. *Let* $m \in \mathbb{N}$ *be sufficiently large and* $l_1, l_2, \cdots, l_m$ *be mutually different lines in* $\mathbb{R}^2$. *Construct an approximate solution of the density distribution* $f(x,y)$ *from the observed data* $F_1, F_2, \cdots, F_m$ *(* $F_i \approx Rf(l_i)$, $i = 1, 2, \cdots, m$ *) necessarily containing errors.*

In numerical analysis, we usually directly discretize a mathematical formula obtained by mathematical analysis in order to implement it for practical application. However, the essence of Hounsfield's idea is to discretize the mathematical model itself, not a mathematical formula. It is very interesting and worked very well at the initial stage of the practicalization of CT.

We can assume that supp$f$ is compact and $f \in L^1(\mathbb{R}^2)$ since f is a density distribution of the human body. Cover supp$f$ with n squares $c_1, c_2, \cdots, c_n$, whose sides are of the same length and parallel to the x- or y-axis, whose areas are all the same as $c = |c_j|$, and any pair of whose interiors are mutually disjoint. We approximate the function f by a function $g(x,y)$ defined as

$$g_c(x,y) = \sum_{j=1}^{n} x_j \chi_{c_j}(x,y), \tag{12}$$

where $\chi_{c_j}(x,y)$ is the characteristic function of the square c_j and x_j are unknowns. For example, if we take x_j as the integral mean of $f(x,y)$ in the square c_j

$$x_j = \frac{1}{c} \int_{c_j} f(x,y)dxdy, \tag{13}$$

then it seems easy to understand Hounsfield's idea. Let us call the function $g_c(x,y)$ as *a pixel function*. Since $\inf_{(x,y)\in c_j} f(x,y) \leq x_j \leq \sup_{(x,y)\in c_j} f(x,y)$, by the definition of the Lebesgue integral, there holds that

$$\lim_{c \to 0} g_c(x,y) = f(x,y) \quad \text{in } L^1(\mathbb{R}^2). \tag{14}$$

Therefore, it is very important in practice to construct approximate solutions for x_j's for small $c > 0$ with observation data containing errors and noises, which Hounsfield tried. He never tried to reconstruct the original function $f(x,y)$, from the observed data necessarily containing errors in various senses. This idea is very nice. Since the best we can hope is to obtain an approximation of f, not to reconstruct f itself, it is very flexible to approximate f by a suitably simple function g_c so that the problem would be simplified. Assume that m X-rays, $I_1, I_2, \cdots, I_m$, are projected to the human body. We assume that for $i = 1, 2, \cdots, m$, the strength of I_i before the projection is I_i^0 and after the projection is I_i^1. By $l_1, l_2, \cdots, l_m$, we denote the lines where the X-ray $I_1, I_2, \cdots, I_m$ rectilinearly propagates, respectively and by a_{ij}, $i = 1, 2, \cdots, m$, $j = 1, 2, \cdots, n$, we denote the length of $l_i \cap c_j$. Letting $s_i := \log I_i^0 - \log l_i^1$, $i = 1, 2, \cdots, m$ together with (12), the problem we have to solve turns out to be the following one.

Problem 3.4. *Solve the following system of linear equations in* $x_1, x_2, \cdots, x_n$.

$$\begin{cases} a_{11}x_1 + a_{12}x_2 + \cdots + a_{1n}x_n = s_1, \\ a_{21}x_1 + a_{22}x_2 + \cdots + a_{2n}x_n = s_2, \\ \qquad \cdots\cdots\cdots \\ a_{m1}x_1 + a_{m2}x_2 + \cdots + a_{mn}x_n = s_m, \end{cases} \tag{15}$$

or equivalently

$$A\boldsymbol{x} = \boldsymbol{s}. \tag{16}$$

In the medical CT, we have to treat a huge system like $m \geq 9 \times 10^6$, $n \geq 3 \times 10^4$. The fact $m \gg n$ and the effect of the errors we mentioned above, the overdetermined system (15) must have no solution. Although the system (15) has no solution, the density distribution $f(x,y)$ of the human body exists with no doubt, which must be approximately solved. Therefore, we have to solve the following problem.

Problem 3.5. *Construct an alternative solution to the system of linear equations* (15) *with no solution.*

This is the problem Hounsfield tried to solve. His idea is what is now called ART (algebraic reconstruction technique) or Kaczmarz method. He hit upon this idea all by himself without knowing ART nor Kaczmarz method (for these methods, see [11]). In the rest of this section, we shall introduce Hounsfield's solution of Problem 3.5.

We first note that each line

$$a_{i1}x_1 + a_{i2}x_2 + \cdots + a_{in}x_n = s_i \tag{17}$$

in (15) is an equation of the hyperplane $H_i \subset \mathbb{R}^n$ whose normal vector is $\boldsymbol{a}_i := (a_{i1}, a_{i2}, \cdots, a_{in})$. Take any $\boldsymbol{x}_0 \in \mathbb{R}^n$ and define the sequence $\{\boldsymbol{x}_k\}$ by

$$\boldsymbol{x}_k := P\boldsymbol{x}_{k-1} \equiv P_m P_{m-1} \cdots P_1 \boldsymbol{x}_{k-1}, \ k = 1, 2, \cdots \tag{18}$$

where

$$P_i\boldsymbol{x} := \boldsymbol{x} - \frac{\boldsymbol{a}_i \cdot \boldsymbol{x} - s_i}{\|\boldsymbol{a}_i\|} \frac{\boldsymbol{a}_i}{\|\boldsymbol{a}_i\|} \tag{19}$$

is the orthogonal projection of $\boldsymbol{x}$ onto the hyperplane H_i. If the system (15) has the unique solution, then it is easily proved that the limit

$$\lim_{k \to \infty} \boldsymbol{x}_k \tag{20}$$

gives the unique solution of (15), which is called ART or Kaczmarz method. Of course, the system has no solution in practice, because of errors in approximation of the original function f by the pixel function g, errors in observation, numerical rounding errors by computers, some noises and so on, all of which are small. Therefore, it can be said that the system (15) is "close to have the unique solution". Therefore Hounsfield considered that (20) would give an approximate solution of (15), which worked very well in practice. It is known that this iteration method by Hounsfield almost converges in a few steps, $k = 3$ or 4 in (20), independently of the size of the system (cf. Figure 2). We also note that if the errors in the each equation in the system (15) is very small, then an approximate solution to (15) constructed by Hounsfield's iteration method and the least square solution

are very close together and the both of them approximate what is required, the density distribution of the human body, very well, for whose image, see Figure 2.
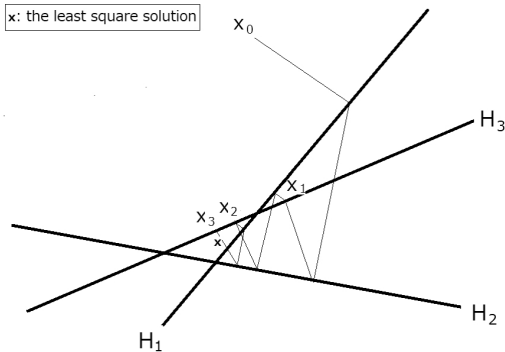
Figure 2: Iterated approximation and the least square solution

There are a number of works on such overdetermined systems of linear equations, cf. [2, 16] for example. There had been are few papers studying such system in relation with the idea by Hounsfield. In [15], the author has given a theoretical justification why Hounsfield's idea works well, which we shall review.

The iteration method by Hounsfield is justified in terms of the least square solutions. If a linear system (15) has a solution $\boldsymbol{x}$, then it holds that $A\boldsymbol{x} - \boldsymbol{s} = \boldsymbol{0}$, in view of which the following the idea of the least square solution is defined.

Definition 3.1. A vector $\boldsymbol{x} \in \mathbb{R}^n$ is called *a least square solution* to (15) (or (16)) if and only if it minimizes the norm

$$\|A\boldsymbol{x} - \boldsymbol{s}\|, \tag{21}$$

where $\|\boldsymbol{y}\| := \sqrt{y_1^2 + \cdots + y_m^2}$ for $\boldsymbol{y} \in \mathbb{R}^m$.

We note that there are many researches on the least square solutions to overdetermined systems (15), cf. [2, 16] for example, our theory is different from them in the following points.

- We a priori know that the least square solution to the overdetermined system (15) is unique, since the rank of the coefficient matrix A in (15) must be n. There being very many X-ray are projected to the human body, for $i < n$, we can take the $i+1$-th line l_{i+1} inductively such that it goes through only one new pixel and some of i pixels where some of the lines $l_1, \cdots, l_i$ have already gone through. In this process, we have to remember the fact $m \gg n$.

- We know by experience that the more observation X-ray data we have (the larger the number m is), the better resolution we can obtain, which shall be discussed and justified in a stochastic way (Theorem 3.1 below).

In the following, we assume the following conditions.

(I) $f(x, y) \in L^1 \cap L^2(\mathbb{R}^2)$.

(II) For any line $l \subset \mathbb{R}^2$, $f|_l \in L^1(l)$ and is piecewisely continuous.

(III) $m \gg n$.

Note that these conditions, (I) and (II), are satisfied by the density distribution of the human body. We also assume that

In the system (15), we divide the right hand side into the following there components;

$$\boldsymbol{s} = \boldsymbol{s}^0 + \boldsymbol{s}_c^{app} + \boldsymbol{s}_c^{obs}, \tag{22}$$

where $\boldsymbol{s}^0 := A\boldsymbol{x}^0$ with

$$\boldsymbol{x}^0 = (x_1^0, \cdots, x_n^0), \quad x_j^0 := \frac{1}{c} \int_{c_j} f(x, y) dx dy, \tag{23}$$

$\boldsymbol{s}_c^{app} := ((s_c^{app})_1, \cdots, (s_c^{app})_m)$ with $(s_c^{app})_i = \int_{l_i} f(x, y) dl - s_i^0$ and $\boldsymbol{s}_c^{obs} = \boldsymbol{s}_X := (s_1^X, \cdots, s_m^X)$ with s_i^X, $i = 1, \cdots, m$, being random variables whose probability density functions are supported by $[-\varepsilon_i, \varepsilon_i]$ for small $\varepsilon_i > 0$ and whose expectation value $E(s_i^X)$ is 0.

Under these assumptions, the author [15] gave a stochastic justification why the idea by Hounsfield worked well for the practicalization of CT.

Theorem 3.1. *We know by experience that even for a fixed number n, the larger the number m is, the better resolution we can obtain, which is proved to be stochastic theoretically right.*

Theorem 3.2. *The pixel function*

$$g_c(x, y) := \sum_{j=1}^{n} x_j \chi_{c_j}(x, y). \tag{24}$$

converges almost surely to the density distribution function $f(x, y)$, that is,

$$\lim_{c \to 0} g_c(x, y) = f(x, y), \quad a.s. \tag{25}$$

Note that by the assumption (III), $c \to 0$ yields $m \gg n \to \infty$. Remember also that

$$g_c(x, y) = g_c^0(x, y) + g_c^{app}(x, y) + g_c^{obs}(x, y). \tag{26}$$

For the proofs of these theorems, we refer the readers to [15]. Theorems 3.1 and 3.2 stochastically prove that the idea by Hounsfield is theoretically right, in the sense that his solution approximates the unique least square solution to (15) if the number n of the pixels are sufficiently large, we have enough number $m > n$ of the X-ray data and the errors are sufficiently small, which can be naturally assumed in usual practical applications.

4   A numerical approach to USI

In this section, we review a numerical approach to Problem 2.1 introduced in [14], where the idea by Hounsfield play an important role.

Let $\Omega \subset \mathbb{R}^3$ be a domain where the object locates, and $C(x)$ be the propagation velocity of the ultrasound at the point $x \in \Omega$. For $\alpha, \beta \in \partial\Omega$, we denote by $\gamma_{\alpha,\beta}$ a route from α to β contained in Ω. Mathematical solution to Problem 2.1 being very difficult and open, we can establish and solve practical problems related to Problem 2.1.

If the object is small or close to homogeneous, then we can apply the same algorithm with the X-ray CT, that is, we assume that the ultrasound rectilinearly propergates and apply the same algorithm with the X-ray CT to obtain a rough sketch of the distribution of the reciprocal $1/C(x)$ of the propagation velocity of the ultrasound. This idea is successful in medical imaging where the object is very small (cf. [1]).

In this section, we review the numerical approach to USI proposed in T1, whose idea is based on Property 2.1 and Hounsfield's idea. The essential idea of this approach is that if the ultrasound rectilinearly propagates then Problems 2.1 and 3.1 are equivalent.

Theorem 4.1. *Assume the same assumption as Problem 2.1. If we further assume that the ultrasound rectilinearly propagates then the fastest route between the two boundary points $\alpha, \beta \in \partial\Omega$ becomes the segment $l(\alpha, \beta)$*

$$l(\alpha, \beta) = \{t\alpha + (1-t)\beta \mid 0 < t < 1\} \tag{27}$$

between α and β. In this case, the integral (1) is the line integral along the segment between the two boundary points $\alpha, \beta \in \partial\Omega$. Therefore, if the ultrasound rectilinearly propagates then Problems 2.1 and 3.1 are equivalent by identifying $f(x) = 1/C(x)$ for $x \in \mathbb{R}^2$ or $\mathbb{R}^3$.

By this theorem, if we assume the ultrasound rectilinearly propagates, then applying the same algorithm as X-ray CT, then we obtain some approximation for the section of the reciprocal velocity $1/C(x)$ distribution.

In this subsection, we shall propose more precise three dimensional reiterating reconstruction algorithm for $1/C(x)$ in USI, where we shall apply Theorem 4.1 as the first step.

Method 4.1. *For USI, we propose the following reiterating procedure.*

(1) *Divide the object into boxels.*

(2) *As for the first step of this reiterating method, assume that the ultrasound rectilinearly propagates and apply the idea by Hounsfield to obtain the boxel function g_1 as the least square solution to (15), which approximates $1/C(x)$, the reciprocal of the sonic velocity $C(x)$. In this procedure, the elements a_{ij} of the matrix in (15) is given by the length of intersection between the (assumed) linear orbit of the i-th ultrasound and j-th boxel and s_i is the travel time of the i-th ultrasound.*

(3) *Taking the boxel function g_1 obtained in the procedure (2) as the first image, we can calculate the new orbit of the ultrasound. Then we change the elements a_{ij} of the matrix by the length of intersection between the new orbit of the i-th ultrasound and j-th boxel. Giving the least square solution g_2 to (15) with new matrix elements gives better approximation.*

(4) *Taking the boxel function g_2 as the second image and repeat the same procedure as procedure (3) to obtain a better approximation boxel function g_3 than g_2.*

(5) *Repeat the procedure (4) until $\sup_{1 \le k \le n} |g_{k+1} - g_k|$ is sufficiently small.*

Note that in the procedure (3), the new calculated orbit of the ultrasound in any boxel must be a segment. Hence the new orbit must be piecewisely linear. For more detail of this method, cf. [14]. In order to practicalize Method 4.1, it is very important to solve the following problem.

Problem 4.1. *Assume that the distribution $C(x)$ of the velocity , $x \in \Omega \subset \mathbb{R}^3$ is known. For any $\alpha, \beta \in \partial\Omega$, determine the fastest route γ from α to β though Ω, that is,*

$$\min_{\gamma_{\alpha,\beta}} \int_{\gamma_{\alpha,\beta}} 1/C(x) d\gamma = \int_{\gamma} 1/C(x) d\gamma. \tag{28}$$

This problem is challenging and interesting. The complete solution to Problem 4.1 seeming to be difficult, it is sufficient to solve this problem by assuming that the distribution $C(x)$ of the velocity is a boxel function. Furthermore, giving an algorithm to find the fastest route for a given boxel function is also practically sufficient. For a numerical approach to USI without sloving Problem 4.1, confer [15].

At the end of this section, let us compare the accuracy of the algorithms for X-ray CT and USI. Method 4.1 is as accurate as Hounsfield's algorithm for CT, where both algorithms are as accurate as each other. The algorithm for today's X-ray CT, however, is much sharper than Hounsfield's. while we have not developed its counterpart for USI and it may be difficult. That is why we mentioned in Introduction that it may be very hard for USI to be accurate as CT and MRI. We, however, claim that the development of USI is very important. USI costs very cheap, requires no protection facility and is very safe. That is why USI is very suitable for non-destructive inspection for infrastructures, especially, for concrete structures, since they are huge, cheaply running, safe and running-with-small-device inspection is required. It is also possible for USI to be an alternative to CT or MRI in the place where it is impossible to build big hospitals, for example, in conflict areas. We also claim that the resolution of USI can be better than that of the other new non-destructive or non-invasive inspection techniques, such as the optical tomogahy, the photo-acoustic tomography and so on, by developing the numerical approach (Method 4.1) posed in this section.

5 Summary

In order to conclude this paper, we shall summarize the conclusions in this paper and mention some open problems to be solved for further development. We first summarize our conclusions.

Conclusion 5.1. *We summarize the conclusion of this paper.*

- *A mathematical problem for USI was reviewed (Problem 2.1).*

- *A theoretical justification of Hounsfield's idea for the practicalization of CT was reviewed (Theorems 3.1 and 3.2).*

- *A numerical approach to USI was given (Method 4.1).*

The first conclusion is the origin of this research. The second one, being interesting itself from the view point of CT, gives a theoretical background for our algorithm (Method 4.1). The third one is very important for numerical implementation to practicalize USI, which contains many points to improve, and requires numerical and practical experiments.

In view of Conclusion 5.1, we mention some open problems to be solved for further development.

Problem 5.1. *We pose open problems to be solved for further development.*

- *It is very important to study the analytic solution to Problem 2.1, which may be very difficult.*

- *It is important to solve the open problem (Problem 4.1) mentioned in the previous section, the solution of which yields a better numerical solution to USI.*

- *Development of a good numerical solution to Problem 4.1 would be of great help to improve the numerical solutions to USI.*

- *Practical and numerical experiments of Method 4.1 are of great importance.*

Let us give some comments on Problem 5.1. First of all, it is very important to establish the reconstruction formula for USI, which is posed in the first problem. The second problem is posed for the development of Method 4.1. If Problem 4.1 is solved then the iteration algorithm in Method 4.1 will improve very much. Even if the analytic solution to Problem 4.1 is difficult, its numerical solution would be sufficient to improve Method 4.1, which is what the third problem claims. Finally, we pose a problem that it is very important to give practical and numerical experiments of Method 4.1.

References

[1] Arakawa, M., Kanai, H., Ishikawa, K., Nagaoka, R., Kobayashi, K. and Saijo, Y. : *A method for the design of ultrasonic devices for scanning acoustic microscopy using impulsive signals*, Ultrasonics **84** (2018) pp.172–179, doi.10.1016/j.ultras.2017.10.023.

[2] Censor, Y., Eggermont, P. P. B. and Gordon, D. : *Storng Underrelaxation in Kacmarz's Method for Inconsistent Systems*, Numer. Math., **41** (1983) pp. 83-92.

[3] Chen, I-K. and Kawagoe, D. : *Propagation of boundary-induced discontinuity in stationary radiative transfer and its application to the optical tomography,* Inverse Problems and Imaging, **13** (2019) pp. 337-351, doi.10.3934/ipi.2019017.

[4] Deans, S. R. : *The Radon Transform and Some of Its Applications*, John Wiley & Sons, Inc., New York, 1983.

[5] Gorzelańczyk, T., Hola, J., Sadowski, L. and Schabowicz, K. : *Methodology of nondestructive identification of defective concrete zones in unilaterally accessible massive members,* Journal of Civil Engineering and Management, **19** (2013) pp. 775-786.

[6] Helgason, S. : *The Radon Transform (second edition)*, Birkhauser, Boston, 1999.

[7] Herman, G. T. : *Image Reconstruction From Projections*, Academic Press, New York, 1980.

[8] Hirasawa, T., Iwatate, R. J., Kamiya. M., Okawa, S., Fujita. M., Urano, Y., and Ishihara, M. : *Spectral-differential-based unmixing for multispectral photoacoustic imaging,* Applied Optics, **57** (2018) pp. 2383-2393, doi.10.1364/AO.57.002383.

[9] Hobbs, B. : *Ultrasonic NDE for assessing the quality of structural brickwork,* Journal of Nondestructive Testing and Evaluation, **12** (1995) pp. 75-85.

[10] Mita, N. and Takiguchi, T. : *Principle of ultrasonic tomography for concrete structures and non-destructive inspection of concrete cover for reinforcement,* Pacific Journal of Mathematics for Industry, (2018) 10:6, doi.10.1186/s40736-018-0040-0

[11] Natterer, F. : *The Mathematics of Computerized Tomography (second edition),* SIAM (Classics in Applied Mathematics, Vol. 32), Philadelphia, PA, 2001.

[12] Radon, J. : *Über die Bestimung von Funktionen durich ihre Integralwarte längs gewisser Mannigfaltigkeiten,* Ber. Verh. Sächs. Akad. Wiss. Leipzig, Math-Nat. **69** (1917) pp. 262-277.

[13] Schabowicz, K. : *Ultrasonic tomography – The latest nondestructive technique for testing concrete members – Description, test methodology, application example,* Archives of Civiland Mechanical Engineering, **14** (2014) pp. 295-303.

[14] Takiguchi, T. : *Ultrasonic tomographic technique and its applications,* Applied Sciences, **9** (2019) 1005, doi.10.3390/app9051005.

[15] —— : *A theoretical study of the algorithm to practicalize CT by G. N. Hounsfield and its applications,* Japan Journal of Industrial and Applied Mathematics, **37** (2020) pp. 115-130, doi.org/10.1007/s13160-019-00391-1.

[16] Tanabe, K. : *Projection method for solving a singular system of linear equations and its applications,* Numer. Math., **17** (1971) pp. 203–214.

An overview of ultrasonic imaging and its develpment

Takashi TAKIGUCHI

National Defense Academy of Japan

New technologies for non-destructive and non-invasive inspections
and their applications
Oct. 29th, 2019 at IMI, Kyushu University

---

1 Introduction

2 Housfield's idea

3 USI

4 Conclusion

1. Introduction

Ultrasonic Imaging (Mita-T, 2018)

- The first arrival wave of the ultrasonic one takes the route where the travel time is the shotest (which is called the fastest route) in the cement paste, the mortar and the concrete.

- In the concrete structures of the length less than 1200mm, there is no decay of the speed of the ultrasonic waves with respect to the length.

Problem 1.1 (Ultrasonic Imaging (Mita-T, 2018))

Let $\Omega \subset \mathbb{R}^3$ be a domain and $f(x), \ (x \in \Omega)$ be the propagation velocity of the sound. For $\alpha, \beta \in \partial\Omega$, we denote by $\gamma_{\alpha,\beta}$ a route from α to β through Ω. Reconstruct $f(x) \ (x \in \Omega)$ out of the data

$$\min_{\gamma_{\alpha,\beta}} \int_{\gamma_{\alpha,\beta}} 1/f(x)d\gamma, \qquad (1)$$

for $\forall \alpha, \beta \in \partial\Omega$.

Remark 1.2 (Remarks on Problem 1.1)

- It is impossible to reconstruct the information of some points x's where $f(x)$'s are very small. However, it does not matter very much. For some problems, we only focus on the part where the density is relatively large, for others, the part where the density is relatively small can be determined by the phenomena that the ultrasonic wave would not go through it.

- It is an interesting problem to determine the optimal subset reconstructible by the acoustic imaging established by the study of Problem 1.1.

Remark 1.3 (Importance of Problem 1.1 in mathematics)

- It is a very interesting problem to establish an reconstruction formula for Problem 1.1 in view of pure mathematics.

- In view of both applied math and integral geometry, it is another interesting problem in Problem 1.1 to determine the subset of Ω where the reconstruction is impossible because it has no intersection with any γ giving **(1)**.

- In practice, we have to study various incomplete data problems of Problems 1.1 by the restriction arisen from various reasons in practical application, which is interesting in view of pure mathematics (integral geometry with incomplete data), applied mathematics and practice.

Problem 1.4 (Problems in this talk)

- Numerical solution to Problem 1.1 and its related problems
- Further development

2. Housfield's idea for CT

Sir Godfrey Newbold Hounsfield
(28 August 1919 – 12 August 2004)

- an English electrical engineer
- developed the diagnostic technique of X-ray computerized tomography (CT)
- received the Nobel Prize in Physiology or Medicine in 1979 (with Allan McLeod Cormack)

Other awards, titles and so on

- elected to the Royal Society in 1975

- appointed Commander of the British Empire in 1976

- awarded the Howard N. Potts Medal in 1977

- knighted in 1981

- Hounsfield scale : a quantitative measure of radiodensity used in evaluating X-ray CT scans, whose unit is defined as Hounsfield unit (HU)

Mathematical model of CT

The section
of a human's body

The X-ray

strength
of the X-ray   I(a)   I(x)   I(b)

coordinates   a   x   b

density   f(a)   f(x)   f(b)
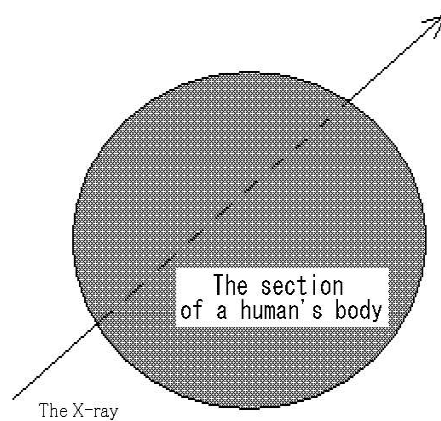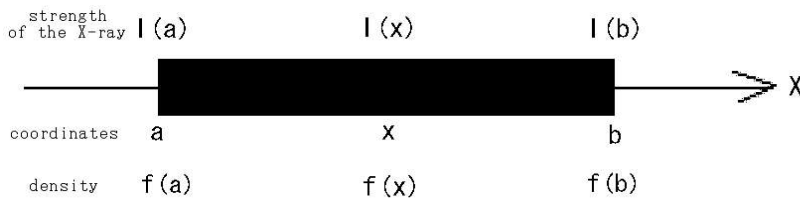
$$I(x + dx) - I(x) = -f(x)I(x)dx$$

$$I'(x) = -f(x)I(x)$$

$$\log I(a) - \log I(b) = \int_a^b f(x)dx$$

Mathematical problem of CT

Reconstruct the function $f(x, y)$ from the data

$$\left\{ \int_l f(x, y)dl \mid l \text{ is a line in } \mathbb{R}^2 \right\}.$$

The Radon transform

Let $\xi = \{x \in \mathbb{R}^n \mid x \cdot \theta = s\}$ be a hyperplane in $\mathbb{R}^n$, where $\theta \in S^{n-1}, \; s \geq 0$.

$$Rf(\xi) = Rf(\theta, s) = \int_{x \cdot \theta = s} f(x) dx.$$

An inversion formula for the Radon transform

For $f(x)$ defined on $\mathbb{R}^n$ and $\forall \alpha < n$,

$$I^\alpha f(x) := F^{-1}(|\xi|^{-\alpha} Ff(\xi))(x),$$

$$Ff(\xi) := \int_{\mathbb{R}^n} e^{-ix \cdot \xi} f(x) dx, \; F^{-1}\varphi(x) := \frac{1}{(2\pi)^n} \int_{\mathbb{R}^n} e^{ix \cdot \xi} \varphi(\xi) d\xi.$$

$$I^\alpha \psi(\theta, s) := F^{-1}(|\rho|^{-\alpha} \psi(\theta, \rho))(x),$$

$$F\psi(\theta, \rho) := \int_{\mathbb{R}} e^{-is\rho} \psi(\theta, s) ds, \; F^{-1}\psi(\theta, s) := \frac{1}{2\pi} \int_{\mathbb{R}} e^{is\rho} \psi(\theta, \rho) d\rho.$$

An inversion formula for the Radon transform

$$f(x) = \frac{1}{2}(2\pi)^{1-n}I^{-\alpha}R^*I^{\alpha-n+1}Rf(x), \qquad (2)$$

$$R^*\psi(x) := \int_{S^{n-1}} \psi(\theta, x \cdot \theta)d\theta.$$

Johann Karl August Radon

(16 December 1887 – 25 May 1956)

- an Austrian mathematician whose doctoral dissertation was on the calculus of variations

  (in 1910, at the University of Vienna)

- Über die Bestimung von Funktionen durich ihre Integralwarte längs gewisser Mannigfaltigkeiten, Ber. Verh. Sächs. Akad. Wiss. Leipzig, Math-Nat. **69** (1917), pp. 262-277.

J. Radon's inversion formulas

For $n = 3$. Let $\alpha = 2$ in (2) then

> **J. Radon's inversion formula for $n = 3$**
>
> $$f(x) = -\frac{1}{8\pi^2}\Delta \int_{S^2} Rf(\theta, x \cdot \theta)d\theta \qquad (3)$$

For $n = 2$. Let $\alpha = 1$ in (2) then the symmetry $Rf(-\theta, -s) = Rf(\theta, s)$ of the Radon transform yields that

> **J. Radon's inversion formula for $n = 2$**
>
> $$f(x) = -\frac{1}{\pi}\int_0^\infty \frac{F_x'(q)}{q}dq \qquad (4)$$

$$F_x(q) := \frac{1}{2\pi}\int_{S^1} Rf(\theta, x \cdot \theta + q)d\theta$$

A present-day algorithmic idea for CT

Let $n = 2,\ \alpha = 1$ in (2)

$$f(x) = \frac{1}{4\pi} I^{-1}\left(\int_{S^1} Rf(\theta, x \cdot \theta)d\theta\right). \tag{5}$$

Hounsfield's idea

Divide the picture into n pixels.

$$f(x, y) \approx g_c(x, y) = \sum_{j=1}^{n} x_j \chi_{c_j}(x, y), \tag{6}$$

where $f(x, y)$ is the density at (x, y).

$c_j,\ j = 1, 2, \cdots , n$: the pixels

c : the size of all pixels

$I_i,\ i = 1, 2, \cdots , m$: the projected X-rays

l_i : the line I_i passes through

$a_{ij} := |l_i \cap c_j|$: the length of $l_i \cap c_j$

I_i^0, I_i^1 : strength of the X-ray I_i before and after
passing through the human body, respectively

$s_i := \log I_i^0 - \log I_i^1$

x_j : the density of the human body on the pixel c_j

Problem 2.1

Solve the following system of linear equations in $x_1, x_2, \cdots , x_n$.

$$\begin{cases} a_{11}x_1 + a_{12}x_2 + \cdots + a_{1n}x_n &= s_1, \\ a_{21}x_1 + a_{22}x_2 + \cdots + a_{2n}x_n &= s_2, \\ \quad \cdots\cdots\cdots \\ a_{m1}x_1 + a_{m2}x_2 + \cdots + a_{mn}x_n &= s_m \end{cases} \tag{7}$$

$$Ax = s \tag{8}$$

Back

The equation (7) allows the unique solution x if and only if

$$Ax - s = 0$$

Definition 2.1 (Least square solutions)

A vector $x \in \mathbb{R}^n$ is called as a least square solution to (7) (or (8)) if and only if it minimizes the norm

$$\|Ax - s\|$$

Lemma 2.2

For $A \in M_{mn}(\mathbb{R})$, the following conditions are equivalent.

  (i) $x \in \mathbb{R}^n$ is a LSS to (7).

 (ii) $(Az, \ Ax - s) = 0$ for any $z \in \mathbb{R}^n$.

(iii) There holds the following equation.

$$^tAAx - \ ^tAs = 0. \qquad\qquad (9)$$

Corollary 2.3

If $^t A A$ is regular then the LSS to (7) is unique.

Lemma 2.4

For any $A \in M_{mn}(\mathbb{R})$,

$$\mathrm{rank}(^t A A) = \mathrm{rank}(A).$$

Corollary 2.5

Let $A \in M_{mn}$, $m \geq n$. If $\mathrm{rank}(A) = n$ then $^t A A$ is regular.

Lemma 2.6

For any $A \in M_{mn}(\mathbb{R})$ and $s \in \mathbb{R}^m$, there always exists a solution to (9). Futhermore, if $m \geq n$ and $\mathrm{rank}(A) = n$ then the solution to (9) is unique.

On the data of the X-rays in (7)

- In G.N. Hounsfield's CT, $m \approx const \times 10^6, \ n \approx 3 \times 10^5$
- In the present-day CT, $m \approx 5 \times 10^9, \ n \approx 3 \times 10^7$ and
- The pixel size in the present-day high precision CT is about (a few μm)^2.

ART
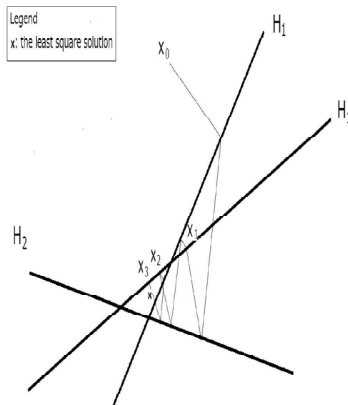
Figure 1:　Image of ART

$$a_i =: (a_{i1}, a_{i2}, \cdots, a_{in}), \quad i = 1, 2, \cdots, m \tag{10}$$

$$H_i : a_{i1}x_1 + a_{i2}x_2 + \cdots + a_{in}x_n = s_i \tag{11}$$

H_i : a hyperplane whose normal vector is a_i

Orthogonal projection $P_i x$ of $x \in \mathbb{R}^n$ to H_i is given by

$$P_i x := x - \frac{a_i \cdot x - s_i}{\|a_i\|} \frac{a_i}{\|a_i\|} \tag{12}$$

Take a suitable $\boldsymbol{x_0} \in \mathbb{R}^n$ and define the sequence $\{\boldsymbol{x_k}\}$ by

$$\boldsymbol{x_k} := P\boldsymbol{x_{k-1}} \equiv P_m P_{m-1} \cdots P_1 \boldsymbol{x_{k-1}}, \ k = 1, 2, \cdots$$

G.N. Hounsfield's algorithm for CT

$$\boldsymbol{x^H} := \lim_{k \to \infty} \boldsymbol{x_k} \approx \boldsymbol{x} \qquad (13)$$

Theoretical justification of Hounsfield's idea

$$\boldsymbol{s} = \boldsymbol{s_c^0} + \boldsymbol{s_c^{app}} + \boldsymbol{s_c^{obs}}, \qquad (14)$$

$\boldsymbol{s_c^0} := A\boldsymbol{x^0}$ with

$$\boldsymbol{x^0} = (x_1^0, \cdots, x_n^0), \ x_j^0 := \frac{1}{c} \int_{c_j} f(x, y) dx dy \qquad (15)$$

$$s_c^{app} := ((s_c^{app})_1, \cdots, (s_c^{app})_m) \text{ with } (s_c^{app})_i = \int_{l_i} f(x,y)dl - (s_c^0)_i$$

$$s_c^{obs} = s_X := (s_1^X, \cdots, s_m^X)$$

$s_i^X, \ i = 1, \cdots, m,$ being random variables whose probability density functions are supported by $[-\varepsilon_i, \varepsilon_i]$ for small $\varepsilon_i > 0$ and whose expectation value $E(s_i^X)$ is 0.

Theorem 2.7

We know by experience that even for a fixed number n, the larger the number m is, the better resolution we can obtain. This knowledge by experience is proved to be stochastic theoretically right.

Theorem 2.8 ((T, 2019))

The pixel function

$$g_c(x, y) := \sum_{j=1}^{n} x_j \chi_{c_j}(x, y). \tag{16}$$

converges almost surely to the density distribution function $f(x, y)$, that is,

$$\lim_{c \to 0} g_c(x, y) = f(x, y), \quad a.s. \tag{17}$$

3. Ultrasonic Imaging

Theorem 3.1

If we assume that the ultrasound rectilinearly propagates then the fastest route between the two boundary points $\alpha, \beta \in \partial\Omega$ becomes the segment $l(\alpha, \beta)$

$$l(\alpha, \beta) = \{t\alpha + (1 - t)\beta \mid 0 < t < 1\} \tag{18}$$

between α and β. In this case, the integral (1) is the line integral along the segment between the two boundary points $\alpha, \beta \in \partial\Omega$. Therefore, if the ultrasound rectilinearly propagates then Problem 1.1 becomes the inverse problems of the X-ray transform by identifying $f(x) = 1/C(x)$ for $x \in \mathbb{R}^2$ or $\mathbb{R}^3$.

A reiterating numarical algorithm for USI

1. Divide the object into boxels.

2. Assume that the ultrasound rectilinearly propagates and apply the idea by Hounsfield to obtain the boxel function g_1.

3. Taking the boxel function g_1 obtained in the procedure **2.** as the first image, we can calculate the new orbit of the ultrasound.

4. Change the elements a_{ij} of the matrix by the length of intersection between the new orbit of the i-th ultrasound and j-th boxel.

5. Give the least square solution g_2 to (7) with new matrix elements gives better approximation.

6. Taking the boxel function g_2 as the second image and repeat the same procedure to obtain a better approximation boxel function g_3 than g_2.

7. Repeat the above procedure until $\sup_{1 \le k \le n} |g_{k+1} - g_k|$ is sufficiently small.

Problem 3.2

Assume that the distribution $C(x)$ of the velocity , $x \in \Omega \subset \mathbb{R}^3$ is known. For any $\alpha, \beta \in \partial\Omega$, determine the fastest route γ from α to β though Ω, that is,

$$\min_{\gamma_{\alpha,\beta}} \int_{\gamma_{\alpha,\beta}} 1/C(x)d\gamma = \int_{\gamma} 1/C(x)d\gamma. \tag{19}$$

4. Conclusion

Conclusion of this talk

■ We introduced theoretical justification how Hounsfield's algorithm worked well for practicalization of CT (Theorem 2.8).

■ We have introduced a numerical solution to USI, where Hounsfield's idea plays an important role.

Open problems left for further development

- Analytic solution to Problem 1.1
- A better numerical approach to USI than ours
- Solution to Problem 3.2

Regularity of solutions to the stationary transport equation and its application to the optical tomography

Daisuke Kawagoe [*]

2019/10/30

Abstract

We consider a boundary value problem of the stationary transport equation in a bounded convex domain with the incoming boundary condition, and we obtain two results on regularity of its solutions. The first result is to describe discontinuity of the solution which arises from discontinuous points of the incoming boundary condition, and we show the exponential decay of a jump of the solution on a discontinuous point. The second one is to give a precise estimate in a two dimensional case. We obtain a $W^{1,p}$ estimate of the solution for $1 \le p < p_m$, where p_m is a real number depending only on the shape of the domain. These two results are applied to solve the inverse problem to determine a coefficient of the stationary transport equation, which is a model of the optical tomography.

0 Introduction

The optical tomography is a new noninvasive medical imaging technology using near-infrared light [5], and it is mathematically modeled by the inverse problem to determine a coefficient in the stationary transport equation (STE).

STE is an integro-differential equation of the following form

$$\xi \cdot \nabla_x f(x,\xi) + \mu_t(x) f(x,\xi) = \mu_s(x) \int_{S^{d-1}} p(x,\xi,\xi') f(x,\xi') \, d\sigma_{\xi'}. \tag{1}$$

Here, the function $f(x,\xi)$ represents density of photon at a position $x \in \mathbb{R}^d$ with a direction $\xi \in S^{d-1}$. In STE, we focus on two phenomena inside a media; absorption and scattering. We consider STE (1) in the pair of a bounded convex domain Ω in $\mathbb{R}^d$ ($d = 2$ or 3) with C^1 boundary and the unit sphere S^{d-1}.

We introduce a notion of "boundaries" associated with STE. Let Ω be a bounded convex domain in $\mathbb{R}^d$ with the C^1 boundary. Then, we can define the outer unit normal vector $n(x)$ to $\partial\Omega$ for all $x \in \partial\Omega$. The outgoing boundary Γ_+ and the incoming boundary Γ_- are defined by

$$\Gamma_{\pm} := \{(x,\xi) \in \partial\Omega \times S^{d-1} | \pm n(x) \cdot \xi > 0\},$$

respectively. Here, $n(x) \cdot \xi$ denotes the Euclid inner product of two vectors $n(x)$ and ξ in $\mathbb{R}^d$.

We pose the incoming boundary condition to STE (1): Let f_0 be a given function on Γ_-. Then, the incoming boundary condition reads

$$f(x,\xi) = f_0(x,\xi) \text{ on } \Gamma_-. \tag{2}$$

The final goal of this research is to solve the inverse problem to determine the coefficient μ_t in STE (1) from boundary measurements; f_0 and $f|_{\Gamma_+}$, where f is a solution to the boundary value problem (1)–(2). This inverse problem was already solved mathematically using the albedo operator

---

[*]d.kawagoe@acs.i.kyoto-u.ac.jp

[6] [9] [14]. However, it is quite difficult to observe the albedo operator in a practical situation. This motivates us to consider another approach to solve the inverse problem in a practical setting. In this note, we discuss two approaches.

The first one is to make use of propagation of the boundary-induced discontinuity, which is discontinuity of a solution to the boundary value problem (1)-(2) arising from discontinuous incoming boundary data. We will see the detail in Section 1.

Anikonov et al. [3] also made use of it in order to solve the inverse problem. They showed that a jump of the boundary-induced discontinuity propagates along a positive characteristic line when the boundary data has a jump with respect to direction ξ, and it is observed as a jump of the outgoing boundary data on a discontinuous point, which locates on the tip of the characteristic line. The exponential decay of the jump contains information about the X-ray transform of the attenuation coefficient μ_t, which is defined by

$$(X\mu_t)(x,\xi) := \int_{\mathbb{R}} \mu_t(x - r\xi)\, dr, \quad (x,\xi) \in \mathbb{R}^d \times S^{d-1}.$$

They applied the inverse X-ray transform to the observed data in order to determine the unknown coefficient μ_t from its image $X\mu_t$ [13].

On the other hand, a jump of the boundary-induced discontinuity also propagates along a positive characteristic line when the boundary data has a jump with respect to space x. Aoki et al. [4] showed this property for the case of the two dimensional half homogeneous space with an incoming boundary data independent of ξ. In this note, we extend the result in [4] to a bounded convex domain. In addition to the discontinuity with respect to direction ξ, which is presented in Anikonov et al [3], we also discuss the discontinuity with respect to space x.

The second one is by iterative numerical computation [12]. In particular, we apply the discrete-ordinate discontinuous Galerkin method as a numerical scheme. Although its numerical analysis was done by Han et al. [11] under the assumption that the gradient of the solution to the boundary value problem (1)-(2) belongs to $L^2(\Omega \times S^{d-1})$, it is not known under which condition the above assumption holds true. In section 2, we consider a bounded convex domain of two dimensions with the C^2 boundary in order to obtain an L^p estimate for the gradient $\nabla_x f$ for $1 \le p < p_m$, where p_m is a real number depending only on the shape of the boundary $\partial\Omega$. Moreover, with the polar coordinate $\xi = (\cos\theta, \sin\theta)$, we also obtain an L^p estimate for the derivative f_θ with respect to θ for $1 \le p < p_m$.

There are few researches about estimates for the gradient $\nabla_x f$ of the solution f. Anikonov [2] gave a formula of the gradient to see its unboundedness. We should note that Agoshkov [1] also analyzed regularity of the solution in a Besov space, although he did not give an L^p estimate for the gradient.

1 Propagation of boundary-induced discontinuity in stationary radiative transfer

In this section, we describe propagation of the boundary-induced discontinuity under the following setting.

Let Ω be a bounded convex domain in $\mathbb{R}^d$ with the C^1 boundary $\partial\Omega$. We assume that $\overline{\Omega} = \cup_{j=1}^{N} \overline{\Omega_j}$, where Ω_j, $1 \le j \le N$, are disjoint (open) subdomains of Ω with piecewise C^1 boundaries. Let $\Omega_0 := \cup_{j=1}^{N} \Omega_j$. We assume that, for all $(x,\xi) \in \Omega \times S^{d-1}$, the half line $\{x - t\xi | t \ge 0\}$ intersects with $\partial\Omega_0$ at most finite times. In other words, for all $(x,\xi) \in \Omega \times S^{d-1}$, there exist positive integer $l(x,\xi)$ and real numbers $\{t_j(x,\xi)\}_{j=1}^{l(x,\xi)}$ such that $0 \le t_1(x,\xi) < t_2(x,\xi) < \cdots < t_{l(x,\xi)}(x,\xi)$, $x - t\xi \in \partial\Omega_0$ if and only if $t = t_j(x,\xi)$, and $\sup_{(x,\xi)\in\Omega\times S^{d-1}} l(x,\xi) < \infty$. This assumption is called generalized convexity condition for Ω_0 [3]. In what follows, we use these notations $t_j(x,\xi)$ and $l(x,\xi)$ for the generalized convexity, and we put $t_0(x,\xi) = 0$.

We assume that μ_t and μ_s are nonnegative bounded functions on $\mathbb{R}^d$ such that μ_t and μ_s are continuous on Ω_0, $\mu_t(x) \ge \mu_s(x)$ for $x \in \Omega_0$, $\mu_t(x) = \mu_s(x) = 0$ for $x \in \mathbb{R}^d\backslash\Omega_0$, and discontinuity may occur only at $\partial\Omega_0$. We also assume that the integral kernel p is a nonnegative bounded

function on $\mathbb{R}^d \times S^{d-1} \times S^{d-1}$ which is continuous on $\Omega_0 \times S^{d-1} \times S^{d-1}$ and $p(x, \xi, \xi') = 0$ for $(x, \xi, \xi') \in (\mathbb{R}^d \backslash \Omega_0) \times S^{d-1} \times S^{d-1}$, and satisfies

$$\int_{S^{d-1}} p(x, \xi, \xi') \, d\sigma_{\xi'} = 1$$

for all $(x, \xi) \in \Omega_0 \times S^{d-1}$. We regard the directional derivative $\xi \cdot \nabla_x f(x, \xi)$ as

$$\xi \cdot \nabla_x f(x, \xi) := \frac{d}{dt} f(x + t\xi, \xi) \Big|_{t=0}.$$

Finally, the measure $d\sigma_{\xi'}$ is the Lebesgue measure on the sphere S^{d-1}.

We introduce some notations. Let

$$D := (\Omega \times S^{d-1}) \cup \Gamma_-, \quad \overline{D} := D \cup \Gamma_+,$$

and we define two functions $\tau_\pm$ on $\overline{D}$ by

$$\tau_\pm(x, \xi) := \inf\{t > 0 | x \pm t\xi \notin \Omega\}.$$

Let $\Gamma_{-,\xi}$ and $\Gamma_{-,x}$ be projections of Γ_- on $\partial\Omega$ and S^{d-1} respectively;

$$\Gamma_{-,\xi} := \{x \in \partial\Omega | n(x) \cdot \xi < 0\}, \quad \xi \in S^{d-1}$$

and

$$\Gamma_{-,x} := \{\xi \in S^{d-1} | n(x) \cdot \xi < 0\}, \quad x \in \partial\Omega.$$

Let $\mathrm{disc}(f)$ be a set of the discontinuous points for a function f.

We define a solution to the boundary value problem (1)-(2). We call a bounded measurable function f on D a solution to the boundary value problem (1)-(2) if (i) it has the directional derivative $\xi \cdot \nabla_x f(x, \xi)$ at all $(x, \xi) \in \Omega_0 \times S^{d-1}$, (ii) it satisfies the stationary transport equation (1) for all $(x, \xi) \in \Omega_0 \times S^{d-1}$ and the boundary condition (2) for all $(x, \xi) \in \Gamma_-$, (iii) $f(\cdot, \xi)$ is continuous along the line $\{x + t\xi | t \in \mathbb{R}\} \cap (\Omega \cup \Gamma_{-,\xi})$ for all $(x, \xi) \in D$, and (iv) $\xi \cdot \nabla_x f(\cdot, \xi)$ is continuous on the open line segments $\{x - t\xi | t \in (t_{j-1}(x, \xi), t_j(x, \xi))\}$, $j = 1, \ldots, l(x, \xi)$ with $t_0(x, \xi) = 0$ for all $(x, \xi) \in \Omega_0 \times S^{d-1}$.

The first main result shows how the boundary-induced discontinuity propagates in the media.

Theorem 1. *Suppose that a boundary data f_0 is bounded and that it satisfies at least one of the following two conditions.*

1. *$f_0(x, \cdot)$ is continuous on $\Gamma_{-,x}$ for almost all $x \in \partial\Omega$,*

2. *$f_0(\cdot, \xi)$ is continuous on $\Gamma_{-,\xi}$ for almost all $\xi \in S^{d-1}$.*

Then, there exists a unique solution f to the boundary value problem (1)-(2), and we have

$$\mathrm{disc}(f) = \{(x_* + t\xi_*, \xi_*) | (x_*, \xi_*) \in \mathrm{disc}(f_0), 0 \le t < \tau_+(x_*, \xi_*)\}.$$

Theorem 1 shows that the boundary-induced discontinuity propagates only along a positive characteristic line starting from a discontinuous point of the incoming boundary data. Here, a positive characteristic line from a point $(x, \xi) \in \Gamma_-$ is defined by $\{(x + t\xi, \xi) | t \ge 0\}$.

Remark 1. Theorem 1 implies that, for a bounded continuous boundary data f_0 on Γ_-, there exists a unique solution f, which is bounded continuous on D.

Remark 2. Anikonov et al. [3] showed Theorem 1 with the condition 2. Our main contribution is to show Theorem 1 with the condition 1.

As the second main result, we shall discuss the boundary-induced discontinuity of the solution extended up to Γ_+. In other words, we can extend the domain of the solution f up to Γ_+, and we see that the boundary-induced discontinuity propagates along a positive characteristic line up to Γ_+.

Theorem 2. *Let a boundary data f_0 satisfy assumptions in Theorem 1 and let f be the solution to the boundary value problem* (1)-(2). *Then, it can be extended up to Γ_+, which is denoted by $\overline{f}$, by*

$$\overline{f}(x,\xi) := \begin{cases} f(x,\xi), & (x,\xi) \in D, \\ \lim_{t\downarrow 0} f(x - t\xi, \xi), & (x,\xi) \in \Gamma_+. \end{cases}$$

Moreover, we have

$$\mathrm{disc}(\overline{f}) = \{(x_* + t\xi_*, \xi_*) | (x_*, \xi_*) \in \mathrm{disc}(f_0), 0 \leq t \leq \tau_+(x_*, \xi_*)\}.$$

We state the decay of the boundary-induced discontinuity in some situation. Let γ be two points in $\partial\Omega$ when $d = 2$, while let γ be a simple closed curve in $\partial\Omega$ when $d = 3$. Then, γ splits $\partial\Omega$ into two connected components A and B, that is $\partial\Omega = A \cup B \cup \gamma$ and $A \cap B = A \cap \gamma = B \cap \gamma = \emptyset$. We put an incoming boundary data f_0 by

$$f_0(x,\xi) = \begin{cases} I, & (x,\xi) \in ((A \cup \gamma) \times S^{d-1}) \cap \Gamma_-, \\ 0, & (x,\xi) \in (B \times S^{d-1}) \cap \Gamma_-, \end{cases} \tag{3}$$

where I is a non-zero constant. We note that f_0 satisfies the condition 1 of Theorem 1, and that $\mathrm{disc}(f_0) = \{(x_*, \xi_*) | x_* \in \gamma, \xi_* \in \Gamma_{-,x_*}\}$.

For $(\overline{x}, \overline{\xi}) \in \mathrm{disc}(\overline{f})$, we define a jump $[\overline{f}](\overline{x}, \overline{\xi})$ by

$$[\overline{f}](\overline{x}, \overline{\xi}) := \lim_{\substack{x \to \overline{x} \\ P(x,\overline{\xi}) \in (A \cup \gamma)}} f(x, \overline{\xi}) - \lim_{\substack{x \to \overline{x} \\ P(x,\overline{\xi}) \in B}} f(x, \overline{\xi}),$$

where

$$P(x,\xi) := x - \tau_-(x,\xi)\xi.$$

We note that, in our situation, $[f_0](x,\xi) = I$ for all $(x,\xi) \in \mathrm{disc}(f_0) = (\gamma \times S^{d-1}) \cap \Gamma_-$. In this situation, we have the following theorem, which is the most important in this paper.

Theorem 3. *Let $\overline{f}$ be the extended solution to the boundary value problem* (1)-(2) *with the incoming boundary data given by* (3), *and let $(x^*, \xi^*) \in \mathrm{disc}(\overline{f})$. Then,*

$$[\overline{f}](x^*, \xi^*) = I \exp\left(-\int_0^{\tau_-(x^*,\xi^*)} \mu_t(x^* - r\xi^*)\,dr\right).$$

In particular, we take a point $(x^*, \xi^*) \in \mathrm{disc}(\overline{f}) \cap \Gamma_+$. From Theorem 3, we have

$$X\mu_t(x^*, \xi^*) = \int_0^{\tau_-(x^*,\xi^*)} \mu_t(x^* - r\xi^*)\,dr = -\log\left([\overline{f}](x^*, \xi^*)/I\right).$$

The right hand side is obtained from observed data. By arranging γ, we can observe the image $X\mu_t$ of the X-ray transform of μ_t. Then, applying the well-known method in [13], we can reconstruct the attenuation coefficient μ_t.

We omit proofs of the above theorems in this note. For detail, see [8].

2 $W^{1,p}$ estimate for solutions to the stationary transport equation

In this section, we give a $W^{1,p}$ estimate of the solution to the boundary value problem (1)-(2) for $1 \leq p < p_m$, where p_m is a real number depending only on the shape of the domain.

We introduce a condition for the domain Ω as follows.

Definition 1. Let $m \geq 2$ or ∞, and let Ω be a bounded convex domain in $\mathbb{R}^2$ with C^2 boundary. We say that the boundary $\partial\Omega$ has the uniform outer generalized contact order m if there exist positive numbers a and δ such that the following statement holds: For a point $y_0 \in \partial\Omega$, we choose a Cartesian coordinates system (x_1, x_2) so that $y_0 = (0,0)$ and $n(y_0) = (0,-1)$ in the system. Then, the curve $x_2 = a|x_1|^m$, $|x_1| < \delta$ touches the boundary $\partial\Omega$ at y_0 from outside of Ω.

We assume that μ_t and μ_s are nonnegative functions in $W^{1,\infty}(\Omega)$ such that $\mu_t(x) \geq \mu_s(x)$ for almost all $x \in \Omega$. We also assume that there exists a nonnegative function $\tilde{p}$ in $W^{1,\infty}(\Omega \times (-1, 1))$ such that

$$p(x, \xi, \xi') = \tilde{p}(x, \xi \cdot \xi')$$

for almost all $(x, \xi, \xi') \in \Omega \times S^1 \times S^1$ and

$$\int_{S^1} \tilde{p}(x, \xi \cdot \xi') \, d\sigma_{\xi'} = 1$$

for almost all $(x, \xi) \in \Omega \times S^1$. For simplicity, in what follows, we only consider $\tilde{p}$ and omit the tilde on p.

We introduce a function space $W^{1,\infty}(\Gamma_-)$. Firstly, we define the derivative on the boundary $\nabla_{x,v} f_0(x, \xi)$ by

$$\nabla_{x,v} f_0(x, \xi) := \frac{d}{dt} f_0(g(t), \xi),$$

where $g : (-\delta, \delta) \to \partial\Omega$ with a small number δ is a local parametrization of $\partial\Omega$ around x such that

$$g(0) = x, \quad g'(0) = v.$$

Also, we introduce the polar coordinate $\xi = (\cos\theta, \sin\theta)$ to identify the unit circle S^1 with the interval $[-\pi, \pi]$. Then, the function space $W^{1,\infty}(\Gamma_-)$ is defined by

$$W^{1,\infty}(\Gamma_-) := \{f_0 \in L^\infty(\Gamma_-) | \|f_0\|_{W^{1,\infty}} < \infty\},$$

where

$$\|f_0\|_{W^{1,\infty}(\Gamma_-)} := \|f_0\|_{L^\infty(\Gamma_-)} + \|\nabla_x f_0\|_{L^\infty(\Gamma_-)} + \|f_{0,\theta}\|_{L^\infty(\Gamma_-)},$$

$$\|\nabla_x f_0\|_{L^\infty(\Gamma_-)} := \operatorname*{esssup}_{(x,\xi) \in \Gamma_-} \left(\operatorname*{esssup}_{\substack{v \in T_x(\partial\Omega) \\ |v|=1}} |\nabla_{x,v} f_0(x, \xi)| \right),$$

$T_x(\partial\Omega)$ is the tangent space at $x \in \partial\Omega$, and $f_{0,\theta}$ is the first derivative of the function f_0 with respect to θ. We assume that the boundary data f_0 belongs to $W^{1,\infty}(\Gamma_-)$.

The main result in this section is the following:

Theorem 4. *Suppose that the boundary $\partial\Omega$ has the uniform outer generalized contact order m. Then, the solution f to the boundary value problem (1)-(2) belongs to $W^{1,p}(\Omega \times S^1)$ for $1 \leq p < p_m$, where $p_m := 2 + 1/(m-1)$.*

Here, a solution f to the boundary value problem (1)-(2) satisfies the stationary transport equation (1) and the boundary condition (2) almost everywhere. We show existence and uniqueness of a solution to the boundary value problem (1)-(2) in the L^p sense.

As a corollary, we obtain the following estimate, which answers to our original question.

Corollary 1. *Suppose that the boundary $\partial\Omega$ has the uniform outer generalized contact order $m > 2$. Then, the solution f to the boundary value problem (1)-(2) belongs to $W^{1,2}(\Omega \times S^1)$.*

The outline of a proof is the following. We reduce the boundary value problem (1)-(2) into the following integral equation.

$$f(x, \xi) = F_0(x, \xi) + F_1(x, \xi) + F_2(x, \xi),$$

where

$$F_0(x,\xi) := \exp\left(-\int_0^{\tau_-(x,\xi)} \mu_t(x-r\xi)\,dr\right) f_0(P(x,\xi),\xi),$$

$$F_1(x,\xi) := \int_0^{\tau_-(x,\xi)} \mu_s(x-t\xi)\exp\left(-\int_0^t \mu_t(x-r\xi)\,dr\right) G_1(x-t\xi,\xi')\,dt,$$

$$F_2(x,\xi) := \int_0^{\tau_-(x,\xi)} \mu_s(x-t\xi)\exp\left(-\int_0^t \mu_t(x-r\xi)\,dr\right) G_2(x-t\xi,\xi')\,dt,$$

$$G_1(x,\xi) := \int_{S^1} p(x,\xi\cdot\xi')F_0(x,\xi')\,d\sigma_{\xi'},$$

$$G_2(x,\xi) := \int_{S^1} p(x,\xi\cdot\xi')\int_0^{\tau_-(x,\xi')} \mu_s(x-t\xi')\exp\left(-\int_0^t \mu_t(x-r\xi')\,dr\right)$$

$$\times \int_{S^1} p(x-t\xi',\xi'\cdot\xi'')f(x-t\xi',\xi'')\,d\sigma_{\xi''}\,dt\,d\sigma_{\xi'}$$

$$= \int_\Omega p\left(x,\xi\cdot\frac{x-y}{|x-y|}\right)\mu_s(y)\exp\left(-|x-y|\int_0^1 \mu_t(x-r(x-y))\,dr\right)$$

$$\times \left(\int_{S^1} p\left(y,\frac{x-y}{|x-y|}\cdot\xi''\right)f(y,\xi'')\,d\sigma_{\xi''}\right)\frac{dy}{|x-y|}.$$

Thanks to the above formula, we can consider the formal derivative of the solution f. However, a strong singularity appears after the differentiation. In order to control the singularity, we first derive a local Hölder estimate for the solution with respect to x. This estimate helps us to prove differentiability of the solution with respect to x. After justification of the differentiation, we investigate an L^p estimates of spatial derivatives of the solution. We further use these estimates to obtain an L^p estimate for the derivative of the solution with respect to θ. We omit the detail of the proof because the calculation is quite complicated and tedious.

References

[1] V. Agoshkov, *Boundary value problems for transport equations. Modeling and simulation in science, Engineering and Technology*, Birkhäuser, Boston, (1998).

[2] D. S. Anikonov, A formula for the gradient of the transport equation solution, *J. Inv. Ill-Posed Prob.*, **4**, no. 2, pp. 85–100, (1996).

[3] D. S. Anikonov, I. V. Prokhorov, A. E. Kovtanyuk, Investigation of scattering and absorbing media by the methods of X-ray tomography, *J. Inv. Ill-Posed Problems*, **1**, no. 4, pp. 259–281, (1993).

[4] K. Aoki, C. Bardos, C. Dogbe, F. Golse, A note on the propagation of boundary induced discontinuities in kinetic theory, *Math. Models Methods Appl. Sci.* **11**, no. 9 pp. 1581–1595, (2001).

[5] S. R. Arridge, J. C. Schotland, Optical tomography: forward and inverse problems, *Inverse Problems*, **25**, no. 12, 123010, 59 pp., (2009)

[6] G. Bal, A. Jollivet, Stability estimates in stationary inverse transport, *Inverse Probl. Imaging*, **2**, no. 4, pp. 427–454, (2008).

[7] I.-K. Chen, C.-H. Hsia, D. Kawagoe, Regularity for diffuse reflection boundary problem to the stationary linearized Boltzmann equation in a convex domain, *Ann. Inst. Henri Poincaré*, **36**, no. 3, pp. 745–782, (2019).

[8] I. Chen, D. Kawagoe, Propagation of boundary-induced discontinuity in stationary radiative transfer and its application to the optical tomography, *Inverse Problems & Imaging* **13** no. 2, pp. 337–351, (2019).

[9] M. Choulli, P. Stefanov, An inverse boundary value problem for the stationary transport equation, *Osaka J. Math.*, **36**, no. 1, pp. 87–104, (1999).

[10] H. Egger, M. Schlottbom, An L^p theory for stationary radiative transfer, *Applicable Analysis*, **93**, no. 6, pp. 1283–1296, (2014).

[11] W. Han, J. Huang, J. A. Eichholz, Discrete-ordinate discontinuous Galerkin methods for solving the radiative transfer equation, *SIAM J. Sci. Comput.*, **20**, no. 2, pp. 477–497, (2010).

[12] A. D. Klose, A. H. Hielscher, Optical tomography using the time-independent equation of radiative transfer–Part 2: inverse model, *J. Quant. Spect. Rad. Trans.*, **72**, pp. 715–732, (2002).

[13] F. Natterer, *The Mathematics of Computerized Tomography*, SIAM, Germany, (2001).

[14] J.-N. Wang, Stability estimates of an inverse problem for the stationary transport equation, *Ann. Inst. Henri Poincaré*, **70**, pp. 473–495, (1999).

Regularity of solutions to the stationary transport equation and its application to the optical tomography

Daisuke Kawagoe

Graduate School of Informatics, Kyoto University

2019/10/30

Optical Tomography (OT)

- A new medical imaging technology
- Using near-infrared light
- Noninvasive
- Related to brain science
  (cf. MRI)

(https://neurosciencenews.com/alzheimers-brain-activity-8803/)
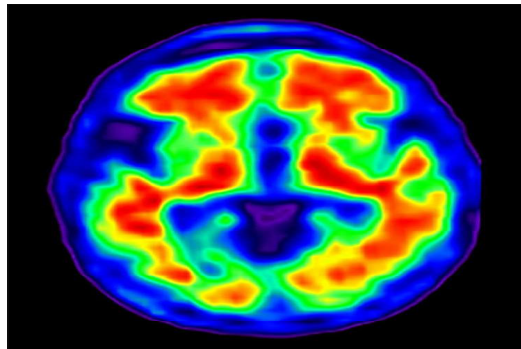
Property of near-infrared light

Transillumination imaging of blood vessels

① 47 mm thickness ③ 67 mm thickness

② 53 mm thickness ④ 58 mm thickness
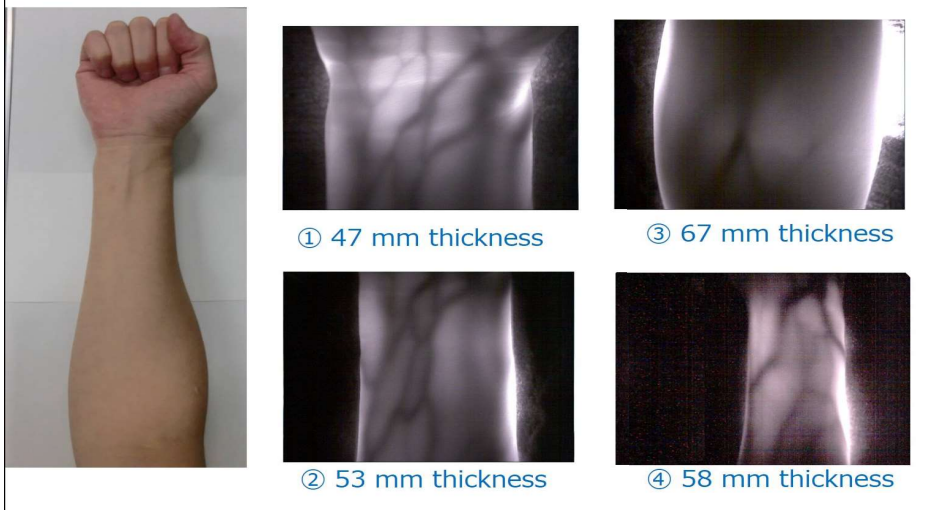
(https://www.ist.hokudai.ac.jp/netjournal/net_35_ex.html)

Stationary Transport Equation (STE)

Stationary transport equation

$$\xi \cdot \nabla_x f(x,\xi) + \mu_t(x) f(x,\xi) = \mu_s(x) \int_{S^{d-1}} p(x,\xi,\xi') f(x,\xi') \, d\sigma_{\xi'}. \tag{1}$$

- $x = (x_1, \ldots, x_d) \in \Omega \subset \mathbb{R}^d, \ (d = 2, 3)$
  Ω : a bounded convex domain, C^1 boundary
- $\xi = (\xi_1, \ldots, \xi_d) \in S^{d-1}$ (the unit sphere)
- $f(x,\xi)$: density of photon at a position x with a direction ξ
- μ_t : the attenuation coefficient
- μ_s : the scattering coefficient
- p : the scattering phase function

Incoming boundary condition

- Ω : a bounded convex domain, C^1 boundary
- $\Gamma_\pm := \{(x,\xi) \in \partial\Omega \times S^{d-1} | \pm n(x) \cdot \xi > 0\}$
- $n(x)$: the outer normal vector at $x \in \partial\Omega$
- f_0 : given on Γ_-

Incoming boundary condition

$$f(x,\xi) = f_0(x,\xi), \quad (x,\xi) \in \Gamma_-. \tag{2}$$
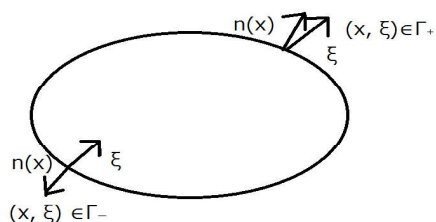
Motivation

Problem

To reconstruct the attenuation coefficient μ_t from boundary data, f_0 and $f|_{\Gamma_+}$, with μ_s and p unknown.

$$\begin{cases} \xi \cdot \nabla_x f(x,\xi) + \mu_t(x)f(x,\xi) = \mu_s(x) \int_{S^{d-1}} p(x,\xi,\xi')f(x,\xi')\,d\sigma_{\xi'}, \\ \qquad\qquad\qquad\qquad\qquad\qquad\qquad\qquad (x,\xi) \in \Omega \times S^{d-1}, \\ f(x,\xi) = f_0(x,\xi), \quad (x,\xi) \in \Gamma_- \end{cases}$$

Conventional approach

Albedo operator

$$\mathcal{A} : f_0 \mapsto f|_{\Gamma_+}.$$

- M. Choulli, P. Stefanov, An inverse boundary value problem for the stationary transport equation, *Osaka J. Math.*, **36**, no. 1, pp. 87–104, (1999)
- J. N. Wang, Stability estimates of an inverse problem for the stationary transport equation, *Ann. Inst. Henri Poincaré*, **70**, pp. 473–495, (1999)
- G. Bal, A. Jollivet, Stability estimates in stationary inverse transport, *Inverse Prob. Imaging*, **2**, no. 4, pp. 427–454, (2008)

Not practical! $\rightarrow$ Another approach?

Two practical(?) approaches

1. theoretical approach
   propagation of boundary-induced discontinuity

2. numerical approach

1. Propagation of boundary-induced discontinuity in stationary radiative transfer

Joint work with I-Kun Chen (National Taiwan University)

Assumptions

- $\Omega \subset \mathbb{R}^d$, $d = 2$ or 3: bounded convex , with C^1 boundary $\partial\Omega$
- $\overline{\Omega} = \cup_{j=1}^{N} \overline{\Omega_j}$
- Ω_j, $1 \leq j \leq N$: disjoint subdomains of Ω with piecewise C^1 boundaries
- $\Omega_0 := \cup_{j=1}^{N} \Omega_j$
- Generalized convexity: for all $(x, \xi) \in \Omega \times S^{d-1}$, there exist a positive integer $l(x, \xi)$ and real numbers $\{t_j(x, \xi)\}_{j=0}^{l(x,\xi)}$ such that $0 \leq t_0(x, \xi) < t_1(x, \xi) < \cdots < t_{l(x,\xi)}(x, \xi)$, $x - t\xi \in \partial\Omega_0$ if and only if $t = t_j(x, \xi)$, and

$$\sup_{(x,\xi)\in\Omega\times S^{d-1}} l(x, \xi) < \infty.$$

Generalized convexity
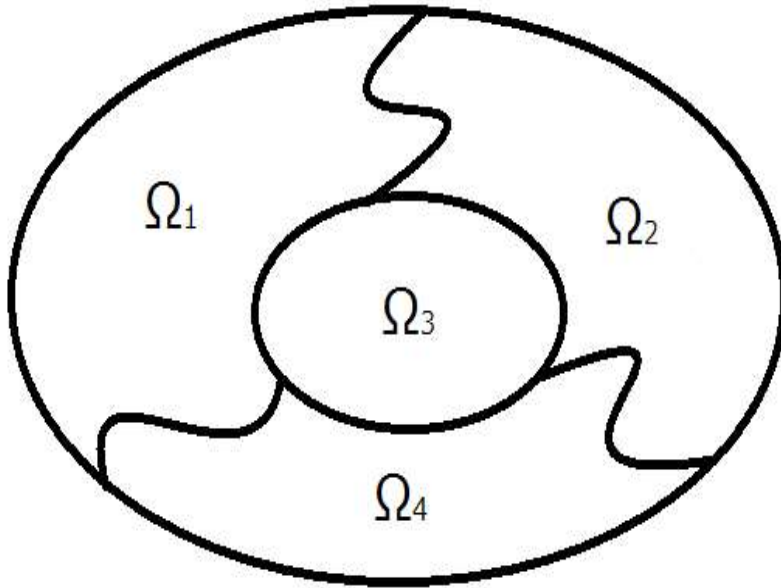
Assumptions

- μ_t, μ_s nonnegative bounded functions on $\mathbb{R}^d$ such that
  - continuous on Ω_0,
  - $\mu_t(x) \geq \mu_s(x)$ for $x \in \Omega_0$,
  - $\mu_t(x) = \mu_s(x) = 0$ for $x \in \mathbb{R}^d \backslash \Omega_0$

- p: a nonnegative bounded function on $\mathbb{R}^d \times S^{d-1} \times S^{d-1}$ such that
  - continuous on $\Omega_0 \times S^{d-1} \times S^{d-1}$,
  - $p(x, \xi, \xi') = 0$ for $(x, \xi, \xi') \in (\mathbb{R}^d \backslash \Omega_0) \times S^{d-1} \times S^{d-1}$,
  - $\int_{S^{d-1}} p(x, \xi, \xi') \, d\sigma_{\xi'} = 1$ for all $(x, \xi) \in \Omega_0 \times S^{d-1}$.

- $\xi \cdot \nabla_x f(x, \xi) := \frac{d}{dt} f(x + t\xi, \xi)|_{t=0}$.

- $d\sigma_{\xi'}$: the Lebesgue measure on the unit sphere S^{d-1}.

Notations

- $D := (\Omega \times S^{d-1}) \cup \Gamma_-$.

- $\tau_\pm(x, \xi) := \inf\{t > 0 | x \pm t\xi \notin \Omega\}$.

- $P(x, \xi) := x - \tau_-(x, \xi)\xi$.

- $\Gamma_{-,\xi} := \{x \in \partial\Omega | n(x) \cdot \xi < 0\}, \quad \xi \in S^{d-1}$.

- $\Gamma_{-,x} := \{\xi \in S^{d-1} | n(x) \cdot \xi < 0\}, \quad x \in \partial\Omega$.

- disc(f): the set of discontinuous points of a function f

Main results

Theorem 1 (Chen, K.)

Suppose that a boundary data f_0 is bounded and that it satisfies at least one of the following two conditions.

1. $f_0(x, \cdot)$ is continuous on $\Gamma_{-,x}$ for almost all $x \in \partial\Omega$,
2. $f_0(\cdot, \xi)$ is continuous on $\Gamma_{-,\xi}$ for almost all $\xi \in S^{d-1}$.

Then, there exists a unique solution f to the boundary value problem (1)-(2), and we have

$$\text{disc}(f) = \{(x_* + t\xi_*, \xi_*) | (x_*, \xi_*) \in \text{disc}(f_0), 0 \le t < \tau_+(x_*, \xi_*)\}.$$

Remark

Definition

we call a bounded function f on D a solution to the boundary value problem (1)-(2) if it has the directional derivative $\xi \cdot \nabla_x f(x, \xi)$ at all $(x, \xi) \in \Omega_0 \times S^{d-1}$, if it satisfies the stationary transport equation (1) for all $(x, \xi) \in \Omega_0 \times S^{d-1}$ and the boundary condition (2) for all $(x, \xi) \in \Gamma_-$, and if $f(\cdot, \xi)$ is continuous on the line $\{x + t\xi | t \in \mathbb{R}\} \cap (\Omega \cup \Gamma_{-,\xi})$ for all $(x, \xi) \in D$.

Remark

If the boundary data f_0 is bounded continuous on Γ_-, then there exists a unique solution f. Moreover, since $\mathrm{disc}(f_0)$ is the empty set, $\mathrm{disc}(f)$ is also the empty set, which implies that the solution f is also bounded continuous on D.

Main results

Theorem 2 (Chen, K.)

Let a boundary data f_0 satisfy assumptions in 1, and let f be the solution to the boundary value problem (1)-(2). Then, f can be extended up to Γ_+, which is denoted by $\overline{f}$, by

$$\overline{f}(x, \xi) := \begin{cases} f(x, \xi), & (x, \xi) \in D, \\ \lim_{t \downarrow 0} f(x - t\xi, \xi), & (x, \xi) \in \Gamma_+. \end{cases}$$

Moreover, we have

$$\mathrm{disc}(\overline{f}) = \{(x_* + t\xi_*, \xi_*) | (x_*, \xi_*) \in \mathrm{disc}(f_0), 0 \leq t \leq \tau_+(x_*, \xi_*)\}.$$

- γ: a simple closed curve in $\partial\Omega$ when $d = 3/$
  two points in $\partial\Omega$ when $d = 2$.

- A, B: two connected components of $\partial\Omega\backslash\gamma$, that is,
  - $\partial\Omega = A \cup B \cup \gamma$
  - $A \cap B = A \cap \gamma = B \cap \gamma = \emptyset$.

-
$$f_0(x, \xi) = \begin{cases} I, & (x, \xi) \in ((A \cup \gamma) \times S^{d-1}) \cap \Gamma_-, \\ 0, & (x, \xi) \in (B \times S^{d-1}) \cap \Gamma_-. \end{cases}$$

  - I: a non-zero constant.
  - $\mathrm{disc}(f_0) = \{(x_*, \xi_*) | x_* \in \gamma, \xi_* \in \Gamma_{-, x_*}\}$.

$$\begin{cases} \xi \cdot \nabla_x f(x, \xi) + \mu_t(x) f(x, \xi) = \mu_s(x) \int_{S^{d-1}} p(x, \xi, \xi') f(x, \xi') \, d\sigma_{\xi'}, (x, \xi) \in \Omega \times S^{d-1}, \\ f(x, \xi) = f_0(x, \xi), \quad (x, \xi) \in \Gamma_-. \end{cases}$$

- $d = 2, 3$
- μ_t, μ_s, p : bounded piecewise continuous
  $+$ generalized convexity
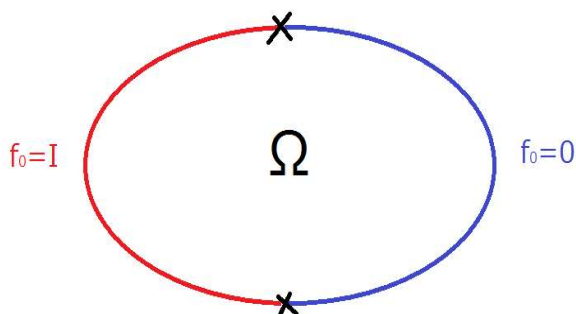
For $(\overline{x}, \overline{\xi}) \in \mathrm{disc}(\overline{f})$, the jump discontinuity $[\overline{f}]$ on $disc(\overline{f})$ by

$$[\overline{f}](\overline{x}, \overline{\xi}) := \lim_{\substack{x \to \overline{x} \\ P(x,\overline{\xi}) \in (A \cup \gamma)}} \overline{f}(x, \overline{\xi}) - \lim_{\substack{x \to \overline{x} \\ P(x,\overline{\xi}) \in B}} \overline{f}(x, \overline{\xi}).$$

$$(P(x, \xi) = x - \tau_-(x, \xi)\xi.)$$

$$\begin{cases} \xi \cdot \nabla_x f(x, \xi) + \mu_t(x) f(x, \xi) = \mu_s(x) \int_{S^{d-1}} p(x, \xi, \xi') f(x, \xi') \, d\sigma_{\xi'}, (x, \xi) \in \Omega \times S^{d-1}, \\ f(x, \xi) = f_0(x, \xi), \quad (x, \xi) \in \Gamma_-. \end{cases}$$
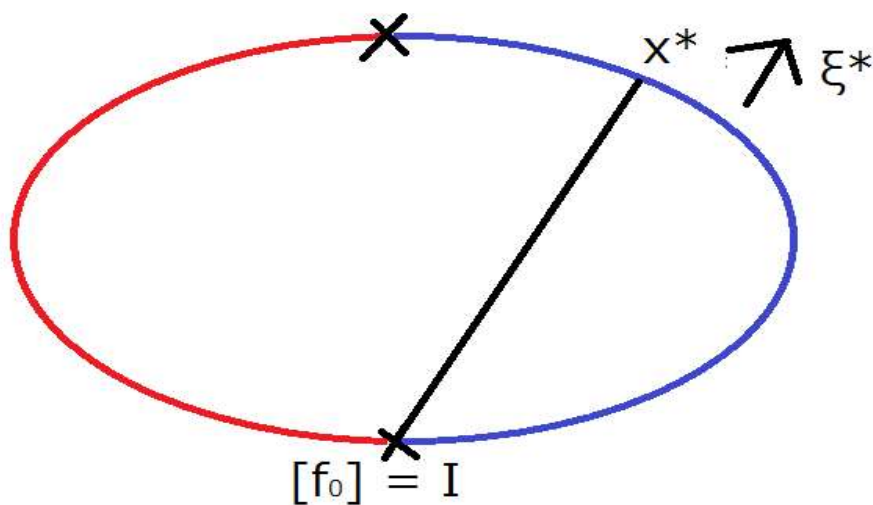
Main results

Theorem 3 (Chen, K.)

Let $(x^*, \xi^*) \in \mathrm{disc}(\overline{f}) \cap \Gamma_+$. Then, we have

$$[f](x^*, \xi^*) = I \exp\left(-\int_0^{\tau_-(x^*, \xi^*)} \mu_t(x^* - r\xi^*)\, dr\right).$$

$$(X\mu_t)(x^*, \xi^*) := \int_0^{\tau_-(x^*, \xi^*)} \mu_t(x^* - r\xi^*)\, dr : \ \text{X-ray transform of } \mu_t.$$
$$= -\log([f](x^*, \xi^*)/I).$$

F. Natterer, *The Mathematics of Computerized Tomography*, SIAM, Germany, (2001)

$f_0 = I$

$f_0 = 0$
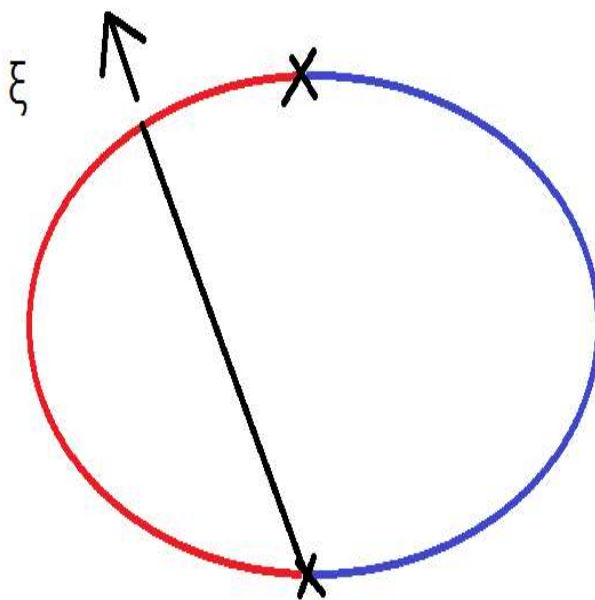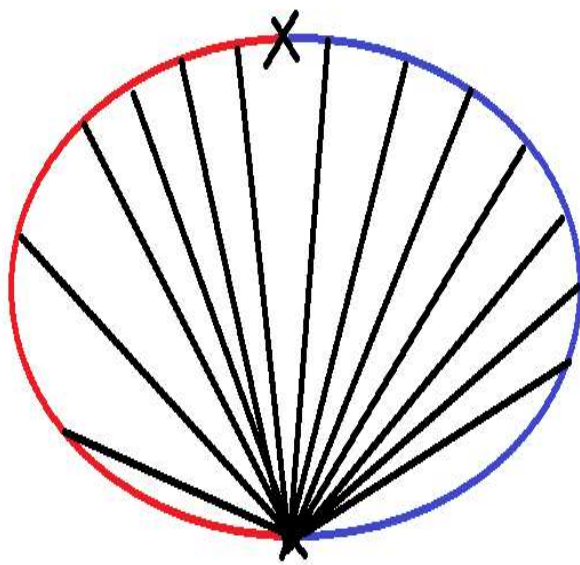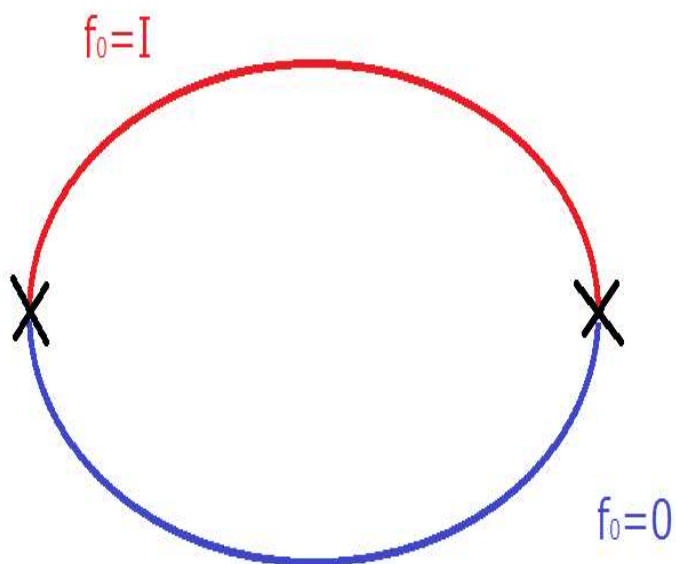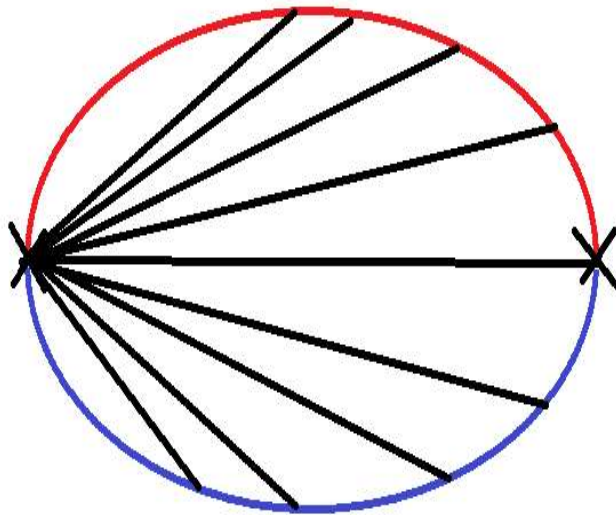
Propagation of boundary-induced discontinuity

- D. S. Anikonov, I. V. Prokhorov, A. E. Kovtanyuk, Investigation of scattering and absorbing media by the methods of X-ray tomography, *J. Inv. Ill-Posed Prob.*, **1**, no. 4, pp. 259–281, (1993) $\cdots$ discontinuity with respect to ξ, a three dimensional bounded convex domain

- K. Aoki, C. Bardos, C. Dogbe, F. Golse, A note on the propagation of boundary induced discontinuities in kinetic theory, *Math. Models Methods Appl. Sci.* **11**, no. 9 pp. 1581–1595, (2001) $\cdots$ discontinuity with respect to x, a two dimensional half plane

- D. Kawagoe, I.-K. Chen, Propagation of boundary-induced discontinuity in stationary radiative transfer, *J. Stat. Phys.*, **170**, no.1 pp. 127–140, (2018) $\cdots$ discontinuity with respect to x and ξ, a multidimensional slab domain

Strategy of proof

1. Reduction to an integral equation

2. Construction of the unique solution to the integral equation

3. Regularity discussion

4. Trace theorem

5. Decay of a jump

Reduction to an integral equation

Integration STE (1) along the line $\{x - t\xi \,|\, t > 0\}$ with the incoming boundary condition (2).

$$f(x, \xi) = \exp\left(-M_t(x, \xi; \tau_-(x, \xi))\right) f_0(P(x, \xi), \xi)$$
$$+ \int_0^{\tau_-(x, \xi)} \mu_s(x - s\xi) \exp\left(-M_t(x, \xi; s)\right)$$
$$\times \int_{S^{d-1}} p(x - s\xi, \xi, \xi') f(x - s\xi, \xi') \, d\sigma_{\xi'} ds. \qquad (3)$$

- $\tau_-(x, \xi) = \inf\{t > 0 \,|\, x - t\xi \notin \Omega\}$
- $P(x, \xi) = x - \tau_-(x, \xi)\xi$
- $M_t(x, \xi; s) := \int_0^s \mu_t(x - r\xi) \, dr$

Construction of the solution

$$f^{(0)}(x,\xi) := \exp\left(-M_t(x,\xi;\tau_-(x,\xi))\right) f_0(P(x,\xi),\xi) \qquad (4)$$

$$f^{(n+1)}(x,\xi) := \int_0^{\tau_-(x,\xi)} \mu_s(x-s\xi) \exp\left(-M_t(x,\xi;s)\right)$$

$$\times \int_{S^{d-1}} p(x-s\xi,\xi,\xi') f^{(n)}(x-s\xi,\xi') \, d\sigma_{\xi'} ds. \qquad (5)$$

Then, $f(x,\xi) := \sum_{n=0}^{\infty} f^{(n)}(x,\xi)$ is the unique solution.

Lemma

$$\sup_{(x,\xi)\in D} |f^{(n+1)}(x,\xi)| \leq M \sup_{(x,\xi)\in D} |f^{(n)}(x,\xi)|, \quad \forall n \geq 0.$$

- $M_t(x,\xi;s) := \int_0^s \mu_t(x-r\xi)\, dr$
- $M := \sup_{(x,\xi)\in D}(1 - \exp(-M_t(x,\xi;\tau_-(x,\xi)))) < 1$
- $P(x,\xi) = x - \tau_-(x,\xi)\xi$

Regularity discussion

$$f(x,\xi) = F_0(x,\xi) + F_1(x,\xi)$$

- $F_0 := f^{(0)}$: discontinuous on D,

$$\text{disc}(F_0) = \{(x_*+t\xi_*,\xi_*)|(x_*,\xi_*) \in disc(f_0), 0 \leq t < \tau_+(x_*,\xi_*)\}.$$

- $F_1 := \sum_{n=1}^{\infty} f^{(n)}$: continuous on D

$$f^{(0)}(x,\xi) := \exp\left(-M_t(x,\xi;\tau_-(x,\xi))\right) f_0(P(x,\xi),\xi)$$

$$f^{(n+1)}(x,\xi) := \int_0^{\tau_-(x,\xi)} \mu_s(x-s\xi) \exp\left(-M_t(x,\xi;s)\right)$$

$$\times \int_{S^{d-1}} p(x-s\xi,\xi,\xi') f^{(n)}(x-s\xi,\xi') \, d\sigma_{\xi'} ds.$$

Discontinuity of F_0

$$F_0(x, \xi) = f^{(0)}(x, \xi) = \exp\left(-M_t(x, \xi; \tau_-(x, \xi))\right) f_0(x - \tau_-(x, \xi)\xi, \xi)$$

Proposition 4

$$\text{disc}(F_0) = \{(x_* + t\xi_*, \xi_*) | (x_*, \xi_*) \in \text{disc}(f_0), 0 \leq t < \tau_+(x_*, \xi_*)\},$$

where $\text{disc}(f)$ is a set of the discontinuity points for a function f.

Lemma

$M_t(x, \xi; \tau_-(x, \xi))$ is continuous on $\Omega \times S^{d-1}$.

$$(x, \xi) \in \text{disc}(F_0) \Leftrightarrow (x - \tau_-(x, \xi)\xi, \xi) \in \text{disc}(f_0),$$

- $\tau_\pm(x, \xi) := \inf\{t > 0 | x \pm t\xi \notin \Omega\}$
- $M_t(x, \xi; s) := \int_0^s \mu_t(x - r\xi)\, dr$

Continuity of $f^{(n)}$

$$f^{(n+1)}(x, \xi) := \int_0^{\tau_-(x, \xi)} \mu_s(x - s\xi) \exp\left(-M_t(x, \xi; s)\right)$$
$$\times \int_{S^{d-1}} p(x - s\xi, \xi, \xi') f^{(n)}(x - s\xi, \xi')\, d\sigma_{\xi'} ds.$$

Proposition 5

$$f^{(n)} \in C_b(D) \Rightarrow f^{(n+1)} \in C_b(D)$$

Lemma

$M_t(x, \xi; s)$ is continuous on $\Omega \times S^{d-1}$ for all $s \geq 0$.

- $\tau_-(x, \xi) := \inf\{t > 0 | x - t\xi \notin \Omega\}$
- $M_t(x, \xi; s) := \int_0^s \mu_t(x - r\xi)\, dr$
- $C_b(D)$: the space of all bounded continuous functions on D

$$f_0 \to f^{(0)} \to f^{(1)} \to f^{(2)} \to f^{(3)} \to \dots$$

$$f_0 \to f^{(0)} \to f^{(1)} \to f^{(2)} \to f^{(3)} \to \dots$$

$$\text{Q. } f^{(1)} \in C_b(D) \text{ ?}$$

Regularity of $f^{(1)}$

$$f^{(1)}(x,\xi) = \int_0^{\tau_-(x,\xi)} \mu_s(x - s\xi) \exp\left(-M_t(x,\xi;s)\right)$$

$$\times \int_{S^{d-1}} p(x - s\xi, \xi, \xi') f^{(0)}(x - s\xi, \xi') \, d\sigma_{\xi'} ds$$

$$= \int_0^{\tau_-(x,\xi)} \mu_s(x - s\xi) \exp\left(-M_t(x,\xi;s)\right) G(x - s\xi, \xi) \, ds.$$

$$G(x,\xi) = \int_{S^{d-1}} p(x,\xi,\xi') \exp\left(-M_t(x,\xi';\tau_-(x,\xi'))\right) f_0(P(x,\xi'),\xi') \, d\sigma_{\xi'}.$$

- $f^{(0)}(x,\xi) := \exp\left(-M_t(x,\xi;\tau_-(x,\xi))\right) f_0(P(x,\xi),\xi)$
- $P(x,\xi) = x - \tau_-(x,\xi)\xi$

Regularity of G

> **Proposition 6**
>
> Under the assumption in Theorem 1, $G \in C_b(\Omega_0 \times S^{d-1})$.

<u>Case 2.</u> $f_0(\cdot,\xi)$ is continuous on $\Gamma_{-,\xi}$ for almost all $\xi \in S^{d-1}$.

$$G(x,\xi) = \int_{S^{d-1}} p(x,\xi,\xi') \exp\left(-M_t(x,\xi';\tau_-(x,\xi'))\right)$$
$$\times f_0(P(x,\xi'),\xi') \, d\sigma_{\xi'}.$$

- τ_- is continuous on $\Omega \times S^{d-1}$. (Guo, 2010)
- $\left| p(x,\xi,\xi') \exp\left(-M_t(x,\xi';\tau_-(x,\xi'))\right) f_0(x - \tau_-(x,\xi')\xi',\xi') \right|$
  $\leq \sup_{(x,\xi,\xi') \in \Omega \times S^{d-1} \times S^{d-1}} |p(x,\xi,\xi')| \sup_{(x,\xi) \in \Gamma_-} |f_0(x,\xi)|$.
- p is continuous on $\Omega_0 \times S^{d-1} \times S^{d-1}$

$\Rightarrow G$ is continuous on $\Omega_0 \times S^{d-1}$.
(by the dominated convergence theorem)

Regularity of G

<u>Case 1.</u> $f_0(x, \cdot)$ is continuous on $\Gamma_{-,x}$ for almost all $x \in \partial\Omega$.

> **Lemma**
>
> $$d\sigma_{\xi'} = \frac{|n(y) \cdot (x - y)|}{|x - y|^d} \, d\sigma_y \text{ via } y = P(x, \xi') = x - \tau_-(x, \xi')\xi'$$

$$
\begin{aligned}
G(x, \xi) &= \int_{S^{d-1}} p(x, \xi, \xi') \exp\left(-M_t(x, \xi'; \tau_-(x, \xi'))\right) \\
&\qquad\qquad\qquad\qquad \times f_0(P(x, \xi'), \xi') \, d\sigma_{\xi'} \\
&= \int_{\partial\Omega} p\left(x, \xi, \frac{x - y}{|x - y|}\right) \exp\left(-M_t\left(x, \frac{x - y}{|x - y|}; |x - y|\right)\right) \\
&\qquad \times f_0\left(y, \frac{x - y}{|x - y|}\right) \frac{|n(y) \cdot (x - y)|}{|x - y|^d} \, d\sigma_y.
\end{aligned}
$$

Regularity of G

> **Proposition 3**
>
> Under the assumption in Theorem 1, $G \in C_b(\Omega_0 \times S^{d-1})$.

<u>Case 1.</u> $f_0(x, \cdot)$ is continuous on $\Gamma_{-,x}$ for almost all $x \in \partial\Omega$.
Fix $\overline{x} \in \Omega_0$.

- $p\left(x, \xi, \frac{x-y}{|x-y|}\right) \exp\left(-M_t\left(x, \frac{x-y}{|x-y|}; |x-y|\right)\right) f_0\left(y, \frac{x-y}{|x-y|}\right) \frac{|n(y) \cdot (x-y)|}{|x-y|^d}$
  is continuous at $(\overline{x}, \xi) \in \Omega_0 \times S^{d-1}$ for almost all $y \in \partial\Omega$.

- $\left| p\left(x, \xi, \frac{x-y}{|x-y|}\right) \exp\left(-M_t\left(x, \frac{x-y}{|x-y|}; |x-y|\right)\right) f_0\left(y, \frac{x-y}{|x-y|}\right) \frac{|n(y) \cdot (x-y)|}{|x-y|^d} \right|$
  $\leq \dfrac{\sup_{(x,\xi,\xi') \in \Omega_0 \times S^{d-1} \times S^{d-1}} |p(x, \xi, \xi')| \sup_{(x,\xi) \in \Gamma_-} |f_0(x, \xi)|}{(|\overline{x} - y| - \epsilon/2)^d}$
  for all $x \in B_{\epsilon/2}(\overline{x})$, with $\epsilon = d(\overline{x}, \partial\Omega_0)$.

$\Rightarrow G$ is continuous on $\Omega_0 \times S^{d-1}$.
  (by the dominated convergence theorem)

Regularity of $f^{(1)}$

- $G \in C_b(\Omega_0 \times S^{d-1})$

- $f^{(1)}(x, \xi) =$
$$\int_0^{\tau_-(x,\xi)} \mu_s(x - s\xi) \exp\left(-M_t(x, \xi; s)\right) G(x - s\xi, \xi) \, ds.$$

$$\Rightarrow f^{(1)} \in C_b(D)$$

Regularity discussion

$$f(x, \xi) = F_0(x, \xi) + F_1(x, \xi).$$

- $F_0 = f^{(0)}$: discontinuous on D,

  $disc(F_0) = \{(x_* + t\xi_*, \xi_*) | (x_*, \xi_*) \in disc(f_0), 0 \le t < \tau_+(x_*, \xi_*)\}.$

- $F_1 = \sum_{n=1}^{\infty} f^{(n)}$: continuous on D

$$\mathrm{disc}(f) = \mathrm{disc}(F_0)$$
$$= \{(x_* + t\xi_*, \xi_*) | (x_*, \xi_*) \in \mathrm{disc}(f_0), 0 \le t < \tau_+(x_*, \xi_*)\}.$$

Trace theorem

For all $(x, \xi) \in \Gamma_+$, the trace

$$\overline{f}(x, \xi) := \lim_{t \downarrow 0} f(x - t\xi, \xi)$$

exists.

By the fundamental theorem of calculus,

$$f(x, \xi) = f_0(x - \tau_-(x, \xi)\xi, \xi) - \sum_{j=1}^{l(x,\xi)} \int_{t_{j-1}(x,\xi)}^{t_j(x,\xi)} \xi \cdot \nabla_x f(x - s\xi, \xi) \, ds.$$

Trace theorem

$$|f(x, \xi) - f(x - t\xi, \xi)| = \left| \int_0^t \xi \cdot \nabla_x f(x - s\xi, \xi) \, ds \right|$$

$$\leq \left(\sup_{(x,\xi) \in \Omega_0 \times S^{d-1}} |\xi \cdot \nabla_x f(x, \xi)| \right) t.$$

- $\tau_-(x - t\xi, \xi) = \tau_-(x, \xi) - t$

Trace theorem

- $\{\overline{f}^{(n)}\}$: extended functions of $\{f^{(n)}\}$ upto Γ_+
- $\overline{F_0}(x, \xi) := \overline{f}^{(0)}(x, \xi)$
- $\overline{F_1}(x, \xi) := \sum_{n=1}^{\infty} \overline{f}^{(n)}$
- $\overline{D} := D \cup \Gamma_+$

Proposition 7

$\mathrm{disc}(\overline{F_0}) = \{(x_* + t\xi_*, \xi_*)|(x_*, \xi_*) \in \mathrm{disc}(f_0), 0 \leq t \leq \tau_+(x_*, \xi_*)\}.$

Proposition 8

Under the assumption in Theorem 1, $\overline{F_1}$ is bounded continuous on $\overline{D}$.

Decay of a jump

Lemma

For $(x^*, \xi^*) \in \mathrm{disc}(\overline{f})$,

$$[\overline{F_0}](x^*, \xi^*) = I \exp\Big(-M_t(x^*, \xi^*; \tau_-(x^*, \xi^*))\Big).$$

- $\overline{F_0}(x, \xi^*) = I \exp\Big(-M_t(x, \xi^*; \tau_-(x, \xi^*))\Big), \quad x \in \overline{\Omega_{A,\xi^*}}.$
  $\overline{\Omega_{A,\xi^*}} = \{x \in \overline{\Omega}|P(x, \xi^*) \in (A \cup \gamma) \cap \Gamma_{-,\xi^*}\}.$

- $\overline{F_0}(x, \xi^*) = 0, \quad x \in \overline{\Omega_{B,\xi^*}}.$
  $\overline{\Omega_{B,\xi^*}} = \{x \in \overline{\Omega}|P(x, \xi^*) \in B \cap \Gamma_{-,\xi^*}\}.$

Decay of a jump

Lemma

For $(x^*, \xi^*) \in \operatorname{disc}(\overline{f})$,

$$[\overline{F_1}](x^*, \xi^*) = 0.$$

$$\therefore [\overline{f}](x^*, \xi^*) = [F_0](x^*, \xi^*) + [F_1](x^*, \xi^*)$$
$$= I \exp\left(-M_t(x^*, \xi^*; \tau_-(x^*, \xi^*))\right).$$

2. $W^{1,p}$ estimate for solutions to the stationary transport equation

Numerical approach

Boundary Value Problem

$$\begin{cases} \xi \cdot \nabla_x f(x,\xi) + \mu_t(x)f(x,\xi) = \mu_s(x) \int_{S^{d-1}} p(x,\xi,\xi')f(x,\xi') \, d\sigma_{\xi'}, \\ f(x,\xi) = f_0(x,\xi), \quad (x,\xi) \in \Gamma_-. \end{cases}$$

1. Give an initial guess μ_t, μ_s and p.
2. Solve the boundary value problem numerically.
3. Compare numerical results with experimental data.
   - They coincide with each other. $\rightarrow$ The initial guess is correct!
   - They do *not* coincide with each other.
     $\rightarrow$ The initial guess is wrong.
     $\rightarrow$ Change the initial guess and go back to the step 2.

A. D. Klose, A. H. Hielscher, Optical tomography using the time-independent equation of radiative transfer—Part 2: inverse model, *J. Quant. Spect. & Rad. Trans.* **72**, pp. 715–732, (2002)

Discrete-ordinate discontinuous Galerkin methods

W. Han, J. Huang, J. A. Eichholz, Discrete-ordinate discontinuous Galerkin methods for solving the radiative transfer equation, *SIAM J. Sci. Comput.*, **20**, no. 2, pp. 477–497, (2010)

Error analysis under the assumption that $\nabla_x f \in L^2(\Omega \times S^{d-1})^d$.

Problem
$$\nabla_x f \in L^p(\Omega \times S^{d-1})^d \text{ for some } 1 \le p \le \infty?$$

Previous Results

Equivalent Integral Equation

$$f(x, \xi) = \exp\left(-M_t(x, \xi; \tau_-(x, \xi))\right) f_0(P(x, \xi), \xi)$$
$$+ \int_0^{\tau_-(x, \xi)} \mu_s(x - s\xi) \exp\left(-M_t(x, \xi; s)\right)$$
$$\times \int_{S^{d-1}} p(x - s\xi, \xi, \xi') f(x - s\xi, \xi') \, d\sigma_{\xi'} \, ds.$$

- $\tau_-(x, \xi) = \inf\{t > 0 | x - t\xi \notin \Omega\}$
- $P(x, \xi) = x - \tau_-(x, \xi)\xi$
- $M_t(x, \xi; s) := \int_0^s \mu_t(x - r\xi) \, dr$

Previous Results

1. H. Egger and M. Schlottbom, An L^p theory for stationary radiative transfer, Applicable Analysis, **93**, (6), pp. 1283–1296, (2014)

   Remark

   $$\|\xi \cdot \nabla_x f\|_{L^p(\Omega \times S^{d-1})} \le \||\nabla_x f|\|_{L^p(\Omega \times S^{d-1})}.$$

2. D. S. Anikonov, A formula for the gradient of the transport equation solution, *J. Inv. Ill-Posed Prob.*, **4**, (2), pp. 85–100, (1996)

Previous Results

③ V. Agoshkov, *Boundary value problems for transport equations. Modeling and simulation in science, Engineering and Technology*, Birkhäuser, Boston, (1998)

Slobodeckij semi-norm

$1 \leq p \leq \infty$, $0 < s < 1$, $f \in L^p(\Omega \times S^{d-1})$,

$$[f]_{s,p} := \left(\int_\Omega \int_\Omega \int_{S^{d-1}} \frac{|f(x,\xi) - f(y,\xi)|^p}{|x-y|^{sp+d}} \, d\sigma_\xi \, dxdy \right)^{1/p}.$$

④ I. K. Chen, C. H. Hsia and D. Kawagoe, Regularity for diffuse reflection boundary problem to the stationary linearized Boltzmann equation in a convex domain, *Ann. I. H. Poincaré (C)*, **36**, (3), pp. 745—782, (2019)

Assumptions

- $\Omega \subset \mathbb{R}^2$: bounded, convex, C^2 boundary.

- uniform outer generalized contact order m
  - $y_0 \in \partial\Omega$.
  - Choose a Cartesian coordinate system (x_1, x_2) such that
    - $y_0 = (0,0)$,
    - x_1-axis is tangent to the boundary $\partial\Omega$ at y_0.
    - $n(y_0) = (0, -1)$.
  - Assume that there exist constants $a > 0$, $m \geq 2$ and $\delta > 0$ such that the curve $x_2 = a|x_1|^m$, $|x_1| < \delta$ touches the boundary $\partial\Omega$ at y_0 from outside of Ω.
  - Also assume that we can take these a, δ and m independently of y_0.

- $p_m := 2 + 1/(m-1)$.

Remark We allow the case $m = \infty$.

X_2

$X_2 = a|X_1|^m$

O X_1
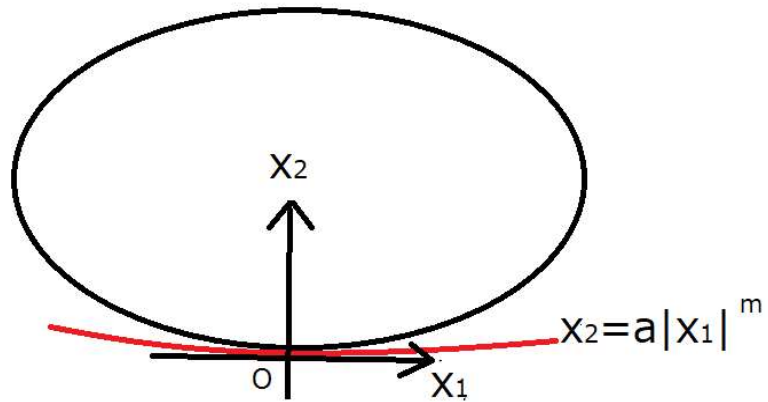
Assumptions

- μ_t, μ_s: nonnegative functions in $W^{1,\infty}(\Omega)$ such that $\mu_t(x) \geq \mu_s(x)$ for almost all $x \in \Omega$.

- There exists a nonnegative function $\tilde{p}$ in $W^{1,\infty}(\Omega \times (-1,1))$ such that $p(x, \xi, \xi') = \tilde{p}(x, \xi \cdot \xi')$ for almost all $(x, \xi, \xi') \in \Omega \times S^1 \times S^1$ and

$$\int_{S^1} \tilde{p}(x, \xi \cdot \xi') \, d\sigma_{\xi'} = 1$$

for almost all $(x, \xi) \in \Omega \times S^1$.

Notations

$W^{1,\infty}(\Gamma_-)$.

- $\nabla_{x,v} f_0(x,\xi) := \dfrac{d}{dt} f_0(g(t),\xi)$.
- $g : (-\delta,\delta) \to \partial\Omega$: a local parametrization of $\partial\Omega$ around x such that
$$g(0) = x, \quad g'(0) = v.$$
- $\xi = (\cos\theta,\sin\theta)$, $\theta \in (-\pi,\pi]$: the polar coordinate on the unit circle S^1.
- $W^{1,\infty}(\Gamma_-) := \{f_0 \in L^\infty(\Gamma_-) | \|f_0\|_{W^{1,\infty}} < \infty\}$.
- $\|f_0\|_{W^{1,\infty}(\Gamma_-)} := \|f_0\|_{L^\infty(\Gamma_-)} + \|\nabla_x f_0\|_{L^\infty(\Gamma_-)} + \|f_{0,\theta}\|_{L^\infty(\Gamma_-)}$.
-
$$\|\nabla_x f_0\|_{L^\infty(\Gamma_-)} := \operatorname*{ess\,sup}_{(x,\xi)\in\Gamma_-} \left(\operatorname*{ess\,sup}_{v\in T_x(\partial\Omega), |v|=1} |\nabla_{x,v} f_0(x,\xi)| \right).$$
- $T_x(\partial\Omega)$: the tangent space at $x \in \partial\Omega$.
- $f_{0,\theta}$: the first derivative of the function f_0 with respect to θ.

We assume that the boundary data f_0 belongs to $W^{1,\infty}(\Gamma_-)$.

Main Result

Theorem

Suppose that the boundary $\partial\Omega$ has uniform outer generalized contact order m. Then, the solution f to the boundary value problem $(1)-(2)$ belongs to $W^{1,p}(\Omega \times S^1)$ for $1 \le p < p_m$, where $p_m := 2 + 1/(m-1)$.

- $W^{1,p}(\Omega \times S^1) := \{f \in L^p(\Omega \times S^1) | \|f\|_{W^{1,p}(\Omega\times S^1)} < \infty\}$.

- $\|f\|_{W^{1,p}(\Omega\times S^1)} :=$
$$\|f\|_{L^p(\Omega\times S^1)} + \|\,|\nabla_x f|\,\|_{L^p(\Omega\times S^1)} + \|f_\theta\|_{L^p(\Omega\times S^1)}.$$

Sketch of Proof

The solution $f(x,\xi) = F_0(x,\xi) + F_1(x,\xi) + F_2(x,\xi)$.

$$F_0(x,\xi) := \exp\left(-\int_0^{\tau_-(x,\xi)} \mu_t(x - r\xi)\, dr\right) f_0(P(x,\xi),\xi),$$

$$F_1(x,\xi) := \int_0^{\tau_-(x,\xi)} \mu_s(x - t\xi) \exp\left(-\int_0^t \mu_t(x - r\xi)\, dr\right) G_1(x - t\xi, \xi')\, dt,$$

$$F_2(x,\xi) := \int_0^{\tau_-(x,\xi)} \mu_s(x - t\xi) \exp\left(-\int_0^t \mu_t(x - r\xi)\, dr\right) G_2(x - t\xi, \xi')\, dt.$$

- $\tau_-(x,\xi) := \inf\{t > 0 \,|\, x - t\xi \notin \Omega\}$.
- $P(x,\xi) := x - \tau_-(x,\xi)\xi$.

Sketch of Proof

$$G_1(x,\xi) := \int_{S^1} p(x, \xi \cdot \xi') F_0(x, \xi')\, d\sigma_{\xi'},$$

$$G_2(x,\xi) := \int_{S^1} p(x, \xi \cdot \xi') \int_0^{\tau_-(x,\xi')} \mu_s(x - t\xi') \exp\left(-\int_0^t \mu_t(x - r\xi')\, dr\right)$$

$$\times \int_{S^1} p(x - t\xi', \xi' \cdot \xi'') f(x - t\xi', \xi'')\, d\sigma_{\xi''}\, dt\, d\sigma_{\xi'}$$

$$= \int_\Omega p\left(x, \xi \cdot \frac{x - y}{|x - y|}\right) \mu_s(y) \exp\left(-|x - y| \int_0^1 \mu_t(x - r(x - y))\, dr\right)$$

$$\times \left(\int_{S^1} p\left(y, \frac{x - y}{|x - y|} \cdot \xi''\right) f(y, \xi'')\, d\sigma_{\xi''}\right) \frac{dy}{|x - y|}.$$

Bootstrap Argument

1. Hölder continuity of f

2. Differentiability of f

3. Integrability of $\nabla_x f$

4. Integrability of f_θ

Hölder continuity of f

Lemma

Fix $\epsilon \in (0,1)$. Let f be the solution to the boundary value problem (1)-(2). Then, for all $x_1, x_2 \in \Omega$ and $\xi \in S^1$,

$$|f(x_1, \xi) - f(x_2, \xi)| \leq C_\epsilon \left(\frac{1}{N(x_1, \xi)} + \frac{1}{N(x_2, \xi)} \right) |x_1 - x_2|^{1-\epsilon}$$

with some positive constant C_ϵ depending on ϵ, where

$$N(x, \xi) := |n(P(x, \xi)) \cdot \xi|.$$

- $|F_0(x_1, \xi) - F_0(x_2, \xi)| \leq C \left(\dfrac{1}{N(x_1, \xi)} + \dfrac{1}{N(x_2, \xi)} \right) |x_1 - x_2|.$

- $|F_1(x_1, \xi) - F_1(x_2, \xi)| \leq C \left(\dfrac{1}{N(x_1, \xi)} + \dfrac{1}{N(x_2, \xi)} \right) |x_1 - x_2|.$

- $|F_2(x_1, \xi) - F_2(x_2, \xi)| \leq C_\epsilon \left(\dfrac{1}{N(x_1, \xi)} + \dfrac{1}{N(x_2, \xi)} \right) |x_1 - x_2|^{1-\epsilon}.$

$$G_1(x, \xi) := \int_{S^1} p(x, \xi \cdot \xi') F_0(x, \xi') \, d\sigma_{\xi'},$$

$$G_2(x, \xi) := \int_{S^1} p(x, \xi \cdot \xi') \int_0^{\tau_-(x, \xi')} \mu_s(x - t\xi') \exp\left(-\int_0^t \mu_t(x - r\xi') \, dr\right)$$

$$\times \int_{S^1} p(x - t\xi', \xi' \cdot \xi'') f(x - t\xi', \xi'') \, d\sigma_{\xi''} \, dt \, d\sigma_{\xi'}$$

$$= \int_{\Omega} p\left(x, \xi \cdot \frac{x - y}{|x - y|}\right) \mu_s(y) \exp\left(-|x - y| \int_0^1 \mu_t(x - r(x - y)) \, dr\right)$$

$$\times \left(\int_{S^1} p\left(y, \frac{x - y}{|x - y|} \cdot \xi''\right) f(y, \xi'') \, d\sigma_{\xi''}\right) \frac{dy}{|x - y|}.$$

Hölder continuity of f

Lemma

For $z_1, z_2 \in \Omega$, we have

$$|G_1(z_1, \xi) - G_1(z_2, \xi)| \leq C(1 + |\log d_{z_1}| + |\log d_{z_2}|)|z_1 - z_2|$$

for some positive constant C, where $d_x := d(x, \partial\Omega)$.

Lemma

For any $0 < \epsilon < 1$, there exists a positive constant C_ϵ such that

$$|G_2(z_1, \xi) - G_2(z_2, \xi)| \leq C_\epsilon |z_1 - z_2|^{1-\epsilon}$$

for all $z_1, z_2 \in \Omega$.

Reminder

The solution $f(x, \xi) = F_0(x, \xi) + F_1(x, \xi) + F_2(x, \xi)$.

$$F_0(x, \xi) := \exp\left(-\int_0^{\tau_-(x,\xi)} \mu_t(x - r\xi)\, dr\right) f_0(P(x, \xi), \xi),$$

$$F_1(x, \xi) := \int_0^{\tau_-(x,\xi)} \mu_s(x - t\xi) \exp\left(-\int_0^t \mu_t(x - r\xi)\, dr\right) G_1(x - t\xi, \xi')\, dt,$$

$$F_2(x, \xi) := \int_0^{\tau_-(x,\xi)} \mu_s(x - t\xi) \exp\left(-\int_0^t \mu_t(x - r\xi)\, dr\right) G_2(x - t\xi, \xi')\, dt.$$

- $\tau_-(x, \xi) := \inf\{t > 0 | x - t\xi \notin \Omega\}$.
- $P(x, \xi) := x - \tau_-(x, \xi)\xi$.

Estimates for P and τ_-

Proposition

Let $x, y \in \Omega$ and $\xi \in S^1$. Suppose that $\tau_-(x, \xi) \leq \tau_-(y, \xi)$. Then,

$$|P(x, \xi) - P(y, \xi)| \leq \frac{|x - y|}{N(x, \xi)},$$

$$|\tau_-(x, \xi) - \tau_-(y, \xi)| \leq \frac{2|x - y|}{N(x, \xi)}.$$

Corollary

Let $x \in \Omega$ and $\xi \in S^1$. Then,

$$|P_{x_i}(x, \xi)| \leq \frac{1}{N(x, \xi)}, \quad |\tau_{-,x_i}(x, \xi)| \leq \frac{2}{N(x, \xi)}.$$

- $\tau_-(x, \xi) = \inf\{t > 0 | x - t\xi \notin \Omega\}$.
- $P(x, \xi) = x - \tau_-(x, \xi)\xi$.
- $N(x, \xi) := |n(P(x, \xi)) \cdot \xi|$.

Key Lemma

> **Lemma**
>
> Let Ω be a bounded convex domain with a C^2 boundary. Then,
>
> $$\int_{S^1} \frac{1}{N(x,\xi)} \, d\sigma_\xi \leq C(1 + |\log d_x|)$$
>
> for all $x \in \Omega$, where $d_x := d(x, \partial\Omega)$.

<u>Remark</u> We use the uniform interior sphere condition.

Differentiability of f

> **Lemma**
>
> Let f be the solution to the boundary value problem (1)-(2).
> Then, the partial derivative f_{x_i} exists.

> **Lemma**
>
> Let f be the solution to the boundary value problem (1)-(2).
> Then, the partial derivative f_θ of f with respect to θ exists.

$$F_0(x,\xi) := \exp\left(-\int_0^{\tau_-(x,\xi)} \mu_t(x - r\xi) \, dr\right) f_0(P(x,\xi), \xi),$$

$$F_j(x,\xi) := \int_0^{\tau_-(x,\xi)} \mu_s(x - t\xi) \exp\left(-\int_0^t \mu_t(x - r\xi) \, dr\right) G_j(x - t\xi, \xi') \, dt.$$

Differentiability of f

$$F_{0,x_i}(x,\xi) = \frac{\partial}{\partial x_i}\left(\exp\left(-\int_0^{\tau_-(x,\xi)}\mu_t(x-r\xi)\,dr\right)f_0(P(x,\xi),\xi)\right)$$

$$= \left\{-\mu_t(x)\tau_{-,x_i}(x,\xi) - \int_0^{\tau_-(x,\xi)}\mu_{t,x_i}(P(x,\xi)+r\xi)\,dr\right.$$

$$\left. +\tau_{-,x_i}(x,\xi)\int_0^{\tau_-(x,\xi)}\frac{d}{dr}\mu_t(P(x,\xi)+r\xi)\,dr\right\}F_0(x,\xi)$$

$$+\exp\left(-\int_0^{\tau_-(x,\xi)}\mu_t(x-r\xi)\,dr\right)\nabla_{x,P_{x_i}(x,\xi)}f_0(P(x,\xi),\xi).$$

Differentiability of f

$$F_{j,x_i}(x,\xi) = \tau_{-,x_i}(x,\xi)\mu_s(x)G_j(x,\xi)$$

$$+\int_0^{\tau_-(x,\xi)}\mu_{s,x_i}(P(x,\xi)+t\xi)\exp\left(-\int_t^{\tau_-(x,\xi)}\mu_t(P(x,\xi)+r\xi)\,dr\right)$$

$$\times G_j(P(x,\xi)+t\xi,\xi)\,dt$$

$$-\int_0^{\tau_-(x,\xi)}\mu_s(P(x,\xi)+t\xi)\exp\left(-\int_t^{\tau_-(x,\xi)}\mu_t(P(x,\xi)+r\xi)\,dr\right)$$

$$\times\left(-\int_t^{\tau_-(x,\xi)}\mu_{t,x_i}(P(x,\xi)+r\xi)\,dr\right)G_j(P(x,\xi)+t\xi,\xi)\,dt$$

$$+\int_0^{\tau_-(x,\xi)}\mu_s(P(x,\xi)+t\xi)\exp\left(-\int_t^{\tau_-(x,\xi)}\mu_t(P(x,\xi)+r\xi)\,dr\right)$$

$$\times G_{j,x_i}(P(x,\xi)+t\xi,\xi)\,dt$$

$$-\tau_{-,x_i}(x,\xi)\int_0^{\tau_-(x,\xi)}\frac{d}{dt}\left\{\mu_s(P(x,\xi)+t\xi)\right.$$

$$\left.\times\exp\left(-\int_t^{\tau_-(x,\xi)}\mu_t(P(x,\xi)+r\xi)\,dr\right)G_j(P(x,\xi)+t\xi,\xi)\right\}\,dt.$$

Differentiability of G

Lemma

For $(x, \xi) \in \Omega \times S^1$, we have

$$|G_{j,x_i}(x, \xi)| \leq C(1 + |\log d_x|).$$

T. A. Germogenova, *Local Properties of Solutions of the Transport Equation*, Nauka, Moscow, (1986) (in Russian).

Corollary

G_{j,x_i} belongs to $L^p(\Omega \times S^1)$ for $1 \leq p < \infty$.

$$G_1(x, \xi) = \int_{S^1} p(x, \xi \cdot \xi') F_0(x, \xi') \, d\sigma_{\xi'},$$

$$G_2(x, \xi) = \int_{\Omega} p\left(x, \xi \cdot \frac{x - y}{|x - y|}\right) \mu_s(y) \exp\left(-|x - y| \int_0^1 \mu_t(x - r(x - y)) \, dr\right)$$

$$\times \left(\int_{S^1} p\left(y, \frac{x - y}{|x - y|} \cdot \xi''\right) f(y, \xi'') \, d\sigma_{\xi''}\right) \frac{dy}{|x - y|}.$$

Differentiability of f

$$f(x, \xi) = \exp\left(-\int_0^{\tau_-(x, \xi)} \mu_t(P(x, \xi) + r\xi) \, dr\right) f_0(P(x, \xi), \xi)$$

$$+ \int_0^{\tau_-(x, \xi)} \mu_s(P(x, \xi) + t\xi)$$

$$\times \exp\left(-\int_t^{\tau_-(x, \xi)} \mu_t(P(x, \xi) + r\xi) \, dr\right) G(P(x, \xi) + t\xi, \xi) \, dt,$$

$$G(x, \xi) := G_1(x, \xi) + G_2(x, \xi).$$

Differentiability of G

$$G := G_1 + G_2.$$

> **Lemma**
>
> G_θ belongs to $L^\infty(\Omega \times S^1)$.

$$G_1(x, \xi) = \int_{S^1} p(x, \xi \cdot \xi') F_0(x, \xi') \, d\sigma_{\xi'},$$

$$G_2(x, \xi) = \int_\Omega p\left(x, \xi \cdot \frac{x - y}{|x - y|}\right) \mu_s(y) \exp\left(-|x - y| \int_0^1 \mu_t(x - r(x - y)) \, dr\right)$$
$$\times \left(\int_{S^1} p\left(y, \frac{x - y}{|x - y|} \cdot \xi''\right) f(y, \xi'') \, d\sigma_{\xi''}\right) \frac{dy}{|x - y|}.$$

Integrability of $\nabla_x f$

> **Lemma**
>
> Let f be the solution to the boundary value problem (1)-(2). Then, the partial derivative f_{x_i} belongs to $L^p(\Omega \times S^1)$ for $1 \le p < p_m$.

> **Lemma**
>
> $1/N$ belongs to $L^p(\Omega \times S^1)$ for $1 \le p < p_m$.

> **Corollary**
>
> P_{x_i} and τ_{-,x_i} belong to $L^p(\Omega \times S^1)$ for $1 \le p < p_m$.

Integrability of f_θ

Lemma

Let f be the solution to the boundary value problem (1)-(2). Then, the partial derivative f_θ belongs to $L^p(\Omega \times S^1)$ for $1 \le p < p_m$.

Lemma

Let Ω be a bounded convex domain in $\mathbb{R}^2$ with the C^1 boundary $\partial\Omega$. Then, τ_- is continuously differentiable with respect to θ and

$$\tau_{-,\theta}(x,\xi) = \frac{\tau_-(x,\xi)}{N(x,\xi)}\Big(\xi_\theta \cdot n\big(P(x,\xi)\big)\Big).$$

Corollary

P_θ and $\tau_{-,\theta}$ belong to $L^p(\Omega \times S^1)$ for $1 \le p < p_m$.

Optimality of $W^{1,p}$ estimates

$$\begin{cases} \xi \cdot \nabla_x f(x,\xi) + 2f(x,\xi) = \dfrac{1}{2\pi}\int_{S^1} f(x,\xi')\,d\sigma_{\xi'}, & (x,\xi) \in \Omega \times S^1, \\ f(x,\xi) = 1, & (x,\xi) \in \Gamma_-. \end{cases}$$

$$(\mu_t = 2, \quad \mu_s = 1, \quad p = 1/2\pi)$$

$$f_{x_i}(x,\xi) = e^{-2\tau_-(x,\xi)}\big(G(P(x,\xi)) - 2\big)\tau_{-,x_i}(x,\xi)$$
$$+ \int_0^{\tau_-(x,\xi)} e^{-2t} G_{x_i}(x - t\xi)\,dt,$$

where

$$G(x) := \frac{1}{2\pi}\int_{S^1} f(x,\xi')\,d\sigma_{\xi'}.$$

Optimality of $W^{1,p}$ estimates

Lemma

$$\int_0^{\tau_-(x,\xi)} e^{-2t} G_{x_i}(x - t\xi)\, dt \in L^p(\Omega \times S^1), \quad 1 \le p < \infty.$$

Lemma (Maximum Value Principle)

$$\|f\|_{L^\infty(\Omega \times S^1)} \le \|f_0\|_{L^\infty(\Gamma_-)} = 1.$$

Corollary

$$|G(x)| \le 1, \quad x \in \overline{\Omega}.$$

Optimality of $W^{1,p}$ estimates

1. Disk domain: $\Omega = \{x \in \mathbb{R}^2 \mid |x| < R\}$. ($m = 2, p_m = 3$)
   - $\tau_-(x, \xi) = \xi \cdot x + \sqrt{R^2 + (\xi \cdot x)^2 - |x|^2}$.
   - τ_{-,x_i} does not belong to $L^3(\Omega \times S^1)$.
   - $|e^{-2\tau_-(x,\xi)}(G(P(x,\xi)) - 2)\tau_{-,x_i}(x,\xi)| \ge e^{-2R}|\tau_{-,x_i}(x,\xi)|$.

2. Circuit domain ($m = \infty, p_m = 2$)
   - $\tau_-(x, \xi) = x_2/\xi_2$ if $P(x, \xi)$ lies in the bottom flat part.
   - τ_{-,x_2} does not belong to $L^2(\Omega \times S^1)$.
   - $e^{-2\tau_-(x,\xi)}(G(P(x,\xi)) - 2)\tau_{-,x_2}(x,\xi) \ge e^{-2R}|\tau_{-,x_i}(x,\xi)|$.

Summary

- We discuss boundary-induced discontinuity, which is discontinuity of the solution to the boundary value problem arising from discontinuous incoming boundary data.

- We propose a way to reconstruct the attenuation coefficient from jumps in boundary measurements.

- We discuss a $W^{1,p}$ estimate for solutions to the boundary value problem of the stationary transport equation in two dimensional convex domain.

- The upper bound of the exponent p seem to depend on the shape of the domain heavily.

- This estimate helps us to work on error analysis of a numerical scheme.

3D reconstruction of the asteroid Ryugu

as an inverse problem

Makoto Maruya

National Institute of Advanced Industrial Science and Technology / Geo Insight LLC

Email: maruya@kta.biglobe.ne.jp

Abstract: This report discusses an inverse problem involved in digital image processing for 3D reconstruction of the asteroid Ryugu conducted in the Hayabusa 2 project of the Japan Aerospace Exploration Agency.   When the spacecraft arrived at the asteroid, the observation process started with imaging of the body with its cameras. The obtained 2D images were transmitted from the spacecraft to the ground stations and processed for 3D reconstruction, that is, obtaining information including rotation axis, rotation period, and surface shape of the body. This 3D reconstruction is one of the main issues of computer vision and is closely related to inverse problems.   This report focuses on the mathematical aspect of the Ryugu 3D reconstruction, including formulation as an optimization problem and relation to inverse problems.

(This report is supported by the JAXA Hayabusa2 project)

Key Words: 3D reconstruction, asteroid Ryugu, Hayabusa2, inverse problems

1.   Introduction

   This report discusses an inverse problem involved in digital image processing for 3D reconstruction of the asteroid Ryugu conducted in the Hayabusa 2 project of the Japan Aerospace Exploration Agency (JAXA).

  The Hayabusa 2 is a Japanese mission launched in December 2014 to study the asteroid Ryugu and to collect samples to bring to Earth. The Hayabusa 2 spacecraft arrived at the asteroid in June 2018.

   When the spacecraft arrived at an asteroid, an observation process started with imaging of the body with its cameras. These 2D images were transmitted from the spacecraft to the ground stations and processed for 3D reconstruction, that is, obtaining information including

rotation axis, rotation period, and surface shape of the body. This kind of reconstruction is one of the main issues of computer vision and is closely related to inverse problems.

The report focuses on the mathematical aspect of the Ryugu 3D reconstruction, including formulation as an optimization problem and relation to inverse problems. Figure 1 shows the relation of this report to three fields; asteroid exploration, 3D reconstruction, and inverse problems.
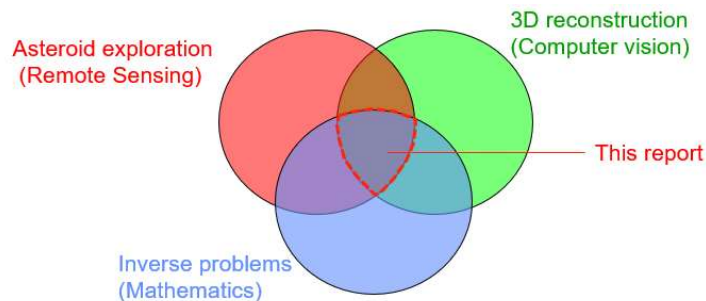
Fig.1 The relation of this report to three fields:
asteroid exploration, 3D reconstruction, and inverse problems.

It should be noted that the images and results of this report were quoted from already published materials and presentations [1][2][3]. Until now, some Ryugu data are not allowed for publication. So, in these materials and also in this report, unpublishable images have been substituted by similar publishable ones.

2. The inputs and outputs of Ryugu 3D reconstruction

2-1. The inputs of 3D reconstruction

The primary source of 3D reconstruction process is the images captured with a telescopic framing camera called ONC-T (hereinafter called "camera"). The field of view of the camera is about 6 x 6 degrees.

The secondary source is the range data from the *Light Detection And Ranging* (LIDAR) instrument, which measures the distance from spacecraft to the asteroid surface, was used to determine the absolute scale of the 3D data.

These data were transmitted from the spacecraft to the ground stations and processed with computers.

2-2. The outputs of 3D reconstruction

The outputs of 3D reconstruction are (1) asteroid coordinates (X-Y-Z orthogonal coordinates), (2) feature points or ground control points (GCPs), and (3) surface shape model. The asteroid coordinates are defined such that its origin is the position of asteroid volume center, Z-axis is parallel to the asteroid rotation axis, and XZ-plane includes the meridian. The feature points represent unique terrain elements such as boulders and craters that are selected manually by operators from the Ryugu images. The 3D positions of feature points and the surface shape model are expressed in the asteroid coordinates.

The feature point data were used with GCP based navigation [3]. The surface shape model was also used for navigation including touchdown area search.
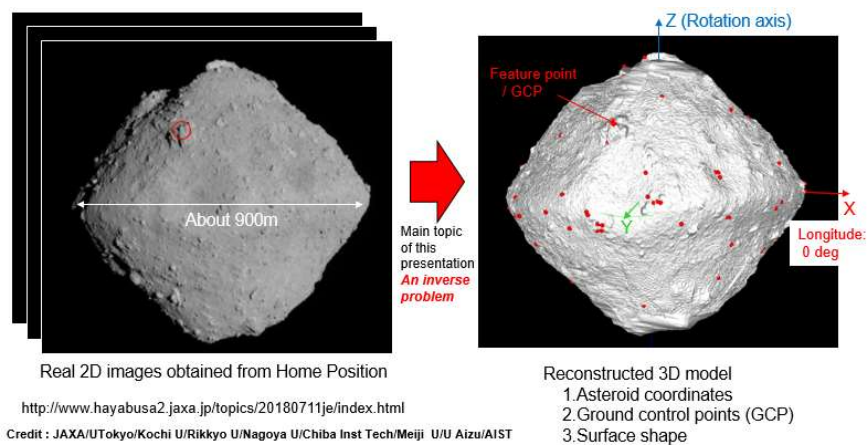
Fig.2 The inputs and outputs of Ryugu 3D reconstruction

3. The process of Ryugu 3D reconstruction

3-1. Image acquisition

The process of Ryugu 3D reconstruction in the Hayabusa 2 project is basically the same as that in the Hayabusa for asteroid Itokawa, but some image acquisition parameters including the number of images and the spacecraft-to-asteroid distance were modified to adapt the new situation.

In the Hayabusa2 project, image acquisition for 3D reconstruction was conducted at a distance of 20 km and 6 km. The 20 km-distance images covered the whole area of Ryugu, and 6 km-distance images provided detailed information around the equatorial region.

In total, 79 images were prepared for 3D reconstruction and 92 feature points were selected by manual. At that stage, the known variables were only feature point positions on the images. Other variables, for example, the orientation of the rotation axis and the rotation period of the Ryugu, and also the positions and orientations of the camera (or the spacecraft) from the

asteroid, were unknown.
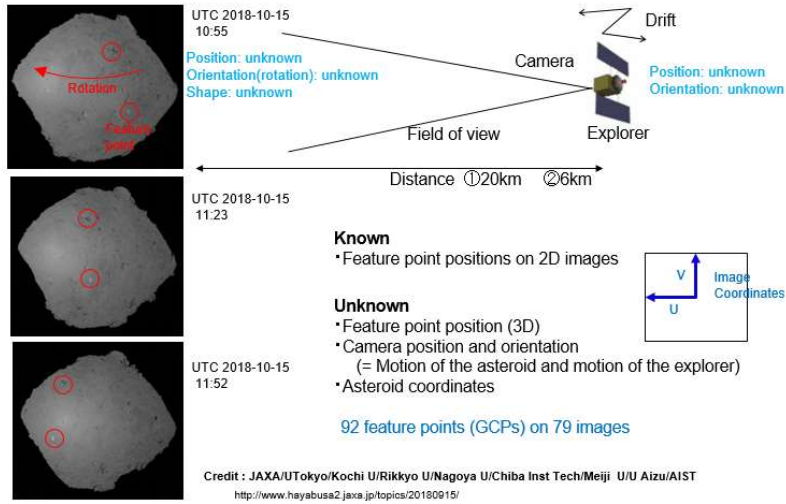
Fig. 3 Acquisition of the Ryugu images

3-2. The basic idea of 3D reconstruction

One fundamental idea of reconstructing 3D data from 2D images is called bundle adjustment [4], and this idea was applied to this work. Figure 4 shows the basic imaging geometry of a single view case which explains the projection mechanism from 3D to 2D. The function $f()$ is a projection function from 3D to 2D. In a single view case, projection from 3D to 2D is computable, but determining 3D from 2D is not computable.
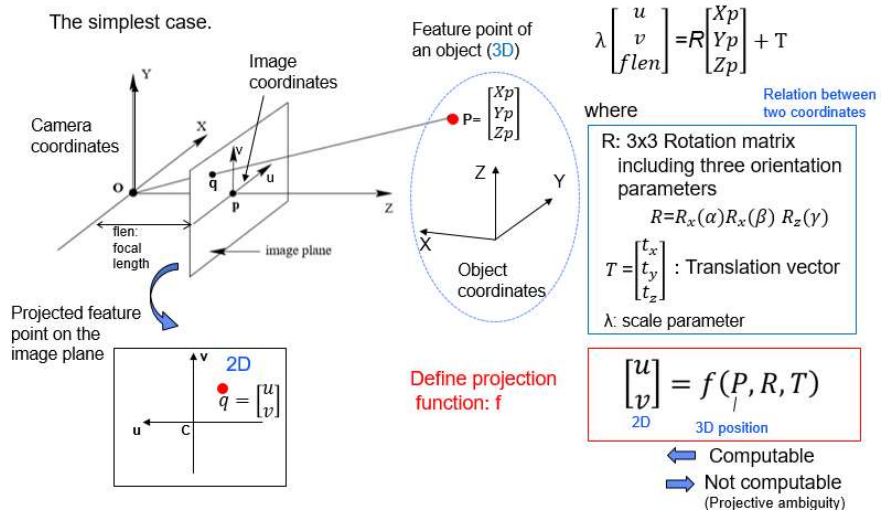
Fig. 4 Basic imaging geometry: single view

Figure 5 shows the imaging geometry of a multiple view case. In a multiple view case and under certain conditions, the number of projection equations exceeds the number of unknown variables and the 2D to 3D computation becomes capable.
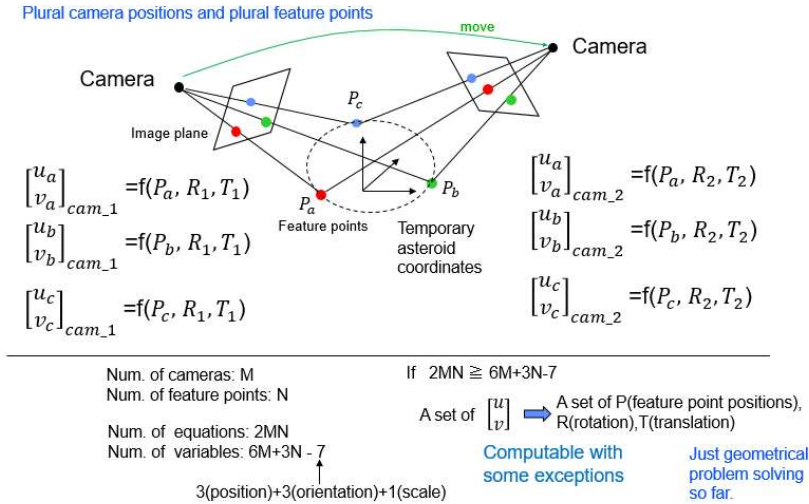
Fig. 5 Basic imaging geometry: multiple views

As the projection functions are not linear, we first obtained an initial (preliminary) solution by dividing the whole problem into small-sized problems (Fig.6). One small-sized problem is estimating positions and orientations of neighboring three cameras and positions of four feature points. Solutions of small-sized problems were merged to make an initial solution.
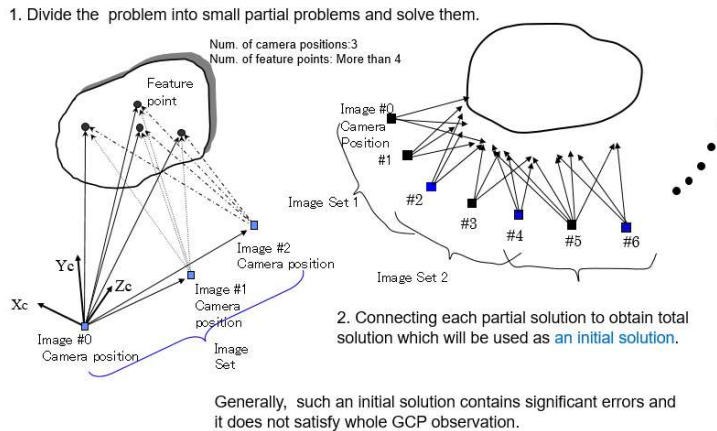
Fig. 6 Obtaining initial values of non-linear optimization

Unfortunately, the obtained initial solution contains some errors that are due to slight misregistrations of feature points on images (Fig.7). This slight misregistration could cause significant errors in the 3D data. It is one of the typical phenomena in inverse problems. The magnitude of error can be measured by reprojection error.
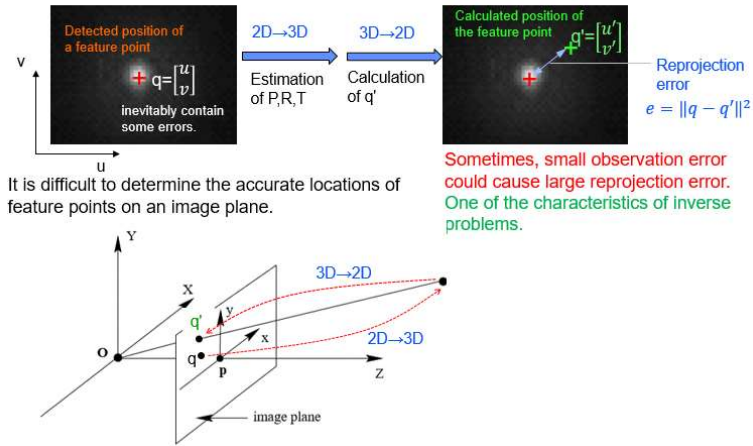
Fig. 7 Observation errors and their effect

In order to obtain an optimal solution, we formulate an object function $E(\boldsymbol{x})$ and find the solution which minimizes the object function.

The object function is defined as follows:

$$E(\boldsymbol{x}) = \sum_{i=1}^{M} \sum_{j=1}^{N} e_{i,j}(\boldsymbol{x}).$$

where

$\boldsymbol{x}$: unknonw variables (camera positions/rotations, feature point positions)

$e_{i,j}(\boldsymbol{x})$: reprojection error

i: camera number

j: feature point number

M: Total number of camera positions = 79

N: Total number of feature points = 92

As the object function is complex and non-linear, it was difficult to obtain an optimal solution at a lump, so it was locally linearized, and a piecewise least square method was applied to approach for the final results step by step.

After local linearization, the following linear observation equation is obtained.

Ax = y.

where

y： 2D projected position (Known variables)

A： Sensitivity Matrix

Then, least-square estimation was conducted using the following equation,

$$\mathbf{x} = (\mathbf{A^T A})^{-1} \cdot \mathbf{A^T y}.$$

By repeating local linearization around new **x,** and least square estimation, final resolutions were obtained. The absolute scale of the 3D data was determined based on LIDAR data.

4. The computational results of the Ryugu 3D reconstruction

Figure 8 shows estimated camera positions (left) and estimated 3D positions (right) on the asteroid coordinates. The left image indicates the circular motion of the spacecraft around the asteroid, mainly due to the asteroid spinning motion.
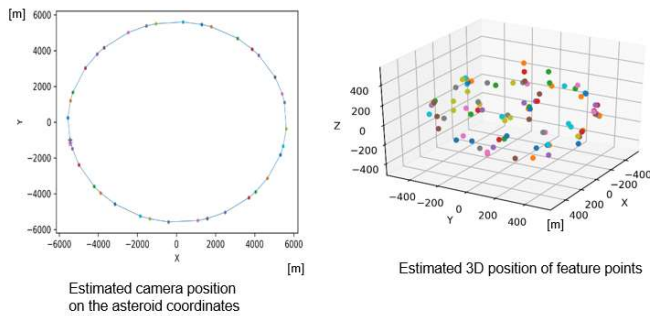
Fig. 8 The computational results (Position of cameras and feature points)

In Figure 9, the reconstructed surface model (right) and real images (left) are arranged for comparison. There are no significant differences between them, and it means the 3D reconstruction has been successful. Red dots on the right images indicate feature points. Touchdown areas are also shown in the images.

Credit : JAXA/UTokyo/Kochi U/Rikkyo U/Nagoya U/Chiba Inst Tech/Meiji U/U Aizu/AIST
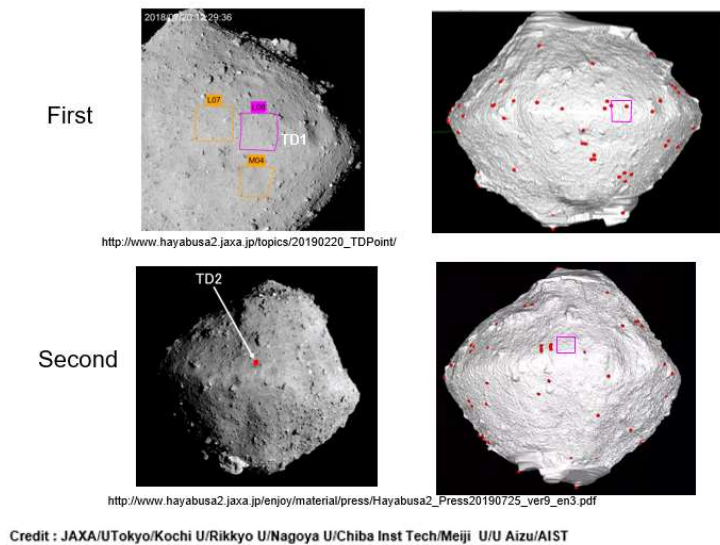
Fig. 9 The touchdown areas

5. Summary

 This report discussed an inverse problem involved in digital image processing for the 3D reconstruction of the asteroid Ryugu conducted in the Hayabusa 2 project. From the 2D images, the 3D data including the asteroid coordinates, the positions of feature points, the positions and orientations of the spacecraft, and surface shape model was successfully determined.

Reference
[1] Maruya, An inverse problem in 3D reconstruction of asteroids, RIMS Workshop on Inverse problems for partial differential equations and related areas, January 2019.
https://sites.google.com/view/rims-ws-ip-2019en

[2] Makoto Maruya, Hiroshi Ohyama, Masashi Uo, Noboru Muranaka, Hideo Morita, Takashi Kubota, Tatsuaki Hashimoto, Jun Saito, Jun'ichiro Kawaguchi, 2006. Navigation Shape and Surface Topography Model of Itokawa, AIAA Guidance, Navigation, and Control Conference.

[3] Fuyuto Terui, Yuichi Tsuda, Naoko Ogawa, Yuya Mimasu, Autonomy for Guidance, Navigation and Control of Hayabusa 2, Journal of the Japanese Society for Artificial Intelligence 29(4), 327-334, 2014-07-01.

[4] Bill Triggs, Philip McLauchlan, Richard Hartley and Andrew Fitzgibbon. Bundle Adjustment — A Modern Synthesis, Vision Algorithms: Theory and Practice, 2000 Springer.

New technologies for non-destructive and non-invasive inspections and their applications

3D reconstruction of the asteroid
Ryugu
as an inverse problem

Makoto Maruya

maruya@kta.biglobe.ne.jp

National Institute of Advanced Industrial Science and Technology /

Geo Insight LLC

This presentation is supported by Hayabusa2 project of the Japan Aerospace Exploration Agency (JAXA).

Oct. 30, 2019. Institute of Mathematics for Industry,   Kyushu University.

1

Contents
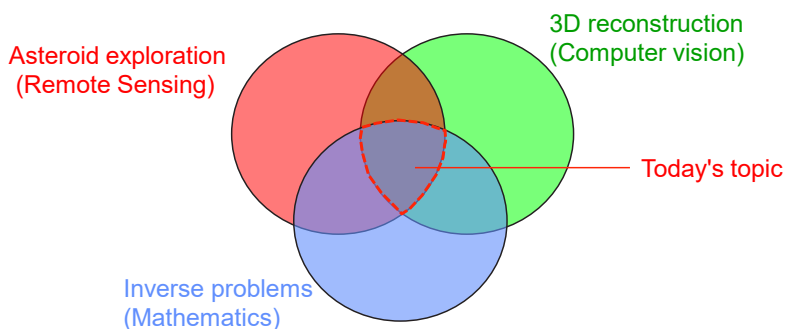
Asteroid exploration
(Remote Sensing)

3D reconstruction
(Computer vision)

Today's topic

Inverse problems
(Mathematics)

1. Hayabusa2 and touch down operation
2. A method of 3D reconstruction
3. Computational results of Ryugu reconstruction
4. Some remote sensing topics related to inverse problems
5. Summary

------- from published materials

} from RIMS WS*

* Maruya, An inverse problem in 3D reconstruction of asteroids, RIMS Workshop on Inverse problems for partial differential equations and related areas, January 2019.
https://sites.google.com/view/rims-ws-ip-2019en

2

Hayabusa2 components

3

Hayabusa2 Mission flow and status

4

Where is Ryugu ?

2018.12.31

2018.11.20

Earth

Sun

Ryugu

Positions of Ryugu and the Earth

©JAXA

About 2AU

Round-trip delay time from the earth to Ryugu: 30+ minutes.

http://www.hayabusa2.jaxa.jp/enjoy/material/press/Hayabusa2_Press20181108_ver6_en2.pdf

5

Definition of operation boxes

Earth Sun

Communication / power

20[km]

1[km] BOX-A

BOX-B

1~5[km]

BOX Y_{HP}-direction size
BOX-A : 1[km](±500[m])
BOX-B : 20[km](±10[km])
BOX-C : 1[km](±500[m])

BOX-C

20[km]

5[km]+
asteroid average radius

Z_{HP}

Gravity

A

X_{HP}

asteroid center of mass
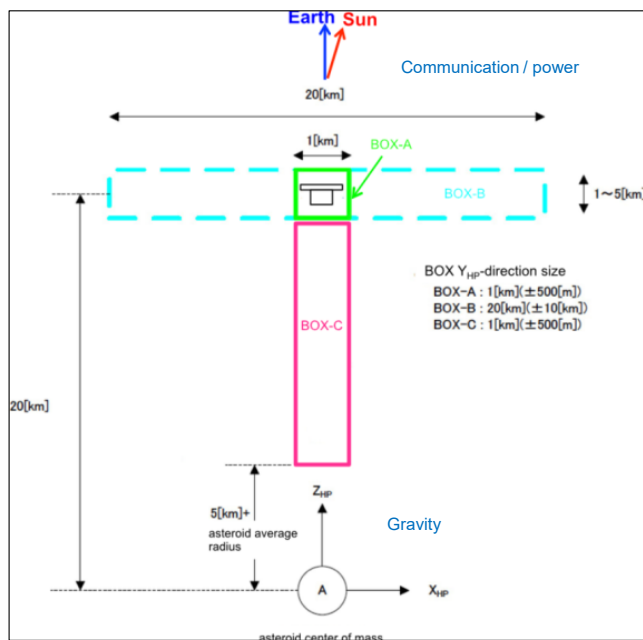
http://www.hayabusa2.jaxa.jp/topics/20180725je/index_e.html

6

First touchdown （During descent）

3. Results of the touchdown operation

During descent

Home position→ 20km height

Time of start of descent (original plan) 2/21 08:13

Descent start 2/21 13:13

90cm/s

40cm/s

nominal trajectory

Nominal trajectory return 2/21 17:33

Descent deceleration 2/21 18:33

touchdown 2/22 07:29

Note) Touchdown detected by change in attitude.

10cm/s

65cm/s

Value of speed is approximate

Time (JST、onboard time)

(image credit：JAXA)

2019/03/05　　Hayabusa2 reporter briefing

24 hours

http://www.hayabusa2.jaxa.jp/enjoy/material/press/Hayabusa2_Press20190305_ver9_en.pdf

First touchdown （Low altitude）

3. Results of the touchdown operation

Low altitude

Antenna change HGA→LGA

TM capture with GCP-NAV guidance system

Antenna change LGA→HGA

07:50

45m

07:07

TM capture

07:10

LIDAR→LRF takeover

TM tracking during descent

TM relative horizontal motion

Horizontal movement while viewing TM

Hover at TM relative offset point

Rising

Landing attitude final adjustment (tail up)

07:19

07:27

Tilt to landing posture

Final descent

8.5m

LRF altitude measurement

LIDAR altitude measurement

07:29

Touchdown

Pinpoint method

0m

TM

L08-E1

TM: Target Marker

Time is JST on February 22 (onboard time)

TM

(Image credit：JAXA)

2019/03/05　　Hayabusa2 reporter briefing

http://www.hayabusa2.jaxa.jp/enjoy/material/press/Hayabusa2_Press20190305_ver9_en.pdf
http://www.hayabusa2.jaxa.jp/enjoy/material/press/Hayabusa2_Press20181108_ver6_en2.pdf

Credit : JAXA/UTokyo/Kochi U/Rikkyo U/Nagoya U/Chiba Inst Tech/Meiji U/U Aizu/AIST

GCP* based navigation (GCP-NAV)

*Ground Control Point: feature point with 3D position data.   GCP data must be prepared prior to touch down operation.
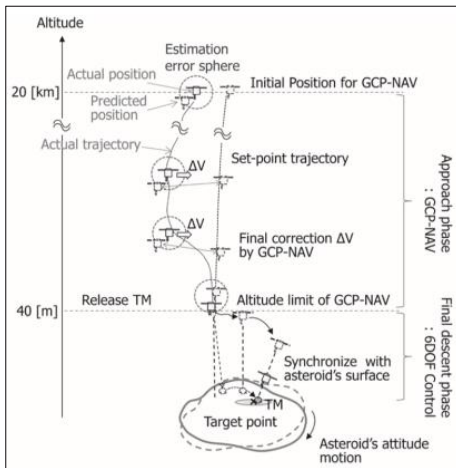
Touch down sequence.
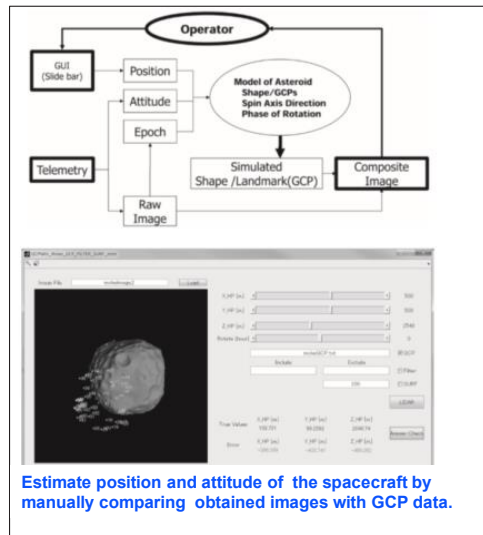
Estimate position and attitude of the spacecraft by manually comparing obtained images with GCP data.

Terui el.al., Autonomy for Guidance, Navigation and Control of Hayabusa, Journal of the Japanese Society for Artificial Intelligence 29(4), 327-334, 2014-07-01

9

Difficulties in asteroid exploration

・Limited prior information about target asteroids

・Long communication delay
  → difficulty in real-time manual operation

・Limited bandwidth of earth-explorer communication

・Limited duration of observation

・Limited fuel of explorers

  ➡ Importance of in-situ reconstruction of 3D shape (3D map) of the target asteroid and navigation planning based on that 3D data

10

Contents
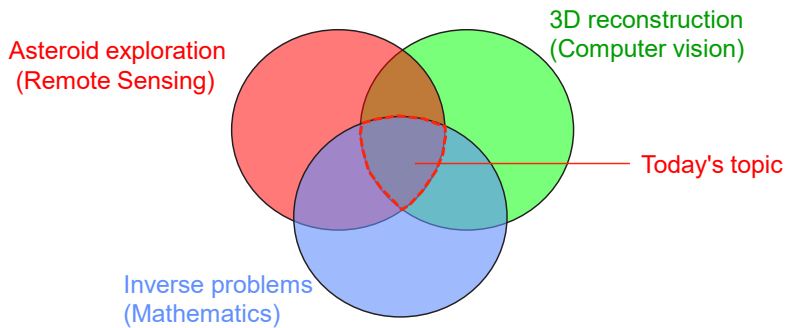
Asteroid exploration (Remote Sensing)

3D reconstruction (Computer vision)

Today's topic

Inverse problems (Mathematics)

1. Hayabusa2 and touch down operation
2. A method of 3D reconstruction
3. Computational results of Ryugu reconstruction
4. Some remote sensing topics related to inverse problems
5. Summary

3D reconstruction of Ryugu (Hayabusa2)

Z (Rotation axis)

Feature point / GCP

X

Longitude: 0 deg

Main topic of this presentation
An inverse problem

About 900m

Real 2D images obtained from Home Position

http://www.hayabusa2.jaxa.jp/topics/20180711je/index.html

Credit : JAXA/UTokyo/Kochi U/Rikkyo U/Nagoya U/Chiba Inst Tech/Meiji U/U Aizu/AIST
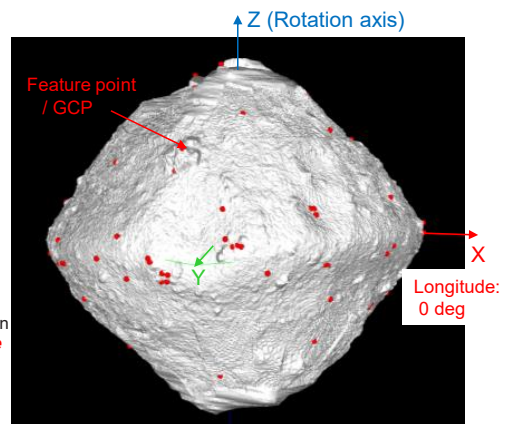
Reconstructed 3D model
1. Asteroid coordinates
2. Ground control points (GCP)
3. Surface shape

Navigation

Image acquisition

UTC 2018-10-15 10:55

Position: unknown
Orientation(rotation): unknown
Shape: unknown

Rotation

Feature point

Drift

Camera

Field of view

Explorer

Position: unknown
Orientation: unknown

Distance ①20km ②6km

UTC 2018-10-15 11:23

Known
・Feature point positions on 2D images

Unknown
・Feature point position (3D)
・Camera position and orientation
　(= Motion of the asteroid and motion of the explorer)
・Asteroid coordinates

92 feature points (GCPs) on 79 images

UTC 2018-10-15 11:52

V
U
Image Coordinates

Credit : JAXA/UTokyo/Kochi U/Rikkyo U/Nagoya U/Chiba Inst Tech/Meiji U/U Aizu/AIST
http://www.hayabusa2.jaxa.jp/topics/20180915/

13

Basic Imaging Geometry: single view

The simplest case.

Camera coordinates

Y
X
v
u
O
q
p
Z
Image coordinates

flen: focal length

image plane

Projected feature point on the image plane

2D
$q = \begin{bmatrix} u \\ v \end{bmatrix}$

Feature point of an object (3D)

$P = \begin{bmatrix} Xp \\ Yp \\ Zp \end{bmatrix}$

Z
Y
X
Object coordinates

$\lambda \begin{bmatrix} u \\ v \\ flen \end{bmatrix} = R \begin{bmatrix} Xp \\ Yp \\ Zp \end{bmatrix} + T$

Relation between two coordinates

where

R: 3x3 Rotation matrix including three orientation parameters

$R = R_x(\alpha) R_x(\beta) R_z(\gamma)$

$T = \begin{bmatrix} t_x \\ t_y \\ t_z \end{bmatrix}$: Translation vector

λ: scale parameter

Define projection function: f

$\begin{bmatrix} u \\ v \end{bmatrix} = f(P, R, T)$

2D　　3D position

⟸ Computable

⟹ Not computable
(Projective ambiguity)

14

Basic Imaging Geometry: multiple views

Plural camera positions and plural feature points

$$\begin{bmatrix} u_a \\ v_a \end{bmatrix}_{cam\_1} = f(P_a, R_1, T_1)$$

$$\begin{bmatrix} u_b \\ v_b \end{bmatrix}_{cam\_1} = f(P_b, R_1, T_1)$$

$$\begin{bmatrix} u_c \\ v_c \end{bmatrix}_{cam\_1} = f(P_c, R_1, T_1)$$

$$\begin{bmatrix} u_a \\ v_a \end{bmatrix}_{cam\_2} = f(P_a, R_2, T_2)$$

$$\begin{bmatrix} u_b \\ v_b \end{bmatrix}_{cam\_2} = f(P_b, R_2, T_2)$$

$$\begin{bmatrix} u_c \\ v_c \end{bmatrix}_{cam\_2} = f(P_c, R_2, T_2)$$
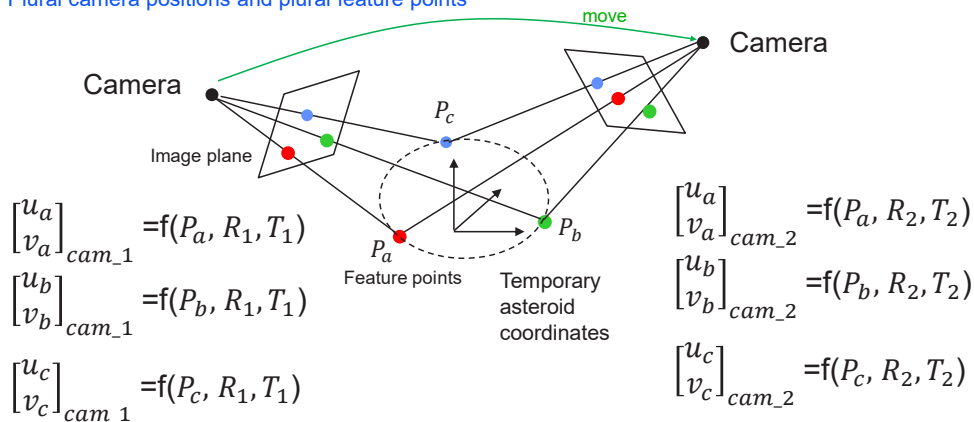
Num. of cameras: M
Num. of feature points: N

Num. of equations: 2MN
Num. of variables: 6M+3N - 7

3(position)+3(orientation)+1(scale)

If $2MN \geqq 6M+3N-7$

A set of $\begin{bmatrix} u \\ v \end{bmatrix}$ ⟹ A set of P(feature point positions), R(rotation),T(translation)

Computable with some exceptions

Just geometrical problem solving so far.

15

Computational process: step1

1. Divide the problem into small partial problems and solve them.

Num. of camera positions:3
Num. of feature points: More than 4
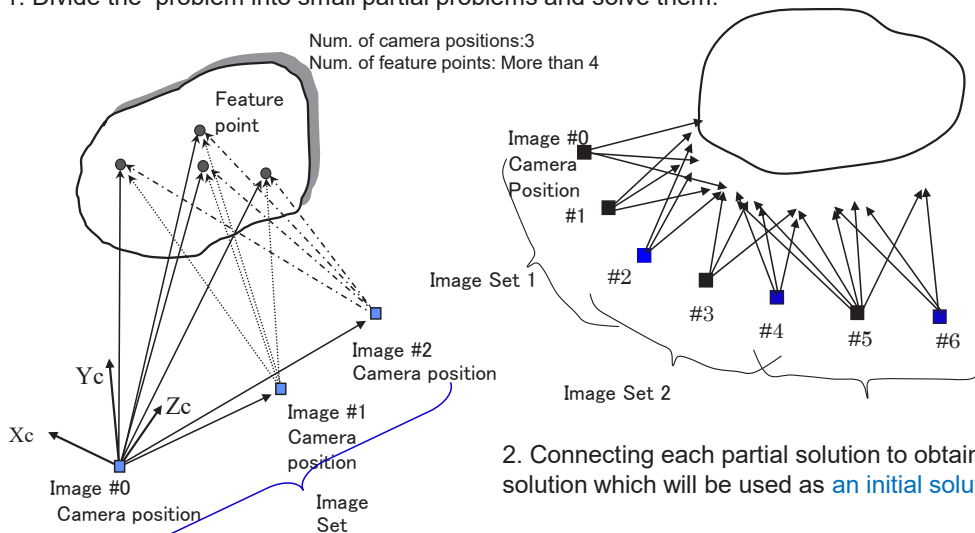
2. Connecting each partial solution to obtain total solution which will be used as an initial solution.

Generally, such an initial solution contains significant errors and it does not satisfy whole GCP observation.

16

Observation errors and their effect

Detected position of
a feature point

v

$+$ q=$\begin{bmatrix} u \\ v \end{bmatrix}$

inevitably contain
some errors.

u

2D→3D

Estimation
of P,R,T

3D→2D

Calculation
of q'

Calculated position of
the feature point

q'=$\begin{bmatrix} u' \\ v' \end{bmatrix}$

$+$

Reprojection
error

$e = \|q - q'\|^2$
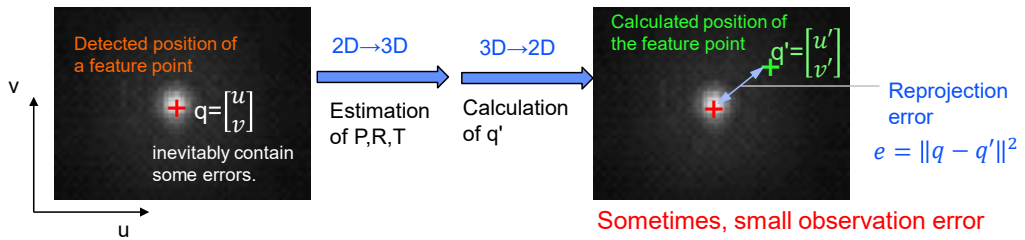
It is difficult to determine the accurate locations of
feature points on an image plane.

Sometimes, small observation error
could cause large reprojection error.
One of the characteristics of inverse
problems.

Y

X

3D→2D

y

q'

x

q $\bullet$ $\mathbf{p}$

$\mathbf{O}$

2D→3D

Z

image plane

Observation errors and their effect

Detected position of
a feature point

v

$+$ q=$\begin{bmatrix} u \\ v \end{bmatrix}$

inevitably contain
some errors.

u

2D→3D

Estimation
of P,R,T

3D→2D

Calculation
of q'

Calculated position of
the feature point

q'=$\begin{bmatrix} u' \\ v' \end{bmatrix}$

$+$

Reprojection
error

$e = \|q - q'\|^2$
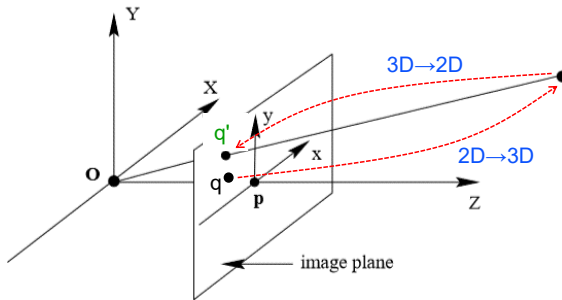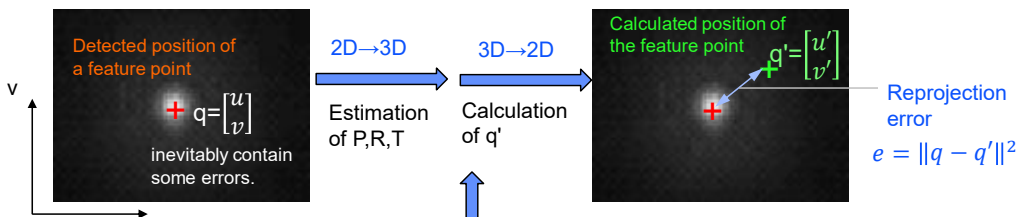
It is difficult in determining the accurate
locations of feature points on an image
plane.

Sometimes,
small observation error
could cause large
reprojection error.

Iteration

For improvement
of solution

Modification of P,R,T

Formulation as an optimization problem

$$\widehat{x} = \underset{x}{\text{argmin}} \; E(x)$$

$E(x)$: Total reprojection error

$$E(x) = \sum_{i=1}^{M} \sum_{j=1}^{N} e_{i,j}(x)$$

where

x : A set of P,R,T

・3D position of feature points
・Camera rotation and translation

M: Num. of camera positions = 79
N: Num. of feature points = 92

We tried to obtain $\widehat{x}$ by numerical computation.

Computational process: step 2

Optimization by piecewise least square estimation

Linear approximation

Observation Equation: $Ax = y$

Least Square Estimation: $x = (A^{T}A)^{-1} \cdot A^{T}y$

x : Camera Position/Rotation, GCP position　（Dimension: 743 ）
y : 2D projection state （Dimension: about 14k) ⇒ calculate total reprojection error
A : Sensitivity Matrix

Additional effort: accuracy improvement by iteration of finding and omitting "inconsistent" (poor quality) feature point data.

Num. of trial	1	2	3	4	5
Average reprojection error[pixel]	1.44	1.11	0.90	0.87	0.82

Remaining problems
- requires large computing time including manual operation
- insufficient convergence (occasionally).
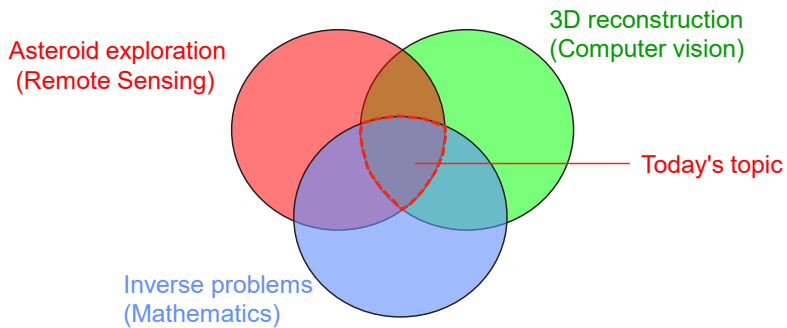
Contents

Asteroid exploration
(Remote Sensing)

3D reconstruction
(Computer vision)

Today's topic

Inverse problems
(Mathematics)
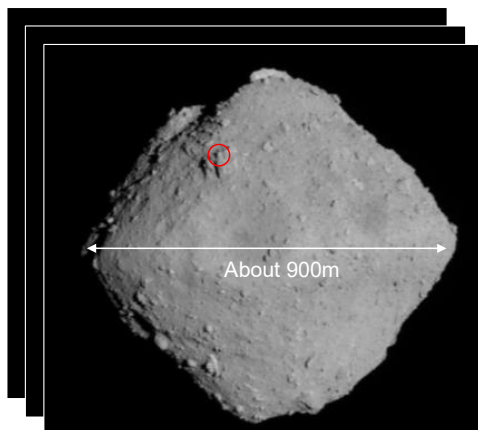
1. Hayabusa2 and touch down operation
2. A method of 3D reconstruction
3. Computational results of Ryugu reconstruction
4. Some remote sensing topics related to inverse problems
5. Summary

---

Computational results (Position of cameras and feature points)

After determining asteroid coordinates·····

Estimated camera position
on the asteroid coordinates

Estimated 3D position of feature points
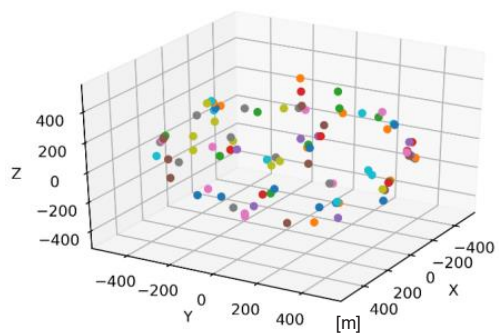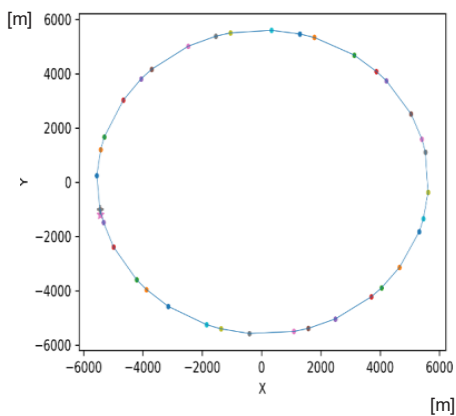
Surface reconstruction by stereo measurement
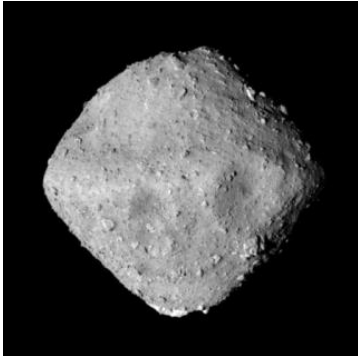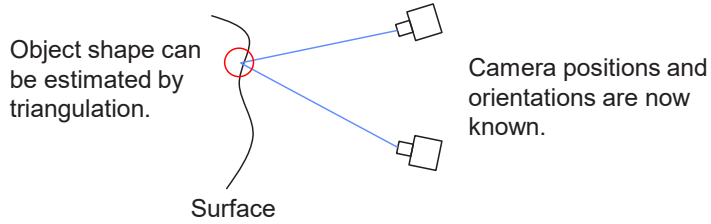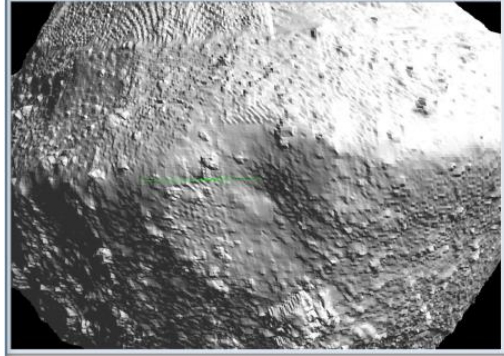
Object shape can be estimated by triangulation.

Camera positions and orientations are now known.

Surface

Image

Reconstructed surface

23

Computational results （GCPs and Shape）
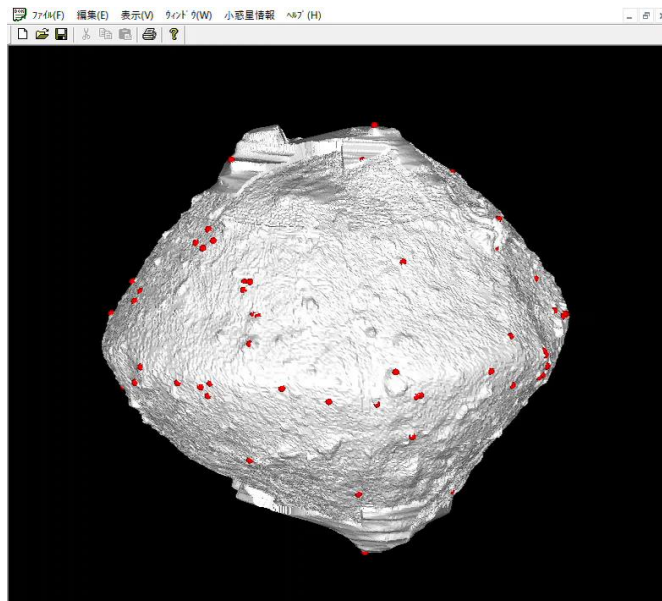
24

Touch down areas

First
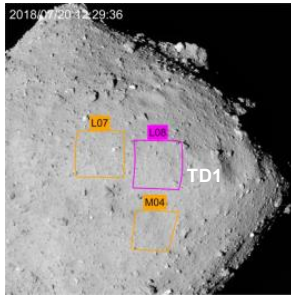
http://www.hayabusa2.jaxa.jp/topics/20190220_TDPoint/
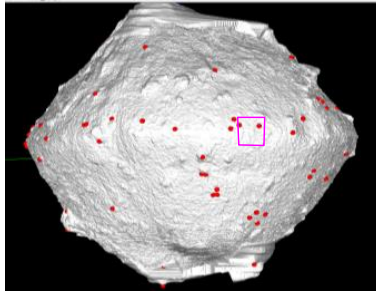
Second
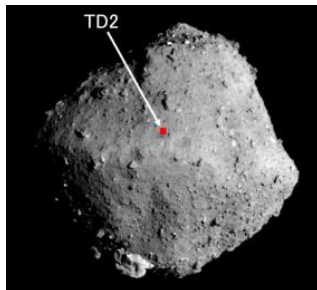
http://www.hayabusa2.jaxa.jp/enjoy/material/press/Hayabusa2_Press20190725_ver9_en3.pdf
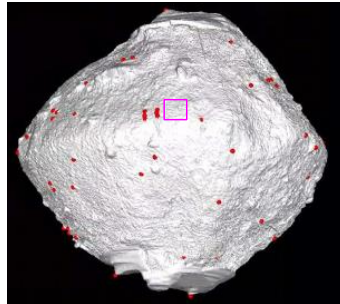
Credit : JAXA/UTokyo/Kochi U/Rikkyo U/Nagoya U/Chiba Inst Tech/Meiji U/U Aizu/AIST

25

Why do we explore asteroids?

・Scientific interest (History of solar system)
・Potentially hazardous objects
・Planetary resources in future

Almost
< 100km in diameter

Photos not to scale

Example of
asteroids
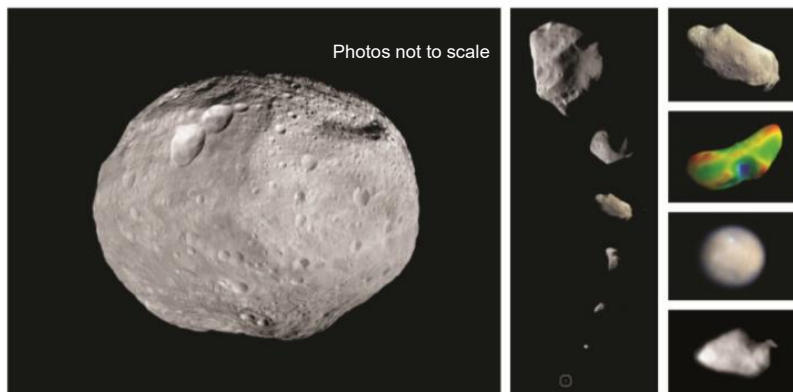
https://solarsystem.nasa.gov/docs/000-SolarSystemLithosCombined_Rev1_FC_optimized.pdf

These image data are the results of past exploration efforts.

26

Other asteroid explorers

【Mission completed】

Hayabusa(JAXA)　　Itokawa

http://jda.jaxa.jp/result.php?lang=j&id=2e3206
1fbb157c8658e2d17df7c6bfaf

Sample return (2010)

NEAR Shoemaker(NASA)　433 Eros

www.aerospaceguide.net/spacecraft/near.html

Landing (2001)

【Mission in progress】

OSIRIS-REx(NASA)　Bennu

Arrived on Nov. 13, 2018.

https://www.asteroidmission.org/?latest-news=nasas-osiris-
rex-spacecraft-arrives-asteroid-bennu
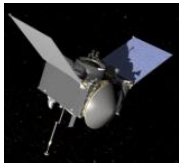
Martian Moons (not asteroid)
Sample return (2029?)

27

Future challenges

Field of view

Small body　　　Explorer
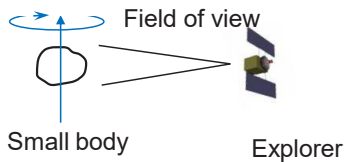
Small inverse problem
・Num. of images < 100
・Num. of GCPs　< 100

Large body
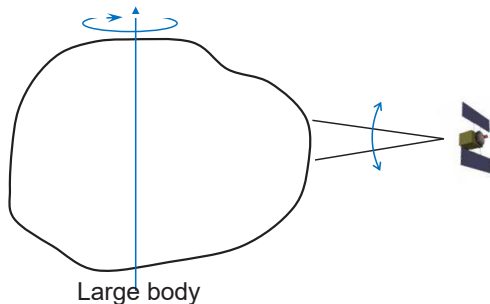
Large inverse problem
・Num. of images: several hundreds
・Num. of GCPs: several hundreds

28

Suggestions received so far

・Analysis using singular value decomposition
・Regularization
・Coarse to fine approach
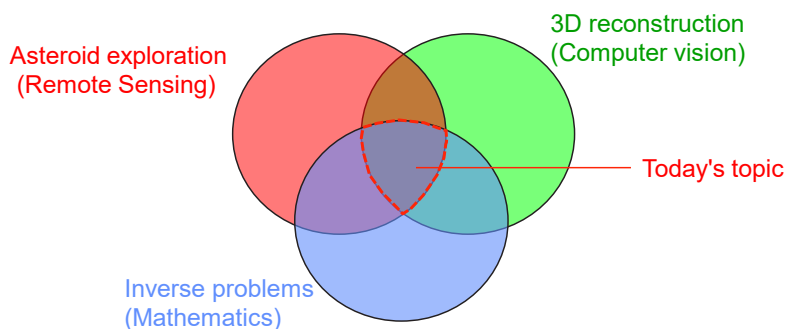
Contents

Asteroid exploration
(Remote Sensing)

3D reconstruction
(Computer vision)

Today's topic

Inverse problems
(Mathematics)

1. Hayabusa2 and touch down operation
2. A method of 3D reconstruction
3. Computational results of Ryugu reconstruction
4. Some remote sensing topics related to inverse problems
5. Summary

Remote sensing and Inverse problems

Sensor → Raw data

Signal
-Ambiguity
-Noise
etc.

Distance

Object

Research effort

Modeling (Forward process) ⟶ Computational algorithm (Inverse process)

Physical quantities to be measured.
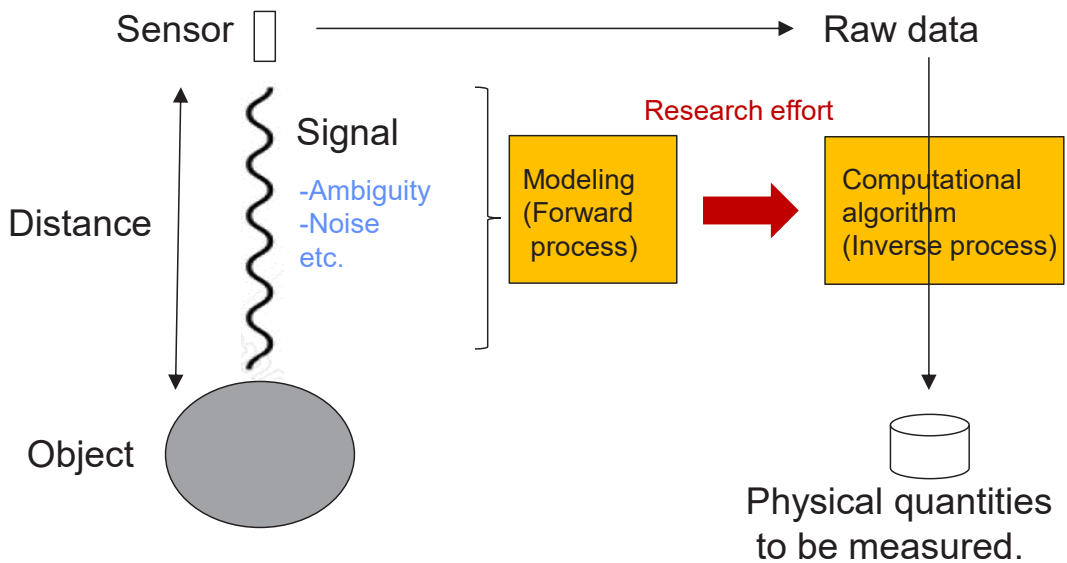
31

Related topics

・Super-resolution of optical images
・Retrieval of atmospheric methane
・Global Navigation Satellite System

32

Summary

・ Introduced a topic "Hayabusa2 and touch down operation".

・Explained a method of 3D reconstruction and discussed
 the relation with inverse problems.

・Demonstrated some results of Ryugu reconstruction and
 discussed future challenge of 3D reconstruction.

・Introduced some remote sensing topics related to
 inverse problems.

33

References

[1] Maruya, An inverse problem in 3D reconstruction of asteroids, RIMS Workshop on Inverse problems for partial differential equations and related areas, January 2019. https://sites.google.com/view/rims-ws-ip-2019en

[2] Makoto Maruya, Hiroshi Ohyama, Masashi Uo, Noboru Muranaka, Hideo Morita, Takashi Kubota, Tatsuaki Hashimoto, Jun Saito, Jun'ichiro Kawaguchi,2006. Navigation Shape and Surface Topography Model of Itokawa, AIAA Guidance, Navigation, and Control Conference.

[3] Fuyuto Terui, Yuichi Tsuda, Naoko Ogawa, Yuya Mimasu, Autonomy for Guidance, Navigation and Control of Hayabusa 2, Journal of the Japanese Society for Artificial Intelligence 29(4), 327-334, 2014

[4] Bill Triggs, Philip McLauchlan, Richard Hartley and Andrew Fitzgibbon. Bundle Adjustment — A Modern Synthesis,　Vision Algorithms : Theory and Practice, 2000 Springer.

34

Perturbations of Rayleigh waves in anisotropic elasticity and Bleustein-Gulyaev waves in piezoelectricity

Kazumi Tanuma* (presenter)

1 Perturbations of Rayleigh waves

1.1 Introduction

Rayleigh waves are elastic surface waves which propagate along the traction-free surface with the phase velocity in the subsonic range, and whose amplitude decays exponentially with depth below the surface. Such waves serve as a useful tool in nondestructive characterization of materials. We consider Rayleigh waves propagating along the traction-free surface of a homogeneous elastic half-space. For isotropic elasticity, such waves are well known: Their phase velocity is determined by the secular equation, which is a bi-cubic equation written in terms of the Lamé constants. For orthorhombic elastic materials, when the traction-free surface is spanned by two symmetry axes and the propagation direction of Rayleigh waves coincides with one of them, the phase velocity of the waves is determined by a bi-cubic equation whose coefficients are written in terms of the components of the elasticity tensor. For general anisotropic materials, however, to derive equations for Rayleigh-wave velocity and to solve them are complicated or difficult. For the approaches along this line, see, for example, [4, 5, 20, 21, 22, 23].

In this section we assume that the elasticity tensor has a principal (unperturbed) part which is orthorhombic and assume that the remaining (perturbative) part of the elasticity tensor is arbitrarily anisotropic. We then investigate the perturbation of the phase velocity and of the polarization ratio (i.e., the ratio of the maximum longitudinal and maximum normal component of the displacements at the surface) of Rayleigh waves, i.e., the shift of phase velocity and the shift of polarization ratio of Rayleigh waves from their respective value pertaining to the comparative orthorhombic state, as caused by the perturbative part of the elasticity tensor. We present perturbation formulas for the phase velocity and for the polarization ratio, which are correct to first order in the components of the perturbative part of the elasticity tensor. These formulas show explicitly how the perturbative part of the elasticity tensor, to first order of itself, affects the phase velocity and the polarization ratio of Rayleigh waves. We obtain these formulas by a consistent method on the basis of the Stroh formalism.

Isotropic materials can be realized by reducing the 9 independent components of the elasticity tensor of orthorhombic materials to the 2 independent Lamé components. Hence our formulas also

*Department of Mathematics, Faculty of Science and Technology, Gunma University, Kiryu 376-8515, Japan.
E-mail: tanuma@gunma-u.ac.jp

apply to such a material that the principal (unperturbed) part of the elasticity tensor is isotropic and the remaining (perturbative) part of the elasticity tensor is arbitrarily anisotropic.

Herein we restrict our study to the forward problem, i.e., the problem of investigating the behavior of Rayleigh waves provided that all the relevant information on material parameters are known. We believe, however, that the results in the forward problem will serve as a guide when considering the inverse problem, i.e., the problem of characterizing material parameters from observation of Rayleigh waves that propagate along the unknown materials.

The study in this section is a joint work with Chi-Sing Man (University of Kentucky, USA) and Wenwen Du (Glenville State College, USA).

1.2 Preliminaries

Let $\boldsymbol{E} = \boldsymbol{E}(\boldsymbol{u}) = \left(\varepsilon_{ij}\right)_{i,j=1,2,3}$ be the infinitesimal strain tensor

$$\varepsilon_{ij} = \frac{1}{2}\left(\frac{\partial u_i}{\partial x_j} + \frac{\partial u_j}{\partial x_i}\right), \tag{1}$$

where $\boldsymbol{u} = \boldsymbol{u}(\mathbf{x}) = (u_1, u_2, u_3)$ is the displacement at the place $\mathbf{x}$ pertaining to the superimposed small elastic motion and (x_1, x_2, x_3) are the Cartesian coordinates of $\mathbf{x}$. In the theoretical context of linear elasticity, the constitutive equation can be written as the generalized Hooke's law:

$$\boldsymbol{\sigma} = \mathbb{C}[\boldsymbol{E}] \qquad \text{or} \qquad \sigma_{ij} = \sum_{k,l=1}^{3} C_{ijkl}\,\varepsilon_{kl}, \tag{2}$$

where $\boldsymbol{\sigma} = (\sigma_{ij})_{i,j=1,2,3}$ is the stress and $\mathbb{C}$ is the elasticity tensor, the latter of which, when regarded as a fourth-order tensor that maps symmetric tensors $\boldsymbol{E}$ onto symmetric tensors, has major and minor symmetries

$$C_{ijkl} = C_{klij} = C_{jikl}, \qquad i,j,k,l = 1,2,3.$$

We assume that the stored energy function is positive for any non-zero strain, which implies that $\mathbb{C} = \left(C_{ijkl}\right)_{i,j,k,\ell=1,2,3}$ is positive definite or it satisfies the following strong convexity condition:

$$\sum_{i,j,k,l=1}^{3} C_{ijkl}\,\varepsilon_{ij}\,\varepsilon_{kl} > 0 \quad \text{for any non-zero } 3 \times 3 \text{ real symmetric matrix } (\varepsilon_{ij}).$$

We say that the elastic material is isotropic if the elasticity tensor $\mathbb{C}$ satisfies

$$C_{ijkl} = \sum_{p,q,r,s=1}^{3} Q_{ip}\,Q_{jq}\,Q_{kr}\,Q_{ls}\,C_{pqrs}, \qquad i,j,k,l = 1,2,3 \tag{3}$$

for any orthogonal tensor $\boldsymbol{Q} = (Q_{ij})_{i,j=1,2,3}$. For isotropic materials, the components C_{ijkl} can be written as

$$C_{ijkl} = \lambda\,\delta_{ij}\delta_{kl} + \mu(\delta_{ik}\delta_{jl} + \delta_{il}\delta_{kj})$$

with the Lamé constants λ and μ. We say that the elastic material is anisotropic if it is not isotropic.

In this section, as a base material we take an orthorhombic medium* with elasticity tensor $\mathbb{C}^{\text{Orth}}$. Suppose the base material can be such that it occupies the half-space $x_3 \leq 0$ and its symmetry axes

---

*We say that an elastic material is orthorhombic if (3) holds for the orthogonal tensor $\boldsymbol{Q} = (Q_{ij})_{i,j=1,2,3}$ corresponding to a right-handed rotation by the angle π around each of the three coordinate axes.

coincide with the three coordinate axes. Then the elasticity tensor $\mathbb{C}^{\text{Orth}}$ is expressed under the Voigt notation[†] as

$$\mathbb{C}^{\text{Orth}} = (C_{\alpha\beta}^{\text{Orth}}) = \begin{pmatrix} C_{11} & C_{12} & C_{13} & 0 & 0 & 0 \\ & C_{22} & C_{23} & 0 & 0 & 0 \\ & & C_{33} & 0 & 0 & 0 \\ & & & C_{44} & 0 & 0 \\ & & & & C_{55} & 0 \\ Sym. & & & & & C_{66} \end{pmatrix}. \tag{4}$$

Suppose that the elasticity tensor $\mathbb{C}$ is composed of an orthorhombic part $\mathbb{C}^{\text{Orth}}$ and a perturbative part $\mathbb{A}$, the latter of which expresses a deviation of the material from its orthorhombic unperturbed state. For the perturbative part $\mathbb{A}$, we assume the major and minor symmetries

$$a_{ijkl} = a_{klij} = a_{jikl}, \qquad i,j,k,l = 1,2,3$$

but do not assume any material symmetry. In the Voigt notation, $\mathbb{A}$ can be written as

$$\mathbb{A} = (a_{\alpha\beta}) = \begin{pmatrix} a_{11} & a_{12} & a_{13} & a_{14} & a_{15} & a_{16} \\ & a_{22} & a_{23} & a_{24} & a_{25} & a_{26} \\ & & a_{33} & a_{34} & a_{35} & a_{36} \\ & & & a_{44} & a_{45} & a_{46} \\ Sym. & & & & a_{55} & a_{56} \\ & & & & & a_{66} \end{pmatrix} \tag{5}$$

and the 21 components in the upper triangular part of matrix (5) are generally all independent. In this setting, $\mathbb{C}$ can be written as a fourth-order tensor on symmetric tensors $\boldsymbol{E}$ in the form

$$\mathbb{C}[\boldsymbol{E}] = \mathbb{C}^{\text{Orth}}[\boldsymbol{E}] + \mathbb{A}[\boldsymbol{E}]. \tag{6}$$

Thus, in our constitutive equation (2) with (6), $\mathbb{A}$ expresses the deviation of the medium in question from its comparative orthorhombic state and then we consider what influence $\mathbb{A}$ exerts upon the phase velocity and the polarization of Rayleigh waves that propagate along the surface of the material half-space.

Let t denote the time and ρ the uniform mass density of the material. Substitution of (1) and (2) into the equation of motion with no body force, namely

$$\sum_{j=1}^{3} \frac{\partial}{\partial x_j} \sigma_{ij} = \rho \frac{\partial^2}{\partial t^2} u_i, \qquad i = 1,2,3,$$

leads us to the elastic wave equation written in terms of the displacement

$$\sum_{j=1}^{3} \frac{\partial}{\partial x_j} \left(C_{ijkl} \frac{\partial u_k}{\partial x_l} \right) = \rho \frac{\partial^2}{\partial t^2} u_i, \qquad i = 1,2,3. \tag{7}$$

[†]For the subscripts ij and kl of $C_{ijkl} \in \mathbb{C}$ we have used the rules of replacing the subscript ij (or kl) by α (or β) as follows:

ij (or kl)		α (or β)	ij (or kl)		α (or β)
11	$\longleftrightarrow$	1	23 or 32	$\longleftrightarrow$	4
22	$\longleftrightarrow$	2	31 or 13	$\longleftrightarrow$	5
33	$\longleftrightarrow$	3	12 or 21	$\longleftrightarrow$	6.

Then the fourth-order tensor $\mathbb{C}$ can be written as a 6×6 symmetric matrix $(C_{\alpha\beta})_{\alpha,\beta=1,2,3,4,5,6}$.

We consider Rayleigh waves that propagate along the traction-free surface $x_3 = 0$ of the half-space $x_3 \leq 0$ in the direction of 2-axis with the phase velocity v_R in the subsonic range, and whose amplitude decays exponentially as $x_3 \longrightarrow -\infty$, and which produce no tractions on $x_3 = 0$. The Stroh formalism (cf., for example, [1, 3, 15, 19]) leads us to the time-harmonic solution to the elastic wave equation (7) which describes such Rayleigh waves

$$\boldsymbol{u} = \sum_{\alpha=1}^{3} c_\alpha \, \mathbf{a}_\alpha \, e^{-\sqrt{-1}\, k(x_2 + p_\alpha x_3 - v\,t)}, \tag{8}$$

where k is the wave number, $\mathbf{a}_\alpha = \mathbf{a}_\alpha(v) \in \mathbb{C}^3$ and $p_\alpha = p_\alpha(v) \in \mathbb{C}^\ddagger$ with $\mathrm{Im}\, p_\alpha > 0$ $(\alpha = 1,2,3)^\S$ are determined from the equation (7), while the traction-free condition at the boundary

$$\sigma_{i3}\,|_{x_3=0} = \sum_{k,l=1}^{3} C_{i3kl} \frac{\partial u_k}{\partial x_l}\bigg|_{x_3=0} = 0, \qquad i = 1, 2, 3$$

determines the phase velocity $v = v_R$ and $c_\alpha = c_\alpha(v_R) \in \mathbb{C}$ $(\alpha = 1, 2, 3)$.

The displacement field $\boldsymbol{u}$ of the Rayleigh waves at the surface $x_3 = 0$ is written through (8) as

$$\boldsymbol{u} = \mathbf{a}_{\mathrm{pol}} \, e^{-\sqrt{-1}\, k(x_2 - v_R\, t)}, \qquad \mathbf{a}_{\mathrm{pol}} = \sum_{\alpha=1}^{3} c_\alpha \mathbf{a}_\alpha.$$

The polarization ratio r_R of Rayleigh waves on the surface $x_3 = 0$ is defined as the ratio of the maximum longitudinal component to the maximum normal component of the displacements on $x_3 = 0$ (see [7]):

$$r_R = \left| \frac{(\mathbf{a}_{\mathrm{pol}})_2}{(\mathbf{a}_{\mathrm{pol}})_3} \right|_{x_3=0},$$

where $(\mathbf{a}_{\mathrm{pol}})_i$ denotes the i-th component of the vector $\mathbf{a}_{\mathrm{pol}}$ and $|z|$ denotes the absolute value of a complex number z.

1.3   Perturbation of phase velocity of Rayleigh waves

For an orthorhombic base material whose elasticity tensor is given by (4), when there exist Rayleigh waves propagating along the surface of the half-space $x_3 \leq 0$ in the direction of the 2-axis, the phase velocity v_R^{Orth} satisfies the secular equation (see [13])

$$R^{\mathrm{Orth}}(v) = 0, \tag{9}$$

where

$$R^{\mathrm{Orth}}(v) = C_{33} C_{44}(C_{22} - V)V^2 - (C_{44} - V)\left(C_{33}(C_{22} - V) - C_{23}^2\right)^2, \qquad V = \rho v^2. \tag{10}$$

Theorem 1 *In an elastic medium whose elasticity tensor $\mathbb{C}$ is given by (6), the phase velocity of Rayleigh waves which propagate along the surface of the half-space $x_3 \leq 0$ in the direction of the 2-axis can be written, up to terms linear in the perturbative part $\mathbb{A}$ of $\mathbb{C}$, as*

$$v_R = v_R^{\mathrm{Orth}} - \frac{1}{2\rho\, v_R^{\mathrm{Orth}}} \left[\gamma_{22}(v_R^{\mathrm{Orth}})\, a_{22} + \gamma_{23}(v_R^{\mathrm{Orth}})\, a_{23} + \gamma_{33}(v_R^{\mathrm{Orth}})\, a_{33} + \gamma_{44}(v_R^{\mathrm{Orth}})\, a_{44}\right], \tag{11}$$

---

‡We also use the symbol $\mathbb{C}$ to denote the classical elasticity tensor. It should be clear from the context what the symbol means when it appears.

§This condition guarantees the exponential decay of the solution (8) in $x_3 \longrightarrow -\infty$.

where

$$\gamma_{ij}(v) = \frac{N_{ij}(v)}{D(v)} \quad (\{ij\} = \{22\}, \{23\}, \{33\}, \{44\}), \tag{12}$$

$$N_{22}(v) = C_{33}[-2C_{44}(C_{22}C_{33} - C_{23}^2) + 2(C_{22}C_{33} - C_{23}^2 + C_{33}C_{44})V + (C_{44} - 2C_{33})V^2],$$

$$N_{23}(v) = 4C_{23}(C_{44} - V)(C_{22}C_{33} - C_{23}^2 - C_{33}V),$$

$$N_{33}(v) = (C_{22} - V)[-2C_{44}(C_{22}C_{33} - C_{23}^2) + 2(C_{22}C_{33} - C_{23}^2 + C_{33}C_{44})V$$

$$+ (C_{44} - 2C_{33})V^2] = \frac{C_{22} - V}{C_{33}} N_{22}(v),$$

$$N_{44}(v) = \frac{-V}{C_{44}}(C_{22}C_{33} - C_{23}^2 - C_{33}V)^2,$$

$$D(v) = (C_{22}C_{33} - C_{23}^2)(C_{22}C_{33} - C_{23}^2 + 2C_{33}C_{44})$$

$$+ 2C_{33}[C_{22}C_{44} - 2(C_{22}C_{33} - C_{23}^2) - C_{33}C_{44}]V + 3C_{33}(C_{33} - C_{44})V^2,$$

$$V = \rho v^2.$$

Remark 2 *Only four components a_{22}, a_{23}, a_{33} and a_{44} of the perturbative part $\mathbb{A}$ of $\mathbb{C}$ affect the first-order perturbation of the phase velocity v_R. This is also true for the case where the base material is unstressed and isotropic [16]. When the base material is generally anisotropic, Song and Fu [14] obtained a formula on the first-order perturbation of the phase velocity of Rayleigh waves; that formula involves the eigenvalues and the eigenvectors of Stroh's eigenvalue problem for the base material. Also, they applied their formula to the case where the base material is monoclinic. There they asserted that for Rayleigh waves polarized in a symmetry plane of the monoclinic material, which we take to be the 2–3 plane in this instance, the first-order perturbation of v_R will not involve any components of $\mathbb{A}$ in which suffix 1 appears at least once, i.e., no components of $\mathbb{A}$ other than $a_{22}, a_{23}, a_{24}, a_{33}, a_{34}$ and a_{44} will affect the first-order perturbation of v_R. For more discussion on work [14] refer to [17].*

In the comparative orthorhombic medium whose elasticity tensor is $\mathbb{C}^{\mathrm{Orth}}$, the polarization ratio is given by

$$r_R^{\mathrm{Orth}} = \sqrt{\frac{C_{33}V_R^{\mathrm{Orth}}}{C_{22}C_{33} - C_{23}^2 - C_{33}V_R^{\mathrm{Orth}}}}, \tag{13}$$

where $V_R^{\mathrm{Orth}} = \rho \left(v_R^{\mathrm{Orth}} \right)^2$ and v_R^{Orth} satisfies (9) and (10) (cf. [13]).

Theorem 3 *In an elastic medium whose elasticity tensor $\mathbb{C}$ is given by (6), the polarization ratio of Rayleigh waves which propagate along the surface of the half-space $x_3 \leq 0$ in the direction of the 2-axis can be written, to within terms linear in the perturbative part $\mathbb{A}$ of $\mathbb{C}$, as*

$$r_R = r_R^{\mathrm{Orth}} + \eta_{22}(v_R^{\mathrm{Orth}}) a_{22} + \eta_{23}(v_R^{\mathrm{Orth}}) a_{23} + \eta_{33}(v_R^{\mathrm{Orth}}) a_{33} + \eta_{44}(v_R^{\mathrm{Orth}}) a_{44}, \tag{14}$$

where

$$\eta_{22}(v) = \frac{-C_{33}C_{44}\sqrt{C_{44}-V}}{2E(v)}\Big[(C_{22}C_{33}-C_{23}^2)^2 - 2(C_{22}C_{33}-C_{23}^2)C_{33}V + (C_{33}^2-C_{23}^2)V^2\Big],$$

$$\eta_{23}(v) = \frac{C_{23}\sqrt{C_{44}-V}}{E(v)}\Big[(C_{22}C_{33}-C_{23}^2)^2C_{44} - 2(C_{22}C_{33}-C_{23}^2)C_{33}C_{44}V + (C_{33}-C_{22})C_{33}C_{44}V^2\Big],$$

$$\eta_{33}(v) = \frac{\sqrt{C_{44}-V}}{2C_{33}E(v)}\Big[2C_{22}(C_{22}C_{33}-C_{23}^2)^2C_{33}C_{44}$$

$$-(C_{22}C_{33}-C_{23}^2)\big((C_{22}C_{33}-C_{23}^2)(2C_{22}C_{33}+C_{23}^2)+4C_{22}C_{33}^2C_{44}\big)V$$

$$+C_{33}\big(2(C_{22}C_{33}-C_{23}^2)(2C_{22}C_{33}+C_{23}^2)-C_{22}(C_{22}C_{33}+C_{23}^2-2C_{33}^2)C_{44}\big)V^2$$

$$-C_{33}\big(C_{22}C_{33}(2C_{33}-C_{44})+C_{23}^2(C_{33}-2C_{44})\big)V^3\Big],$$

$$\eta_{44}(v) = \frac{C_{22}C_{33}-C_{23}^2}{2C_{44}D(v)}\sqrt{C_{33}(C_{22}C_{33}-C_{23}^2-C_{33}V)V},$$

$$E(v) = \sqrt{C_{44}(C_{22}-V)(C_{22}C_{33}-C_{23}^2-C_{33}V)V}\ D(v)V$$

and $D(v)$ is given in (12) and $V = \rho v^2$.

Remark 4 *Only four components a_{22}, a_{23}, a_{33} and a_{44} of the perturbative part $\mathbb{A}$ of $\mathbb{C}$ can affect the first-order perturbation of the polarization ratio r_R. These are the same as the components that affect the first-order perturbation of the phase velocity v_R (cf. Theorem 1). We observe that these components, together with a_{24} and a_{34}, constitute the elasticity tensor pertaining to two-dimensional anisotropic elasticity in the 2-3 plane.*

2 Bleustein-Gulyaev waves in piezoelectricity

2.1 Introduction

Piezoelectric materials have been used in many engineering devices because of their intrinsic direct and converse piezoelectric effects that take place between electric fields and mechanical deformations [10, 12, 18]. In the system of the constitutive equations, the mechanical stress and the electric displacement are related to the mechanical displacement and the electric potential through the elasticity tensor, the piezoelectric tensor and the dielectric tensor, and it is the piezoelectric tensor through which the elastic fields and electric fields can be coupled with each other.

When the piezoelectric material has a hexagonal symmetry, which means that the material has one 6-fold symmetry axis, a subsonic surface wave called the Bleustein-Gulyaev (BG) wave [2, 6] propagates along the surface of a piezoelectric half-space, provided that the 6-fold symmetry axis lies on the surface, the propagation direction on the surface is perpendicular to the 6-fold axis, and that the mechanically-free and electrically-closed boundary condition is imposed at that surface. Its phase velocity is written explicitly in terms of the aforementioned three material tensors.

Now we give a perturbation to the three material tensors of the piezoelectric half-space of hexagonal symmetry. This perturbation consists of a perturbative part of the elasticity tensor (which has

21 components, see (5)), a perturbative part of the piezoelectric tensor (has 18 components) and a perturbative part of the dielectric tensor (has 6 components), for which we do not assume any material symmetry. We then observe how these perturbative tensors (which have 45 components in all) affect the phase velocity of BG waves that propagate along the surface of the piezoelectric half-space.

We present a first order perturbation formula for the velocity of BG waves, which expresses the shift in the velocity from its comparative value for the piezoelectric half-space of hexagonal symmetry, caused by the aforementioned perturbative parts of the three tensors. The formula is correct to within terms linear in those perturbative parts of the tensors, and proves a somewhat surprising fact; only a few components of the perturbative parts of the tensors can affect the first order perturbation of the phase velocity of BG waves.

This section is a brief sketch of the collaborating work [11] with Gen Nakamura (Hokkaido University, Japan) and Xiang Xu (Zhejiang University, China).

2.2 Preliminaries

In the Cartesian coordinate system $\mathbf{x} = (x_1, x_2, x_3)$, the mechanical stress tensor $\boldsymbol{\sigma} = (\sigma_{ij})_{i,j=1,2,3}$ and the electric displacement $\boldsymbol{D} = (D_1, D_2, D_3)$ are related to the mechanical displacement $\boldsymbol{u} = (u_1, u_2, u_3)$ and the electric potential ϕ by the following constitutive equations:

$$
\begin{aligned}
\sigma_{ij} &= \sum_{k,l=1}^{3} C_{ijkl} \frac{\partial u_k}{\partial x_l} + \sum_{l=1}^{3} e_{ijl} \frac{\partial \phi}{\partial x_l}, \qquad i,j = 1,2,3, \\
D_j &= \sum_{k,l=1}^{3} e_{klj} \frac{\partial u_k}{\partial x_l} - \sum_{l=1}^{3} \epsilon_{jl} \frac{\partial \phi}{\partial x_l}, \qquad j = 1,2,3.
\end{aligned}
\tag{15}
$$

Here $\mathbb{C} = (C_{ijkl})_{i,j,k,l=1,2,3}$ is the elasticity tensor, $\boldsymbol{e} = (e_{ijl})_{i,j,l=1,2,3}$ is the piezoelectric tensor, and $\boldsymbol{\epsilon} = (\epsilon_{jl})_{i,l=1,2,3}$ is the dielectric tensor. Hence the elastic and electric fields are coupled through the piezoelectric tensor.

These three tensors $\mathbb{C}$, $\boldsymbol{e}$, and $\boldsymbol{\epsilon}$ satisfy the following symmetry conditions:

$$
C_{ijkl} = C_{jikl} = C_{klij}, \qquad e_{ijl} = e_{jil}, \qquad \epsilon_{jl} = \epsilon_{lj}, \qquad i,j,k,l = 1,2,3.
$$

We assume that the internal energy function is positive, which implies the following positivity conditions for $\mathbb{C}$ and $\boldsymbol{e}$:

$$
\sum_{i,j,k,l=1}^{3} C_{ijkl}\, s_{ij}\, s_{kl} > 0, \qquad \sum_{j,l=1}^{3} \epsilon_{jl}\, E_j\, E_l > 0
$$

for any non-zero 3×3 real symmetric matrix (s_{ij}) and for any non-zero real vector (E_1, E_2, E_3).

The equations of mechanical motion with zero body force and the equation of electric equilibrium with zero free charge are given by

$$
\sum_{j=1}^{3} \frac{\partial \sigma_{ij}}{\partial x_j} = \rho \frac{\partial^2 u_i}{\partial t^2}, \quad i = 1,2,3 \qquad \text{and} \qquad \sum_{j=1}^{3} \frac{\partial D_j}{\partial x_j} = 0,
\tag{16}
$$

respectively, where ρ is the uniform density. Substituting (15) into the preceding equations leads us to a system of the equations for the unknowns $\boldsymbol{u} = (u_1, u_2, u_3)$ and ϕ.

Let $\mathbf{m}$ and $\mathbf{n}$ be orthogonal unit vectors in $\mathbb{R}^3$, and consider surface waves in the piezoelectric half-space $\mathbf{n} \cdot \mathbf{x} \le 0$ which propagate along the surface $\mathbf{n} \cdot \mathbf{x} = 0$ in the direction of $\mathbf{m}$, decay exponentially as $\mathbf{n} \cdot \mathbf{x} \longrightarrow -\infty$, and satisfies the "mechanically-free and electrically-closed (or, grounded) condition"

$$\sum_{j=1}^{3} \sigma_{ij} n_j = 0 \quad (i = 1, 2, 3) \quad \text{and} \quad \phi = 0 \quad \text{at} \quad \mathbf{n} \cdot \mathbf{x} = 0. \tag{17}$$

Lothe and Barnett [8, 9] extended the Stroh formalism to piezoelectricity, which allows us to write the time-harmonic solution to (16) that describes such surface waves in the following form

$$\begin{pmatrix} \boldsymbol{u} \\ \phi \end{pmatrix} = \sum_{\alpha=1}^{4} c_\alpha \, \mathbf{a}_\alpha \, e^{-\sqrt{-1}\,k(\mathbf{m}\cdot\mathbf{x}+p_\alpha \mathbf{n}\cdot\mathbf{x}-v\,t)}, \tag{18}$$

where k is the wave number, $\mathbf{a}_\alpha = \mathbf{a}_\alpha(v) \in \mathbb{C}^4$ and $p_\alpha = p_\alpha(v) \in \mathbb{C}$ with $\operatorname{Im} p_\alpha > 0$ $(1 \le \alpha \le 4)$ are determined from the equations (16), whereas the phase velocity v and $c_\alpha = c_\alpha(v) \in \mathbb{C}$ $(1 \le \alpha \le 4)$ are determined from the boundary condition (17).

We assume that the piezoelectric medium has a hexagonal symmetry, which means that the medium has one 6-fold symmetry axis[¶]. Let the 3-axis be the 6-fold axis. Then the elasto-piezo-dielectric matrix is written as

$$\mathrm{P}_{\mathrm{hex}} = \left(\mathrm{P}_{\mathrm{hex}}\right)^T = \left[\begin{array}{cccccc|ccc} C_{11} & C_{12} & C_{13} & 0 & 0 & 0 & 0 & 0 & e_{23} \\ C_{12} & C_{11} & C_{13} & 0 & 0 & 0 & 0 & 0 & e_{23} \\ C_{13} & C_{13} & C_{33} & 0 & 0 & 0 & 0 & 0 & e_{33} \\ 0 & 0 & 0 & C_{44} & 0 & 0 & e_{41} & e_{42} & 0 \\ 0 & 0 & 0 & 0 & C_{44} & 0 & e_{42} & -e_{41} & 0 \\ 0 & 0 & 0 & 0 & 0 & \frac{C_{11}-C_{12}}{2} & 0 & 0 & 0 \\ \hline 0 & 0 & 0 & e_{41} & e_{42} & 0 & -\epsilon_{22} & 0 & 0 \\ 0 & 0 & 0 & e_{42} & -e_{41} & 0 & 0 & -\epsilon_{22} & 0 \\ e_{23} & e_{23} & e_{33} & 0 & 0 & 0 & 0 & 0 & -\epsilon_{33} \end{array}\right], \tag{20}$$

where we have used the contracted notation (Voigt notation) which expresses the tensors $\mathbb{C}, \boldsymbol{e}$ and $\boldsymbol{\epsilon}$ in terms of a 9×9 matrix as shown above.[‖]

2.3 Bleustein-Gulyaev waves and their perturbations

When the 6-fold axis lies on the surface of the piezoelectric half-space, a subsonic surface wave called the Bleustein-Gulyaev (BG) wave propagates along that surface in the direction perpendicular to the 6-fold axis. Let us take $\mathbf{m} = (1, 0, 0)$ and $\mathbf{n} = (0, 1, 0)$.

[¶]In this case, besides the relation (3), relations

$$e_{ijl} = \sum_{p,q,r=1}^{3} Q_{ip}\,Q_{jq}\,Q_{lr}\,e_{pqr} \quad (i, j, l = 1, 2, 3), \qquad \epsilon_{jl} = \sum_{p,q=1}^{3} Q_{jp}\,Q_{lq}\,\epsilon_{pq} \quad (j, l = 1, 2, 3) \tag{19}$$

hold for the orthogonal tensor $\boldsymbol{Q} = (Q_{ij})_{i,j=1,2,3}$ corresponding to a right-handed rotation by the angle $2\pi/6$ around that axis. A piezoelectric medium of hexagonal symmetry is proved to be transversely isotropic with its 6-fold axis being an axis of rotational symmetry, which implies that (3) and (19) hold for the orthogonal transformation $\boldsymbol{Q} = (Q_{ij})_{i,j=1,2,3}$ corresponding to a right-handed rotation by an arbitrary angle around the axis of rotational symmetry.

[‖]For the subscript ij (the first two indices) of $e_{ijl} \in \boldsymbol{e}$ we have used the same rules as have been adopted in (4) and (5). Then the elasto-piezo-dielectric matrix is defined as a 9×9 symmetric matrix $\left[\begin{array}{c|c} (C_{\alpha\beta}) & (e_{\alpha l}) \\ \hline (e_{\alpha l})^T & -(\epsilon_{jl}) \end{array}\right]$. We do not use these rules for the subscript of $\boldsymbol{\epsilon}$.

Proposition 5 ([2, 6])   *Suppose that $e_{42} \neq 0$. There exists a surface wave which propagates along the surface $x_2 = 0$ of the piezoelectric half-space $x_2 \leq 0$ in the direction of the 1-axis and which satisfies a mechanically-free and electrically-closed condition at the boundary, i.e., $(\sigma_{i2})_{i\downarrow 1,2,3} = \mathbf{0}$ and $\phi = 0$ at $x_2 = 0$. Its phase velocity $v = v_{\mathrm{B}}^{\mathrm{hex}}$ is given by*

$$V_{\mathrm{B}}^{\mathrm{hex}} = \rho \left(v_{\mathrm{B}}^{\mathrm{hex}}\right)^2 = \frac{C_{44}\left(C_{44} + 2\dfrac{e_{42}{}^2}{\epsilon_{22}}\right)}{C_{44} + \dfrac{e_{42}{}^2}{\epsilon_{22}}}. \tag{21}$$

The setting of the theorem implies the existence of another surface wave which is determined only from the elastic part $(C_{\alpha\beta})$ of $\mathrm{P_{hex}}$, i.e., the upper left hand 6×6 block of (20). This is a surface wave whose solution (18) has the fourth component being zero (i.e., $\phi = 0$), and agrees with the Rayleigh wave in a transversely isotropic elastic medium. In fact, Lothe and Barnett [8, 9] proved that

- For fixed orthogonal unit vectors $\mathbf{m}$ and $\mathbf{n}$ in $\mathbb{R}^3$, there are at most two surface waves that satisfy the mechanically-free and electrically-closed boundary condition (17).

and the argument therein implies that

- Existence condition of the surface waves is stable under a perturbation of material constants.

Now we give a perturbation to the material constants of the piezoelectric medium of hexagonal symmetry whose elasto-piezo-dielectric matrix is $\mathrm{P_{hex}}$ (20). This perturbation is expressed as a perturbative elasto-piezo-dielectric matrix $\mathrm{P_{ptb}}$:

$$\mathrm{P_{ptb}} = \left(\mathrm{P_{ptb}}\right)^T = \left[\begin{array}{cccccc|ccc} a_{11} & a_{12} & a_{13} & a_{14} & a_{15} & a_{16} & f_{11} & f_{12} & f_{13} \\ & a_{22} & a_{23} & a_{24} & a_{25} & a_{26} & f_{21} & f_{22} & f_{23} \\ & & a_{33} & a_{34} & a_{35} & a_{36} & f_{31} & f_{32} & f_{33} \\ & & & a_{44} & a_{45} & a_{46} & f_{41} & f_{42} & f_{43} \\ & & & & a_{55} & a_{56} & f_{51} & f_{52} & f_{53} \\ & & & & & a_{66} & f_{61} & f_{62} & f_{63} \\ \hline & & & & & & -\delta_{11} & -\delta_{12} & -\delta_{13} \\ & & & & & & & -\delta_{22} & -\delta_{23} \\ & & & & & & & & -\delta_{33} \end{array}\right].$$

Namely, the upper left hand 6×6 block is the perturbative part of the elasticity tensor $\mathbb{C}$, the upper right hand 6×3 block is the perturbative part of the piezoelectric tensor $\boldsymbol{e}$, and the lower right hand 3×3 block is the minus of the perturbative part of the dielectric tensor $\boldsymbol{\epsilon}$, for which we do not assume any material symmetry. Hence the 45 components in the upper triangular part of matrix $\mathrm{P_{ptb}}$ are generally all independent.

We consider BG waves in a piezoelectric half-space whose elasto-piezo-dielectric matrix is given by $\mathrm{P_{hex}} + \mathrm{P_{ptb}}$, and present a perturbation formula which shows how $\mathrm{P_{ptb}}$ affects the phase velocity of BG waves from its comparative value $v_{\mathrm{B}}^{\mathrm{hex}}$ for the piezoelectric half-space of hexagonal symmetry.

Theorem 6   *Suppose that $v_{\mathrm{B}}^{\mathrm{hex}} \neq v_{\mathrm{R}}$, where v_{R} is the velocity of Rayleigh waves determined from the upper left hand 6×6 block in $\mathrm{P_{hex}}$. In a piezoelectric medium whose elasto-piezo-dielectric matrix is given by $\mathrm{P_{hex}} + \mathrm{P_{ptb}}$, the phase velocity v_{B} of BG waves which propagate along the surface $x_2 = 0$ of*

the piezoelectric half-space $x_2 \leq 0$ in the direction of the 1-axis and which satisfies a mechanically-free and electrically-closed condition at $x_2 = 0$ can be written, to within terms linear in the perturbative part P_{ptb}, as

$$V_{\mathrm{B}} = \rho\,(v_{\mathrm{B}})^2 \,=\, V_{\mathrm{B}}^{\mathrm{hex}} \,+\, P_1\,f_{42} \,+\, P_2\,f_{51} \,+\, D_1\,\delta_{11} \,+\, D_2\,\delta_{22} \,+\, E_1\,a_{44} \,+\, E_2\,a_{55}, \qquad (22)$$

where $V_{\mathrm{B}}^{\mathrm{hex}}$ is given by (21) and the coefficients P_i, D_i and E_i $(i = 1, 2)$ are written by

$$P_1 \;=\; \frac{-2\,C_{44}\,e_{42}{}^5}{(C_{44}\,\epsilon_{22} + e_{42}{}^2)^2\,(C_{44}\,\epsilon_{22} + 2\,e_{42}{}^2)}, \qquad P_2 = \frac{2\,C_{44}\,e_{42}}{C_{44}\,\epsilon_{22} + 2\,e_{42}{}^2},$$

$$D_1 \;=\; \frac{-C_{44}{}^2\,e_{42}{}^2}{(C_{44}\,\epsilon_{22} + e_{42}{}^2)\,(C_{44}\,\epsilon_{22} + 2\,e_{42}{}^2)}, \qquad D_2 = \frac{-C_{44}{}^2\,e_{42}{}^4}{(C_{44}L\,\epsilon_{22} + e_{42}{}^2)^2\,(C_{44}\,\epsilon_{22} + 2\,e_{42}{}^2)},$$

$$E_1 \;=\; \frac{e_{42}{}^4}{(C_{44}\,\epsilon_{22} + e_{42}{}^2)^2}, \qquad E_2 = 1.$$

Remark 7 *Only two components f_{42}, f_{51} of the perturbative part of the piezoelectric tensor $\boldsymbol{e}$, two component δ_{11}, δ_{22} of the perturbative part of the dielectric tensor $\boldsymbol{\epsilon}$ and two components a_{44}, a_{55} of the perturbative part of the elasticity tensor $\mathbb{C}$ can affect the first-order perturbation of the phase velocity v_{B} of BG waves that propagate in the direction of the 1-axis on the surface of the half-space $x_2 \leq 0$. For an interpretation of this fact, we refer to Page 59 of the presentation slides.*

Remark 8 *In the formula (22), $a_{\alpha\beta}, f_{\alpha l}$ and δ_{jl} have different units. However, the formula can be justified by regarding $(a_{\alpha\beta}), (f_{\alpha l})$ and (δ_{jl}) as sufficiently small compared with $\mathbb{C}, \boldsymbol{e}$ and $\boldsymbol{\epsilon}$, respectively. For instance, the term $P_1\,f_{42}$ in (22) can be rewritten as $\dfrac{-2C_{44}\left(\frac{e_{42}{}^2}{\epsilon_{22}}\right)^3}{\left(C_{44} + \frac{e_{42}{}^2}{\epsilon_{22}}\right)^2 \left(C_{44} + 2\frac{e_{42}{}^2}{\epsilon_{22}}\right)} \cdot \dfrac{f_{42}}{e_{42}}$, whose unit is pascal (cf. also (21)).*

References

[1] D. M. Barnett and J. Lothe, Free surface (Rayleigh) waves in anisotropic elastic half spaces: the surface impedance method, Proc. R. Soc. Lond. **A 402** (1985) 135-152.

[2] J. L. Bleustein, A new surface wave in piezoelectric materials, Appl. Phys. Lett. **13** (1968) 412–413.

[3] P. Chadwick and G. D. Smith, Foundations of the theory of surface waves in anisotropic elastic materials, Adv. Appl. Mech. **17** (1977) 303–376.

[4] M. Destrade, Explicit secular equation for surface acoustic waves in monoclinic elastic crystals, J. Acoust. Soc. Am. **109** (2001) 1398–1402.

[5] M. Destrade, Rayleigh waves in symmetry planes of crystals; explicit secular equations and some explicit wave speeds, Mech. Mater. **35** (2003) 931–939.

[6] Yu.V. Gulyaev, Electroacoustic surface waves in solids, Sov. Phys. JETP Lett. **9** (1969) 37–38.

[7] M. Junge, J. Qu and L. J. Jacobs, Relationship between Rayleigh wave polarization and state of stress, Ultrasonics **44** (2006) 233–237.

[8] J. Lothe and D. M. Barnett, Integral formalism for surface waves in piezoelectric crystals. Existence considerations, J. Appl. Phys. **47** (1976) 1799–1807.

[9] J. Lothe and D. M. Barnett, Further development of the theory for surface waves in piezoelectric crystals, Phys. Norv. **8** (1976) 239–254.

[10] G. A. Maugin, *Continuum Mechanics of Electromagnetic Solids.* North-Holland, Amsterdam (1988).

[11] G. Nakamura, K. Tanuma and X. Xu, On the perturbation of Bleustein-Gulyaev waves in piezoelectric media, submitted to Mathematical Analysis of Continuum Mechanics and Industrial Applications IV, Proceedings of the International Conference CoMFoS19, Springer.

[12] V. M. Ristic, *Principles of Acoustic Devices.* John Wiley & Sons., New York (1983).

[13] D. Royer and E. Dieulesaint, Rayleigh wave velocity and displacement in orthorhombic, tetragonal, hexagonal, and cubic crystals, J. Acoust. Soc. Am. **76** (1984) 1438–1444.

[14] Y. Q. Song and Y. B. Fu, A note on perturbation formulae for the surface-wave speed due to peturbations in material properties, J. Elasticity **88** (2007) 187–192.

[15] K. Tanuma, Stroh formalism and Rayleigh waves, J. Elasticity **89** (2007) 5–154.

[16] K. Tanuma and C.-S. Man, Perturbation formula for phase velocity of Rayleigh waves in prestressed anisotropic media, J. Elasticity **85** (2006) 21–37.

[17] K. Tanuma, C.-S. Man and W. Du, Perturbation of phase velocity of Rayleigh waves in prestressed anisotropic media with orthorhombic principal part, Math. Mech. Solids **18** (2013) 301–322.

[18] H. F. Tiersten, *Linear Piezoelectric Plate Vibrations.* Plenum Press, New York (1969).

[19] T. C. T. Ting, *Anisotropic Elasticity.* Oxford University Press, New York (1996).

[20] T. C. T. Ting, Explicit secular equations for surface waves in monoclinic materials with the symmetry plane at $x_1 = 0, x_2 = 0$ or $x_3 = 0$, Proc. R. Soc. Lond. **A 458** (2002) 1017–1031.

[21] T. C. T. Ting, An explicit secular equation for surface waves in an elastic material of general anisotropy, Q. J. Mech. Appl. Math. **55** (2002) 297–311.

[22] T. C. T. Ting, Explicit secular equations for surface waves in an anisotropic elastic half-space; from Rayleigh to today, In: *Surface Waves in Anisotropic and Laminated Bodies and Defects Detection*, pp. 95–116, ed., R. V. Goldstein & G. A. Maugin, Kluwer Academic Publishers, 2004.

[23] Pham Chi Vinh and R.W. Ogden, On a general formula for the Rayleigh wave speed in orthotropic elastic solids, Meccanica **40** (2005) 147–161.

Perturbations of
Rayleigh waves in anisotropic elasticity
and
Bleustein-Gulyaev waves in piezoelectricity

Kazumi Tanuma (presenter), *Gunma University, Japan*

Collaborators:

Yue Chen, *Auburn University at Montgomery, USA*

Wenwen Du, *University of Kentucky, USA*

Chi-Sing Man, *University of Kentucky, USA*

Gen Nakamura, *Hokkaido University, Japan*

Xiang Xu, *Zhejiang University, China*

1

§ 1 . Perturbation of Rayleigh Waves in

Macroscopically Homogeneous, Anisotropic,

Elastic Media

Collaboration with

Chi-Sing Man, *University of Kentucky, USA*

Wenwen Du, *University of Kentucky, USA*

2

Rayleigh waves (subsonic surface waves)

Elastic medium : *half-space* $x_3 \leq 0$

v_R : phase velocity
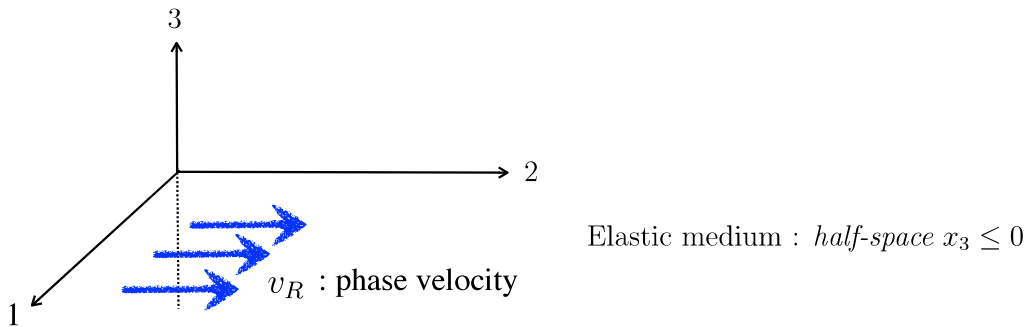
- ●   decay exponentially along the depth

- ● v_R < speed of body waves

- ●   produce No traction on the surface $x_3 = 0$

Usefulness of Rayleigh waves in nondestructive evaluation

- Characterization of anisotropy in materials

Smith & Dahlen 1973 The azimuthal dependence of Love and Rayleigh wave propagation in a slightly anisotropic medium. *J. Geophys. Res.*

Sayers 1985 Angular dependence of the Rayleigh wave velocity in polycrystalline metals with small anisotropy. *Proc. R. Soc. Lond.* A

- Acoustoelasticity $\implies$ Evaluation of initial stress

Man, et al. 2000 Ultrasonic measurement of through-thickness stress gradients in textured sheet metals. *Review of Progress in Quantitative Nondestructive Evaluation*

$$\boxed{\text{from measurements of phase velocity } v_R}$$

Any other physical quantity that can be measured
and can be utilized ?

Possibly, <u>displacements</u> of Rayleigh waves at the boundary
can be used.

polarization ratio r_R
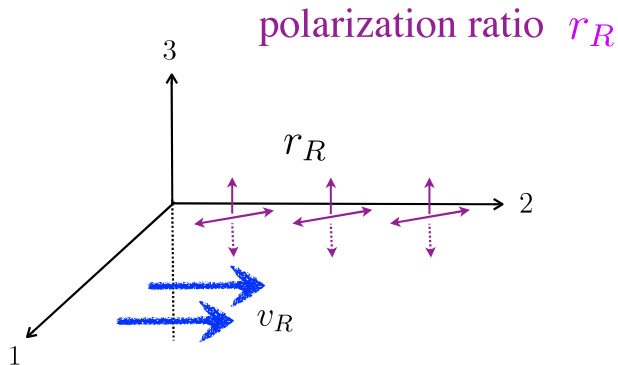
Polarization ratio r_R :

$$r_R \ = \ \frac{\text{maximum longitudinal component}}{\text{maximum normal component}} \quad \text{at the boundary}$$

Junge et al., Ultrasonic (2006)

``the relative polarization is more sensitive to applied stress than relative wave speed''

Herein we study the perturbations of v_R and r_R
caused by perturbation of elasticity tensor.

(Forward Problem)

Displacement of Rayleigh waves on the traction-free surface $x_3 = 0$

$$
\begin{bmatrix} a_1^+ \\ a_2^+ \\ a_3^+ \end{bmatrix} \cos k(x_2 - v_R t) + \begin{bmatrix} a_1^- \\ a_2^- \\ a_3^- \end{bmatrix} \sin k(x_2 - v_R t) \qquad \in \mathbb{R}^3
$$

$\longrightarrow$

- longitudinal component :

$$
a_2^+ \cos k(x_2 - v_R t) + a_2^- \sin k(x_2 - v_R t) = \sqrt{(a_2^+)^2 + (a_2^-)^2} \, \sin \left(k(x_2 - v_R t) + \alpha \right),
$$

- normal component :

$$
a_3^+ \cos k(x_2 - v_R t) + a_3^- \sin k(x_2 - v_R t) = \sqrt{(a_3^+)^2 + (a_3^-)^2} \, \sin \left(k(x_2 - v_R t) + \beta) \right).
$$

Polarization ratio r_R

$$
r_R \;=\; \frac{\text{maximum longitudinal component}}{\text{maximum normal component}} \;=\; \frac{\sqrt{(a_2^+)^2 + (a_2^-)^2}}{\sqrt{(a_3^+)^2 + (a_3^-)^2}}.
$$

7

Equations of motion

$$
\rho \, \frac{\partial^2}{\partial t^2} \, u_i \;=\; \sum_{j=1}^{3} \frac{\partial}{\partial x_j} \, \sigma_{ij} \qquad \text{in} \ \ x_3 \leq 0, \qquad i = 1, 2, 3
$$

$$
\rho : \ \text{mass density}, \quad t : \text{time},
$$

$$
\boldsymbol{u} = (u_1, u_2, u_3) : \ \text{displacement},
$$

$$
\boldsymbol{\sigma} = \Big(\sigma_{ij} \Big)_{i,j=1,2,3} \ : \ \text{stress}.
$$

8

$$\boldsymbol{E} = \left(E_{ij}\right)_{i,j=1,2,3} = \tfrac{1}{2}\left(\nabla\boldsymbol{u} + \nabla\boldsymbol{u}^T\right) \;:\; \text{infinitesimal strain,}$$

Hooke's law

$$\boldsymbol{\sigma} = \left(\sigma_{ij}\right)_{i,j=1,2,3} = \mathbb{C}[\boldsymbol{E}\,] = \left(\sum_{k,l=1}^{3} C_{ijkl}\, E_{kl}\right)_{i,j=1,2,3}$$

$$\mathbb{C} = \left(C_{ijkl}\right)_{i,j,k,l=1,2,3} \;:\; \text{elasticity tensor,}$$

$$C_{ijkl} = C_{klij} = C_{jikl}$$

Elastic wave equations

$$\rho\,\frac{\partial^2}{\partial t^2}\,u_i = \sum_{j,k,l=1}^{3}\frac{\partial}{\partial x_j}\left(C_{ijkl}\frac{\partial u_k}{\partial x_l}\right) \quad \text{in}\;\; x_3 \le 0, \quad i = 1,2,3.$$

&

Traction-free condition at the boundary $x_3 = 0$

$$\boldsymbol{t} = \left(\sigma_{i3}\right)_{i\downarrow 1,2,3}\Big|_{x_3=0} = \left(\sum_{k,l=1}^{3} C_{i3kl}\frac{\partial u_k}{\partial x_l}\right)_{i\downarrow 1,2,3}\Big|_{x_3=0} = \boldsymbol{0}.$$

Elastic medium : $x_3 \leq 0$,

Rayleigh waves : propagate in the direction of the 2-axis.

1. Find a surface-wave solution of the form :

$$\boldsymbol{u} = \sum_{\alpha=1}^{3} c_\alpha \, \mathbf{a}_\alpha \, e^{-\sqrt{-1}\, k\,(x_2 + p_\alpha\, x_3 - v\, t)}$$

k : wave number, $\quad v$: phase velocity

$$c_\alpha \in \mathbb{C}, \quad \mathbf{a}_\alpha \in \mathbb{C}^3$$

Complex
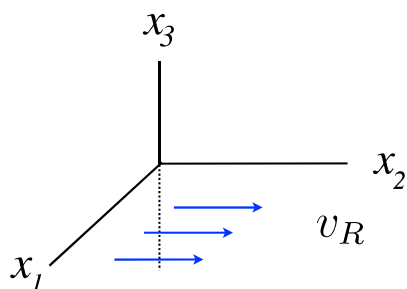
$p_\alpha = p_\alpha(v), \; \mathbf{a}_\alpha = \mathbf{a}_\alpha(v) \; (\alpha = 1, 2, 3) :$

determined from the elastic wave equations.

$v \in$ "subsonic range" $\quad \Longrightarrow \quad$ Im $p_\alpha > 0,$

$\boldsymbol{u}$ decays as $x_3 \longrightarrow -\infty$

2. Compute the traction on the surface $x_3 = 0$

$$\boldsymbol{u} = \sum_{\alpha=1}^{3} c_\alpha \, \mathbf{a}_\alpha \, e^{-\sqrt{-1}\, k\,(x_2 + p_\alpha\, x_3 - v\, t)}$$

$$\boldsymbol{t} = \left(\sigma_{i3}\right)_{i\downarrow 1,2,3}\Big|_{x_3=0} = \left(\sum_{k,l=1}^{3} C_{i3kl}\, \frac{\partial u_k}{\partial x_l}\right)_{i\downarrow 1,2,3}\Bigg|_{x_3=0}$$

$$= -\sqrt{-1}\, k \sum_{\alpha=1}^{3} c_\alpha \, \mathbf{l}_\alpha \, e^{-\sqrt{-1}\, k\,(x_2 - v\, t)}$$

3. Find v_R so that $\boldsymbol{t} = \boldsymbol{0}$

4. Compute r_R from the displacement $\displaystyle\sum_{\alpha=1}^{3} c_\alpha \, \mathbf{a}_\alpha \Big|_{v=v_R}$.

Perturbation assumption on material constants

Elasticity tensor :

$$\mathbb{C} \;=\; \mathbb{C}^{\mathrm{Orth}} \;+\; \mathbb{A}$$

- $\mathbb{C}^{\mathrm{Orth}} = \left(C^{\mathrm{Orth}}_{ijkl}\right)_{i,j,k,l=1,2,3}$: Orthorhombic part of $\mathbb{C}$
  (principal)

  $\Longrightarrow$ Base material

- $\mathbb{A} = \left(a_{ijkl}\right)_{i,j,k,l=1,2,3}$: Perturbative part of $\mathbb{C}$

$$\|\mathbb{A}\| \;\ll\; \|\mathbb{C}^{\mathrm{Orth}}\|$$

13

$$\mathbb{C}^{\mathrm{Orth}} = (C^{\mathrm{Orth}}_{rs}) = \begin{pmatrix} C_{11} & C_{12} & C_{13} & 0 & 0 & 0 \\ & C_{22} & C_{23} & 0 & 0 & 0 \\ & & C_{33} & 0 & 0 & 0 \\ & & & C_{44} & 0 & 0 \\ & & & & C_{55} & 0 \\ & Sym. & & & & C_{66} \end{pmatrix}$$

: 9 independent components

(Base material)

1,2,3-axis : axes of symmetry

$$\mathbb{A} = (a_{rs}) = \begin{pmatrix} a_{11} & a_{12} & a_{13} & a_{14} & a_{15} & a_{16} \\ & a_{22} & a_{23} & a_{24} & a_{25} & a_{26} \\ & & a_{33} & a_{34} & a_{35} & a_{36} \\ & & & a_{44} & a_{45} & a_{46} \\ & & & & a_{55} & a_{56} \\ & Sym. & & & & a_{66} \end{pmatrix}$$

: 21 independent components

Voigt notation:

ij (or kl)		r or s	ij (or kl)		r or s
11	$\longleftrightarrow$	1	23 or 32	$\longleftrightarrow$	4
22	$\longleftrightarrow$	2	31 or 13	$\longleftrightarrow$	5
33	$\longleftrightarrow$	3	12 or 21	$\longleftrightarrow$	6

14

Notes :

Hooke's law

$$\boldsymbol{\sigma} = \left(\sigma_{ij}\right)_{i,j=1,2,3} = \mathbb{C}[\boldsymbol{E}] = \left(\sum_{k,l=1}^{3} C_{ijkl}\, E_{kl}\right)_{i,j=1,2,3}$$

$$\boldsymbol{E} = \left(E_{ij}\right)_{i,j=1,2,3} = \tfrac{1}{2}\left(\nabla\boldsymbol{u} + \nabla\boldsymbol{u}^T\right)$$

$\Longleftrightarrow$ under the Voigt notation applied to $\mathbb{C}$

$$
\begin{bmatrix} \sigma_{11} \\ \sigma_{22} \\ \sigma_{33} \\ \sigma_{23} \\ \sigma_{13} \\ \sigma_{12} \end{bmatrix}
=
\begin{bmatrix}
C_{11} & C_{12} & C_{13} & C_{14} & C_{15} & C_{16} \\
 & C_{22} & C_{23} & C_{24} & C_{25} & C_{26} \\
 & & C_{33} & C_{34} & C_{35} & C_{36} \\
 & & & C_{44} & C_{45} & C_{46} \\
 & \textit{Sym.} & & & C_{55} & C_{56} \\
 & & & & & C_{66}
\end{bmatrix}
\begin{bmatrix}
(u_1)_{x_1} \\
(u_2)_{x_2} \\
(u_3)_{x_3} \\
(u_2)_{x_3} + (u_3)_{x_2} \\
(u_1)_{x_3} + (u_3)_{x_1} \\
(u_1)_{x_2} + (u_2)_{x_1}
\end{bmatrix}
$$

15

● **Isotropic**

$$
\mathbb{C}^{\text{Iso}} = (C_{rs}^{\text{Iso}}) =
\begin{pmatrix}
\lambda + 2\mu & \lambda & \lambda & 0 & 0 & 0 \\
 & \lambda + 2\mu & \lambda & 0 & 0 & 0 \\
 & & \lambda + 2\mu & 0 & 0 & 0 \\
 & & & \mu & 0 & 0 \\
 & & & & \mu & 0 \\
 & \textit{Sym.} & & & & \mu
\end{pmatrix}
$$

$$\left(C_{ijkl}^{\text{Iso}} = \lambda\,\delta_{ij}\delta_{kl} + \mu\,(\delta_{ik}\delta_{jl} + \delta_{il}\delta_{kj}),\ \ \lambda, \mu : \text{Lamé coefficients} \right)$$

● **Transversely isotropic (= hexagonal** in elasticity**)**

3-axis : axis of rotational symmetry

$$
\mathbb{C}^{\text{hex}} = (C_{rs}^{\text{hex}}) =
\begin{pmatrix}
C_{11} & C_{12} & C_{13} & 0 & 0 & 0 \\
 & C_{11} & C_{13} & 0 & 0 & 0 \\
 & & C_{33} & 0 & 0 & 0 \\
 & & & C_{44} & 0 & 0 \\
 & & & & C_{44} & 0 \\
 & \textit{Sym.} & & & & \frac{C_{11}-C_{12}}{2}
\end{pmatrix}
$$

: 5 independent components

16

Orthorhombic

$$\mathbb{C}^{\mathrm{Orth}} = (C_{rs}^{\mathrm{Orth}}) = \begin{pmatrix} C_{11} & C_{12} & C_{13} & 0 & 0 & 0 \\ & C_{22} & C_{23} & 0 & 0 & 0 \\ & & C_{33} & 0 & 0 & 0 \\ & & & C_{44} & 0 & 0 \\ & & & & C_{55} & 0 \\ & \textit{Sym.} & & & & C_{66} \end{pmatrix}$$

Orthorhombic $\supset$ hexagonal $\supset$ isotropic

17

Forward problem
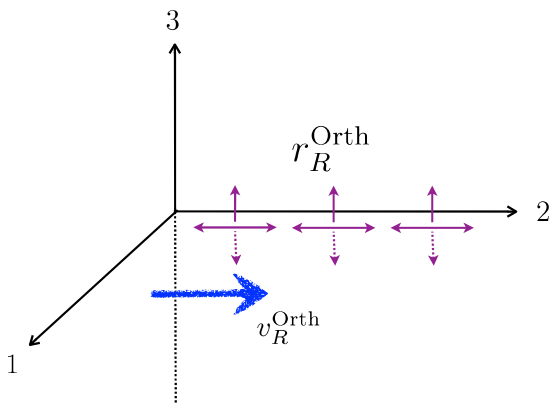
$$\boldsymbol{\sigma} = \mathbb{C}^{\mathrm{Orth}}[\boldsymbol{E}]$$

base material
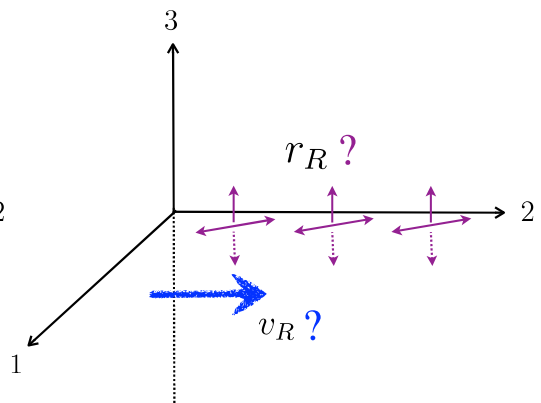
$$\boldsymbol{\sigma} = \big(\mathbb{C}^{\mathrm{Orth}} + \mathbb{A}\big)[\boldsymbol{E}]$$

perturbed medium

18

In the base material,
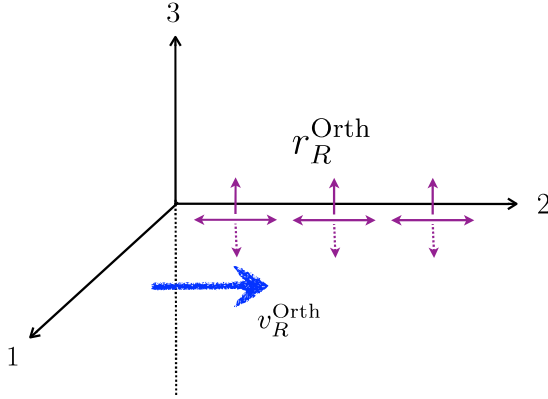
[Stoneley, 1963]

- 🔵 $V_R^{\mathrm{Orth}} = \rho\,(v_R^{\mathrm{Orth}})^2$: the unique root of the cubic equation

$$C_{33}C_{44}(C_{22}-V)V^2 - (C_{44}-V)\left(C_{33}(C_{22}-V) - C_{23}^2\right)^2 = 0$$

- 🟣 $r_R^{\mathrm{Orth}} = \sqrt{\dfrac{C_{33}V_R^{\mathrm{Orth}}}{C_{22}C_{33} - C_{23}^2 - C_{33}V_R^{\mathrm{Orth}}}}$ [Royer, Dieulesaint, 1984]

Theorem [Tanuma, Man & Du, *Mathematics and Mechanics of Solids*
<div align="right">Vol. 18 (3) 2013]</div>

Elastic medium : $x_3 \le 0$,

$\quad$ 1, 2, 3-axes : symmetry axes of $\mathbb{C}^{\mathrm{Orth}}$ of Base material

Rayleigh waves : propagate in the direction of the 2-axis.

$$\Longrightarrow$$

First-order perturbation formula for v_R

$$v_R \;\simeq\; v_R^{\mathrm{Orth}} - \frac{1}{2\rho\,v_R^{\mathrm{Orth}}}$$

$$\times\; \left[\gamma_{22}(v_R^{\mathrm{Orth}})\,a_{22} + \gamma_{23}(v_R^{\mathrm{Orth}})\,a_{23} + \gamma_{33}(v_R^{\mathrm{Orth}})\,a_{33} + \gamma_{44}(v_R^{\mathrm{Orth}})\,a_{44}\right]$$

Each coefficient $\gamma_{ij}(v)$ is written explicitly in terms of $\mathbb{C}^{\mathrm{Orth}}$ and ρ.

$$\gamma_{ij}(v) = \frac{N_{ij}(v)}{D(v)} \qquad (\{ij\} = \{22\}, \{23\}, \{33\}, \{44\}),$$

$$
\begin{aligned}
N_{22}(v) = C_{33}\Big[&-2C_{44}(C_{22}C_{33} - C_{23}^2) + 2(C_{22}C_{33} - C_{23}^2 + C_{33}C_{44})V \\
&+ (C_{44} - 2C_{33})V^2 \Big],
\end{aligned}
$$

$$N_{23}(v) = 4C_{23}(C_{44} - V)(C_{22}C_{33} - C_{23}^2 - C_{33}V),$$

$$
\begin{aligned}
N_{33}(v) = (C_{22} - V)\Big[&-2C_{44}(C_{22}C_{33} - C_{23}^2) + 2(C_{22}C_{33} - C_{23}^2 + C_{33}C_{44})V \\
&+ (C_{44} - 2C_{33})V^2 \Big] = \frac{C_{22} - V}{C_{33}} N_{22}(v),
\end{aligned}
$$

$$N_{44}(v) = \frac{-V}{C_{44}}(C_{22}C_{33} - C_{23}^2 - C_{33}V)^2,$$

$$
\begin{aligned}
D(v) = {}&(C_{22}C_{33} - C_{23}^2)(C_{22}C_{33} - C_{23}^2 + 2C_{33}C_{44}) \\
&+ 2C_{33}\Big[C_{22}C_{44} - 2(C_{22}C_{33} - C_{23}^2) - C_{33}C_{44} \Big]V + 3C_{33}(C_{33} - C_{44})V^2,
\end{aligned}
$$

$$V = \rho\, v^2$$

Theorem (Tanuma & Man, submitted to "Mathematical Methods and Models in Composites", 2nd ed., Imperial College Press)

Elastic medium : $x_3 \leq 0$,

    $1, 2, 3$-axes : symmetry axes of $\mathbb{C}^{\mathrm{Orth}}$ of Base material

Rayleigh waves : propagate in the direction of the 2-axis.

$\Longrightarrow$

1st-order perturbation formula for r_R :
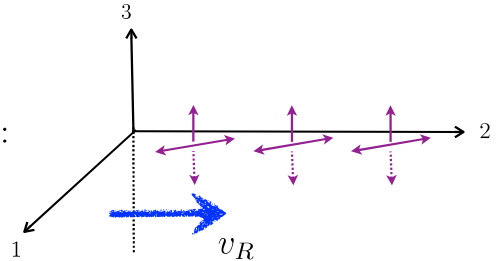
$$r_R = r_R^{\mathrm{Orth}} + \eta_{22}(v_R^{\mathrm{Orth}})\, a_{22} + \eta_{23}(v_R^{\mathrm{Orth}})\, a_{23} + \eta_{33}(v_R^{\mathrm{Orth}})\, a_{33} + \eta_{44}(v_R^{\mathrm{Orth}})\, a_{44}$$

Each coefficient $\eta_{ij}(v)$ is written explicitly in terms of $\mathbb{C}^{\mathrm{Orth}}$ and ρ.

$$\boldsymbol{\sigma} = \Big(\sigma_{ij}\Big)_{i,j=1,2,3} = \big(\mathbb{C}^{\text{Orth}} + \mathbb{A}\big)[\boldsymbol{E}]$$

● Only 4 components of $\mathbb{A} = (a_{rs}) = \begin{pmatrix} a_{11} & a_{12} & a_{13} & a_{14} & a_{15} & a_{16} \\ & a_{22} & a_{23} & a_{24} & a_{25} & a_{26} \\ & & a_{33} & a_{34} & a_{35} & a_{36} \\ & & & a_{44} & a_{45} & a_{46} \\ & & & & a_{55} & a_{56} \\ Sym. & & & & & a_{66} \end{pmatrix}$

can influence the first order perturbation of v_R and r_R.

23

$$\eta_{22}(v) = \frac{-C_{33}C_{44}\sqrt{C_{44}-V}}{2E(v)}\Big[(C_{22}C_{33}-C_{23}^2)^2 - 2(C_{22}C_{33}-C_{23}^2)C_{33}V + (C_{33}^2 - C_{23}^2)V^2\Big],$$

$$\eta_{23}(v) = \frac{C_{23}\sqrt{C_{44}-V}}{E(v)}\Big[(C_{22}C_{33}-C_{23}^2)^2C_{44} - 2(C_{22}C_{33}-C_{23}^2)C_{33}C_{44}V + (C_{33}-C_{22})C_{33}C_{44}V^2\Big],$$

$$\eta_{33}(v) = \frac{\sqrt{C_{44}-V}}{2C_{33}E(v)}\Big[2C_{22}(C_{22}C_{33}-C_{23}^2)^2C_{33}C_{44}$$

$$- (C_{22}C_{33}-C_{23}^2)\big((C_{22}C_{33}-C_{23}^2)(2C_{22}C_{33}+C_{23}^2) + 4C_{22}C_{33}^2C_{44}\big)V$$

$$+ C_{33}\big(2(C_{22}C_{33}-C_{23}^2)(2C_{22}C_{33}+C_{23}^2) - C_{22}(C_{22}C_{33}+C_{23}^2-2C_{33}^2)C_{44}\big)V^2$$

$$- C_{33}\big(C_{22}C_{33}(2C_{33}-C_{44}) + C_{23}^2(C_{33}-2C_{44})\big)V^3\Big],$$

$$\eta_{44}(v) = \frac{C_{22}C_{33}-C_{23}^2}{2C_{44}D(v)}\sqrt{C_{33}(C_{22}C_{33}-C_{23}^2-C_{33}V)V},$$

$$E(v) = \sqrt{C_{44}(C_{22}-V)(C_{22}C_{33}-C_{23}^2-C_{33}V)V}\ D(v)V,$$

$$D(v) = (C_{22}C_{33}-C_{23}^2)(C_{22}C_{33}-C_{23}^2+2C_{33}C_{44}) + 2C_{33}[C_{22}C_{44}-2(C_{22}C_{33}-C_{23}^2)-C_{33}C_{44}]V$$

$$+ 3C_{33}(C_{33}-C_{44})V^2,$$

$$V = \rho\,v^2.$$

24

Related works : on v_R

Base material is Isotropic:

- [Delsanto & Clark, J. Acoust. Soc. Am. (1987)]

    The 6 components of $\mathbb{A}$ can influence the 1st order perturbation of v_R

- [Tanuma & Man, J. Elasticity (2006)]
- [Song & Fu, J. Elasticity (2007)]
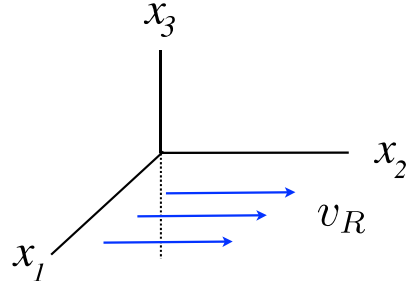
Base material is Monoclinic:

- [Song & Fu, J. Elasticity (2007)]

    The 6 components of $\mathbb{A}$ can influence the 1st order perturbation of v_R

Related works : on r_R

- [Royer, Dieulesaint, *J. Acoust. Soc. Am.* (1984)] : on r_R^{Orth}

- [Junge et al., *Ultrasonic* (2006)]

$\overset{\circ}{\boldsymbol{T}} = \left(\overset{\circ}{T}_{ij} \right)_{i,j=1,2,3}$: residual stress $\Rightarrow$

$$
\begin{aligned}
\mathbb{A}\,[\boldsymbol{E}] = \mathbb{A}(\overset{\circ}{\boldsymbol{T}})\,[\boldsymbol{E}] \;=\;& \beta_1 (\mathrm{tr}\,\boldsymbol{E})(\mathrm{tr}\,\overset{\circ}{\boldsymbol{T}})\boldsymbol{I} + \beta_2 (\mathrm{tr}\,\overset{\circ}{\boldsymbol{T}})\boldsymbol{E} \\
& + \beta_3 \left((\mathrm{tr}\,\boldsymbol{E})\overset{\circ}{\boldsymbol{T}} + (\mathrm{tr}\,\boldsymbol{E}\overset{\circ}{\boldsymbol{T}})\boldsymbol{I} \right) + \beta_4 (\boldsymbol{E}\overset{\circ}{\boldsymbol{T}} + \overset{\circ}{\boldsymbol{T}}\boldsymbol{E})
\end{aligned}
$$

Perturbative part of $\mathbb{C}$

Acoustoelastic Coefficients

Case of Uniaxial Stress (the uniaxial stress $\sigma_2 = \overset{\circ}{T}_{22}$ is applied in the direction of the 2-axis, i.e., in the propagation direction of the Rayleigh wave):

$$
\frac{r_R - r_R^{\text{Iso}}}{r_R^{\text{Iso}}} \;=\; K^r\,\sigma_2, \qquad\qquad \frac{v_R - v_R^{\text{Iso}}}{v_R^{\text{Iso}}} \;=\; K^v\,\sigma_2,
$$

	K^r (1/MPa)	K^v (1/MPa)	K^r/K^v
mild steel	9.184×10^{-6}	-5.710×10^{-7}	-16.08
Al (99.3%)	3.701×10^{-5}	-1.086×10^{-5}	-3.407
Al alloy B53S	2.790×10^{-5}	-2.883×10^{-6}	-9.676
Al alloy D54S	6.673×10^{-5}	-2.045×10^{-5}	-3.263
Al alloy JH77S	6.095×10^{-5}	-2.368×10^{-5}	-2.574
polystyrene	6.939×10^{-4}	-2.958×10^{-5}	-23.46
brass	3.848×10^{-5}	-6.479×10^{-6}	-5.939
aluminum	3.925×10^{-5}	-1.127×10^{-5}	-3.481
copper	1.487×10^{-5}	-5.167×10^{-6}	-2.878
rail steel	9.761×10^{-6}	-4.339×10^{-7}	-22.50
CP titanium	1.805×10^{-5}	-1.874×10^{-6}	-9.634
aluminum oxide	4.170×10^{-6}	2.861×10^{-7}	14.58

sensitivity :

$$|K^r| \;>\; |K^v|$$

polarization ratio   phase velocity

Extension: Vertically-Inhomogeneous, Anisotropic, Prestressed Elastic media

$$\rho = \rho(x_3), \quad \mathbb{C} = \mathbb{C}(x_3), \quad \overset{\circ}{\boldsymbol{T}} = \overset{\circ}{\boldsymbol{T}}(x_3) = \big(\overset{\circ}{T}_{ij}\big)_{i,j=1,2,3}$$

Example : stress profile in tempered metals, glass, ...

tension compression

$$x_3 = 0$$

$$\overset{\circ}{T}_{22}$$

residual stress

$$x_3 \longrightarrow -\infty$$

27

---
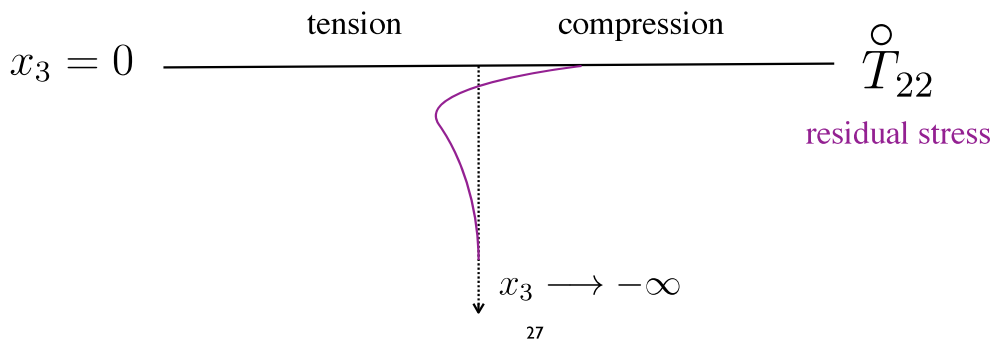
v_R : depends on k : dispersion

dispersion formula

$\eta = (\eta_1, \eta_2, 0)$: direction of propagation

$$v_R = v_R(\eta, k) = \underline{v_0(\eta)} + v_1(\eta)\, k^{-1} + v_2(\eta)\, k^{-2} + \cdots \qquad \text{for large } k$$

§1

Man, Nakamura, Tanuma, Wang, *IMA Journal of Applied Mathematics* (2013)
Tanuma, Man, Chen, *International Journal of Engineering Journal* (2015)
Chen, Man, Tanuma, Kube, *Wave Motion* (2018)

Next to do :

Find

§1

$$r_R = r_R(\eta, k) = \underline{r_0(\eta)} + r_1(\eta)\, k^{-1} + r_2(\eta)\, k^{-2} + \cdots \qquad \text{for large } k.$$

28

§2. Perturbation of Bleustein-Gulyaev waves
in piezoelectricity

Collaboration with

Gen Nakamura, *Hokkaido University, Japan*

Xiang Xu, *Zhejiang University*, *China*

mechanical deformations ⟷ electric fields

piezoelectric effects
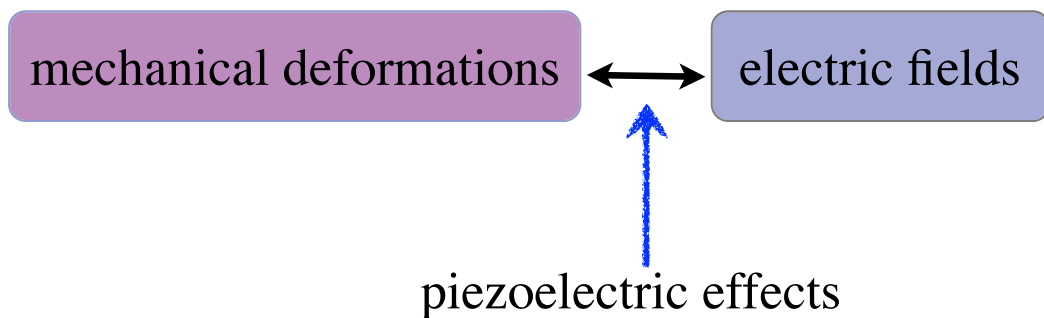
Applications : semiconductor, speaker, cell phone,
ignition device, etc.

30

Constitutive equations

$$\sigma_{ij} = \sum_{k,l=1}^{3} C_{ijkl} \frac{\partial\, u_k}{\partial\, x_l} + \sum_{l=1}^{3} e_{ijl} \frac{\partial\, \phi}{\partial\, x_l}, \qquad i,j = 1,2,3,$$

$$D_j = \sum_{k,l=1}^{3} e_{klj} \frac{\partial\, u_k}{\partial\, x_l} - \sum_{l=1}^{3} \epsilon_{jl} \frac{\partial\, \phi}{\partial\, x_l}, \qquad j = 1,2,3.$$

$\boldsymbol{\sigma} = \left(\sigma_{ij}\right)$: mechanical stress tensor

$\boldsymbol{D} = (D_1, D_2, D_3)$: electric displacement

$\boldsymbol{u} = (u_1, u_2, u_3)$: mechanical displacement

ϕ : electric potential

31

Constitutive equations

Elasticity

$$\sigma_{ij} = \sum_{k,l=1}^{3} C_{ijkl} \frac{\partial\, u_k}{\partial\, x_l} + \sum_{l=1}^{3} e_{ijl} \frac{\partial\, \phi}{\partial\, x_l}, \qquad i,j = 1,2,3,$$

$$D_j = \sum_{k,l=1}^{3} e_{klj} \frac{\partial\, u_k}{\partial\, x_l} - \sum_{l=1}^{3} \epsilon_{jl} \frac{\partial\, \phi}{\partial\, x_l}, \qquad j = 1,2,3.$$

$\boldsymbol{\sigma} = \left(\sigma_{ij}\right)$: mechanical stress tensor

$\boldsymbol{D} = (D_1, D_2, D_3)$: electric displacement

$\boldsymbol{u} = (u_1, u_2, u_3)$: mechanical displacement

ϕ : electric potential

32

Coefficients (material constants)

$$\sigma_{ij} \;=\; \sum_{k,l=1}^{3} C_{ijkl}\,\frac{\partial\, u_k}{\partial\, x_l} \;+\; \sum_{l=1}^{3} e_{ijl}\,\frac{\partial\, \phi}{\partial\, x_l}, \qquad i,j = 1,2,3,$$

$$D_j \;=\; \sum_{k,l=1}^{3} e_{klj}\,\frac{\partial\, u_k}{\partial\, x_l} \;-\; \sum_{l=1}^{3} \epsilon_{jl}\,\frac{\partial\, \phi}{\partial\, x_l}, \qquad j = 1,2,3.$$

$\mathbf{C} = \big(C_{ijkl}\big)$: elasticity tensor $(C_{ijkl} = C_{jikl} = C_{klij}, \; \mathbf{C} > 0)$,

$\boldsymbol{\epsilon} = \big(\epsilon_{jl}\big)$: dielectric tensor $(\epsilon_{jl} = \epsilon_{lj}, \; \boldsymbol{\epsilon} > 0)$,

$\boldsymbol{e} = \big(e_{ijl}\big)$: **piezoelectric tensor** $(e_{ijl} = e_{jil})$.

Serve as a bridge between mechanics and electronics

Voigt notation for $\mathbf{C}$ and $\boldsymbol{e}$: $\quad \big(C_{ijkl}\big) = \big(C_{\alpha\beta}\big), \qquad \big(e_{ijl}\big) = \big(e_{\alpha l}\big)$

(applied for first 2 indices)

ij (or kl)		α or β	ij (or kl)		α or β
11	$\longleftrightarrow$	1	23 or 32	$\longleftrightarrow$	4
22	$\longleftrightarrow$	2	31 or 13	$\longleftrightarrow$	5
33	$\longleftrightarrow$	3	12 or 21	$\longleftrightarrow$	6

The constitutive relations becomes

$$
\begin{bmatrix} \sigma_{11} \\ \sigma_{22} \\ \sigma_{33} \\ \sigma_{23} \\ \sigma_{13} \\ \sigma_{12} \\ \hline D_1 \\ D_2 \\ D_3 \end{bmatrix}
=
\left[
\begin{array}{cccccc|ccc}
C_{11} & C_{12} & C_{13} & C_{14} & C_{15} & C_{16} & e_{11} & e_{12} & e_{13} \\
 & C_{22} & C_{23} & C_{24} & C_{25} & C_{26} & e_{21} & e_{22} & e_{23} \\
 & & C_{33} & C_{34} & C_{35} & C_{36} & e_{31} & e_{32} & e_{33} \\
 & & & C_{44} & C_{45} & C_{46} & e_{41} & e_{42} & e_{43} \\
 & & & & C_{55} & C_{56} & e_{51} & e_{52} & e_{53} \\
 & & & & & C_{66} & e_{61} & e_{62} & e_{63} \\
\hline
 & & \textcolor{blue}{Sym.} & & & & -\epsilon_{11} & -\epsilon_{12} & -\epsilon_{13} \\
 & & & & & & & -\epsilon_{22} & -\epsilon_{23} \\
 & & & & & & & & -\epsilon_{33}
\end{array}
\right]
\begin{bmatrix} (u_1)_{x_1} \\ (u_2)_{x_2} \\ (u_3)_{x_3} \\ (u_2)_{x_3} + (u_3)_{x_2} \\ (u_1)_{x_3} + (u_3)_{x_1} \\ (u_1)_{x_2} + (u_2)_{x_1} \\ \hline \phi_{x_1} \\ \phi_{x_2} \\ \phi_{x_3} \end{bmatrix}
$$

elasto-piezo-dielectric matrix (**9-by-9 symmetric**)

Equations of mechanical motion + Equation of electric equilibrium :

$$\sum_{j=1}^{3} \frac{\partial \sigma_{ij}}{\partial x_j} = \rho \frac{\partial^2 u_i}{\partial t^2}, \quad i = 1, 2, 3, \qquad \sum_{j=1}^{3} \frac{\partial D_j}{\partial x_j} = 0$$

(ρ : uniform density)

System for the unknowns $\boldsymbol{u} = (u_1, u_2, u_3)$ and ϕ.

$\mathbf{m}$, $\mathbf{n}$: orthogonal unit vectors in $\mathbb{R}^3$

$\mathbf{m}$: propagation direction

$\mathbf{n}$: unit outer normal of the surface

<u>Surface-wave solution</u>

in the half-space $\mathbf{n} \cdot \mathbf{x} \leq 0$:
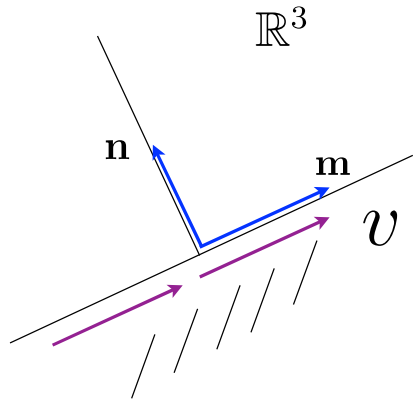
$$\begin{pmatrix} \boldsymbol{u} \\ \phi \end{pmatrix} = \sum_{\alpha=1}^{4} c_\alpha \, \mathbf{a}_\alpha \, e^{-\sqrt{-1}\, k\, (\mathbf{m}\cdot\mathbf{x} + p_\alpha \mathbf{n}\cdot\mathbf{x} - v\,t)} \quad \in \mathbb{C}^4$$

c_α, $p_\alpha(v) \in \mathbb{C}$, $\mathbf{a}_\alpha(v) \in \mathbb{C}^4$, k : wave number, v : phase velocity

$v \in$ "subsonic range" $\longleftrightarrow$ Im $p_\alpha > 0$ $(\alpha = 1, 2, 3, 4)$ $\longrightarrow$ $\begin{pmatrix} \boldsymbol{u} \\ \phi \end{pmatrix}$ decays as $\mathbf{n} \cdot \mathbf{x} \longrightarrow -\infty$

Two types of boundary conditions

a Mechanically-free and electrically-open condition at the boundary
i.e.,

$$\sum_{j=1}^{3} \sigma_{ij} n_j = 0, \quad i = 1,2,3, \qquad \sum_{j=1}^{3} D_j n_j = 0 \ \text{ at } \ \mathbf{n} \cdot \mathbf{x} = 0$$

b Mechanically-free and electrically-closed condition at the boundary
i.e.,

$$\sum_{j=1}^{3} \sigma_{ij} n_j = 0, \quad i = 1,2,3, \qquad \phi = 0 \ \text{ at } \ \mathbf{n} \cdot \mathbf{x} = 0$$
$$(\text{ grounded })$$

a mechanically-free, electrically-open boundary condition

$$\begin{pmatrix} \boldsymbol{u} \\ \phi \end{pmatrix} = \sum_{\alpha=1}^{4} c_\alpha \, \mathbf{a}_\alpha \, e^{-\sqrt{-1}\,k\,(\mathbf{m}\cdot\mathbf{x}+p_\alpha\mathbf{n}\cdot\mathbf{x}-v\,t)} \qquad \longrightarrow \qquad \text{Compute } \mathbf{l}_\alpha(v)\text{'s so that}$$

$$\begin{pmatrix} \left(\sum_{j=1}^{3} \sigma_{ij} n_j\right)_{i\downarrow 1,2,3} \\ \sum_{j=1}^{3} D_j n_j \end{pmatrix}_{\mathbf{n}\cdot\mathbf{x}=0} = -i\,k \sum_{\alpha=1}^{4} c_\alpha \, \mathbf{l}_\alpha(v) \, e^{-i\,k(\mathbf{m}\cdot\mathbf{x}-v\,t)} \bigg|_{\mathbf{n}\cdot\mathbf{x}=0} \in \mathbb{C}^4$$

Find $v = v_R$ such that

$$\sum_{\alpha=1}^{4} c_\alpha \, \mathbf{l}_\alpha(v) = \mathbf{0} \iff \det\left[\, \mathbf{l}_1(v) \ \mathbf{l}_2(v) \ \mathbf{l}_3(v) \ \mathbf{l}_4(v) \,\right] = 0.$$

b **mechanically-free, electrically-closed boundary condition**

$\mathbf{a}_\alpha(v)$'s $\mathbf{l}_\alpha(v)$'s in the previous steps

$$\Longrightarrow\quad \begin{pmatrix} -i\,k\,\phi \\ \left(\sum_{j=1}^{3}\sigma_{ij}n_j\right)_{i\downarrow 1,2,3} \end{pmatrix}_{\mathbf{n\cdot x}=0} = -i\,k\sum_{\alpha=1}^{4} c_\alpha \begin{pmatrix} (\mathbf{a}_\alpha)_4 \\ (\mathbf{l}_\alpha)_1 \\ (\mathbf{l}_\alpha)_2 \\ (\mathbf{l}_\alpha)_3 \end{pmatrix} e^{-i\,k(\mathbf{m\cdot x}-v\,t)}\Bigg|_{\mathbf{n\cdot x}=0}.$$

Find $v = v_B$ such that $\quad \det \begin{pmatrix} (\mathbf{a}_1)_4 & (\mathbf{a}_2)_4 & (\mathbf{a}_3)_4 & (\mathbf{a}_4)_4 \\ (\mathbf{l}_1)_1 & (\mathbf{l}_2)_1 & (\mathbf{l}_3)_1 & (\mathbf{l}_4)_1 \\ (\mathbf{l}_1)_2 & (\mathbf{l}_2)_2 & (\mathbf{l}_3)_2 & (\mathbf{l}_4)_2 \\ (\mathbf{l}_1)_3 & (\mathbf{l}_2)_3 & (\mathbf{l}_3)_3 & (\mathbf{l}_4)_3 \end{pmatrix} = 0.$

Barnett & Lothe's integral formalism for piezoelectricity based on Stroh formalism (1976)

a **Mechanically-free and electrically-free condition at the boundary**

$\Longrightarrow$ For fixed $\mathbf{m}$ and $\mathbf{n}$, there is at most one surface wave.

$$v = v_{\mathrm{R}}$$

b **Mechanically-free and electrically-closed condition at the boundary**

$\Longrightarrow$ For fixed $\mathbf{m}$ and $\mathbf{n}$, there is at most two surface waves.

$$v = v_{\mathrm{R}},\ \ v_{\mathrm{B}}$$

● Existence condition of surface waves is locally stable under the change of material constants.

We are interested in surface waves

- which carry clear information on the piezoelectric tensor $\boldsymbol{e} = (e_{ijl})$,
- which can be used as observation data for recovering $\boldsymbol{e} = (e_{ijl})$.

Derive a formula for surface-wave velocity in terms of
$$\mathbf{C} = (C_{ijkl}), \boldsymbol{\epsilon} = (\epsilon_{jl}) \text{ and } \boldsymbol{e} = (e_{ijl}).$$

(Forward Problem)

Bleustein-Gulyaev surface waves (BG waves) (1968, 1969)

1. <u>Piezoelectric material of Symmetry **6** (hexagonal, transversely isotropic)</u>

3-axis : axis of Symmetry **6** of $\mathbf{P}^{\text{hex}}$

$$\mathbf{P}^{\text{hex}} = \left[\begin{array}{cccccc|ccc} C_{11} & C_{12} & C_{13} & 0 & 0 & 0 & 0 & 0 & e_{23} \\ C_{12} & C_{11} & C_{13} & 0 & 0 & 0 & 0 & 0 & e_{23} \\ C_{13} & C_{13} & C_{33} & 0 & 0 & 0 & 0 & 0 & e_{33} \\ 0 & 0 & 0 & C_{44} & 0 & 0 & e_{41} & e_{42} & 0 \\ 0 & 0 & 0 & 0 & C_{44} & 0 & e_{42} & -e_{41} & 0 \\ 0 & 0 & 0 & 0 & 0 & \frac{C_{11}-C_{12}}{2} & 0 & 0 & 0 \\ \hline 0 & 0 & 0 & e_{41} & e_{42} & 0 & -\epsilon_{22} & 0 & 0 \\ 0 & 0 & 0 & e_{42} & -e_{41} & 0 & 0 & -\epsilon_{22} & 0 \\ e_{23} & e_{23} & e_{33} & 0 & 0 & 0 & 0 & 0 & -\epsilon_{33} \end{array}\right] \qquad e_{42} \neq 0$$

2. Piezoelectric medium : $x_2 \leq 0$,   Propagation direction : $(1, 0, 0)$

3. **Mechanically-free** and **electrically-closed** condition at $x_2 = 0$.

x_3 : axis of symmetry 6

$v_\mathrm{B}^\mathrm{hex}$

medium $\mathbf{P}^\mathrm{hex} : x_2 \leq 0$

x_2

$\mathbf{m} = (1, 0, 0)$

x_1
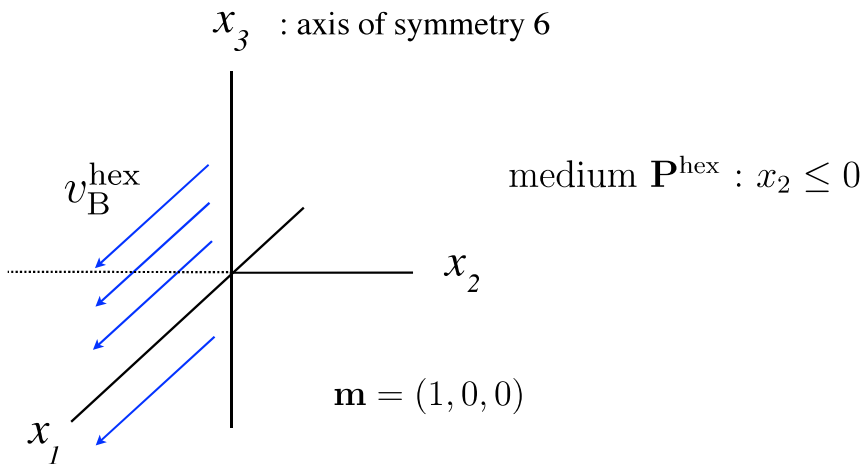
The velocity $v_\mathrm{B} = v_\mathrm{B}^\mathrm{hex}$ is given by

$$V_\mathrm{B}^\mathrm{hex} = \rho \left(v_\mathrm{B}^\mathrm{hex} \right)^2 = \frac{C_{44} \left(C_{44} + 2 \dfrac{e_{42}^2}{\epsilon_{22}} \right)}{C_{44} + \dfrac{e_{42}^2}{\epsilon_{22}}}$$

43

To the best of the authors' knowledge, however, there are no surface waves, aside from BG waves, whose velocity carries clear information on the piezoelectric tensor and can be used as observation data for recovering the material tensors.

44

$v_{\mathrm{B}}^{\mathrm{hex}}$ has very restrictive information on the material constants; i.e.,

$v_{\mathrm{B}}^{\mathrm{hex}}$ depends on just one component C_{44} of $\mathbf{C}$,

one component e_{42} of $\boldsymbol{e}$, and

one component ϵ_{22} of $\boldsymbol{\epsilon}$.

Consider perturbation.

Now we give an *arbitrary* perturbation to the medium of $\mathbf{P}^{\mathrm{hex}}$, i.e.,

elasto-piezo-dielectric matrix

$$
=
\left.
\begin{bmatrix}
C_{11} & C_{12} & C_{13} & 0 & 0 & 0 & 0 & 0 & e_{23} \\
C_{12} & C_{11} & C_{13} & 0 & 0 & 0 & 0 & 0 & e_{23} \\
C_{13} & C_{13} & C_{33} & 0 & 0 & 0 & 0 & 0 & e_{33} \\
0 & 0 & 0 & C_{44} & 0 & 0 & e_{41} & e_{42} & 0 \\
0 & 0 & 0 & 0 & C_{44} & 0 & e_{42} & -e_{41} & 0 \\
0 & 0 & 0 & 0 & 0 & \frac{C_{11}-C_{12}}{2} & 0 & 0 & 0 \\
0 & 0 & 0 & e_{41} & e_{42} & 0 & -\epsilon_{22} & 0 & 0 \\
0 & 0 & 0 & e_{42} & -e_{41} & 0 & 0 & -\epsilon_{22} & 0 \\
e_{23} & e_{23} & e_{33} & 0 & 0 & 0 & 0 & 0 & -\epsilon_{33}
\end{bmatrix}
\right) \mathbf{P}^{\mathrm{hex}}
$$

$$
+
\left.
\begin{bmatrix}
a_{11} & a_{12} & a_{13} & a_{14} & a_{15} & a_{16} & f_{11} & f_{12} & f_{13} \\
 & a_{22} & a_{23} & a_{24} & a_{25} & a_{26} & f_{21} & f_{22} & f_{23} \\
 & & a_{33} & a_{34} & a_{35} & a_{36} & f_{31} & f_{32} & f_{33} \\
 & & & a_{44} & a_{45} & a_{46} & f_{41} & f_{42} & f_{43} \\
 & & & & a_{55} & a_{56} & f_{51} & f_{52} & f_{53} \\
 & & & & & a_{66} & f_{61} & f_{62} & f_{63} \\
 & & \textit{Sym.} & & & & -\delta_{11} & -\delta_{12} & -\delta_{13} \\
 & & & & & & & -\delta_{22} & -\delta_{23} \\
 & & & & & & & & -\delta_{33}
\end{bmatrix}
\right)
\begin{array}{l} \mathbf{P}^{\mathrm{ptb}} \\ \text{(perturbation} \\ \text{with no} \\ \text{material symmetry)} \end{array}
$$

Problem

How v_{B} deviates from its comparative value $v_{\mathrm{B}}^{\mathrm{hex}}$ in Symmetry 6 due to the influence of $\mathbf{P}^{\mathrm{ptb}}$?

More precisely,

How does each component of
$$
\left[
\begin{array}{cccccc|ccc}
a_{11} & a_{12} & a_{13} & a_{14} & a_{15} & a_{16} & f_{11} & f_{12} & f_{13} \\
 & a_{22} & a_{23} & a_{24} & a_{25} & a_{26} & f_{21} & f_{22} & f_{23} \\
 & & a_{33} & a_{34} & a_{35} & a_{36} & f_{31} & f_{32} & f_{33} \\
 & & & a_{44} & a_{45} & a_{46} & f_{41} & f_{42} & f_{43} \\
 & & & & a_{55} & a_{56} & f_{51} & f_{52} & f_{53} \\
 & & & & & a_{66} & f_{61} & f_{62} & f_{63} \\
\hline
 & & & & & & -\delta_{11} & -\delta_{12} & -\delta_{13} \\
 & & & & & & & -\delta_{22} & -\delta_{23} \\
 & & & & & & & & -\delta_{33}
\end{array}
\right\} \mathbf{P}^{\mathrm{ptb}}
$$

affect the first order perturbation of v_{B} ?

---

axis of symmetry 6

x_3

medium : $x_2 \leq 0$

$v_{\mathrm{B}}^{\mathrm{hex}}$

x_2

x_1

$\mathbf{P}^{\mathrm{hex}}$

Propagation direction : $(1, 0, 0)$

x_3

medium : $x_2 \leq 0$

v_{B} ?

x_2

x_1

$\mathbf{P}^{\mathrm{hex}} + \mathbf{P}^{\mathrm{ptb}}$

Propagation direction : $(1, 0, 0)$
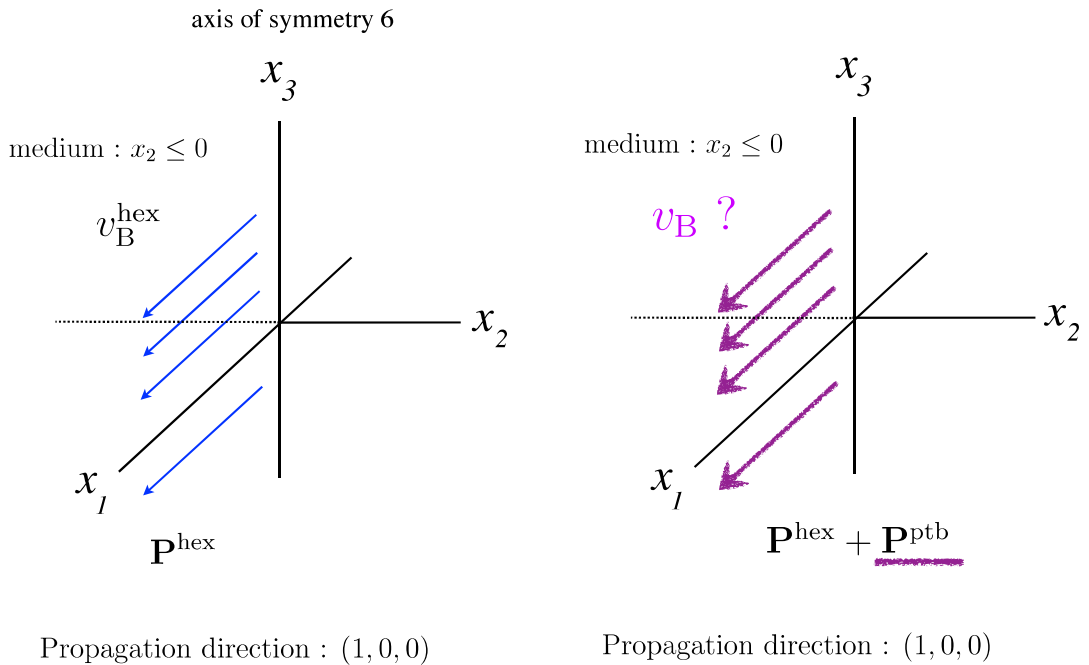
Theorem (Perturbation of BG waves) [submitted]

Suppose that $v_{\mathrm{B}}^{\mathrm{hex}} \neq v_{\mathrm{R}}^{\mathrm{hex}}$, where $v_{\mathrm{R}}^{\mathrm{hex}}$ is Rayleigh-wave velocity determined from the elastic part of $\mathbf{P}^{\mathrm{hex}}$

$$\Longrightarrow$$

First-order perturbation formula for v_B : (correct up to terms linear in $\mathbf{P}^{\mathrm{ptb}}$)

$$V_{\mathrm{B}} = \rho\,(v_{\mathrm{B}})^2 \approx V_{\mathrm{B}}^{\mathrm{hex}} + P_1\,f_{42} + P_2\,f_{51} + D_1\,\delta_{11} + D_2\,\delta_{22} + E_1\,a_{44} + E_2\,a_{55}$$

Each coefficient P_i, D_i and E_i $(i = 1, 2)$ is written explicitly in terms of $\mathbf{P}^{\mathrm{hex}}$.

$$P_1 = \frac{-2\,C_{44}\,e_{42}{}^5}{(C_{44}\,\epsilon_{22} + e_{42}{}^2)^2\,(C_{44}\,\epsilon_{22} + 2\,e_{42}{}^2)}, \qquad P_2 = \frac{2\,C_{44}\,e_{42}}{C_{44}\,\epsilon_{22} + 2\,e_{42}{}^2},$$

$$D_1 = \frac{-C_{44}{}^2\,e_{42}{}^2}{(C_{44}\,\epsilon_{22} + e_{42}{}^2)\,(C_{44}\,\epsilon_{22} + 2\,e_{42}{}^2)}, \qquad D_2 = \frac{-C_{44}{}^2\,e_{42}{}^4}{(C_{44}\,\epsilon_{22} + e_{42}{}^2)^2\,(C_{44}\,\epsilon_{22} + 2\,e_{42}{}^2)},$$

$$E_1 = \frac{e_{42}{}^4}{(C_{44}\,\epsilon_{22} + e_{42}{}^2)^2}, \qquad E_2 = 1.$$

Remark

$$\begin{bmatrix} a_{11} & a_{12} & a_{13} & a_{14} & a_{15} & a_{16} & f_{11} & f_{12} & f_{13} \\ & a_{22} & a_{23} & a_{24} & a_{25} & a_{26} & f_{21} & f_{22} & f_{23} \\ & & a_{33} & a_{34} & a_{35} & a_{36} & f_{31} & f_{32} & f_{33} \\ & & & \boxed{a_{44}} & a_{45} & a_{46} & f_{41} & \boxed{f_{42}} & f_{43} \\ & & & & \boxed{a_{55}} & a_{56} & \boxed{f_{51}} & f_{52} & f_{53} \\ & & & & & a_{66} & f_{61} & f_{62} & f_{63} \\ & & Sym. & & & & \boxed{-\delta_{11}} & -\delta_{12} & -\delta_{13} \\ & & & & & & & \boxed{-\delta_{22}} & -\delta_{23} \\ & & & & & & & & -\delta_{33} \end{bmatrix}$$

Only the circled components can affect the first order perturbation of v_B.

Outline of the Proof

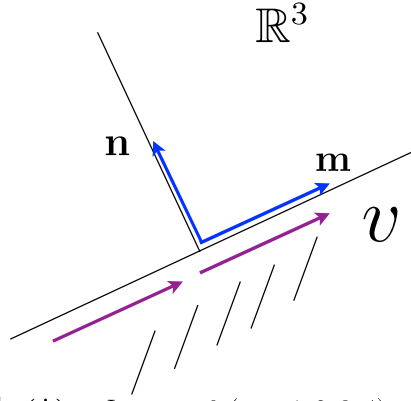$\mathbf{m}$, $\mathbf{n}$: orthogonal unit vectors in $\mathbb{R}^3$

$\mathbf{m}$: propagation direction

$\mathbf{n}$: unit outer normal of the surface

Surface-wave solution

in the half-space $\mathbf{n} \cdot \mathbf{x} \leq 0$:

$\mathbb{R}^3$

$$\begin{pmatrix} \boldsymbol{u} \\ \phi \end{pmatrix} = \sum_{\alpha=1}^{4} c_\alpha \, \mathbf{a}_\alpha \, e^{-\sqrt{-1}\, k\,(\mathbf{m}\cdot\mathbf{x}+p_\alpha\,\mathbf{n}\cdot\mathbf{x}-v\,t)} \in \mathbb{C}^4 \quad (*) \qquad \operatorname{Im} p_\alpha > 0 \; (\alpha = 1,2,3,4)$$

$$\begin{pmatrix} \left(\sum_{j=1}^{3} \sigma_{ij} n_j\right)_{i\downarrow 1,2,3} \\ \sum_{j=1}^{3} D_j n_j \end{pmatrix}_{\mathbf{n}\cdot\mathbf{x}=0} = -i\,k \sum_{\alpha=1}^{4} c_\alpha \, \mathbf{l}_\alpha \, e^{-i\,k(\mathbf{m}\cdot\mathbf{x}-v\,t)} \Bigg|_{\mathbf{n}\cdot\mathbf{x}=0} \in \mathbb{C}^4$$

51

Barnett & Lothe's integral formalism for piezoelectricity
based on the Stroh formalism [J. Appl. Phys. & Phys. Norv. (1976)]

$$\widetilde{\mathbf{m}} = \widetilde{\mathbf{m}}(\phi) = \mathbf{m}\cos\phi + \mathbf{n}\sin\phi, \qquad \widetilde{\mathbf{n}} = \widetilde{\mathbf{n}}(\phi) = -\mathbf{m}\sin\phi + \mathbf{n}\cos\phi$$

$$\implies \quad \mathbf{N}(\phi)\begin{pmatrix} \mathbf{a}_\alpha \\ \mathbf{l}_\alpha \end{pmatrix} = p_\alpha(\phi)\begin{pmatrix} \mathbf{a}_\alpha \\ \mathbf{l}_\alpha \end{pmatrix}, \qquad \alpha = 1,2,3,4 \qquad \text{for all } \phi$$

$$p_\alpha'(\phi) = -1 - p_\alpha(\phi)^2, \quad p_\alpha(0) = p_\alpha \text{ in } (*)$$

where

$$\mathbf{N} = \mathbf{N}(\phi) = \begin{pmatrix} -\mathbf{T}(\phi)^{-1}\mathbf{R}(\phi)^T & \mathbf{T}(\phi)^{-1} \\ -\mathbf{Q}(\phi)+\mathbf{R}(\phi)\mathbf{T}(\phi)^{-1}\mathbf{R}(\phi)^T & -\mathbf{R}(\phi)\mathbf{T}(\phi)^{-1} \end{pmatrix} \qquad 8 \times 8$$

52

and

$$\mathbf{Q}(\phi) = \left(\begin{array}{c|c} \left(\sum_{j,l=1}^{3} C_{ijkl}\widetilde{m}_j\widetilde{m}_l\right)_{i\downarrow k\rightarrow 1,2,3} - \rho\, v^2 \cos^2\phi\, \mathbf{I} & \left(\sum_{j,l=1}^{3} e_{ijl}\widetilde{m}_j\widetilde{m}_l\right)_{i\downarrow 1,2,3} \\ \hline \left(\sum_{j,l=1}^{3} e_{klj}\widetilde{m}_j\widetilde{m}_l\right)_{k\rightarrow 1,2,3} & -\sum_{j,l=1}^{3} \varepsilon_{jl}\widetilde{m}_j\widetilde{m}_l \end{array} \right),$$

$$\mathbf{R}(\phi) = \left(\begin{array}{c|c} \left(\sum_{j,l=1}^{3} C_{ijkl}\widetilde{m}_j\widetilde{n}_l\right)_{i\downarrow k\rightarrow 1,2,3} + \rho\, v^2 \cos\phi\sin\phi\, \mathbf{I} & \left(\sum_{j,l=1}^{3} e_{ijl}\widetilde{m}_j\widetilde{n}_l\right)_{i\downarrow 1,2,3} \\ \hline \left(\sum_{j,l=1}^{3} e_{klj}\widetilde{m}_j\widetilde{n}_l\right)_{k\rightarrow 1,2,3} & -\sum_{j,l=1}^{3} \varepsilon_{jl}\widetilde{m}_j\widetilde{n}_l \end{array} \right),$$

$$\mathbf{T}(\phi) = \left(\begin{array}{c|c} \left(\sum_{j,l=1}^{3} C_{ijkl}\widetilde{n}_j\widetilde{n}_l\right)_{i\downarrow k\rightarrow 1,2,3} - \rho\, v^2 \sin^2\phi\, \mathbf{I} & \left(\sum_{j,l=1}^{3} e_{ijl}\widetilde{n}_j\widetilde{n}_l\right)_{i\downarrow 1,2,3} \\ \hline \left(\sum_{j,l=1}^{3} e_{klj}\widetilde{n}_j\widetilde{n}_l\right)_{k\rightarrow 1,2,3} & -\sum_{j,l=1}^{3} \varepsilon_{jl}\widetilde{n}_j\widetilde{n}_l \end{array} \right). \quad (13)$$

Take angular average of both sides

$$\implies \qquad \begin{pmatrix} \mathbf{S}_1 & \mathbf{S}_2 \\ \mathbf{S}_3 & \mathbf{S}_1^T \end{pmatrix} \begin{pmatrix} \mathbf{a}_\alpha \\ \mathbf{l}_\alpha \end{pmatrix} = \mathrm{i} \begin{pmatrix} \mathbf{a}_\alpha \\ \mathbf{l}_\alpha \end{pmatrix}, \qquad \alpha = 1,2,3,4,$$

where

$$\mathbf{S}_1 = \frac{1}{2\pi} \int_{-\pi}^{\pi} -\mathbf{T}(\phi)^{-1}\mathbf{R}(\phi)^T\, d\phi, \qquad \mathbf{S}_2 = \frac{1}{2\pi} \int_{-\pi}^{\pi} \mathbf{T}(\phi)^{-1}\, d\phi,$$

$$\mathbf{S}_3 = \frac{1}{2\pi} \int_{-\pi}^{\pi} -\mathbf{Q}(\phi) + \mathbf{R}(\phi)\mathbf{T}(\phi)^{-1}\mathbf{R}(\phi)^T\, d\phi.^4$$

Recall that

$$\sum_{\alpha=1}^{4} c_\alpha \begin{pmatrix} (\mathbf{a}_\alpha)_4 \\ (\mathbf{l}_\alpha)_1 \\ (\mathbf{l}_\alpha)_2 \\ (\mathbf{l}_\alpha)_3 \end{pmatrix} = \mathbf{0} \quad \text{at } v = v_{\mathrm{B}},$$

and

$$\begin{pmatrix} \mathbf{S}_1 & \mathbf{S}_2 \\ \mathbf{S}_3 & \mathbf{S}_1^T \end{pmatrix} \sum_{\alpha=1}^{4} c_\alpha \begin{pmatrix} \mathbf{a}_\alpha \\ \mathbf{l}_\alpha \end{pmatrix} = \mathrm{i} \sum_{\alpha=1}^{4} c_\alpha \begin{pmatrix} \mathbf{a}_\alpha \\ \mathbf{l}_\alpha \end{pmatrix}.$$

Pick up 4th to 7th components from both sides

$$\implies \qquad \underbrace{\begin{pmatrix} (\mathbf{S}_1)_{\substack{i=4 \\ k\rightarrow 1,2,3}} & (\mathbf{S}_2)_{\substack{i=4 \\ k=4}} \\ (\mathbf{S}_3)_{\substack{i\downarrow 1,2,3 \\ k\rightarrow 1,2,3}} & (\mathbf{S}_1^T)_{\substack{i\downarrow 1,2,3 \\ k=4}} \end{pmatrix}}_{\substack{\| \\ \widetilde{\mathbf{S}}_3 = \widetilde{\mathbf{S}}_3(v)}} \sum_{\alpha=1}^{4} c_\alpha \begin{pmatrix} (\mathbf{a}_\alpha)_1 \\ (\mathbf{a}_\alpha)_2 \\ (\mathbf{a}_\alpha)_3 \\ (\mathbf{l}_\alpha)_4 \end{pmatrix} = \mathbf{0} \quad \text{at } v = v_{\mathrm{B}}$$

$$\implies \qquad \boxed{\det \widetilde{\mathbf{S}}_3 = 0 \qquad at \ \ v = v_B}$$

: secular equation written by $\mathbf{C} = (C_{ijkl}), \boldsymbol{\epsilon} = (\epsilon_{jl}), \boldsymbol{e} = (e_{ijl})$ and v.

(1) *The symmetric matrix $\widetilde{\mathbf{S}}_3$ is negative definite at $v = 0$.*
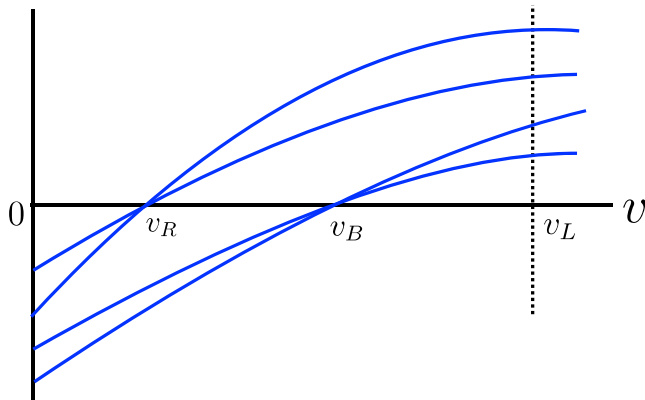
(2) *The symmetric matrix $\dfrac{d}{dv}\widetilde{\mathbf{S}}_3$ is positive definite* ***unless***

$$\Big(\sum_{j,l=1}^{3} e_{ijl}m_j m_l\Big)_{i\downarrow 1,2,3} = \mathbf{0}, \quad \Big(\sum_{j,l=1}^{3} e_{ijl}n_j n_l\Big)_{i\downarrow 1,2,3} = \mathbf{0}, \quad \Big(\sum_{j,l=1}^{3} e_{ijl}(m_j n_l + n_j m_l)\Big)_{i\downarrow 1,2,3} = \mathbf{0}.$$

(3) *The eigenvalues of $\widetilde{\mathbf{S}}_3$ are monotonic increasing functions of v.*

(4) *When one eigenvalue of $\widetilde{\mathbf{S}}_3$ is zero at some v in the interval $0 < v < v_L$, two eigenvalues of $\widetilde{\mathbf{S}}_3$ are simultaneously zero at that v.*

Behavior of eigenvalues of $\widetilde{\mathbf{S}}_3 = \widetilde{\mathbf{S}}_3(v)$

Example

$$\widetilde{\mathbf{S}}_3^{\text{hex}} = \begin{pmatrix} R(V) & 0 & 0 & 0 \\ 0 & \sqrt{\dfrac{C_{11}\left(C_{11} - C_{12} - 2V\right)}{\left(C_{11} - V\right)\left(C_{11} - C_{12}\right)}}\, R(V) & 0 & 0 \\ 0 & 0 & -Z_{33}\left(1 + \dfrac{e_{41}^2}{\Delta}\right) & -Z_{33}\dfrac{e_{41}}{\Delta} \\ 0 & 0 & -Z_{33}\dfrac{e_{41}}{\Delta} & -Z_{33}\dfrac{1}{\Delta} \end{pmatrix},$$

where

$$R(V) \;=\; \frac{1}{V}\left(\sqrt{\frac{C_{11} - C_{12}}{C_{11} - C_{12} - 2V}}\,(C_{11} - C_{12} - V)^2 - \sqrt{\frac{C_{11} - V}{C_{11}}}\,(C_{11} - C_{12})^2\right),$$

$$\Delta \;=\; \sqrt{\left(C_{44}\,\varepsilon_{22} + e_{42}^2\right)\left((C_{44} - V)\varepsilon_{22} + e_{42}^2\right)}, \qquad Z_{33} = \frac{1}{\varepsilon_{22}}(\Delta - e_{42}^2), \qquad V = \rho\,v^2.$$

$$\begin{cases} v_R \;:\; R(V) = 0 \quad \text{(Rayleigh waves)} \\[2ex] v_B \;:\; Z_{33} = 0 \quad \text{(BG waves)} \qquad\qquad \text{(2) of the lemma} \;\Longleftrightarrow\; e_{42} \neq 0 \end{cases}$$

Observation on the fact below:

$$\begin{bmatrix} a_{11} & a_{12} & a_{13} & a_{14} & a_{15} & a_{16} & f_{11} & f_{12} & f_{13} \\ & a_{22} & a_{23} & a_{24} & a_{25} & a_{26} & f_{21} & f_{22} & f_{23} \\ & & a_{33} & a_{34} & a_{35} & a_{36} & f_{31} & f_{32} & f_{33} \\ & & & \boxed{a_{44}} & a_{45} & a_{46} & f_{41} & \boxed{f_{42}} & f_{43} \\ & & & & \boxed{a_{55}} & a_{56} & \boxed{f_{51}} & f_{52} & f_{53} \\ & & & & & a_{66} & f_{61} & f_{62} & f_{63} \\ \hline & & & & & & -\boxed{\delta_{11}} & -\delta_{12} & -\delta_{13} \\ & & & & & & & -\boxed{\delta_{22}} & -\delta_{23} \\ & & & & & & & & -\delta_{33} \end{bmatrix}$$

Only the circled components can affect the first order perturbation of v_B.

BG waves $\implies$ $\begin{pmatrix} \boldsymbol{u} \\ \phi \end{pmatrix} = \begin{pmatrix} 0 \\ 0 \\ u_3(x_1, x_2) \\ \phi(x_1, x_2) \end{pmatrix}$

$$\begin{bmatrix} C_{11} & C_{12} & C_{13} & 0 & 0 & 0 & 0 & 0 & e_{23} \\ C_{12} & C_{11} & C_{13} & 0 & 0 & 0 & 0 & 0 & e_{23} \\ C_{13} & C_{13} & C_{33} & 0 & 0 & 0 & 0 & 0 & e_{33} \\ 0 & 0 & 0 & C_{44} & 0 & 0 & e_{41} & e_{42} & 0 \\ 0 & 0 & 0 & 0 & C_{44} & 0 & e_{42} & -e_{41} & 0 \\ 0 & 0 & 0 & 0 & 0 & \frac{C_{11}-C_{12}}{2} & 0 & 0 & 0 \\ 0 & 0 & 0 & e_{41} & e_{42} & 0 & -\epsilon_{22} & 0 & 0 \\ 0 & 0 & 0 & e_{42} & -e_{41} & 0 & 0 & -\epsilon_{22} & 0 \\ e_{23} & e_{23} & e_{33} & 0 & 0 & 0 & 0 & 0 & -\epsilon_{33} \end{bmatrix} \begin{bmatrix} (u_1)_{x_1} \\ (u_2)_{x_2} \\ (u_3)_{x_3} \\ (u_2)_{x_3} + (u_3)_{x_2} \\ (u_1)_{x_3} + (u_3)_{x_1} \\ (u_1)_{x_2} + (u_2)_{x_1} \\ \phi_{x_1} \\ \phi_{x_2} \\ \phi_{x_3} \end{bmatrix}$$

$\mathbf{P}^{\text{ptb}}$ $\begin{bmatrix} a_{11} & a_{12} & a_{13} & a_{14} & a_{15} & a_{16} & f_{11} & f_{12} & f_{13} \\ & a_{22} & a_{23} & a_{24} & a_{25} & a_{26} & f_{21} & f_{22} & f_{23} \\ & & a_{33} & a_{34} & a_{35} & a_{36} & f_{31} & f_{32} & f_{33} \\ & & & a_{44} & a_{45} & a_{46} & f_{41} & f_{42} & f_{43} \\ & & & & a_{55} & a_{56} & f_{51} & f_{52} & f_{53} \\ & & & & & a_{66} & f_{61} & f_{62} & f_{63} \\ & & & & & & -\delta_{11} & -\delta_{12} & -\delta_{13} \\ & & & & & & & -\delta_{22} & -\delta_{23} \\ & & & & & & & & -\delta_{33} \end{bmatrix}$

59

observation data

$$V_{\text{B}} = \rho\,(v_{\text{B}})^2 \approx V_{\text{B}}^{\text{hex}} + P_1\,f_{42} + P_2\,f_{51} + D_1\,\delta_{11} + D_2\,\delta_{22} + E_1\,a_{44} + E_2\,a_{55}$$

get information on the material constants

A simple structure of the first order perturbation of v_B,

but from the point of view of **inverse problems**,

the first order perturbation of v_B has poor information on $\mathrm{P_{ptb}}$.

Two attempts towards the inverse problem :

60

1. Determination of piezoelectric components f_{rj} in P_{ptb}.

Piezoelectric medium : $\mathbf{P}^{hex} + \mathbf{P}^{ptb}$ in $-x_1 \sin\theta + x_2 \cos\theta \le 0$

3-axis : axis of Symmetry $\mathbf{6}$ of $\mathbf{P}^{hex}$

Propagation direction of perturbed BG waves : $(\cos\theta, \sin\theta, 0)$

Velocity : v_B^θ

$$
\begin{aligned}
V_B^\theta &= \rho\,(v_B^\theta)^2 = V_B^{hex} + \cos^2\theta\left(\underline{P_1\,f_{42} + P_2\,f_{51}} + D_1\,\delta_{11} + D_2\,\delta_{22} + E_1\,a_{44} + E_2\,a_{55}\right)\\
&+\ \cos\theta\sin\theta\left((P_2-P_1)(\underline{f_{52}+f_{41}}) + 2(D_1-D_2)\delta_{12} + 2(E_2-E_1)a_{45}\right)\\
&+\ \sin^2\theta\left(\underline{P_2\,f_{42} + P_1\,f_{51}} + D_2\,\delta_{11} + D_1\,\delta_{22} + E_2\,a_{44} + E_1\,a_{55}\right).
\end{aligned}
$$

Two piezoelectric components f_{42} and f_{51} and one linear combination $f_{52} + f_{41}$ can be determined once we already know P_{hex} and the components $\delta_{11}, \delta_{22}, \delta_{12}, a_{44}, a_{55}, a_{45}$ in P_{ptb}.

2. Determination of P_{hex} without P_{ptb}.

Piezoelectric medium : $\mathbf{P}^{hex}$ in $x_2 \le 0$,

3-axis : axis of Symmetry $\mathbf{6}$

Propagation direction of perturbed BG waves : $(\cos\theta, 0, \sin\theta)$ θ : sufficiently small

$$
V_B^\theta = \rho\,(v_B^\theta)^2 = V_B^{hex} + P_1\,f_{42} + P_2\,f_{51} + D_1\,\delta_{11} + D_2\,\delta_{22} + E_1\,a_{44} + E_2\,a_{55},
$$

$$
\begin{aligned}
f_{42} &= f_{232} = Q_{2p}Q_{3q}Q_{2r}\,e_{pqr} - e_{232} = (\cos\theta - 1)e_{42},\\
f_{51} &= f_{131} = Q_{1p}Q_{3q}Q_{1r}\,e_{pqr} - e_{131} = (\cos^3\theta - \cos\theta\sin^2\theta - 1)e_{51} + \cos\theta\sin^2\theta(e_{33}-e_{13}),\\
\delta_{11} &= Q_{1p}Q_{1q}\,\epsilon_{pq} - \epsilon_{11} = (\cos^2\theta - 1)\epsilon_{11} + \sin^2\theta\,\epsilon_{33} = \sin^2\theta(\epsilon_{33}-\epsilon_{22}), \quad \delta_{22} = Q_{2p}Q_{2q}\,\epsilon_{pq} - \epsilon_{22} = 0,\\
a_{44} &= a_{2323} = Q_{2p}Q_{3q}Q_{2r}Q_{3s}\,C_{pqrs} - C_{2323} = (\cos^2\theta - 1)C_{2323} + \sin^2\theta\,C_{2121} = \sin^2\theta\left(\frac{A-N}{2} - L\right),\\
a_{55} &= a_{1313} = Q_{1p}Q_{3q}Q_{1r}Q_{3s}\,C_{pqrs} - C_{1313} = (\cos^4\theta - 2\cos^2\theta\sin^2\theta + \sin^4\theta - 1)C_{1313}\\
&\qquad -2\cos^2\theta\sin^2\theta\,C_{1133} + \cos^2\theta\sin^2\theta(C_{1111}+C_{3333}) = \cos^2\theta\sin^2\theta\,(A + C - 2F - 4L),
\end{aligned}
$$

all of which are of order θ^2 as $\theta \longrightarrow 0$.

How to overcome this difficulty?

$$
\begin{bmatrix}
\lambda+\mu & \lambda & \lambda & 0 & 0 & 0 & 0 & 0 & 0 \\
\lambda & \lambda+\mu & \lambda & 0 & 0 & 0 & 0 & 0 & 0 \\
\lambda & \lambda & \lambda+\mu & 0 & 0 & 0 & 0 & 0 & 0 \\
0 & 0 & 0 & \mu & 0 & 0 & 0 & 0 & 0 \\
0 & 0 & 0 & 0 & \mu & 0 & 0 & 0 & 0 \\
0 & 0 & 0 & 0 & 0 & \mu & 0 & 0 & 0 \\
\hline
0 & 0 & 0 & 0 & 0 & 0 & -\epsilon & 0 & 0 \\
0 & 0 & 0 & 0 & 0 & 0 & 0 & -\epsilon & 0 \\
0 & 0 & 0 & 0 & 0 & 0 & 0 & 0 & -\epsilon
\end{bmatrix}
$$

isotropic configuration

$$
+
\begin{bmatrix}
a_{11} & a_{12} & a_{13} & a_{14} & a_{15} & a_{16} & f_{11} & f_{12} & f_{13} \\
 & a_{22} & a_{23} & a_{24} & a_{25} & a_{26} & f_{21} & f_{22} & f_{23} \\
 & & a_{33} & a_{34} & a_{35} & a_{36} & f_{31} & f_{32} & f_{33} \\
 & & & a_{44} & a_{45} & a_{46} & f_{41} & f_{42} & f_{43} \\
 & & & & a_{55} & a_{56} & f_{51} & f_{52} & f_{53} \\
 & & & & & a_{66} & f_{61} & f_{62} & f_{63} \\
\hline
 & & & & & & -\delta_{11} & -\delta_{12} & -\delta_{13} \\
 & & & & & & & -\delta_{22} & -\delta_{23} \\
 & & & & & & & & -\delta_{33}
\end{bmatrix}
$$

perturbative part

How v_{R} deviates from its comparative value in an isotropic state ?

63

「マス・フォア・インダストリ研究」シリーズ刊行にあたり

本シリーズは，平成 23 年 4 月に設立された九州大学マス・フォア・インダストリ研究所 (IMI)が，平成 25 年 4 月に共同利用・共同研究拠点「産業数学の先進的・基礎的共同研究拠点」として，文部科学大臣より認定を受けたことにともない刊行するものである．本シリーズでは，主として，マス・フォア・インダストリに関する研究集会の会議録，共同研究の成果報告等を出版する．各巻はマス・フォア・インダストリの最新の研究成果に加え，その新たな視点からのサーベイ及びレビューなども収録し，マス・フォア・インダストリの展開に資するものとする．

平成 30 年 10 月

マス・フォア・インダストリ研究所

所長 佐伯 修

シリーズ既刊

Issue	Author／Editor	Title	Published
マス・フォア・インダストリ研究　No.1	穴田　啓晃 安田　貴徳 Xavier Dahan 櫻井　幸一	Functional Encryption as a Social Infrastructure and Its Realization by Elliptic Curves and Lattices	26 February 2015
マス・フォア・インダストリ研究　No.2	滝口　孝志 藤原　宏志	Collaboration Between Theory and Practice in Inverse Problems	12 March 2015
マス・フォア・インダストリ研究　No.3	筧　三郎	非線形数理モデルの諸相：連続，離散，超離散，その先 $\left(\begin{array}{l}\text{Various aspects of nonlinear mathematical models}\\ \text{: continuous, discrete, ultra-discrete, and beyond}\end{array}\right)$	24 March 2015
マス・フォア・インダストリ研究 No.4	穴田　啓晃 安田　貴徳 櫻井　幸一 寺西　勇	Next-generation Cryptography for Privacy Protection and Decentralized Control and Mathematical Structures to Support Techniques	29 January 2016
マス・フォア・インダストリ研究 No.5	藤原　宏志 滝口　孝志	Mathematical Backgrounds and Future Progress of Practical Inverse Problems	1 March 2016
マス・フォア・インダストリ研究 No.6	松谷　茂樹 佐伯　修 中川　淳一 上坂　正晃 濵田　裕康	結晶のらせん転位の数理	10 January 2017
マス・フォア・インダストリ研究 No.7	滝口　孝志 藤原　宏志	Collaboration among mathematics, engineering and industry on various problems in infrastructure and environment	1 March 2017
マス・フォア・インダストリ研究 No.8	藤原　宏志 滝口　孝志	Practical inverse problems based on interdisciplinary and industry-academia collaboration	20 February 2018
マス・フォア・インダストリ研究 No.9	阿部　拓郎 高島　克幸 縫田　光司 安田　雅哉	代数的手法による数理暗号解析 Workshop on analysis of mathematical cryptography via algebraic methods	1 March 2018
マス・フォア・インダストリ研究 No.10	阿部　拓郎 落合　啓之 高島　克幸 縫田　光司 安田　雅哉	量子情報社会に向けた数理的アプローチ Mathematical approach for quantum information society	26 December 2018

Issue	Author／Editor	Title	Published
マス・フォア・インダストリ研究 No.11	松谷　茂樹 佐伯　修 中川　淳一 濵田　裕康 上坂　正晃	結晶転位の先進数理解析 Advanced Mathematical Investigation for Dislocations	7 January 2019
マス・フォア・インダストリ研究 No.12	滝口　孝志	Non-destructive inspection for concrete structures and related topics	13 February 2019
マス・フォア・インダストリ研究 No.13	宇波　耕一 長野　智絵 吉岡　秀和 田上　大助 白井　朋之	数理農学における時系列データのモデル化と解析 Modeling and Analysis of Time Series Data in Math-Agro Sciences	28 February 2019
マス・フォア・インダストリ研究 No.14	佐久間　弘文 大津　元一 小嶋　泉 福本　康秀 山本　昌宏 納谷　昌之	ドレスト光子に関する基礎的数理研究	18 March 2019
マス・フォア・インダストリ研究 No.15	松谷　茂樹 佐伯　修 中川　淳一 濵田　裕康 富安　亮子	結晶の界面，転位，構造の先進数理解析	2 December 2019
マス・フォア・インダストリ研究 No.16	Takuro Abe Yasuhiko Ikematsu Koji Nuida Yutaka Shikano Katsuyuki Takashima Masaya Yasuda	Quantum computation, post-quantum cryptography and quantum codes	17 January 2020
マス・フォア・インダストリ研究 No.17	河村　彰星 津曲　紀宏 西澤　弘毅 溝口　佳寛	代数・論理・幾何と情報科学―理論から実世界への展開	10 February 2020

Institute of Mathematics for Industry
Kyushu University